Responsiveness and dynamics of asynchronous states and Gamma oscillations in cerebral cortex

Eduarda Susin

Thèse présentée pour obtenir le grade de docteur

Sorbonne Université

❧

Institut des Neurosciences Paris-Saclay
École doctorale ED 158 - Cerveau, cognition, comportement

Discipline : Neurosciences

Responsiveness and dynamics of asynchronous states and Gamma oscillations in cerebral cortex

---

Par : **Eduarda DEMORI SUSIN**

Sous la direction de Alain Destexhe, Directeur de Recherche au CNRS, Directeur adjoint de NeuroPSI, Université Paris-Saclay

Membres du jury:

Rapporteur : Laure Buhry, Université de Lorraine.

Rapporteur : María Victoria Sánchez-Vives, Universitat de Barcelona

Examinateur : Diego Contreras, University of Pennsylvania, School of Medicine

Examinateur : Demian Battaglia, Aix-Marseille l'Université

Président du jury : Stéphane Charpier, Sorbonne Université

Directeur de Thèse : Alain Destexhe, Université Paris-Saclay

Date de soutenance : 24 novembre 2021

À minha querida mãe e a meu querido pai que partiu deste mundo sem poder ver este trabalho concluído.

Résumé

Comprendre la cognition et ses mécanismes sous-jacents (comment l'information est codée, décodée et traitée) est l'un des objectifs des neurosciences. Certaines observations indiquent l'implication des oscillations Gamma (30-90 Hz) dans le traitement de l'information en étant associées à différentes fonctions cognitives de haut niveau, telles que la mémoire, la perception, l'attention, l'éveil focalisé et la prédiction. Néanmoins, malgré ces corrélations, le rôle exact des oscillations Gamma est encore débattu. Afin d'étudier les principes neuronaux de la transmission de l'information dans le cerveau, nous avons profité de l'analyse des données électrophysiologiques acquises chez l'homme. Cette analyse a indiqué comment des neurones individuels participent aux rythmes Gamma, nous permettant d'utiliser ces caractéristiques pour construire et contraindre des modèles de réseaux informatiques. Nous avons construit trois modèles de réseaux générant des rythmes Gamma par trois mécanismes différents : soit par l'interaction exclusive entre neurones inhibiteurs [*Interneuron Gamma* (ING)], soit par l'interaction de neurones inhibiteurs et excitateurs via *Pyramidal-Interneuron Gamma* (PING) ou via un mécanisme lié à la présence d'un type particulier de neurone excitateur - appelée *Chattering cell* en anglais, le *Chattering Induced Gamma* (CHING). Ces modèles ont été explorés et comparés à des états électrophysiologiques asynchrones, afin de déterminer quelles sont les conséquences de chaque mécanisme oscillatoire dans la manière dont l'information est traitée par le réseau. La transmission de l'information a été évaluée à travers de la mesure de la réactivité du réseau (*responsiveness*), qui a été acquise dans des conditions saines et dans des conditions pathologiques, imitant des états hallucinatoires ou semblables à des conditions observées dans des patients schizophréniques. Ce travail apporte alors une compréhension du rôle des oscillations Gamma non seulement dans des conditions saines, mais aussi dans des conditions pathologiques.

Abstract

Understanding cognition and its underlying mechanisms (how information is encoded, decoded and processed) is one of the purposes of neuroscience. Gamma oscillations (30-90 Hz) are believed to be involved in information processing, and have been associated to different high-level cognitive functions, such as memory, perception, attention, focused arousal and prediction. Regardless of these observations the exact role of these oscillations is still debated. In order to study the neuronal principles of information transmission in the brain, we took advantage of multi-unit electrophysiological data acquired in human. The analysis of this data indicated how individual neurons participate to Gamma rhythms, and these features were used to build and constrain computational network models. We built three network models generating Gamma rhythms by three different mechanisms: either by the exclusive interaction between inhibitory neurons [*Interneuron Gamma* (ING)] or by the interaction of inhibitory and excitatory neurons via *Pyramidal-Interneuron Gamma* (PING) or via *Chattering Induced Gamma* (CHING). These models were explored and compared to asynchronous states, in order to determine what are the consequences of each oscillatory mechanism in the way information is processed by the network. Information transmission was assessed by means of the measurement of network responsiveness, which was acquired in healthy and in pathological states mimicking hallucinatory states or schizophrenia disease. This work provides insight into the role of Gamma oscillations during healthy and pathological conditions.

Remerciements

Ce travail n'aurait pas été possible sans le soutien de l'École des Neurosciences de Paris (ENP), la Fondation pour la Recherche Médicale (FRM) et la Fondation des Treilles, qui m'ont permis, grâce à une allocation de recherches et diverses aides financières, de me consacrer sereinement à l'élaboration de ma thèse.

Je remercie Alain Destexhe, Directeur de Recherche au CNRS, qui m'a encadré tout au long de cette thèse et qui m'a fait partager ses brillantes intuitions. Qu'il soit aussi remercié pour sa gentillesse, sa disponibilité permanente et pour le soutien qu'il m'a prodigué.

J'adresse tous mes remerciements au président du comité de cette thèse Stéphane Charpier (Professeur Sorbonne Université et Chef d'équipe à l'Institut du Cerveau et de la Moelle épinière), à Laure Buhry (Maître de Conférence - HDR et Professeur associé à l'Institut des sciences du digital Management & Cognition, Université de Lorraine) et María Victoria Sánchez-Vives, (Professeur chercheur à l'Institut d'Investigacions Biomèdiques August Pi i Sunyer, Universitat de Barcelona), ainsi qu'à Diego Contreras (Professeur chercheur au département de Neurosciences à University of Pennsylvania, School of Medicine) et Demian Battaglia (Chercheur au CNRS à l'Institut de Neuro-sciences des Systèmes, Aix-Marseille l'Université), de l'honneur qu'ils m'ont fait en acceptant d'être rapporteurs et examinateurs de cette thèse.

Je tiens à remercier Mallory Carlu et Damien Depannemaecker, mes collègues de laboratoire, pour leurs amitié, compagnie, soutien, encouragements et discussions éclairées.

J'exprime ma gratitude à Leonardo Gregory Brunnet, Professor titular de l'Universidade Federal do Rio Grande do Sul, à Rita Maria Cunha de Almeida, Professora associada de l'Universidade Federal do Rio Grande do Sul et à Sandra Denise Prado, Professora associada de l'Universidade Federal do Rio Grande do Sul, pour leur accompagnement pendant ma Licence et mon Master au Brésil. Ils ont toujours été là pour me soutenir et c'est grâce à eux que j'ai découvert la recherche.

Je remercie mes amis proches que m'ont apporté le soutien émotionnel pour franchir les difficultés et toutes les personnes avec qui j'ai partagé mes études, notamment ces années de thèse.

Finalement, il m'est impossible d'oublier le soutien inconditionnel de ma mère, Luciana Isabel Demori, de mon père, Enelsir Bernart, de ma marraine Eliane Delegrave et de mon compagnon Siegfried Nebel. Cette thèse est aussi à vous.

Summary

Part I

Introduction

Key Biological Concepts

The Brain, Neurons and Synapses

The brain[1] is the center of the nervous system and is the most complex organ in all vertebrates. In all mammals, the outer layer of the brain is denominated as the *cerebral cortex*. In humans, it can be divided into four distinct lobes: parietal, occipital, frontal and temporal. Each region of the cerebral cortex has its specificities: different cellular composition with different patterns of connectivity.

The cerebral cortex is composed by two main categories of cells, the *glia cells* (required for structural stabilization and energy supply) and another very heterogeneous class of cells called *neurons*. Even though recent works have shown the possible implication of glia cells in information processing [1], the main elementary computing units of the nervous system are thought to be the neurons.

Neurons, like all livings cells, present an electric membrane potential, due to the difference between positive and negative charges in the intra- and extra-cellular domain. On the other hand, unlike most cells, neurons are excitable. This means that the electric membrane potential of neurons is capable of fluctuating and, as a consequence, generating and transmitting electrical and chemical stimuli to other cells.

In spite of the large variety of neuronal shapes, a typical neuron can be divided into three structural parts: soma, dendrites and axon. While the dendrites and the axon can be seen as input and output "devices" of the neuron, the soma[2] can be seen as the "information processing center" of the cell. This information processing happens in a way that if the total input leads the membrane potential to exceed a certain threshold, then an output signal is generated and transmitted to other neurons by the axon. When this signal is generated, we say that the neuron *spiked* and that an *Action Potential*[3] was produced. The place where this signal exchange takes place is called *synapse*. Neurons which are sending and receiving this signal are respectively called presynaptic and postsynaptic neurons. This process can happen in different ways depending on the nature of the synapse: electrical

[1]The brain is the ensemble of three structures: the cerebrum, the cerebellum and the brain stem.

[2]The soma, or cell body, is the part of the cell where the genetic information is stored and where most of the physiological processes take place.

[3]The Action Potential is a rapid variation in the neuronal membrane potential, composed of a fast period of depolarization (due to the opening of Na^+ channels), and a slow period of repolarization and hyperpolarization (due to inactivation of Na^+ channels and opening of K^+ channels). It is known as the *Absolute Refractory Period*, the period of time that covers the effects of the increase in the K^+ conductivity (with respect to the *resting state*) and the effects of the residual inactivation of the Na^+ channels.

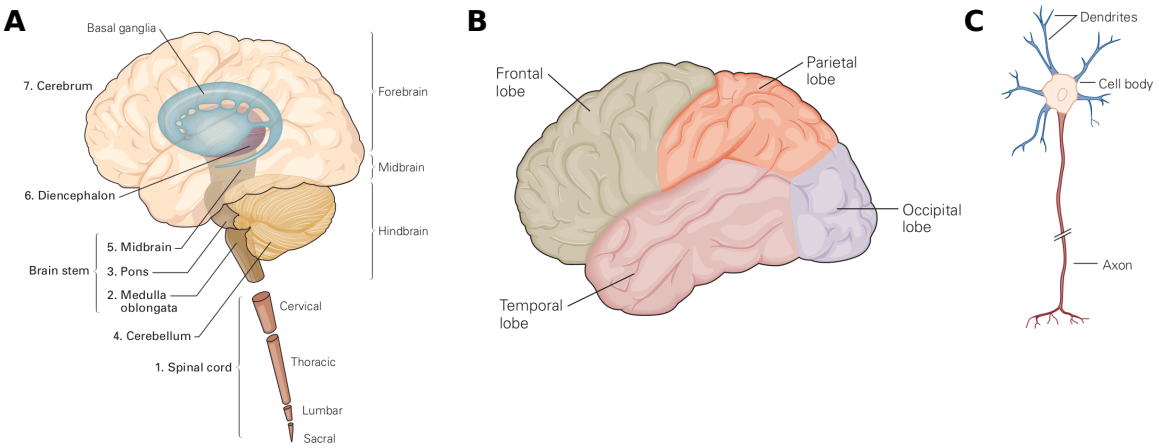

Figure 1: **The central nervous system parts and its units**. A) Anatomical parts of the central nervous system. It can be divided into 7 main parts (as indicated in the figure). The brain is the ensemble of three structures: the cerebrum, the cerebellum and the brain stem. The Cerebrum is composed by the cerebral cortex and several subcortical structures (the hippocampus, the basal ganglia, and the olfactory bulb). The Diencephalon is composed by the thalamus, the hypothalamus, the epithalamus and the subthalamus. B) Anatomical division of the cerebral cortex into 4 lobes. C) General structure of a neuron. Figures A, B and C were adapted from [2] (pages 9 and 25).

or chemical.

In chemical synapses, presynaptic and postsynaptic neurons are completely separated from each other in space. On the other hand, in electrical synapses, pre- and postsynaptic cells are directly connected (sharing their cytoplasm) by means of special channels called *gap-junctions*.

Gap-junctions have been proposed to contribute to *brain rhythms* both experimentally and theoretically [3, 4, 5, 6, 7]. However in the network models developed in this thesis, we decided to ignore this level of description, and only included chemical synapses in our models.

Chemical Synapses, Neuro-transmitters and Receptors

At chemical synapses, the synaptic transmission happens by means of vesicles of small organic molecules, called neurotransmitters, released by the presynaptic cell, due to the rise of Ca^{2+} concentration within the synaptic terminal, following an Action Potential. These vesicles diffuse in the extracellular medium between the pre- and the postsynaptic cells, the *synaptic cleft*, and bind to the receptors on the postsynaptic neuron. This binding leads to the opening of ion channels at the postsynaptic neuron, generating a change in its membrane potential (see Figure 2). All these processes generate a time difference between

the presynaptic spike and the postsynaptic response. This time difference is called *synaptic delay*.

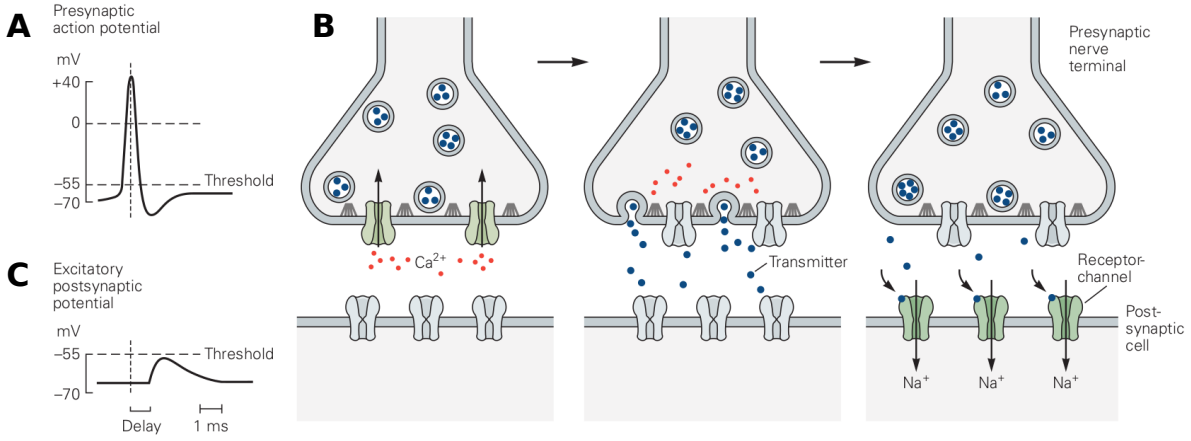

Figure 2: **Synaptic transmission at chemical synapses**. A) Membrane potential variation during an Action Potential on the presynaptic cell. B) Succession of events composing the chemical synaptic transmission: the action potential arriving at the terminal of a presynaptic axon causes voltage-gated Ca^{2+} channels at the presynaptic terminal to open (left panel). This opening generates an intracellular high concentration of Ca^{2+} in the presynaptic terminal, allowing vesicles containing neurotransmitter to fuse with the presynaptic cell membrane and release their contents into the synaptic cleft (middle panel). Subsequently, the released neurotransmitter molecules diffuse across the synaptic cleft and bind specific receptors on the postsynaptic membrane. These receptors cause ion channels to open (or close), thereby changing the membrane conductance and the membrane potential of the postsynaptic cell (right panel). C) Postsynaptic potential fluctuation due to the synaptic transmission. This figure was adapted from [2].

Conductance changes by means of chemical synapses can either increase the postsynaptic membrane potential (excitatory synapse) or decrease it (inhibitory synapses), depending on the type of neurotransmitter released. Glutamate and γ-aminobutyric acid (GABA) are respectively the main excitatory and inhibitory neurotransmitters in the brain.

The glutamate-gated channels conduct both Na^+ and K^+ ions, with nearly equal permeability. The two major glutamate receptors are α-amino-3-hydroxy-5-methyl-4-isoxazolepropionic (AMPA) and N-methyl-D-aspartate (NMDA) receptors. Unlike AMPA, NMDA channels are additionally highly permeable to Ca^{2+}, which is crucial for induction of synaptic plasticity [8]. While the AMPA-mediated currents are fast (0.34-11ms), the NMDA-mediated are considerably slower (6–350 ms) and present a complex relation with respect to the membrane potential [9, 10, 11, 12]. Both AMPA and NMDA receptors are *ionotropic*, meaning that these channels open directly when glutamate binds to them. However, the opening of NMDA channels depends not only on the biding of neurotransmitters but also on the membrane voltage. At the resting membrane potential extracellular Mg^{2+} ions are tightly bond to NMDA channel pores, blocking ionic current. When the

membrane is depolarized (for example, by the opening of AMPA receptor-channels), Mg^{2+} is expelled by electrostatic repulsion, allowing the flux of ions. Due to this Mg^{2+} block, NMDA receptor channels rarely initiate neuronal excitation on their own. The magnesium block of the NMDA receptor channel (B) is accurately modeled by the following phenomenological expression as a function of voltage of the membrane potential (V) [13] :

$$B(V) = \frac{1}{1 + exp(-0.062V).([Mg^{2+}]_o/3.57)} \quad (1)$$

where $[Mg^{2+}]_o$ is the external magnesium concentration (1 to 2 mM in physiological conditions). NMDA-mediated synapses have been reported to participate in both thalamo-cortical and intracortical synaptic pathways [14] acting on excitatory and inhibitory neurons [15].

The main receptors of the inhibitory neurotransmitters GABA are $GABA_A$ and $GABA_B$. While $GABA_A$ receptors are ionotropic, directly opening Cl^- channels, $GABA_B$ receptors are metabotropic, meaning that they activate second-messenger cascades, opening indirectly other channels (often K^+ channels). For this reason the current produced by $GABA_A$ receptor channels are fast, while the ones from $GABA_B$ are slow. Most ofthe fast inhibitory postsynaptic potentials are mediated by $GABA_A$ receptors in the central nervous system. In this thesis only $GABA_A$ receptors are used in our models. Figure 3 depicts the representative postsynaptic currents due to $GABA_A$, $GABA_B$, AMPA and NMDA receptor channels.

Neuronal Heterogeneity

Although all neurons inherit the same genes, depending on the particular cell's developmental history, only a restricted set of them are expressed. As a consequence, an enormous variety of their enzymes, structural proteins, membrane constituents, ion channels, and secretory products exists among neurons [2, 17, 18, 19]. This rich repertoire of channels allows neurons to generate action potentials with a wide range of shapes (spike waveform), firing rates and duration [20]. These physiological differences can be used to categorized neurons into different types [21, 22, 23, 24].

McCormick and collaborators were the first to describe the so-called Regular-Spiking (RS) and Fast-spiking (FS) neurons. When presented with prolonged stimuli of constant amplitude, RS neurons exhibit pronounced adaptation of the spike frequency while FS neurons undergo little or no adaptation [21] (see Figure 4A and 4B). In 1985, McCormick and colleagues related electrophysiological aspects to morphological and immunocytochemical features, identifying neocortical FS neurons as being GABA-mediated interneurons [21] and RS neurons as being pyramidal neurons. Today, other types of cell are known

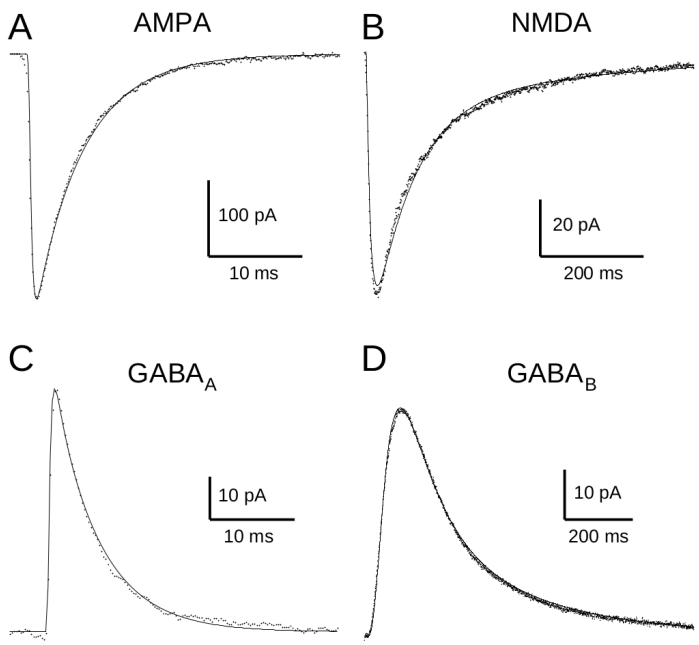

Figure 3: **Postsynaptic currents due to different receptors**. A) AMPA-mediated currents. B) NMDA-mediated currents. C) $GABA_A$-mediated currents. D) $GABA_B$-mediated currents. For all graphs, the averaged recording of the synaptic current (noisy trace) is represented with the best fit obtained using detailed kinetic models (continuous trace) [16]. This figure was adapted from [16]. Original works that provided the experimental curves are cited in [16].

to also display regular spiking activity. This is the case for the Cholecystokinin-positive basket cells (GABA-mediated interneuron) [25]. Likewise, two types of GABA-mediated interneurons are known to display fast spiking activity: Chandelier cells[4] and Parvalbumin-positive (PV) Basket cells [25]. In this thesis three types of cells are used in our models: Regular Spiking pyramidal cells (RS), Fast Spiking basket cells (FS) and Chattering (Ch) cells.

Chattering Cells were proposed to be a biophysically distinct class of pyramidal neurons because of its distinguished intrinsic firing properties [27]. These neurons, found in superficial layers of the cortex, intrinsically generate bursts that repeat with a firing frequency of 20 Hz and upwards due to a suprathreshold depolarizing current injection [27, 28, 29] (see Figure 4C).

[4]Chandelier cells are a type of GABA-mediated interneurons that differs from Basket cells both morphologically and functionally. While Basket cells form axosomatic synapses (axons terminating on the cell bodies of target neurons), Chandelier cells form axo-axonic synapses (axons terminating exclusively on the axons of target neurons). Interestingly this morphological difference (inputs onto axon initial segment) proffer this type of cell an excitatory effect on its postsynaptic neurons [26]. Based on the classification by means of the expression of specific molecular markers, Chandelier cells are also classified as Parvalbumin-positive (PV) [25].

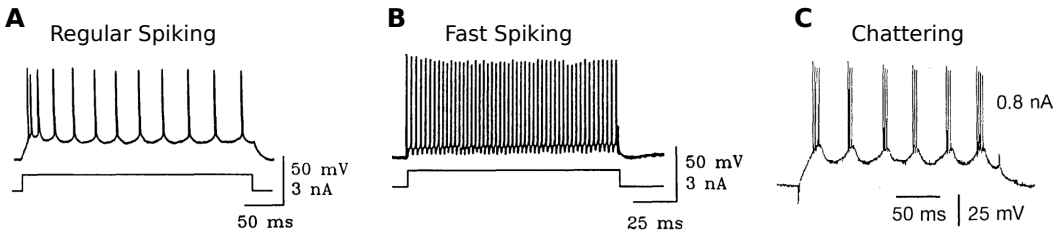

Figure 4: **Intrinsic firing patterns of different cell types**. A) Extracellular recording in mouse thalamocortical slice of a Regular Spiking (RS) pyramidal cell (adapted from [30, 22]). B) Intracellular recording in guinea pig neocortical slices of Fast Spiking (FS) inhibitory cells (adapted from [21, 22]). C) Intracellular recording in the cat neocortex *in vivo* of a Chattering (Ch) neuron (adapted from [27]).

Cortical Layers

The neocortex, external region of cerebral cortex[5], can be morphologically segmented based on the density of specific pyramidal neurons, as well as by their afferent and efferent projections [31]. Most of the neocortex contains six layers, numbered from the outer surface (pia mater) of the cortex to the inner white matter [2]. Layer L4 receives most of the stimulus coming from the primary sensory thalamic nuclei, together with L5b and L6. Layers L1 and L5a receive inputs from associative thalamus, while layer L5b send projections to subcortical areas. The cortical layers communicate with each other in an intricate way. A scheme of their connections is depicted in Figure 5. In this thesis we are particularly interested in layers 2/3.

Inhibitory neurons are present in all layers and usually have axons that remain within the same area where their cell body are [2]. They are believed to receive inputs from the same sources as the principal cells. It is estimated that inhibitory neurons constitute around 20% to 25% of the neurons in the neocortex.

Brain States: States of Consciousness

Different brain states can be categorized based on two important concepts: *awareness* and *arousal*[6] [33]. The level of *arousal* is associated to the global capacity to respond to stimuli. For instance, clinicians use scoring systems such as the *Glasgow Coma Scale* [35] to access the level of arousal in patients. In this protocol, the patient reactions (eye opening, motor response and verbal response) are measured with respect to censorial stimuli and scored accordingly. Scores range from 3 to 15, in which 15 indicates a patient fully alert. The level of *awareness*, on the other hand, is related to the ability to perceive and interact

[5]The neocortex constitutes 90% of the cortex. The remaining 10% is occupied by the *allocortex*, which contains the olfactory system and the hippocampus.

[6]The concept of arousal is also associated to the nomenclature of *wakefulness* or *vigilance* [33, 34]

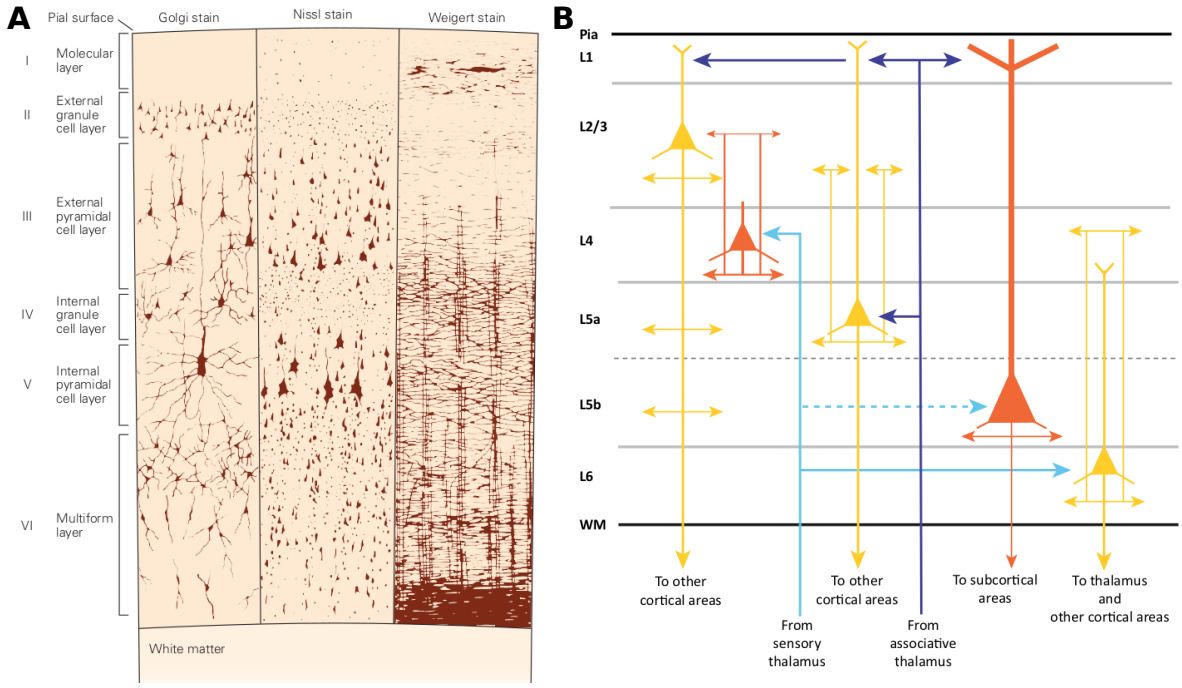

Figure 5: **The six layers of neocortex and their connections**. A) Visualization (by means of 3 different types of stain) of neocortical neurons arrangement in 6 different layers. The Golgi stain unveil a subset of neuronal cell bodies, axons, and dendritic trees, while the Nissl method allows only the visualization of cell bodies and proximal dendrites. The Weigert stain method, on the other hand, enable the visualization of myelinated fibers (like axons). Figure A was adapted from [2] (page 345) and originally extracted from [32]. B) Simplified diagram illustrating localization and input–output connectivity patterns of excitatory neurons in the 6 cortical layers (adapted from [25]). WM stands for white matter.

with the environment in a complex and *conscious* way. In this perspective, awake states are seen as the state in which the patient is fully *aroused* and fully *aware*. While a patient in vegetative state is considered to be in a state in which there is some level of *arousal*, but no level of *awareness*. The scheme depicted in Figure 6, illustrates these concepts.

In mammals and in most bird species, sleep is divided in two distinguishable neurophysiological states: rapid eye movement (REM) and non-rapid eye movement (NREM) sleep [36]. REM sleep is characterized by inhibited muscular tone (as measured by electromyography) and involuntary saccadic eye movements (from where its name is derived). In humans, NREM sleep can be divided into three gradual sleep depth levels [37]: stage N1 (transition between wake and sleep), Stage N2 (light sleep) and Stage N3 (deep sleep, also known as Slow Wave Sleep, SWS). The SWS receives this name because of its characteristic extracellular activity, which exhibits slow oscillations (as will be discussed in the next section).

In general, the level of arousal increases with the increase of awareness. This is what is observed when we compare the different stages of NREM sleep with conscious wakefulness. However, an interesting exception exists: REM sleep. This sleep stage presents

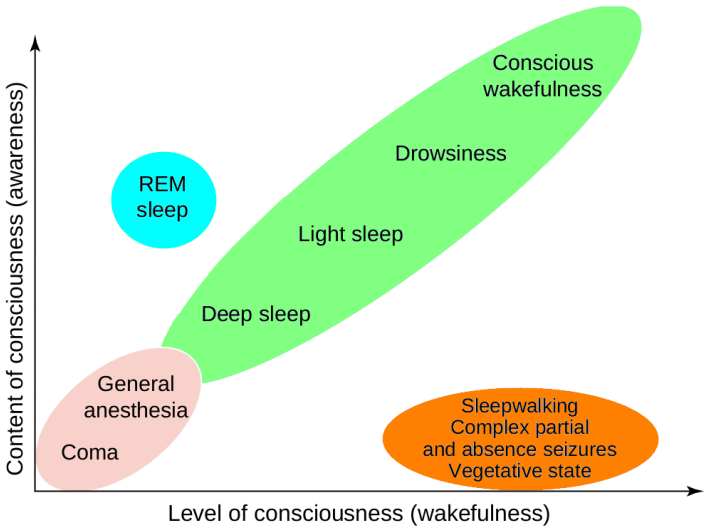

Figure 6: **Scheme illustrating different brain states.** States of Consciousness are classified with respect to the level of awareness and to the level of wakefulness (arousal). Figure adapted from [33]

electrophysiological activity similar to the one observed during Awake states: single units firing tonically, together with extracellular recordings capturing spontaneous bursts of low-amplitude oscillations in the range of 15-90 Hz [38, 39, 40, 41, 42]. For this reason, REM sleep is seen as a state with high awareness but no *arousal*.

Regardless of the difficulties to rigorously define awareness, some authors tried to quantify it, by means of certain concepts of *complexity theory*. The **Complement Research Article** inserted in the end of this thesis reviews some of them.

Brain Rhythms

The discovering of brain oscillations dates from 1929, when a controversial psychiatrist, Hans Berger, trying to prove the existence of psychic phenomena, observed electrical oscillations coming from electrodes placed at the head of one of his patients. This was the first electroencephalogram (EEG) recording registered [43].

Brain rhythms is the generic therm used to describe oscillatory electro-magnetic phenomena generated by the collective activity of neurons in the brain in a mesoscopic scale (few millimeters to centimeters). This type of activity can be measured by methods such as ECoG (electrocorticography), EEG (electroencephalography), LFP (local field potentials) and MEG (magnetoencephalography), with temporal precision varying from the order of milliseconds to seconds [44, 45]. See Figure 7.

The canonical classification of these oscillations has been defined in the following frequency bands: Slow-oscillations (0.3-1 Hz), Delta (1–4 Hz), Theta (4–8 Hz), Alpha (8–12 Hz), Beta (15–30 Hz), Gamma (30–90 Hz), High Gamma (90-140 Hz). In addition,

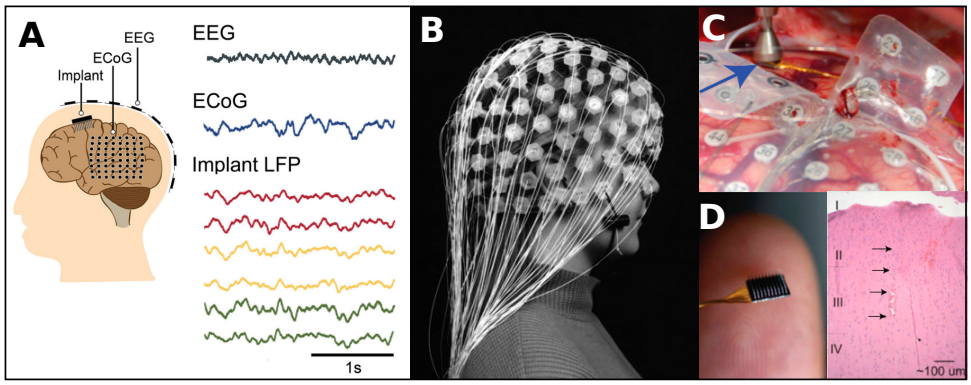

Figure 7: **Brain Rhythm Measurements**. A) Schematic illustration of different techniques of brain rhythm recordings. B) EEG is the less invasive method beeing recorded on the scalp surface. It allows stable recordings over time but presents low spatial resolution (covering a large area) and a low signal-to-noise ratio. C) ECoG is more invasive than EEG, being recorded intracranially, in the surface of the brain. It allows a high signal-to-noise ratio and stable recordings over time. D) Multi-electrode arrays (left). The LFP is measured by means of penetrating electrodes directly in the brain tissue (right). This technique is highly invasive and doesn't allow very long recordings since the neuronal environment deteriorates over time leading to instabilities in the recordings. Its advantage is that it allows a high signal-to-noise ratio close to the neurons. Some types of arrays allow not only the measurement of LFP but also unit activity. This is the case of the experimental data used in this thesis. Figure A was adapted from [44]. Figures B was adapted from [46] and Figures C, D and E were adapted from [47].

other important rhythms are the Spindles and the Ripples oscillations, which are not exclusively defined by their frequency band (see below). In principle, all these rhythms could emerge in the brain at any given time and region, but some correlations between certain rhythms regions and behavior have been established throughout the last decades. Bellow we highlight some of these aspects related to each brain rhythm. These correlations suggest possible mechanistic roles for each oscillation on cognitive phenomena, but the exact function of these oscillations is still debated.

Brain Rhythms Features:

- **Delta and Slow oscillations (SO):** Mostly observed during deep non-REM sleep or during anesthesia. Different evidences suggests that these rhythms, SO (0.3-1 Hz) and Delta (1-4 Hz), have an important role on the formation and consolidation of memories acquired during wakefulness [48, 49, 50, 51, 52]. SO and Delta oscillations have been classically classified as two distinct neurophysiological phenomena with different spatial and temporal properties [53, 51]. For example, while some observations indicate that SO are generated exclusively by cortical networks [54, 55, 56], Delta rhythms generators were found in both cortex and thalamus, with mechanism

of generation specific to each structure [57]. More recent studies indicate that SO and Delta oscillations have competing roles in sleep-dependent memory consolidation [58].

- **Theta :** In Hippocampus, it is observed during spatial navigation, and the precise timing of spikes with respect to the Theta cycle is believed to partially encode spatial information [59]. In addittion, Theta is also believed to play a role in the formation and retrieval of episodic and spatial memory [60] in the hippocampus. In cortex, Theta rhythms have been associated to working memory tasks, both in Human [61] and in Monkey [62] .

- **Alpha :** Frequently observed in the occipital lobe, alpha rhythms are associated with wakeful rest with eyes closed [63].

- **Beta :** Beta rhythms are more frequently associated to the inhibitory control in the motor system. They occur during the preparation for the movement ("readiness state") and cease at the onset of movement execution. Other studies, additionally indicate that Beta oscillations are more generally involved in sensory-motor integration and top-down signaling [64].

- **Gamma :** Gamma oscillations occur in all cortical areas, thalamus and hippocampus [65, 66, 67, 68, 69, 70, 71, 72, 73]. This type of activity has been associated to different high-level cognitive functions, such as memory [74, 75, 76], perception [77, 78, 79, 80], attention [81, 82, 83, 84], focused arousal [85] and prediction [86].

- **High Gamma :** The terms *fast Gamma* [87] and *high Gamma* [88] were coined to describe a frequency band between 90 and 140 Hz in the cortex. Two hypothesis about high Gamma oscillations have been debated. One states that high Gamma play the same role as Gamma oscillations but operate at a shorter timescales [75], while other authors propose that high Gamma power is simply related to a spiking activity increase [89, 90]. Furthermore, different works suggests [91, 92] that Gamma and high Gamma have different mechanisms of generation, which would justify a difference in the nomenclature for rhythms in the 30–90 Hz and the 90–140 Hz bands.

- **Ripple Oscillations :** This type of high frequency oscillation is typically observed during non-REM sleep, anesthesia and during consummatory behaviors (immobility, drinking, eating and grooming). It has been traditionally studied in the hippocampus [93, 67, 94], but recent work has proposed that ripples can also be recorded in the cortex [57, 95, 96]. In hippocampus ripples are observed together with *sharp waves*. Sharp wave ripples in hippocampus are typically characterized by periods of approximately 50 to 100 ms of a large negative *sharp wave* with superimposed

high frequency oscillatory activity (80–200 Hz) called *ripples*, followed by a period of approximately 200 ms of a positive wave [94]. Ripple oscillations have been proposed to play an important role in memory consolidation during non-REM sleep or consummatory behaviors [97, 93], and, more recently, to be involved in memory retrieval during active awake states [97, 95, 96].

- **Spindle Oscillations :** Also known as sleep spindles, it is a characteristic rhythm that occurs during non-REM sleep (stages 2 and 3 [98]). It is typified as oscillations (11-16 Hz) lasting for 0.5 to 3 seconds, whose amplitudes wax and wane [98, 99]. Spindles are the product of the interaction between thalamic reticular, thalamocortical, and cortical pyramidal networks [100, 53]. It has been proposed that spindles may be an essential element for memory formation [48] and short- and middle term synaptic plasticity [51].

Asynchronous and Irregular States

The spontaneous cortical activity observed *in vivo* is characterized by highly stochastic and irregular neuronal spiking with low pairwise spike correlations in different brain states [101, 102, 103, 104].

One of the first works to approach the spontaneous cortical activity in a theoretical point of view, demonstrating it to be an emergent property of large networks of excitatory and inhibitory neurons sparsely connected by strong synapses, was developed by Carl Van Vreeswijk and Haim Sompolinsky [105]. In this seminal work based on binary neurons (see the section Computational Models), the stochastic feature of spiking activity was associated to the approximate balance between its excitatory and inhibitory inputs which was dynamically adjusted by the own network intrinsic properties. This *balanced state* has also been experimentally observed *in vitro* [106] and *in vivo* works [107, 108].

Subsequently, Nicolas Brunel and collaborators [109, 110] extended these results by working with systems in which synaptic time scales were included. By means of spiking networks of *leaky integrate-and-fire neurons* and *mean field models* (see the section Computational Models), they showed that irregular firing activity in low firing rates could be achieved in different conditions in networks with sparsely connected neurons with strong synapses composed of excitatory and inhibitory units. In networks in which the time constants of the membrane potentials of excitatory and inhibitory neurons were the same, this stochastic firing behavior could only emerge when inputs were closely balanced. On the other hand, if inhibitory neurons could depolarize faster than excitatory neurons (through smaller membrane time constants), then this condition could be relaxed, leading to irregular spiking activity close to what is observed *in vivo*, even if excitatory inputs dominated [109]. Sub-sequential works have enlarged this view to more complex neuronal and synaptic dynamics [111, 112]. More generally, this early analysis [110] showed that different activity regimes could be achieved depending on the balance between inhibition and excitation, and on the magnitude of external inputs. These regimes were classified generically due to two main aspects: global activity (synchronous or asynchronous) and individual neuronal activity (regular or irregular). Following this criteria, the observed spontaneous activity observed in cortical regions *in vivo* has been classified to be in an *Asynchronous and Irregular* (AI) state.

The AI state is precisely defined as a stationary global activity with strongly irregular individual firing at low rates. However, spontaneous awake activity is far from being stationary. *In vitro* studies have shown that to be able to correctly explain the *inter-spike intervals* (ISI) of neuronal activity observed *in vivo*, factors such as synchrony need to

be taken into consideration [113]. In addition, human ECoG measurements, in conditions in which the subjects are awake and immobile, show the occurrences of different brain rhythms in different brain regions [114]. Using the terminology developed by [110], resting awake activity could be interpreted as the dynamical switch between *Asynchronous and Irregular* states and *Synchronous and Irregular* states (brain oscillations). This switch, according to these simplified models [110], could be controlled by the strength of an external drive and by the balance between excitation and inhibition. The theoretical description of brain oscillations will be detailed on chapter: Computational Models.

Different brain states are characterized by different levels of occurrences of different brain rhythms [115]. In particular, during Slow-wave sleep (SWS), neuronal activity remains irregular while it is strongly modulated by a Delta rhythm, which is characterized by periods of sustained firing and periods of very low spiking activity called the *Up* and *Down states* [102].

It has been proposed that the neuronal activity displayed during *Up states* of SWS are similar to the activity displayed during awake states both in terms of spiking and rhythmic activity observed on the LFP [38]. In **Work 1**, we review several works that have shown similarities and differences between these two brain states. We compare previously published results with our own analysis of human data provided by one of our collaborators, focusing on differences of spiking patterns (firing rate and spiking correlations) and on different neuronal participation on Gamma rhythms in awake and SWS.

Other properties of Awake-like states (*Asynchronous and Irregular*) are investigated in **Work 2**, in which network responsiveness is measured and compared to periods of increased synchrony where the networks present Gamma oscillations in a *Synchronous and Irregular* manner.

Gamma Oscillations

The first study characterizing Gamma-band activity (30-90 Hz) was developed by Edgar Adrian in 1942 [116], who reported induced activity, due to olfactory stimulus, as sinusoidal oscillations between 30 and 60 Hz lasting for the duration of the stimulation. Nevertheless, the study of Gamma oscillations gained the attention of the general scientific community only in 1987, when Gray and Singer discovered 40 Hz oscillations at the cellular level [66]. A complete review of historical hallmark studies is given by [117].

Gamma rhythms are observed in many brain regions, during both awake and sleep states [118, 38, 69, 119, 74, 47], in different species. They have been reported to appear spontaneously or due to external stimulus, being either induced, evoked, or emitted [120]. Interestingly, the spiking activity, measured concomitantly with Gamma activity on the LFP, is highly irregular. Examples of this neuronal activity were observed *in vivo* in the neocortex and hippocampus, where gamma oscillations were associated with stochastic and sparse spiking activity of individual cells [68, 75, 121, 81, 122, 87, 69, 38, 123, 124].

In the last decades, Gamma oscillations have been associated to different high-level cognitive functions, which lead to the hypotheses that Gamma oscillations are important for information processing and coding. The most popular theories are the Binding-by-synchronization Hypothesis [125, 126], the Phase Coding Theory [127, 128], the Communication Through Coherence Theory [129, 130] and Communication through Resonance Theory [131].

In **Work 2**, we take advantage of the human data provided by one of our collaborators to further characterize individual neuronal activity during Gamma oscillations. We typify neurons according to their phase-locking and firing rate changes inside and outside Gamma bursts, inquiring about behavior changes. In **Work 2** we also compare the result of this analysis with computational models putting into perspective the different theories of information processing and coding involving Gamma previously cited. In addition, we use these computational models to explore three mechanisms of Gamma generation (detailed bellow), and examine their effects on the spiking patterns of individual cells.

Mechanisms of Generation

The mechanisms underlying Gamma oscillations have been widely studied experimentally, both *in vivo* and *in vitro* [70, 132, 133, 134, 135]. Three important mechanisms are the *Interneuron Gamma* (ING), in which Gamma oscillations are generated by the exclusively interaction among inhibitory neurons; the *Pyramidal-Interneuron Gamma* (PING), in

which Gamma is due to the interaction between inhibitory and excitatory neurons; and the *Chattering Induced Gamma* (CHING)[7], in which the rhythm production relies on the presence of pacemaker excitatory cells known as *Chattering neurons* [27, 133]. The theoretical approach to study the underlying mechanisms of Gamma oscillations will be discussed in the next chapter.

Several experimental models have been used to examine oscillation dynamics as an emergent property of neuronal networks. These protocols include the application of agonists or antagonists of certain receptors, and/or the electrical activation of specific cells types [135]. We describe in Figure 8 three important works that reported, by means of extracellular recordings, how Gamma oscillations can be initiated or blocked *in vitro* by means of these techniques.

In the work [136], Gamma oscillations are generated on Hippocampus (CA3) by means of Carbachol, a cholinergic agonist. In this preparation Gamma rhythms are blocked either by NBQX (AMPA receptor antagonist) or by Bicuculline ($GABA_A$ receptor antagonist), showing that both excitatory and inhibitory synapses are involved in Gamma generation, an *in vitro* demonstration of PING mechanism (Figure 8A).

The work [137] reported Gamma oscillation in CA3 due to Kainate (Kainate receptors agonist). In this study, Gamma oscillations were abolished by Bicuculline, but were not affected by the AMPA receptor antagonist GYKI 53655. This results indicate that the observed rhythmic activity was mainly a consequence of inhibitory synaptic activity, an illustration of ING mechanism (Figure 8B).

At last, the work [133] reported the importance of Chattering cells on Gamma rhythm generation (CHING mechanism) on Cortex. In this study, Gamma oscillations were evoked by Kainate and abolish after phenytoin application. Phenytoin is an anticonvulsant drug that blocks persistent sodium conductance, acting preferentially on Chattering cells because of its electrophysiological behavior. It is known that Chattering cells are absent at Hippocampus. The work of [133] showed that Kainate-induced Gamma oscillations were only extinct by phenytoin on cortex and not in Hippocampus, indicating the importance of Chattering cells on the rhythm generation, illustrating the CHING mechanism (Figure 8C).

Even-though these three mechanisms can be observed in cortex *in vitro*, it is still controversial which of these mechanisms are engaged in different cortical regions in different conditions *in vivo* [138, 132, 139, 140].

[7]The term *Chattering Induced Gamma* (CHING) was coined in this thesis to designate the Gamma generation mechanism that relies on the presence of *Chattering neurons*.

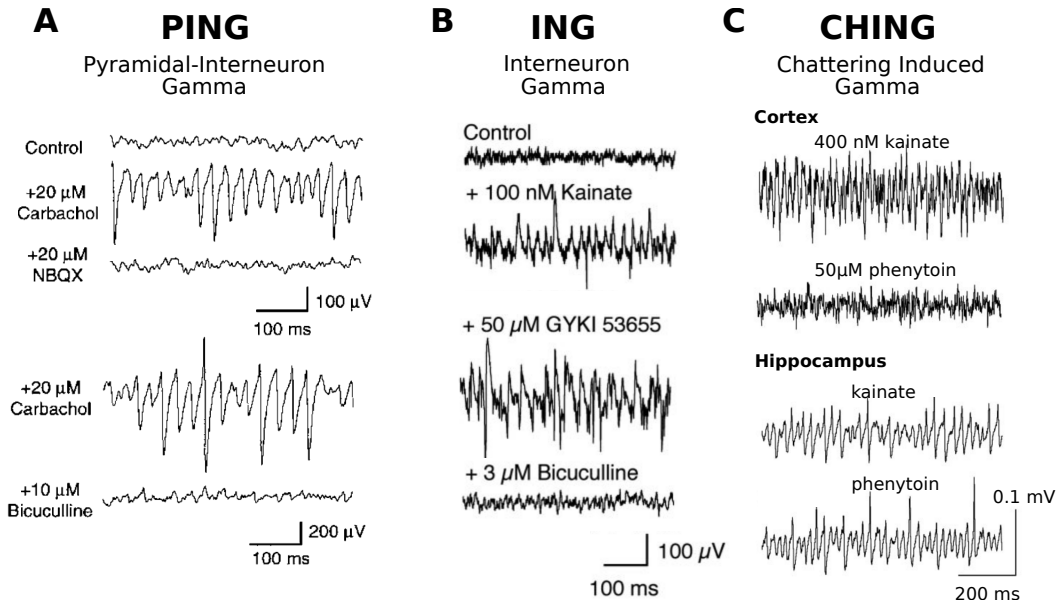

Figure 8: **Extracellular recordings demonstrating different Gamma generation mechanisms *in vitro***. A) Gamma oscillations were evoked on hippocampal region CA3 by means of Carbachol and are blocked by both AMPA receptor antagonist NBQX and the $GABA_A$ receptor antagonist Bicuculline, illustrating PING mechanism. Figure adapted from [136]. B) Kainate-induced Gamma oscillations in CA3 are abolished by Bicuculline but suffer no effect from AMPA receptor antagonist GYKI 53655 application, illustrating ING mechanism. Figure adapted from [137]. C) Phenytoin blocks Kainate-induced Gamma oscillations in cortex, but not in Hippocampus. Since Chattering cells are sensitive to Phenytoin and are absent in Hippocampus, this preparation illustrates the CHING mechanism. Figure adapted from [133].

Gamma Oscillations, NMDA receptors and Schizophrenia

Schizophrenia is a mental disorder that affects around 1% of global population [141]. It is characterized by three classes of symptoms: positive symptoms, which include delusions, hallucinations and disordered thoughts or speech; negative symptoms, which comprehend poverty of speech and deficits of normal emotional response, such as lack of motivation and inability to experience pleasure; and cognitive deficits involving dysfunction of working memory, long-term memory, attention and learning [142, 143, 144].

Several abnormalities have been identified in schizophrenic patients. These abnormalities extend from important differences in neurotransmitters systems to anatomical deficits[8] and are reflected in abnormal neuronal activity.

In healthy subjects, NMDA receptor antagonists can induce a psychotic state that resembles all three classes of schizophrenic symptoms [147, 148, 149]. Likewise, in schizophrenic patients, NMDA receptor antagonists can exacerbate the symptoms [148, 150]. These observations lead to the conception of the *NMDA hypofunction paradigm* [151, 152], which states that the hypofunction of NMDA receptors (NMDAR) might be one of the causes of schizophrenia[9]. Furthermore, a reduced expression or binding of NMDAR in thalamus and in cortex have been identified in postmortem studies [156].

NMDA receptors are critical to the development and to the adult function of GABAergic interneurons. NMDA receptors regulate the expression of GAD67 [157] (GABA synthesizing enzyme) and the expression of parvalbumin[10] (PV) [157]. *In vitro* studies have shown that NMDA receptor antagonists, such as ketamine or phencyclidine, reduce the expression of GAD67 and PV [157, 160, 161], and reduce inhibitory synaptic transmission in cortical slices [162]. Furthermore, post-mortem analysis of schizophrenic patient's brain have shown a reduced expression of PV and GAD67 [163, 164, 165, 166, 167, 142].

[8] Schizophrenia is associated with widespread reductions in the volume of grey matter [145]. Since the overall number of neurons is largely preserved, these volume reductions are believed to reflect a reduction of synaptic connectivity [146].

[9] Another important paradigm used to study schizophrenia is the one of the *hyperdopaminergic hypothesis*. This is supported by the fact that dopamine D2 receptor antagonists are able to provide anti-psychotic effects [153, 154]. D2 dopamine receptor antagonists are one of the most common antipsychotic drug type used to treat schizophrenia. On the other hand, this type of treatment are not effective on negative symptoms or cognitive deficits [155], which has been one of the reasons to focus research attention on the *NMDA hypofunction paradigm*.

[10] Parvalbumin, commonly known as PV, is a protein that modulates neuronal firing properties [158] and neuronal plasticity in inhibitory neurons [159]. It is used as criterion to categorize inhibitory neurons [25].

The reduction of GAD67 in schizophrenic patients have been shown to be principally pronounced in a particular type of inhibitory neurons, the PV-positive neurons [168], which receive an important amount of glutamatergic drive from NMDA channels [157]. In agreement, genetic ablation of NMDA receptors in PV-positive interneurons in rodents mimics important phenotypical (reduction of GAD67 [169], increase of neuronal excitability [169] and increase of spontaneous Gamma power [170, 171, 172]) and behavioral features of schizophrenia [173]. These observations support the idea that the hypofunction of NMDA receptors in PV-positive interneurons are specially important in this illness[11].

An important question, which is still under debate, is whether the alterations observed in Gabaergic neurons are the consequence or the cause of the modifications in the NMDA neurotransmitter system.

NMDA receptor antagonists in sub-anesthetics doses generate increase in neural activity and increase Gamma power

As stated in previous sections, NMDA receptors mediate excitatory synaptic transmission. Hence, it is intuitively expected that when applying NMDAR antagonists neural activity be decreased. In agreement, NMDA receptor antagonists, such as Ketamine, have been extensively used as anesthetics [176]. However, several preparations with sub-anesthetics doses of NMDAR antagonists produce neural excitation [177, 178, 179, 180, 181, 182]. Several explanations have been proposed to explain this apparent paradox [144]. The interpretation we adopt in this thesis, which is supported by experimental observations [15, 183, 162, 184], is that NMDAR antagonists in sub-anesthetics doses act preferentially on inhibitory neurons, therefore increasing network activity indirectly by means of desinhibition[12]. For example, the work reported in [15] showed, on medial prefrontal-cortex of freely moving rats injected with an NMDAR antagonist dizocilpine maleate (MK801), that approximately 69% of inhibitory FS neurons decreased their firing, while 86% of excitatory RS neurons increased their firing after MK801 injection, leading to a global excitatory effect.

Besides of producing neural excitation, Ketamine in sub-anesthetic doses has been associated to the increase of self-generated and evoked Gamma oscillations. Works in human healthy subjects, under sub-anesthetic doses of Ketamine, reported an increase of induced Gamma amplitude during sensory tasks in primary motor and visual cortices

[11] Some works reported conflicting results and have questioned the hypothesis that PV-positive Fast Spiking neurons play a role in Schizophrenia [174, 175]. Furthermore NMDA receptors are expressed in both GABAergic and glutamatergic neurons, and it still remains unclear in which types of cells the NMDA receptor hypofunction cause schizophrenia [175, 144].

[12] One *in vitro* study has reported conflicting results [174].

[185] and an increase of evoked Gamma amplitude in auditory cortex, during steady-state response [186] and in a paired-click paradigm [187]. In agreement, same results were reproduced in animals *in vivo*. In rat neocortex, sub-anesthetic doses of Ketamine increase Gamma power of spontaneous generated Gamma oscillations during free movement [188, 189, 190, 191] and were accompanied by a marked increase in locomotion, hyperactivity, and ataxic behavior. Additionally, experiments in monkey with similar doses of Ketamine also reported robustly induced spontaneous Gamma in primary motor cortex [192].

Gamma Oscillations in Schizophrenic Patients

Power and temporal correlations of neural oscillations during the resting state have been demonstrated in studies with healthy twins to be highly heritable [193]. Following this observation, dysfunctional neural oscillations could represent an *endophenotype* of certain mental illness, guiding the search for its genetic contributions. Regarding schizophrenia, important evidence for the relationship between anomalous neural oscillations and genetic predisposition have been reported [194, 195, 196, 197]. Different abnormalities in Gamma oscillations have been observed in schizophrenic patients, both in sensory-driven (evoked oscillations) and in self-generated oscillations (spontaneous or induced) [198, 199].

Several works have reported evoked Gamma oscillation in schizophrenic patients presenting reduced amplitude and reduced phase synchronization with respect to healthy subjects during cognitive tasks. These studies include observations either during complex tasks, such as during mental arithmetic calculations [200], or simple ones in which Gamma band activity responses are measured due to auditory stimuli (*steady-state evoked potentials* [201, 202, 203, 204, 205, 206, 207] or auditory oddball paradigm [208]), due to visual stimuli (stimulus-locked evoked oscillation) [209, 210], or due to Transcranial Magnetic Stimulation (TMS) [211]. On the other hand, in protocols measuring spontaneous (not evoked) Gamma, several studies have found an increased power in Gamma band [212, 213, 214, 215, 199].

However, contrasting findings reporting an increase of evoked Gamma activity and a decrease in spontaneous activity in schizophrenic patients also exist. Increases of Gamma activity were reported in response to stimulus during both complex and simple tasks, involving working memory [216] for example, or the auditory oddball selective attention task [217]. While a decrease in spontaneous Gamma activity have been reported during some cognitive tasks (not stimulus locked) [218, 219] or during resting conditions (when the subject in not engaged in any cognitive task) [220]. In addition, other works have reported no significant changes between schizophrenic patients and healthy subjects during resting conditions [221, 214]. Similar discrepancies were detailed in [222, 223].

It has been proposed that part of these incompatibilities with respect of evoked Gamma oscillations could be explained by technical reasons. Indeed, several studies [224, 209, 225,

205, 209, 226] analyzed changes on the power of evoked Gammma activity relative to a pre-stimulus baseline rather than relative to the absolute level of Gamma power. However, differences in baseline levels influence directly the calculation of post-stimulus responses. For example, the study [217], showed that the absolute magnitude of Gamma synchrony was enhanced when the reference to this baseline period was removed.

While part of the discrepancies in evoked Gamma could be explained by the observed increase of Gamma activity on stimulus base-line, the discrepant results with respect to spontaneous Gamma activity could be in part related to the stage of the schizophrenic disease of the patients used in each study. Since it has been recently shown that the resting-state Gamma band activity is significantly different in each of the stages of schizophrenia disease [227].

This recently study [227] observed, for example, a widespread decreased of resting-state Gamma activity in frontal, temporal and sensorimotor areas in chronic schizophrenic patients. On the other hand, in first-episode patients[13], an increased activity was observed on the occipital cortex (significant in the band 30-46 Hz, and strong in the band 64-90 Hz), while an activity decrease was only detected on the occipital cortex (significant in the band 30-46 Hz, and moderate in the band 64-90 Hz). This increase of Gamma activity in first-episode schizophrenic patients have also been detect in early works [217], which showed, for example, an increased Gamma activity in first-episode patients in both resting state and under an attention task. Several other works indicating this phenomena have been systematically reviewed by Perrottelli and colleagues [223]. With this review, the authors argue that the increase of Gamma activity could be used as a marker of the illness onset, since the Gamma increase in the early phases of schizophrenia is a well established fact.

Gamma oscillations, psychotic states and NMDAR hypofunction

As stated in previous sections, the administration of sub-anesthetic doses of NMDAR antagonists generate a significant increase of Gamma power on neuronal activity and induces several schizophrenia-relevant symptoms, including hallucinations and delusions [214, 228, 188, 191, 189, 190]

The increase of Gamma activity, even though not well established as a robust feature of schizophrenia disease in chronic patients [198], has been frequently observed in patients in early phases of the disease [223]. In addition, it was recently shown [229] that other features of the early phases of schizophrenia (but not chronic phases), such as hyper-

[13]The term *first-episode patients* refers to patients in the early-course schizophrenia disease, who have experienced only one or few psychotic episodes.

connectivity, could be reproduced by the administration of an NMDAR antagonist [14]. Other evidences in favor of the hypofunction of NMDA receptors as one of the elements related to schizophrenia can be found in the review [144].

In parallel, it has been shown [230] that first-episode patients presented 9.3% higher scores than chronic patients on the *Positive And Negative Syndrome Scale* (PANSS) and 16.3% lower on the negative symptom scale. Concurrently, Gamma-band responses in schizophrenic patients often correlate with positive psychotic symptoms, with higher gamma-band activity corresponding to increased symptom load [225, 205, 209, 226].

On the other hand, despite of these independent observations, the role of the increase of Gamma activity on the occurrence of psychotic states in schizophrenic patients is largely controversial. In **Work 3**, we use network models endowed with NMDA synaptic conductances to mimic schizophrenic states in which the hypo-function of NMDA synapses generate an increase of excitation (due to inhibitory desinhibition) and an increase of the Gamma power generated by the global network activity. In **Work 3** we also explore the effect of NMDA hypo-function on the capability of the network to respond to external stimuli, providing, as a consequence, a possible interpretation with respect to the type of neuronal information processing occurring during hallucinations and/or delusions occurring during psychotic states.

[14] In the referred work [229], a robust hyper-connectivity of the prefrontal cortex was observed in healthy volunteers administered with sub-anesthetic doses of ketamine, similarly to the one observed in patients in early schizophrenic stages. Interestingly this hyper-connectivity was not observed in chronic patients [229].

Computational Models

Historical Perspective

Individual neuron models

The mathematical study of neural activity dates the earliest eighteen century, when Louis Lapicque, in 1907, published a paper on the excitability of nerve cells. Lapicque modeled neurons by means of an analogy to electrical circuits, describing the neuronal membrane as a circuit consisting of a parallel capacitor and a resistor. Lapique's insights about the fundamental relationship between the membrane parameters and its excitability gave rise only decades later (1960s) to the simplified model known today as the Leaky Integrate-and-Fire (LIF) [231].

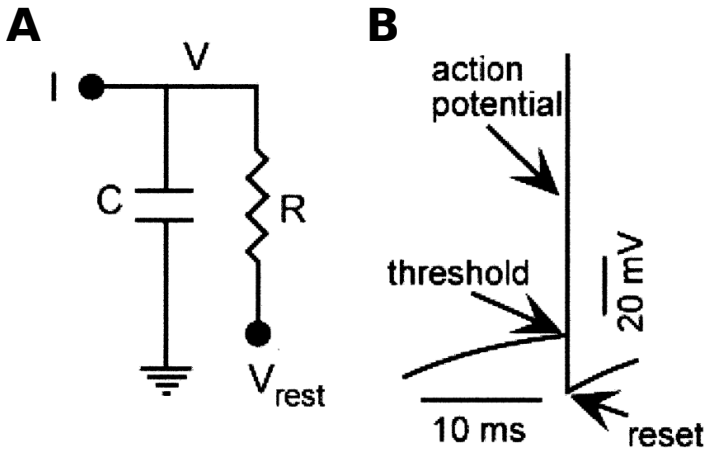

Figure 9: **The neuron as a RC circuit**. A) Equivalent circuit in which the neuronal membrane is seen as capacitor C, coupled in parallel with a resistor R. V is the membrane potential, V_{rest} is the resting membrane potential and I indicates an injected current. B) Scheme representing the voltage trajectory of the integrate-and-fire model imagined by Lapique, indicating that when V reaches a threshold value, an action potential is generated and V is reset to a subthreshold value. Figure adapted from [232].

In 1943, Warren McCulloch and Walter Pitts developed an even more simplified model, *the formal neuron* [233], in which neurons would be either active or inactive, presenting as outputs 0 or 1. This type of model allowed the construction of neural networks which could be simulated computationally with the technology available at the time and gave important insights on the study of associative memory [234]. Subsequently, in 1952, Alan Lloyd Hodgkin and Andrew Fielding Huxley explained and described mathematically for

the first time the ionic mechanisms underlying the initiation and propagation of action potentials in the squid giant axon, receiving for this work the Nobel Prize in Physiology or Medicine in 1963.

Today this model is known as the Hodgkin-Huxley model (HH) [235] and a huge diversity of variations of it is available: from extended versions, describing neurons with several compartments (spines, dendrites, soma, axon segments) [236, 237] to simplified versions, such as the Adaptive Exponential Integrate-and-Fire (AdEx) [238]. In addition, several other models have been developed though-out the decades, the most importants being the FitzHugh–Nagumo Model, [239], the Hindmarsh–Rose Model, [240], the Izhikevich Model [241] and the Quadratic Integrate-and-Fire (QIF) [242]. See the reviews [243, 244, 237].

The network models developed in this thesis used the AdEx model to describe their units. In this model, neurons are described by their membrane potential, that thanks to a supplementary equation, is capable of displaying *spike-frequency adaptation*[15]. Furthermore, neurons in the AdEx model are *point neurons*, that is, their membrane potential is assumed to be homogeneous in the whole cell body, which is the same as assuming that the neuron have no structure: no axon and no dendrites, only a punctual soma. More details about this model are described in the methods section of **Work 2** and **Work 3**.

Network models and Oscillations

Yoshiki Kuramoto started a general theory to treat chemical and biological systems whose elements behave as oscillators [247]. This theory has been proven to be useful in several domains of knowledge, including neuroscience [248]. Nancy Kopell, Bard Ermentrout and collaborators were some of the pioneers to apply Kuramoto's ideas on the field. This branch of theoretical neuroscience got known as the *Coupled Oscillators Theory*, in which neurons are depicted as intrinsically rhythmic units that spike regularly and are coupled by weak synaptic connections [16].

Great amount of our understanding on neural oscillations have been given by the *Coupled Oscillators Theory*, which allowed the investigation of the effect of noise, couplings, and delays on the synchrony and regularity of network dynamics [252, 253, 135, 254, 255,

[15] *Spike-frequency adaptation* is the name given for a phenomenon in which neurons, when stimulated with a step current, display a gradual decrease of their firing frequency (after an initial increase). This phenomena is caused by several biophysical mechanisms, which are reviewed in [245, 246].

[16] Couple Oscillators Theory is a general term assembling different types of description: from simplified models, in which neurons are described by its *Phase Response Curve* (PRC) [249, 250, 251], to more detailed models, in which the ideas from the PRC approach are extended, keeping the assumption of weak synaptic disorder and weak noise. In these more detailed models, neurons fire synchronously with the same firing rate as the network, acting as oscillators [252, 253, 135, 254, 255, 256, 257, 258, 247, 259, 260]. The *Phase Response Curve* (PRC) is a function that describes neuronal phase, characterizing the way a neuron shifts its spike times with respect to the timing of depolarizing currents [249, 250, 251]. Neuronal phase is defined based on neuronal spikes: the phase oscillates between 0 to 2π, being the spike time usually associated to the phase zero. PRC of individual neurons can be coupled and used to build network models [261, 262, 263]

256, 257, 258, 259, 260] and gave important qualitative predictions about the mechanisms of oscillation generation for different neuron types [242, 257, 252, 64]. However, the conditions under which neurons can be considered as coupled oscillators, e.g weak synapses and weak noise, are frequently not fulfilled [264, 70, 265]. Furthermore, the assumed spiking regularity of individual neurons during global oscillatory activity is typically not observed, since, as stated earlier, in general even when coherent oscillations are detected in extracellular recordings *in vivo*, neurons present a stochastic and sparse pattern of firing [68, 75, 121, 81, 122, 87, 69, 38, 123, 124].

Nicolas Brunel and collaborators developed models able of capturing both phenomena: fast network oscillations combined with irregular neuron firing. These models assume fast synapses with strong synaptic weights and synaptic delays [266, 110, 111, 112, 267]. This type of description allows neurons to spike with firing rates much smaller than the network oscillation frequency, in a stochastic way, similarly to what it is observed *in vivo*. This type of dynamical regime is known as the *firing rate regime* [111], in contrast to fully synchronized modes, like the ones observed in *coupled oscillators* models, known as the *spike-to-spike regime*.

Another important theoretical approach, in the study of neural oscillations, is the field of the so-called *rate models* (also known as *mean-field models* or *mass models*). This approach describes the collective properties of a large numbers of neurons instead of focusing on individual neural dynamics, by modeling the average firing rate of a particular population of neurons. These models are obtained by means of heuristic arguments [268, 269, 270], not being directly derived from spiking neurons. The first firing rate models were derived under the assumption that individual neurons spike stochastically [271, 272] being able to characterize (stationary) oscillations in the *firing rate regime* [266, 110, 111, 112, 267]. These models were usually characterized by one single variable (the average population firing rate), evolving according to an differential equation described by a time constant τ and a steady-state input-output transfer function (f-I curve). These models, on the other hand, could not describe neuronal activity if a significant portion of the neurons fired synchronously (like in *spike-to-spike regime*). Recent firing rate models [273, 274] have incorporated a second variable (describing the network synaptic activity) being able to model oscillations in both regimes (*spike-to-spike regime* and *firing rate regime*).

In **Work 2**, we developed different network structures generating Gamma oscillations, working in the *firing rate regime*, using Adaptive exponential integrate-and-fire neurons [238]. These models were improved (with the addition of NMDA channels) in **Work 3**.

Gamma oscillations in theoretical models

Even though several experimental protocols have been used to examine the generation mechanisms of Gamma oscillations, a more complete understanding requires the use of

theoretical models [132, 70]. Gamma oscillations have been extensively modeled in the literature with different neuronal models and networks structures [132, 70, 64]. In **Work 2**, three types of Gamma generation mechanisms were explored: the *Interneuron Gamma* (ING), the *Pyramidal-Interneuron Gamma* (PING) and the *Chattering Induced Gamma* (CHING).

In this section, we describe theoretically each of these mechanisms and reference some of the most important theoretical hallmarks of the literature.

ING Model

The ING mechanism can be qualitatively understood as a succession of events: (1) The rhythm starts when a subset of inhibitory neurons discharge together, generating synchronous inhibitory post-synaptic potentials (IPSPs). (2) The neurons who receive these inputs, have their spike times constrained, being able to spike again only when these inhibitory currents decay. (3) These postsynaptic neurons are forced to discharge their next spike closer in time to their pre-synaptic neurons, which will also spike when the global inhibitory input decays. This spike time restriction increases network synchrony progressively, generating the rhythm.

It has been shown theoretically that Gamma oscillations emerge spontaneously in a networks exclusively composed of mutually connected inhibitory neurons if a sufficient external drive is provided [275, 276, 277, 259, 278, 266, 111, 112] and certain conditions are fulfilled. However, these conditions are different depending on the oscillatory regime studied (*firing rate regime* or *spike-to-spike regime*). While in the *spike-to-spike regime* the oscillation frequency strongly depends on synaptic decay time, allowing synchrony to emerge even without any synaptic latency [275, 276, 277, 259], in the *firing rate regime*, synchronization is generated by the presence of a neuronal phase-lag (either due to synaptic delays or due to the time a conductance-based neuron takes to respond to synaptic currents because of its intrinsic properties) and depends weakly on synaptic decay times [111, 112]. In addition, the frequency of Gamma oscillations generated by the ING mechanism is also differently determined in these two regimes. In the *spike-to-spike regime* the oscillation frequency is mainly determined by the inhibitory synaptic decay time [276, 277], while in the *firing rate regime* it depends much more on the fastest time scales, like latency and the rise times, than on the synaptic decay times.

PING Model

The PING model, based on the reciprocal interaction between pyramidal neurons and interneurons, is the earliest proposed model to explain Gamma oscillations [271, 279, 280, 281, 111, 112]. This mechanism can be understood qualitatively as a succession of cycles of picks of excitation and inhibition that alternate. In these cycles, excitatory neurons

recruit inhibitory neurons that in turn reduce network activity. The new cycle starts when inhibition decays.

PING models can also describe Gamma oscillations in both *spike-to-spike regime* and *firing rate regime*. Furthermore, the parameters defining the oscillation frequency in each of these conditions are similar. In both regimes, the oscillation frequency depends strongly on excitatory and inhibitory synaptic time decays [282, 111].

The phase relationship between excitation and inhibition is an important aspect to be discussed, since it has been suggested to be a marker of the type of Gamma generation mechanism [140]. In theoretical models of PING mechanism, excitatory neurons can spike both before and after inhibitory neurons [283, 284, 112] during Gamma oscillations.

It has been shown theoretically by [112] that in the *firing rate regime*, in models composed of conductance based neurons (neurons that include non-linear spike generation mechanisms in their equations), the spiking order of excitatory and inhibitory populations depends exclusively on single-cell characteristics. When the I_{AMPA}/I_{GABA} ratio is the same in excitatory and inhibitory neurons, excitatory cells tend to follow the inhibitory ones in most of the physiologically plausible parameter space. On the other hand, when the ratio of excitation to inhibition is weaker in excitatory cells than in inhibitory ones, excitatory cells tend to precede inhibitory neurons [111, 112]. Furthermore, [283, 284] have studied neuron phase differences during ING and PING (on the *spike-to-spike regime*) and the conditions in which each mechanism take place when both of them are allowed by the network structure. These works have indicated, in addition, in which conditions during *spike-to-spike* Gamma oscillations inhibitory neurons proceed excitatory ones when the PING mechanism take place.

CHING Model

Chattering cells, also known as Fast Rhythmic Bursting (FRB) cells, were proposed decades ago to be Gamma generators in cortical networks due to certain experimental observations [66, 27, 118]. Nonetheless very few computational models, in our knowledge, were proposed to study the emergence of Gamma oscillations due to the presence of this type of neurons.

By means of multi-compartment neurons and voltage-dependent currents described by the Hodgkin-Huxley formalism, the study of [285] showed that Chattering cells have an important role in recruiting feedback inhibition through their pacemaker rhythmic spiking. They observed that this role is not only due to the increase of firing rate, but specifically due to their bursting firing pattern. The work of [285] argues that Chattering cells would be important on Gamma generation in brain regions in which the synaptic transmission to interneurons is not highly reliable. In agreement, experimental studies have shown that Chattering cells work as amplifiers of Gamma activity due to their

intrinsic suprathreshold properties and to their profuse axonal projections to other chattering cells and to other neurons on the network [27, 118, 133, 286]. In addition, other computational multi-compartment models have shown the importance of the connection via axonal gap junctions of Chattering cells with other pyramidal cells in the generation of Gamma oscillations [133, 287].

In this thesis we developed a single compartment model of Adaptive exponential integrate-and-fire neurons composed of Chattering cells, Regular spiking cells, Fast Spiking cells, in which Gamma oscillations are generated exclusively thanks to presence of Chattering Cells. We coined the term *Chattering Induced Gamma* (CHING) to refer to Gamma oscillations generated thanks to the presence of these pacemaker excitatory cells. This model is discussed in **Work 2**.

Human Recordings Analysis

The data used in this thesis to constrain our models, both during Gamma and AI states, has been already published in other works [288, 47] and was donated by one of our collaborators, Sydney S. Cash (Department of Neurology, Massachusetts General Hospital and Harvard Medical School, Boston).

In this thesis, we extend these prior analysis, focusing on awake states. The data was acquired extracellularly in patients suffering of intractable epilepsy, who had had multi-electrode arrays implanted during therapeutic procedures. The arrays registered simultaneously local field potentials (LFP) and single-unit activity. We considered the data of one patient for which the recording was very stable, and in which several periods of wakefulness could be analyzed. Figure 10A indicates the structure of the recording, in which several brain states during the night could be observed: slow wave sleep (SWS), light sleep, REM sleep and awake periods. Only long and consecutive periods of wakefulness, containing several seconds of Gamma bursts, were considered (Segments 1, 2, 3, 4 and 5 indicated in 10A).

Eighty one electrodes were implanted on the temporal cortex of this patient (layer 2/3) and 91 neurons could be identified (some neurons were recorded by the same electrode). These neurons have been already previously [288, 47] classified as Regular Spiking Cell (RS), putative excitatory, and Fast Spiking Cells (FS), putative inhibitory. From the 91 neurons, 23 were recognized as FS and 68 were recognized as RS. This classification was performed by means of clustering based on the spike shape and functional interactions (determined using cross-correlograms) [289, 288].

In each data part, periods of Gamma oscillations (Gamma bursts) were identified and neural activity was characterized with respect to the Gamma cycles. The duration of these data parts are indicated in Figure 10B, together with the total amount of Gamma periods identified inside of each of them. The identification of Gamma bursts was done separately for each electrode. We considered as Gamma bursts periods in which the amplitude of Hilbert Transform envelope (absolute value) differed from the mean, by at least 2 standard deviations, for a minimum duration of 3 Gamma cycles (See Figure 10C). These criteria were not enough to identify all Gamma bursts (some Gamma bursts were ignored). On the other hand, no false positives were included in the analysis. All the Gamma bursts automatically identified by the algorithm were individually confirmed visually. The oscillation phase was acquired using the angle of the imaginary part of the Hilbert Transform (See Figure 10C).

Individual neuron spike times were analyzed with respect to Gamma periods, both in

regard to their spiking phase and to their spiking frequency inside and outside Gamma bursts. To identify neurons that were particularly phase-locked to Gamma oscillations, we constructed individual phase distributions, which were tested for circular uniformity using a Bonferroni-corrected Rayleigh test [61, 290]. A neuron was considered phase-locked if we could reject circular uniformity at $P < 0.01$ ($Z > Z_c$). Figure 11 depicts in A and B, two examples of distributions of phase-locked neurons.

To identify firing rate changes inside Gamma bursts, the average firing rates inside (f_γ) and outside (f_{out}) of Gamma bursts were computed for each neuron. A neuron was considered to increase its firing significantly if the observed average number of spikes inside Gamma bursts was higher than the *percent point function* of a 95% interval of confidence of a Poissonian distribution with average firing rate f_{out}. Cells which had firing rates smaller than 0.1 Hz or cells whose electrode measured less than 1 second of Gamma bursts, in the respective data segment, were classified as *inconclusive*. Figure 12 indicates an example of this procedure.

The results of this experimental data analysis, which inquired the relationship between individual neuron activity and Gamma rhythms measured on LFP, are characterized in **Work 2**. This study showed, by means of this analysis, that the participation of individual cells of Gamma oscillations is very sparse. During Gamma bursts, only a small percentage of the recorded neurons have been identified to be phase-locked to the rhythm and only some cells increased their firing. Furthermore, throughout the night (different data segments), neurons changed of behavior. That is, neurons that were previously changing their firing during Gamma bursts kept their firing the same and/or neurons that were previously identified to be phase-locked were not phase-locked in other periods of time. In addition, this analysis showed that FS cells presented significant higher level of phase-locking and firing rate increase in comparison to RS cells. Likewise, FS cells changed its behavior less than RS cells. Figure 13 indicates that this neuronal behavior changes across the five data segments used on our analysis. The models described in **Work 2** were capable of displaying most of these features.

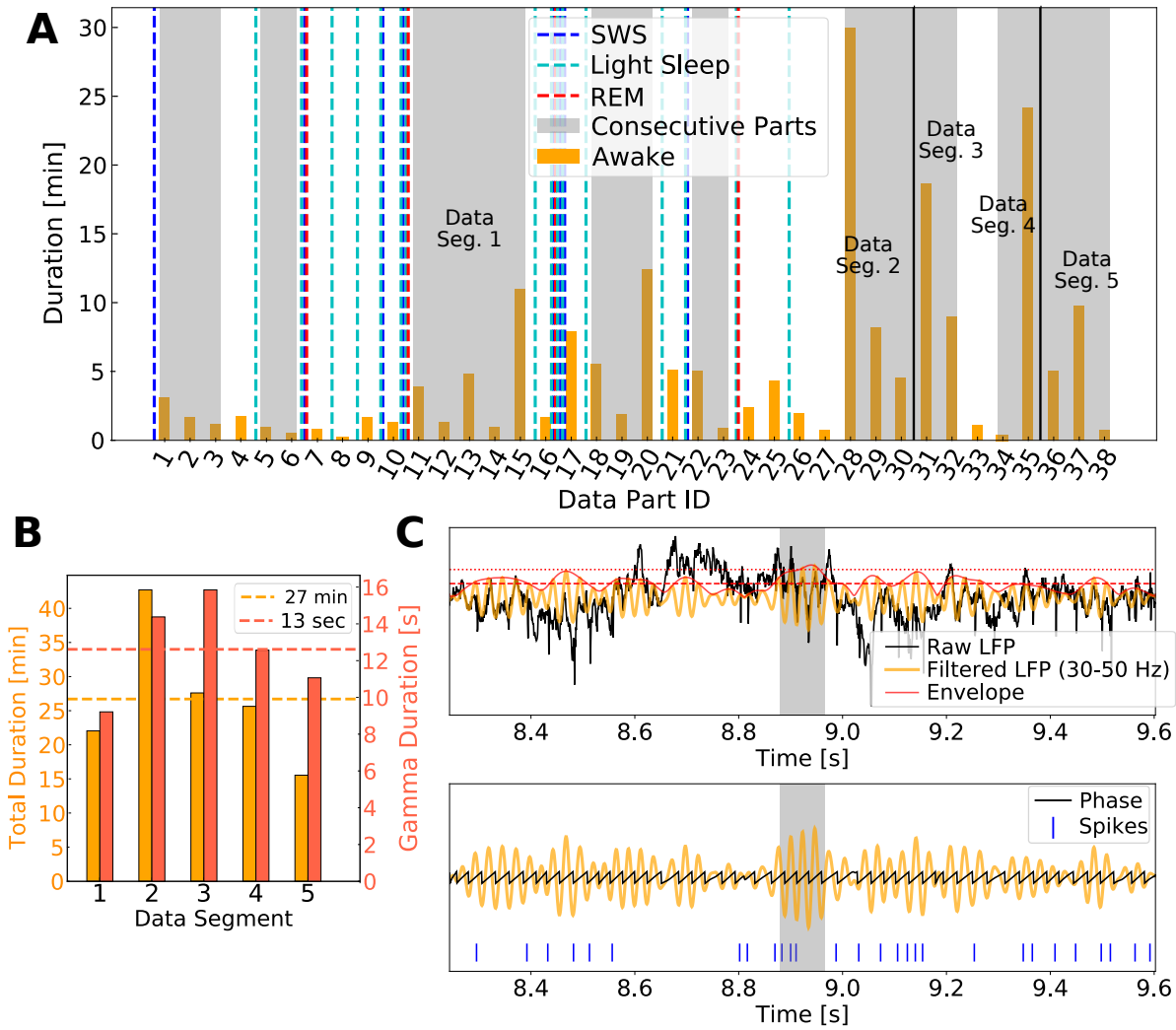

Figure 10: **Human electrophysiological data**. A) Structure of the recordings of one patient during the night. Thirty eight periods of wakefulness (whose duration are indicated) could be recorded. These periods were interspersed with sleep states (SWS, light sleep and REM), represented by colored lines, without the indication of their duration. In our analysis, only long and consecutive periods of wakefulness were considered: Segments 1, 2, 3, 4 and 5. B) Total duration of each of the 5 data parts selected for the analysis and the respective total duration of Gamma bursts inside of each of them. Averages are indicated by the dashed lines. C) Upper graph: Gamma periods detection. Raw LFP (black), band-pass filtered LFP (yellow) and Hilbert Transform Envelope (red) are shown. Gamma bursts were detected by means of the deviation from the average of the Hilbert Transform envelope (dashed red line) of at least 2 SDs (dotted red line), with a minimum duration of 3 Gamma cycles. The gray shaded region indicates one example of identified Gamma burst. Lower graph: Oscillation Phase extraction. The oscillation phase were obtained by the angle of the imaginary part of the Hilbert Transform. Phase distributions per neuron were computed based on the oscillation phases where each neuron spiked.

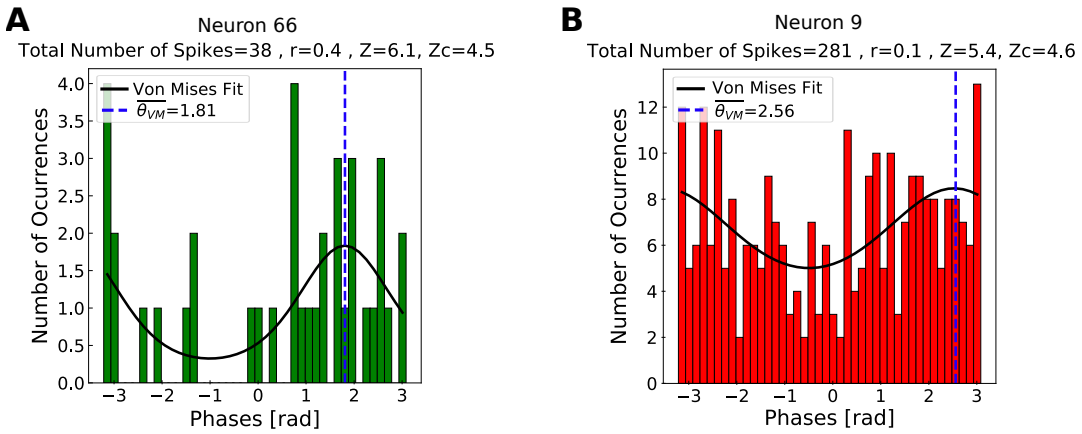

Figure 11: **Phase-locking statistical test**. Phase distribution of two randomly picked cells from the human recordings during *Data segment 1*: one excitatory (A) and one inhibitory (B). The phase distribution of each cell was fitted to a Von Mises curve, which allowed the estimation of its preferred phase $\overline{\theta_{VM}}$. The phase distribution of each neuron was tested for circular uniformity using a Bonferroni-corrected Rayleigh test [61, 290]. A neuron was considered phase-locked if the circular uniformity at $P < 0.01$, ($Z > Z_c$) could be rejected.

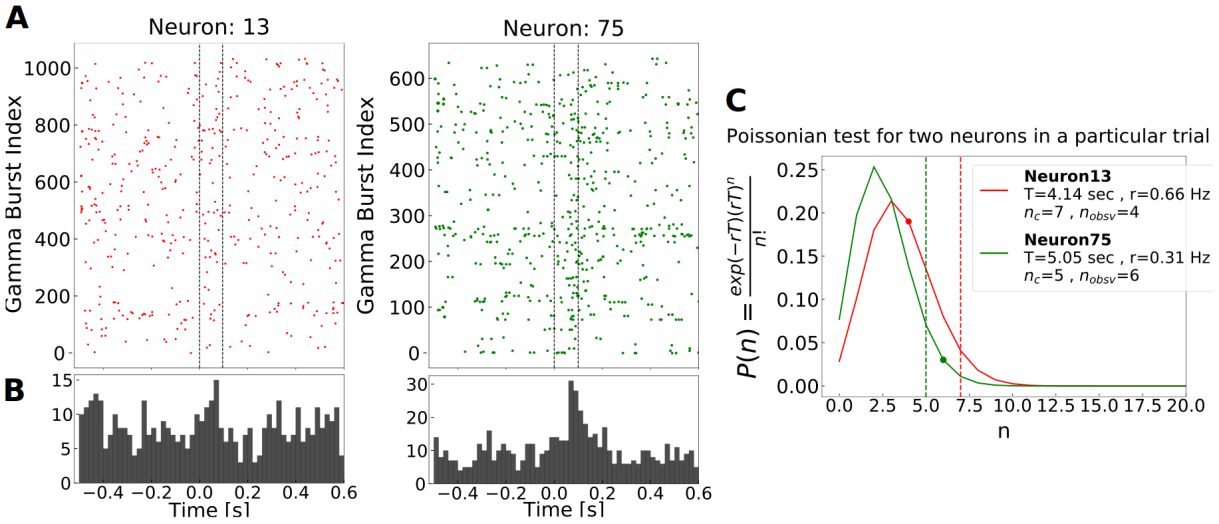

Figure 12: **Firing rate change statistical test**. A: Activity of two randomly picked cells during several Gamma bursts: neuron 13 (inhibitory, left) and neuron 75 (excitatory, right). The graphs display the firing patter around Gamma bursts (indicated by the black doted lines). Each point corresponds to one spike in the correspondent tuple of time and burst ID (y-axis). B: Histogram computing the distributions of all spikes inside all Gamma bursts of neuron 13 (left) and neuron 75 (right). C: Exemplification of firing rate change statistical test. The Poissonian distribution of these two neurons is constructed based on their average firing rate calculated outside of Gamma bursts. The critical number of spikes n_c, indicated by the dotted lines, is calculated based on the *percent point function* of the respective Poissonian Distribution for a period T, with an 95% interval of confidence. The observed number of spikes n_{obsv} is depict as a dot over the curve. According to this procedure, only neuron 75 is considered to increase its firing, since $n_{obsv} > n_c$.

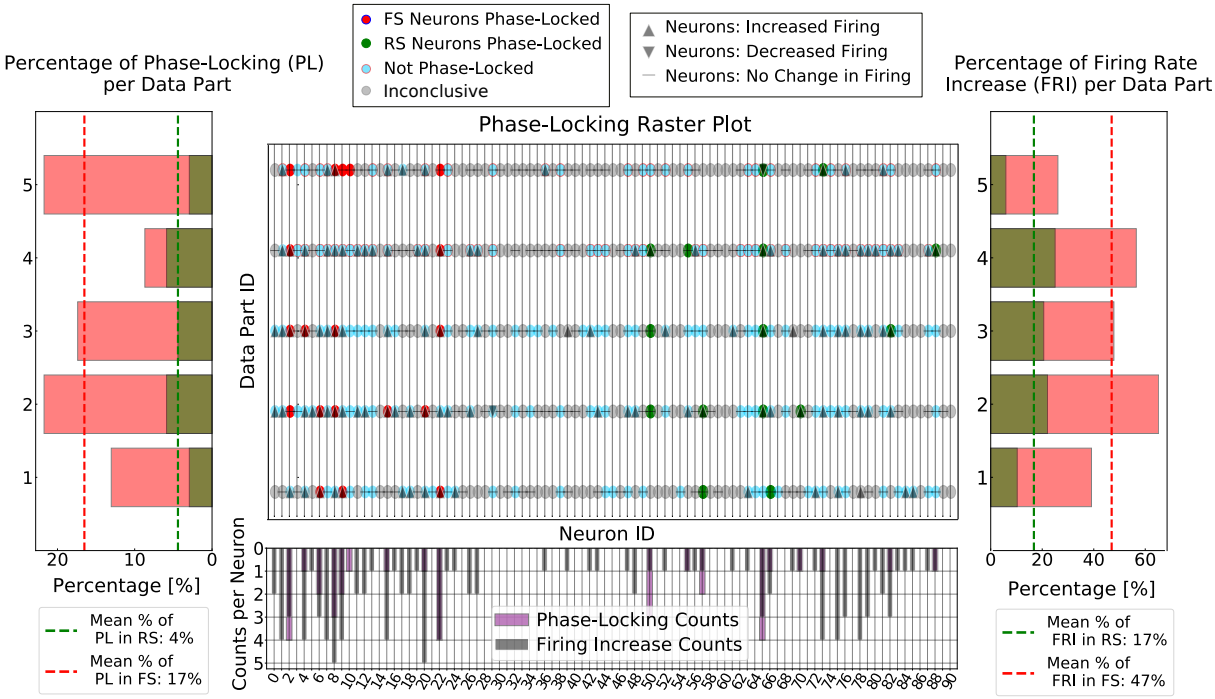

Figure 13: **Change of *Cell Behavior* across time during Gamma in experimental data**. Middle panel represents each cell by a circle in each of the 5 data segments. FS and RS phase-locked cells are depicted respectively as red and green circles, while not phase-locked or inconclusive cells (with respect to phase locked) of both types are depicted as blue and gray circles respectively. Superposed to each cell circle, pointing up and down triangles were added to indicate if the cell increased ($\triangle$) or decreased ($\triangledown$) its firing. If the cell didn't change its firing significantly a minus sign (-) was added. Side box plots indicate, on the left, the percentage of phase-locked FS (red) and RS (green) cells in each of the 5 data segments, and, on the right, the percentage of firing rate increase. Dotted lines indicate the average value between the 5 data segments (phase-locking level: left and firing rate increase: right). The box plot at the bottom depicts the superposed counts of phase-locking and firing rate increase behavior of each individual cell, computed in the 5 data segments.

Developed Models

The models developed in this thesis had their parameters constrained by electrophysiological data acquired in human as described in the previous chapter. We exploit different network structures to investigate three well-known mechanisms of Gamma generation [138, 132, 139, 140, 27, 133]: either by the exclusive interaction between inhibitory neurons [*Interneuron Gamma* (ING)] or by the interaction of inhibitory and excitatory neurons via *Pyramidal-Interneuron Gamma* (PING) or via *Chattering Induced Gamma* (CHING). While networks with a structure similar to the *PING Network* have been largely used in the literature, the structures of *ING* and *CHING Networks* were developed exclusively in this thesis.

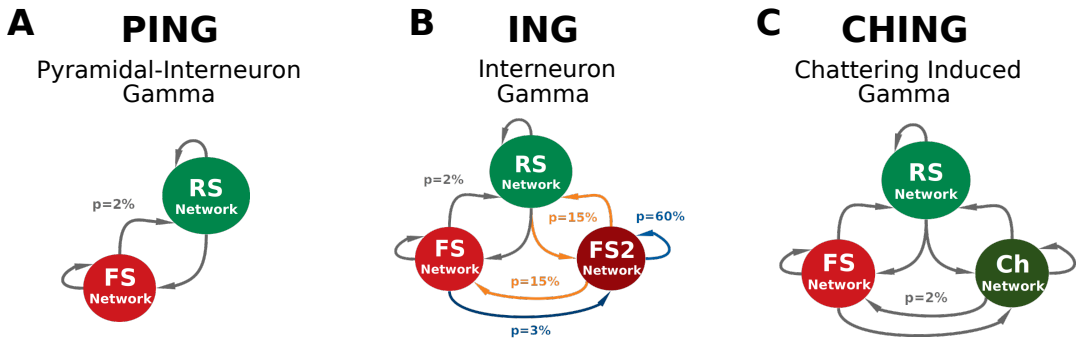

Figure 14: **Network structures of the three developed models**.

Each of the three developed networks used the *Adaptive Exponential Integrate-And-Fire Model* (Adex) [238] for its neural units, and were composed of different types of cells: Regular Spiking Cells (RS), Chattering Cells (Ch) and Fast Spiking Cells (FS). Network structures and individual cell parameters are described in detail in **Work 2**.

Parameter search

An extensive parameter search was performed to identify network and neuronal parameter sets which could, in each model, reproduce experimental features. Physiologically plausible distributions of firing rates, of membrane conductance and of inter-spike intervals were used to constrain these models, the same way as the level of phase-locking and firing rate changes during Gamma oscillations extracted from our data analysis.

Parameter search in PING Network

For PING network, a parameter search with respect to the synaptic decays was performed. Parameters were chosen in such a way that oscillations in the Gamma band would be present in a network composed of neurons with neuronal parameters chosen in accordance with previous publications [291, 292]. Figure 15 indicates this parameter search.

Parameter search in ING Network

The ING network is composed by the mixture of two networks: one being composed by RS and FS neurons (which can not generate oscillations due to the choice of synaptic conductances, τ_e=τ_i= 5 ms, like it is shown on Figure 15D), and one network being composed by FS neurons that are highly connected (FS2 neurons[17]). This network of highly connected FS neurons can generate Gamma oscillations by its own, thanks to its dense connections, like it is shown in Figure 16.

For the ING network, a parameter search was performed to identify which interaction between each population (RS, FS and FS2 neurons) could allow the model to reproduce experimental features. Among these experimental features are the level of phase-locking and the level of firing rate changes during Gamma oscillations, extracted from our data analysis. Because this parameter search was highly multidimensional, it could not be performed as systematically as the previous ones depicted in Figures 15 and 16. For this reason, we present a scheme indicating the qualitative conclusions from this parameter search, which justify the choice of probabilities of connections between each neuronal population, used in this model (Figure 17).

Parameter search in CHING Network

The CHING network is exactly the same network displayed in Figure 15D (with synaptic conductances: τ_e=τ_i= 5 ms), with the difference that 5% of its RS neurons were replaced by Chattering cells. For this reason, the rhythms it presents are exclusively generated by the Chattering activity. Consequently, the parameter search performed in this model was entirely focused on the choice of the intrinsic cellular parameters of this neuronal type. Again, since this parameter search was highly multidimensional, it could not be performed in a systematical way. Several parameter combinations were tested taking into account the following criteria: 1) cells should keep their chattering properties, 2) the oscillation should be on Gamma band, 3) the oscillation should be on the *firings rate regime*, with sparse and irregular firing, 4) cells should present physiologically plausible distributions of firing rates, of membrane conductance and of inter-spike intervals, 5) cells should present

[17]We decided to rename this population as FS2, to stress the different pattern of connectivity between this group of highly connected FS neurons, from the other FS neurons in the network.

levels of phase-locking and firing rate changes during Gamma oscillations similar as the one extracted from our data analysis.

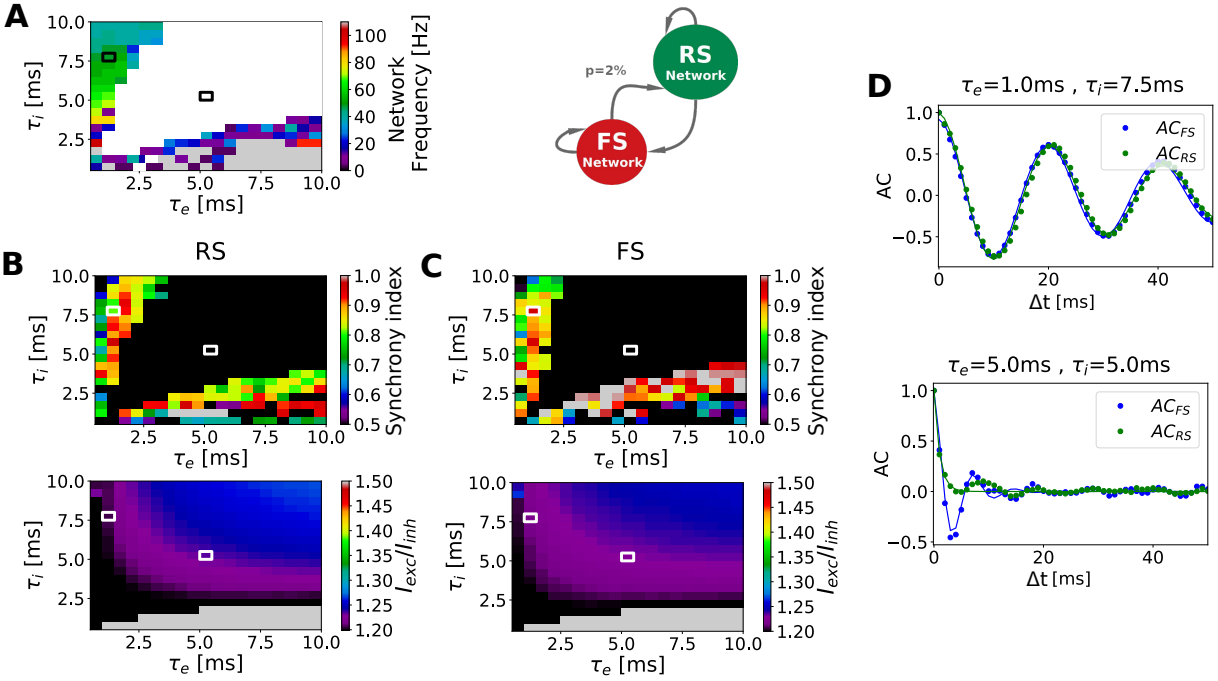

Figure 15: **Synaptic time scale parameter search of a network composed of RS and FS neurons randomly connected**. The network used to produce this figure was composed of 20000 excitatory Regular Spiking and 5000 inhibitory Fast Spiking neurons connected randomly with a probability of connection of 2%. All synapses were delayed by a time delay of 1.5 ms, and had reference synaptic strengths of Q_e^R= 1 nS or Q_i^R= 5 nS and reference synaptic time scales of τ_e^R=τ_i^R= 5 ms. Synaptic strengths ($Q_{e,i}$) were normalized at each tested time scale ($\tau_{e,i}$) to keep the same synaptic gain, such that: $Q_{e,i} = (Q_{e,i}^R.\tau_{e,i}^R)/\tau_{e,i}$. A) Network oscillation frequency depicted in a color scheme as a function of excitatory and inhibitory synaptic time scales. White color corresponds to regions in which no oscillation was identified in RS population. B) Synchrony Index of RS population (top) and network balance (bottom) as a function of synaptic time scales. The Synchrony Index (SI) is based on the auto-correlation of the population frequency of RS cells. To be calculated, the autocorrelation of the population frequency was fitted by a damped cosine function and the value of this fitted function at zero time lag was defined as the SI. If the exponential decay rate was higher than 100, it was considered that there was no global oscillation at the population scale. The network balance was defined as the rate between the average excitatory and inhibitory synaptic currents, $\left\langle \frac{\langle I_{exc}\rangle_N}{\langle I_{inh}\rangle_N} \right\rangle_t$, in which $\langle\rangle_N$ stand for average among neurons and $\langle\rangle_t$ average on time. White squares indicate the two different parameter sets used in our simulations (τ_e=τ_i= 5 ms for *AI Network*, and τ_e=1 ms , τ_i= 7.5 ms for *PING Network*, as decribed in **Work 2**). C) Same as B but calculated for the FS population. D) Population frequency autocorrelation of RS (green dots) and FS population (blue dots) neurons of the two used parameter sets. Solid lines indicate the damped cosine fitted function.

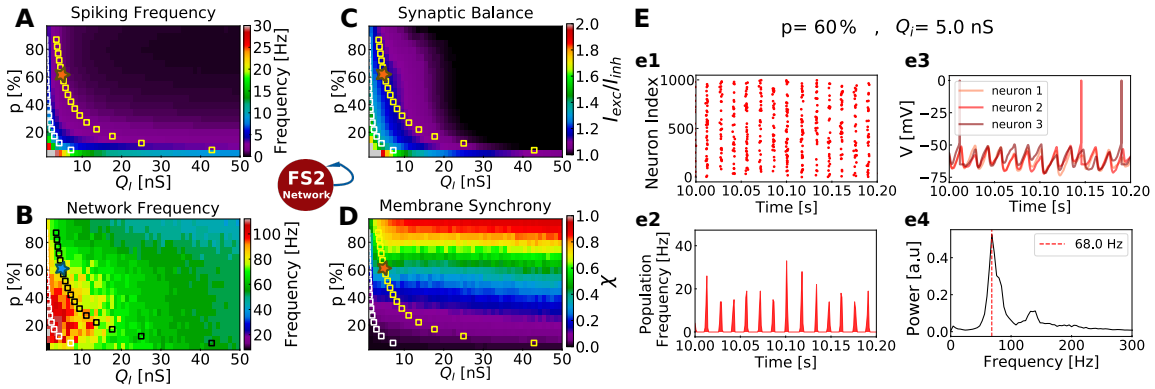

Figure 16: ***Gamma Network* parameter search**. The network connectivity (p) vs. inhibitory synaptic strengths (Q_i) parameter space of the Gamma Network are displayed as color-plots. A) Average spiking frequency. B) Network oscillation frequency. C) Network balance: rate between the average excitatory and inhibitory synaptic currents, $\left\langle \frac{\langle I_{exc} \rangle_N}{\langle I_{Inh} \rangle_N} \right\rangle_t$, in which $\langle\rangle_N$ stand for average among neurons and $\langle\rangle_t$ stand for average on time. D) Membrane Potential Synchrony (χ), calculated by means of the equation: $\chi^2 = \frac{\sigma_V^2}{\frac{1}{N}\Sigma_i^N \sigma_{V_i}^2}$, in which $V(t) = \frac{1}{N}\Sigma_i^N V_i(t)$, ${\sigma_V}^2 = \langle [V(t)]^2 \rangle_t - [\langle V(t) \rangle_t]^2$ and ${\sigma_{V_i}}^2 = \langle [V_i(t)]^2 \rangle_t - [\langle V_i(t) \rangle_t]^2$. The set of parameters which allowed the Gamma Network to oscillate in the Gamma range are indicated by a star symbol. The white and yellow curves depict parameter choices in which the product between p and Q_i are the same. The yellow curve indicates all parameters equivalent to a choice of p=60% and Q_i= 5 nS ($Q_i' = 3/p'$), while the white curve indicates all parameters equivalent to a choice of p=10% and Q_i= 5 nS ($Q_i' = 0.5/p'$), like it is usually used in other works [111]. Every point in each graph is given by the average output of 10 simulations of 5 seconds each. In these simulations, each neuron of the *Gamma Network* received 400 independent and identically distributed excitatory Poissonian spike trains with a spiking frequency μ_{Ext}=5 Hz and a synaptic strength of Q_{Ext}= 1 nS (that decayed with synaptic time constant of τ_E=5 ms). E) Network activity for the parameters indicated with a start in A, B, C and D (p=60% and Q_i= 5 nS). The raster plot of the whole network (e1), the population frequency (e2), the membrane potential of 3 randomly chosen neurons (e3) and the power spectrum of the population frequency (e4) are indicated. The population frequency is calculated as the total number of spikes (spikes of the whole network) in a time bin of 1 ms, divided by the duration of this time bin. Because of the exclusive presence of inhibitory neurons and its high level of recurrent inhibition, this network is capable of generating Gamma rhythms with frequencies around 70Hz by means of an ING mechanism.

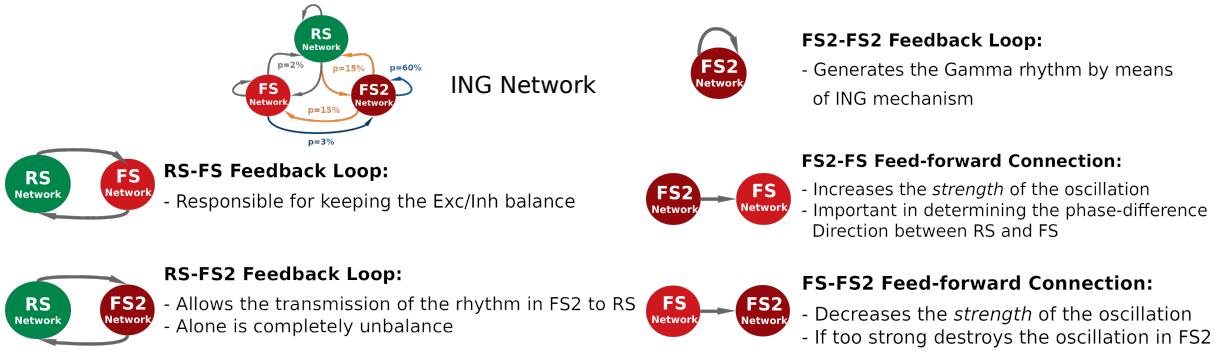

Figure 17: **Qualitative scheme indicating the role of each population interaction on the network dynamics**.

Part II

Research Articles

Cellular correlates of wakefulness and slow-wave sleep: evidence for a key role of inhibition

---

Reference: Susin, Eduarda, and Alain Destexhe. "Cellular correlates of wakefulness and slow-wave sleep: evidence for a key role of inhibition." Current Opinion in Physiology 15 (2020): 68-73.

French Abstract:

Dans cet article, nous avons considéré et discuté certaines études récentes à propos de corrélations cellulaires, dans des états de veille et de sommeil, basés sur des enregistrements d'unités multiples. Ces études concernaient, d'entre autres, une nouvelle forme d'homéostasie observée pendant le sommeil lent profond (SWS de l'anglais), où les cellules les plus actives (haut taux de décharge) ont montré une baisse dans leur taux de décharge pendant le SWS, tandis que, inversement, les cellules les moins actives ont montré une tendance à décharger plus rapidement dans le SWS. Également, autres références ont montré une implication plus forte des neurones inhibiteurs par rapport aux neurones excitateurs lors des oscillations Gamma dans le SWS, et une augmentation des corrélations croisées par paires exclusivement entre les neurones inhibiteurs pendant le SWS. Nous comparons les résultats de ces études (chez des modèles animaux) avec nos analyses effectuées sur des enregistrements chez l'homme. Nous confirmons certaines similitudes dans la dynamique cellulaire observées entre l'état de veille et le SWS, et soulignons les différences qui sont principalement apparentes dans la dynamique et dans les corrélations des neurones inhibiteurs. Ces résultats suggèrent que les réseaux inhibiteurs sont essentiels dans la dynamique du sommeil, et devraient être une cible principale dans les études futures.

Available online at www.sciencedirect.com

ScienceDirect

Current Opinion in Physiology

Cellular correlates of wakefulness and slow-wave sleep: evidence for a key role of inhibition☆

Eduarda Susin and Alain Destexhe

Recent studies have identified interesting cellular dynamics in wakefulness and slow-wave sleep (SWS), as we review here for unit recordings in animals and human. First, a novel form of homeostasis was observed during sleep, where high-firing cells in wake tend to fire slower during SWS, while low-firing cells in wake tend to fire faster in SWS. Second, there seems to be a stronger involvement of inhibitory cells compared to excitatory cells during gamma oscillations in SWS. Third, pairwise cross-correlations between cells seem to increase specifically during SWS, but only for inhibitory neurons. We compare these results between animal and human unit recordings, and confirm the similarities in cellular dynamics in wake and SWS, and highlight that differences are mostly apparent in the dynamics and correlations of inhibitory cells. These results suggest that inhibitory networks are key in the dynamics of sleep, and should be a main target in future studies.

Address
Department of Integrative and Computational Neuroscience (ICN), Paris-Saclay Institute of Neuroscience (NeuroPSI), Centre National de la Recherche Scientifique (CNRS), 91198 Gif-sur-Yvette, France

Corresponding authors: Susin, Eduarda (eduardadsusin@gmail.com), Destexhe, Alain (destexhe@unic.cnrs-gif.fr)

Current Opinion in Physiology 2020, **15**:68–73

This review comes from a themed issue on **Physiology of Sleep**

Edited by **Vladyslav Vyazovskiy** and **Jenny Morton**

For a complete overview see the Issue and the Editorial

Available online 27th December 2019

https://doi.org/10.1016/j.cophys.2019.12.006

Introduction

Slow-wave sleep (SWS) is characterized by the prevalence of slow waves in the delta (0.5–4 Hz) frequency range, which are visible in the electroencephalogram (EEG) and local field potentials (LFPs). Early studies using intracellular recordings in anesthetized sleeping animals [1–3] have shown that the depth-positive (surface-negative) EEG components of slow waves are associated with cellular hyperpolarization and pause of firing. In natural SWS, extracellularly recorded neurons fire in coincidence with the depth-negative component of slow-wave complexes, whereas the depth-positive component is associated with neuronal silence [4–6]. Similar relations were found for delta waves in the intact brain [7], or isolated cortex [8]. Thus it seems that slow-wave complexes are characterized by alternating periods of sustained firing and neuronal silence usually called "Up" and "Down" states, respectively. It was further shown that, in natural sleep, Up and Down states appear synchronously in multiple cells recorded extracellularly [6], and the relation between the slow-wave and cellular hyperpolarization was later confirmed by intracellular recordings of neurons in naturally sleeping animals [9•]. Note that Down states are not periods of complete silence. A possible relation between the residual activity during Down states and memory consolidation has been proposed based on extracellular recordings in prefrontal cortical areas in rats [10]. This residual activity during down states was also observed in human recordings [11•].

Early studies also showed that, in aroused states, cortical cells fire tonically [12–14], and the EEG is dominated by low-amplitude fast activity in the beta/gamma (15–75 Hz) frequency range. Extracellular studies in natural SWS found that all characteristics from the spiking activity, LFP activity or LFP coherence, are identical between the Up-states of SWS, wakefulness or rapid-eye movement (REM) sleep [6]. These seemingly identical properties led to the suggestion that SWS Up-states constitute small episodes of activity replayed from wakefulness, possibly involved in memory consolidation [15]. This view was challenged recently by studies who found subtle differences in firing activity between natural SWS and wakefulness [16•], as we review in this paper.

Cellular correlates of wakefulness and slow-wave sleep

Generic features of brain activity during wake and sleep states in humans are illustrated in Figure 1. We used a dataset where units could be separated into fast-spiking (FS), presumed inhibitory, and regular-spiking (RS), presumed excitatory cells; some of these were confirmed by direct functional identification [19]. In these human recordings, during Wake and REM states, the activity of both RS and FS cells is sustained, asynchronous and

★ Research supported by Centre National de la Recherche Scientifique (CNRS), the European Community (Human Brain Project, H2020-785907), and École des Neurosciences de Paris (ENP).

Figure 1

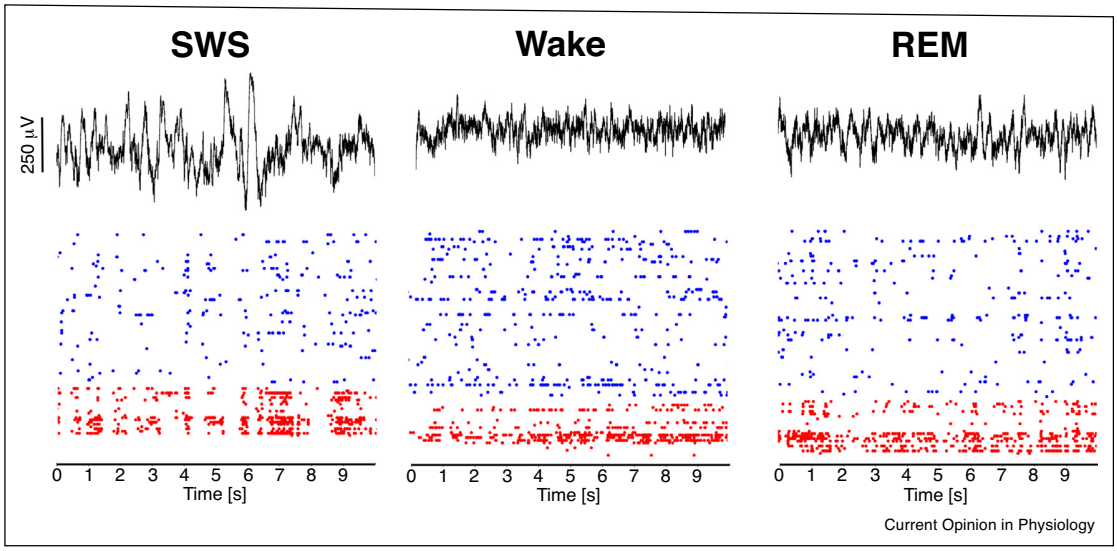

Features of different brain states in Human. Selected parts of 10 s of recordings of LFP (top) and spiking activity (bottom) of SWS, Wake and REM are shown. The data were recorded from the same human subject which had a multielectrode array implanted in temporal cortex before a therapeutic surgery. LFP and spiking activity were simultaneously measured and the spikes were sorted allowing the identification of 68 putative excitatory (blue) and 23 putative inhibitory (red). Data sample from [19].

irregular, and the LFP is dominated by high-frequency activity. In contrast, during SWS, the activity is dominated by slow waves in the LFP, which are paralleled with synchronized silences (Down states) where almost all cells cease firing. Outside these periods (Up states), the dynamics is sustained, asynchronous and irregular, similar to Wake and REM states. These observations lead to the statement that the Down states is what makes SWS dynamics more synchronized, and in a sense, the higher synchrony during SWS does not come from the firing of units, but rather comes from these periods of non-firing.

Consistent with this interpretation, a previous extracellular study in marmoset cortical areas [18], found that there was no significant increase of neural correlation during SWS when recording spontaneous activity, providing another evidence that SWS Up-states display firing dynamics almost identical to wakefulness.

However, several observations have shown differences in spiking activity during wake states and SWS. For instance, a relevant feature that has been taken into consideration is the firing level of single units in different states. A recent work using wide-field calcium imaging in cortical superficial and deep layers in mice [17•] showed that the activity of excitatory neurons was highest during Wake, followed by that of SWS and subsequently followed by that of REM sleep (Wake > SWS > REM). Using two-photon imaging in layer 2/3, the same study [17•] also showed that paralvabumin-positive (PV+) interneuron activity follow the relation: Wake = REM > SWS, while somatostatin-positive interneurons follow: Wake > SWS > REM. In human recordings, the firing rates were comparable in all brain states [21], which would tend to support that the recorded FS cells are PV+ cells, although this should be confirmed with better statistics.

In addition, a recent analysis [16•] found important differences between SWS and Wake by focusing on Up states. By means of silicon probes implanted in frontal cortical areas of rats, measurements of extracellular signals allowed simultaneous identification of brain state and the assessment of the firing pattern of putative excitatory and inhibitory cells. This analysis [16•] showed that during SWS pyramidal cells that displayed high-firing during Wake tended to decrease their activity during SWS, while cells that displayed low-firing during wake tended to increase their firing during SWS. We confirm these findings also in humans through similar recordings and data processing performed previously [19]. Figure 2 compares the results from [16•] with our own analysis based on the data coming from [19]. Despite the small number of cells available in the human data set, in a confidence interval of 95%, it is possible to observe a small slope with respect to the identity (0.67–0.94). These results (in both data sets) indicate that a new type of homeostasis, as argued by [16•], in which a homogenization of firing is observed thorough the differential action in cells with different levels of activity (in opposition to previous homeostatic models [22,23]). On the other hand,

Figure 2

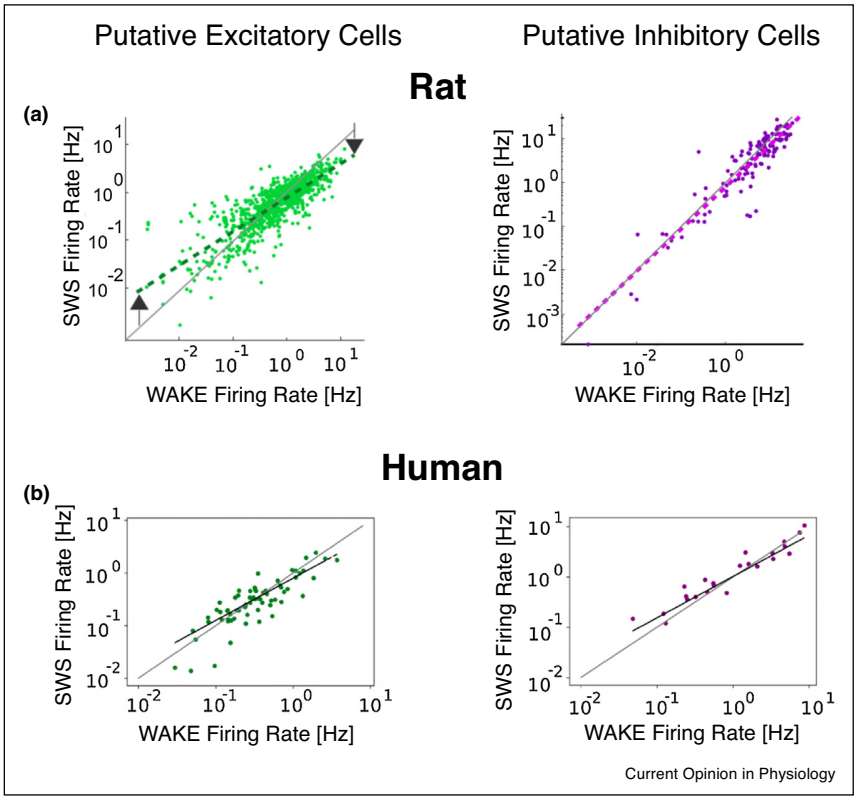

Comparison of firing rate during Wake and SWS states in rat and human cortex. Each point in the graph characterizes the firing rate (log scale) of an individual cell in the two states. Putative excitatory cells, both in rat and humans, suffer a change in their firing rate depending of their level of activity. Neurons that are highly active during wake decrease their firing during SWS, while neurons that have very low firing rates increase their firing (see arrows). Diverging results were found in the two data sets when looking to putative inhibitory cells. **(A)** Putative excitatory and inhibitory neurons in rat (slopes, 95% confidence interval: 0.66-0.71 and 0.996-1.005). Figure adapted with permission from [16•]. **(B)** Putative excitatory and inhibitory neurons in human (slopes, 95% confidence interval: 0.67–0.94 and 0.68–0.94). Data sample from [19].

when considering putative inhibitory cells the result is divergent in the two data sets (rat and human). No firing alteration is observed in the firing of inhibitory cells during Wake and SWS in rat [16•], while a tendency close to that which is observed with excitatory cells is observed in human inhibitory cells. This result should be checked in data sets where more neurons are available.

A further difference observed during Up states in SWS with respect to Wake states is the involvement of inhibitory cells in gamma oscillations. As recently shown in human recordings [11•], both putative excitatory regular-spiking and putative inhibitory fast-spiking populations increase their firing during gamma oscillations. Here, by analyzing the pre-processed data from [19], we noted that there is a significant increase on the average firing of the inhibitory population during SWS with respect to its activity during Wake (see Figure 3D). While no significant increase in firing with respect to Wake is exhibited by the excitatory population during SWS (see Figure 3E). Indicating an increase of FS participation in gamma generation during SWS.

Another key aspect to differentiate the network state between Wake and SWS is the pairwise correlations displayed by unit spikes. Figure 4A shows recordings of multielectrode arrays implanted in two monkey cortical areas (premotor dorsal — PMd — and motor neocortical -MI, layers II/III) [11•], in which spiking activity and LFP were simultaneously recorded. Cross-correlations between spike trains were normalized by the geometric mean of each cell pair's average firing rates to avoid spurious effects from cell-intrinsic firing levels [24]. Remarkably, comparing the correlation matrices between Wake and SWS, one sees that pairs of cells become correlated specifically during SWS (Figure 4). These sleep-specific correlations appear even between distant cortical areas. Interestingly, these pairwise spike train correlations only concern pairs of FS cells. With this observation we emphasize one more time that there

Figure 3

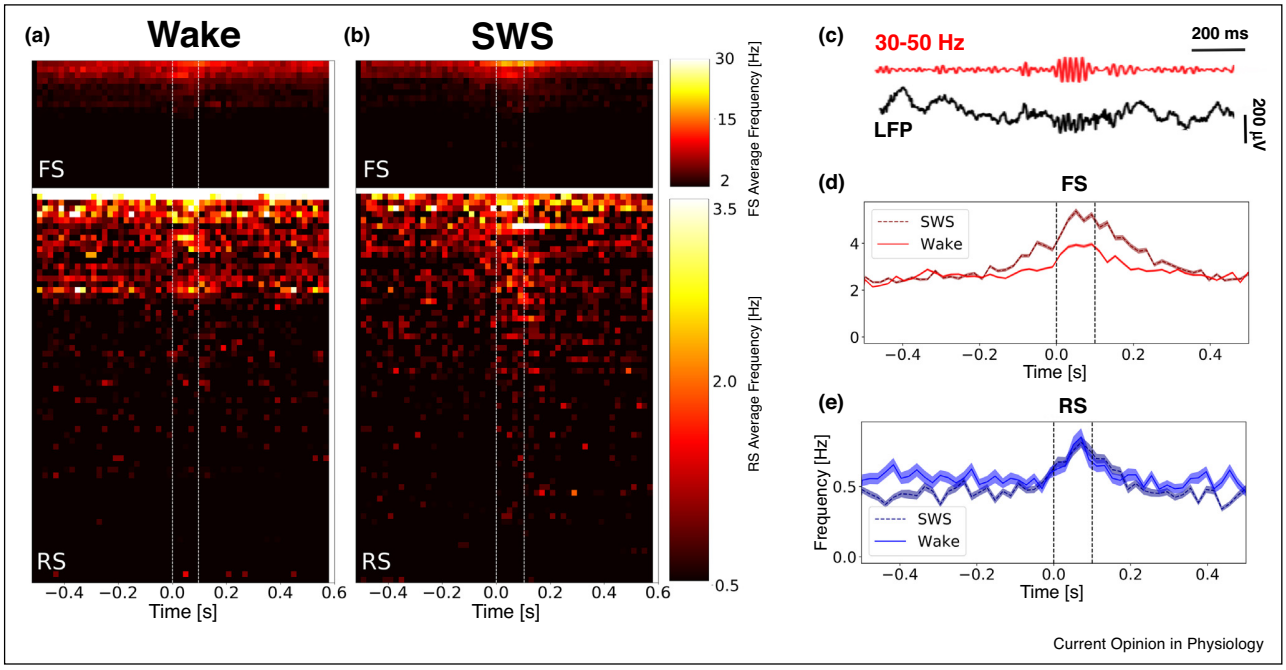

Difference of firing rates during γ events in RS and FS cells in Human Wake and SWS states. The color-maps indicating the average firing rate per cell around γ events in both Wake and SWS states are indicated in **(A)** and **(B)**. The firing of regular spiking (RS) are displayed in the bottom and the fast spiking (FS) cells is displayed in the top. Each line indicates the color-coded firing rate of each neuron in time averaged between all the gamma periods detected. For each γ event the firing rate was calculated in bins of 20 ms around the centered γ period. The white dashed lines indicate the beginning and the average end of γ periods identified in the data. Gamma periods were identified by the variation of the envelope obtained through the Hilbert Transform of the filtered LFP in the range of 30-50 Hz as is schematically shown in **(C)**. Neurons were ordered by their discharge probability during γ. The average firing rate per population during γ events in Wake and SWS are displayed in **(D)** and **(E)**. The color-coded firing rates shown in A and B were average in between neurons for each population: FS (D) and RS (E). The shadowed parts indicate the standard error of the mean. Data sample from [19].

seems to exist a particularly high involvement of inhibitory cells specifically during SWS. In agreement, a previous study [18] also reported an increase of correlations during SWS in the response to auditory stimuli, but no separation between RS and FS cells was attempted in that study.

Furthermore, this particular involvement of inhibition can also be detected from correlated patterns analyzed using maximum entropy models. Such methods can infer correlations from large data sets with the advantage that they can uncover collective dynamics with very few *ad hoc* assumptions. Recently, spiking activity in human recordings were used to infer the parameters of a Maximum Entropy model that takes into account only and exactly the single neurons' spiking probability, and the pairwise covariances observed in the data [20•]. In this work, illustrated in Figure 4B, the empirical probability distributions of population activity of FS and RS cells, during Wake and SWS, were compared to the probability distributions predicted by the model. Population activity was defined as the average number of active cells in a certain time window. This work showed that a model based exclusively on pairwise couplings can successfully predict the activity of both neuron types during Wake states (see the measures of the Kullback–Leibler divergence, D_{KL}, in Figure 4b1). However, it also demonstrated that pairwise interactions alone are not enough to describe the probability distribution displayed by the FS population during SWS (Figure 4b2). This result implies that, in contrast to the RS population, higher-order, or even population-wide, interactions govern the behavior of FS cells during SWS. This indicates another important difference between Wake and SWS states with respect to FS cells.

Discussion

In this paper, we briefly reviewed a few of recent studies about the cellular correlates of wake and sleep states based on multiple unit recordings. Similar to a previous study in cats [6], it was found that in human and monkey multielectrode recordings, wake and sleep states globally display similar levels of firing. Most units fire irregularly and asynchronously, and this pattern is seen in all brain

Figure 4

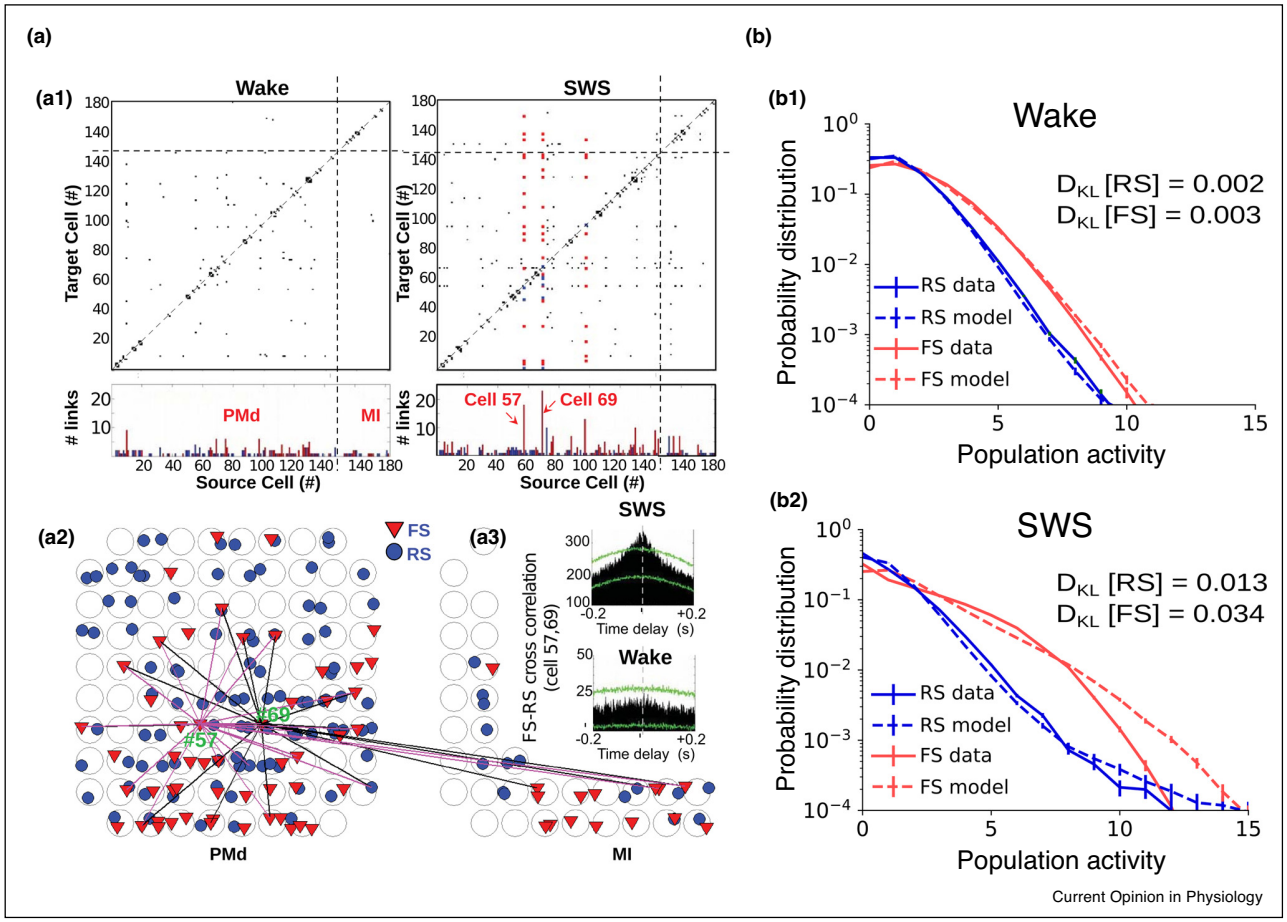

Difference in pairwise spike train cross-correlations among RS and FS cells during Wake and SWS. (A) Spiking activity measured during β oscillations through multielectrod arrays in two cortical areas in monkey (premotor dorsal, PMd, and motor neocortical, MI). Neurons could be identified as RS and FS. a1) Cell-cell correlations matrices containing cells from the two areas (PMd and MI). For cells 57/69 (during SWS) the type of target cells is indicated with colors (red, FS; and blue, RS). a2) Spatial location of different cells in the implanted arrays. Note that FS cells (exemplified by cells 57 and 69) display synchronous activity even with cell recorded in another cortical area (M1). a3) Spike cross-correlogram between cells 57 and 69 during SWS and Wake states. A significant peak is observed only during SWS. Figure A was adapted from [11•]. **(B)** Empirical probability distributions of human spiking activity are compared with the ones predicted by Maximum Entropy model (see main text), both in Wake (b1) and SWS (b2) for two type of cells (FS and RS). Measures of the Kullback-Leibler divergence, D_{KL}, are indicated in the graphs. Figure B was adapted from [20•].

states (Figure 1). Note that, in mice, a different level of activity is observed between Wake and sleep depending on the cell type. In the light of recent studies [11•], we also found differences between Wake and SWS in human: (1) there seems to exist a weak homeostasis of firing activity, where high-firing cells in wake tend to fire lower during SWS, and vice-versa for low-firing cells, as found in rat excitatory neurons [16•] and which we confirm here in human (Figure 2) for RS and FS cells. (2) There is a stronger participation of FS cells during gamma oscillations in SWS compared to Wake (Figure 3). (3) Besides the level of firing, there is also an increase of the spiking correlation between pairs of FS cells, specifically during sleep [11•] (Figure 4).

Taken together, these results show that inhibition seems to be a key to differentiate the network state between Wake and SWS, even though the differences are subtle. This is true for the level of firing of inhibitory cells, which seems to be maximally involved during SWS gamma oscillations. It is also true for the level of correlation between inhibitory cells, which show remarkably high correlations that specifically appear during SWS, sometimes extending to large cortical distances [11•] (Figure 4A).

We presently do not know why inhibitory networks seem different during sleep. A possibility is that the different levels of cholinergic drive in Wake and SWS may

up-regulate some of the inhibitory neurons, resulting in an increase of participation in gamma oscillations, as we observed. However, this does not explain why inhibitory cells are so correlated during SWS, which necessarily comes from an excitatory drive yet to be identified.

Acknowledgements

This research was supported by the Centre National de la Recherche Scientifique (CNRS) and the European Community (Human Brain Project, H2020-785907). E.S. acknowledges a PhD fellowship from the École des Neurosciences de Paris (ENP).

References

1. Steriade M, Nunez A, Amzica F: **Intracellular analysis of relations between the slow (< 1 Hz) neocortical oscillation and other sleep rhythms of the electroencephalogram**. *J Neurosci* 1993, **13**:3266-3283.

2. Steriade M, Contreras D, Dossi RC, Nunez A: **The slow (<1 hz) oscillation in reticular thalamic and thalamocortical neurons: scenario of sleep rhythm generation in interacting thalamic and neocortical networks**. *J Neurosci* 1993, **13**:3284-3299.

3. Contreras D, Steriade M: **Cellular basis of eeg slow rhythms: a study of dynamic corticothalamic relationships**. *J Neurosci* 1995, **15**:604-622.

4. Steriade M, Contreras D, Amzica F, Timofeev I: **Synchronization of fast (30–40 Hz) spontaneous oscillations in intrathalamic and thalamocortical networks**. *J Neurosci* 1996, **16**:2788-2808.

5. Amzica F, Steriade M: **The k-complex: its slow (<1-hz) rhythmicity and relation to delta waves**. *Neurology* 1997, **49**:952-959.

6. Destexhe A, Contreras D, Steriade M: **Spatiotemporal analysis of local field potentials and unit discharges in cat cerebral cortex during natural wake and sleep states**. *J Neurosci* 1999, **19**:4595-4608.

7. Buzsaki G, Bickford RG, Ponomareff G, Thal L, Mandel R, Gage FH: **Nucleus basalis and thalamic control of neocortical activity in the freely moving rat**. *J Neurosci* 1988, **8**:4007-4026.

8. Frost JD Jr, Kellaway P, Gol A: **Single-unit discharges in isolated cerebral cortex**. *Exp Neurol* 1966, **14**:305-316.

9. • Steriade M, Timofeev I, Grenier F: **Natural waking and sleep states: a view from inside neocortical neurons**. *J Neurophysiol* 2001, **85**:1969-1985
first paper having shown the dynamics of slow-wave sleep intracellularly in cats, where the Down-states are clearly associated with cellular hyperpolarization, while Up-states are intracellularly very close to the dynamics found during wakefulness.

10. Todorova R, Zugaro M: **Isolated cortical computations during delta waves support memory consolidation**. *Science* 2019, **366**:377-381.

11. • Le Van Quyen M, Muller LE, Telenczuk B, Halgren E, Cash S, Hatsopoulos NG, Dehghani N, Destexhe A: **High-frequency oscillations in human and monkey neocortex during the wake-sleep cycle**. *Proc Natl Acad Sci* 2016, **113**:9363-9368
this paper investigated the firing of excitatory and inhibitory cells in human and monkey during wake and sleep states, during gamma oscillations. A higher level of participation was found for inhibitory cells, as well as high correlations, specific to SWS, and only between inhibitory cells.

12. Hubel DH: **Single unit activity in striate cortex of unrestrained cats**. *J Physiol* 1959, **147**:226-238.

13. Evarts EV: **Temporal patterns of discharge of pyramidal tract neurons during sleep and waking in the monkey**. *J Neurophysiol* 1964, **27**:152-171.

14. Steriade M, Deschenes M: **Inhibitory processes and interneuronal apparatus in motor cortex during sleep and waking. II. recurrent and afferent inhibition of pyramidal tract neurons**. *J Neurophysiol* 1974, **37**:1093-1113.

15. Destexhe A, Hughes SW, Rudolph M, Crunelli V: **Are corticothalamic 'up' states fragments of wakefulness?** *Trends Neurosci* 2007, **30**:334-342.

16. • Watson BO, Levenstein D, Greene JP, Gelinas JN, Buzsáki G: **Network homeostasis and state dynamics of neocortical sleep**. *Neuron* 2016, **90**:839-852
this paper showed clear evidence for a regulation of the firing of neurons between Wake and SWS states, where neurons with high levels of firing tend to fire lower during SWS, and conversely, neurons with low levels of firing tend to fire higher during SWS. This can be interpreted as a form of homeostasis of firing dynamics between wake and sleep states.

17. • Niethard N, Hasegawa M, Itokazu T, Oyanedel CN, Born J, Sato TR: **Sleep-stage-specific regulation of cortical excitation and inhibition**. *Curr Biol* 2016, **26**:2739-2749
this paper showed features of the neural activity of wake and sleep states in mice. This was done for excitatory cells, which fired more during Wake than the two sleep states, while interneurons also tended to fire more, but with some differences according to the type of inhibitory cell.

18. Issa EB, Wang X: **Increased neural correlations in primate auditory cortex during slow-wave sleep**. *J. Neurophysiol.* 2013, **109**:2732-2738.

19. Peyrache A, Dehghani N, Eskandar EN, Madsen JR, Anderson WS, Donoghue JA, Hochberg LR, Halgren E, Cash SS, Destexhe A: **Spatiotemporal dynamics of neocortical excitation and inhibition during human sleep**. *Proc Natl Acad Sci* 2012, **109**:1731-1736.

20. • Nghiem T-A, Telenczuk B, Marre O, Destexhe A, Ferrari U: **Maximum-entropy models reveal the excitatory and inhibitory correlation structures in cortical neuronal activity**. *Phys Rev E* 2018, **98**:012402
this study confirmed that inhibitory neurons follow a very particular dynamics during sleep, pairwise correlations cannot account for their firing statistics, and higher-order correlations are needed.

21. Dehghani N, Peyrache A, Telenczuk B, Le Van Quyen M, Halgren E, Cash SS, Hatsopoulos NG, Destexhe A: **Dynamic balance of excitation and inhibition in human and monkey neocortex**. *Sci Rep* 2016, **6**:23176.

22. Tononi G, Cirelli C: **Sleep and the price of plasticity: from synaptic and cellular homeostasis to memory consolidation and integration**. *Neuron* 2014, **81**:12-34.

23. Turrigiano GG, Nelson SB: **Homeostatic plasticity in the developing nervous system**. *Nat Rev Neurosci* 2004, **5**:97.

24. De La Rocha J, Doiron B, Shea-Brown E, Josić K, Reyes A: **Correlation between neural spike trains increases with firing rate**. *Nature* 2007, **448**:802.

Work 2

Integration, coincidence detection and resonance in networks of spiking neurons expressing gamma oscillations and asynchronous states

---

Reference: Susin, Eduarda, and Alain Destexhe. "Integration, coincidence detection and resonance in networks of spiking neurons expressing Gamma oscillations and asynchronous states." Plos Computational Biology (2021).

French Abstract:

Pendant l'état de veille, l'activité neuronale observée dans le cerveau est typiquement asynchrone et irrégulière. Cependant, cette activité est également accompagnée de périodes où des oscillations modulent l'activité des neurones. Une de ces oscillations, connues comme des Ondes Gamma (30-90 Hz), a été associée au traitement de l'information. Dans cette étude, nous utilisons des modèles informatiques pour étudier comment les circuits cérébraux génèrent des oscillations d'une manière cohérente avec les enregistrements de microélectrodes chez l'homme. Nous étudions ensuite comment ces réseaux réagissent aux stimuli externes, en comparant les états asynchrones avec les états oscillatoires. Ceci est testé selon plusieurs paradigmes: un *mode intégrative* où des entrées qui variant lentement sont progressivement intégrées; un *mode de détection de coïncidence* où les entrées brèves sont traitées en fonction de la phase des oscillations; et un *mode de résonance* où le réseau est sondé avec des stimuli oscillatoires. Étonnamment, nous constatons que dans tous les cas, la présence d'oscillations Gamma diminue la réactivité aux stimuli externes. Nous discutons des implications possibles de cette diminution de réactivité sur le traitement de l'information et proposons de nouvelles directions pour une exploration plus poussée.

PLOS COMPUTATIONAL BIOLOGY

RESEARCH ARTICLE

Integration, coincidence detection and resonance in networks of spiking neurons expressing Gamma oscillations and asynchronous states

Eduarda Susin*, Alain Destexhe

Institute of Neuroscience (NeuroPSI), Paris-Saclay University, Centre National de la Recherche Scientifique (CNRS), Gif-sur-Yvette, France

* eduardadsusin@gmail.com

OPEN ACCESS

Citation: Susin E, Destexhe A (2021) Integration, coincidence detection and resonance in networks of spiking neurons expressing Gamma oscillations and asynchronous states. PLoS Comput Biol 17(9): e1009416. https://doi.org/10.1371/journal.pcbi.1009416

Editor: Arvind Kumar, Royal Institute of Technology (KTH), SWEDEN

Received: May 4, 2021

Accepted: September 2, 2021

Published: September 16, 2021

Peer Review History: PLOS recognizes the benefits of transparency in the peer review process; therefore, we enable the publication of all of the content of peer review and author responses alongside final, published articles. The editorial history of this article is available here: https://doi.org/10.1371/journal.pcbi.1009416

Data Availability Statement: Codes written in support of this publication are publicly available at ModelDB: http://modeldb.yale.edu/267039.

Abstract

Gamma oscillations are widely seen in the awake and sleeping cerebral cortex, but the exact role of these oscillations is still debated. Here, we used biophysical models to examine how Gamma oscillations may participate to the processing of afferent stimuli. We constructed conductance-based network models of Gamma oscillations, based on different cell types found in cerebral cortex. The models were adjusted to extracellular unit recordings in humans, where Gamma oscillations always coexist with the asynchronous firing mode. We considered three different mechanisms to generate Gamma, first a mechanism based on the interaction between pyramidal neurons and interneurons (PING), second a mechanism in which Gamma is generated by interneuron networks (ING) and third, a mechanism which relies on Gamma oscillations generated by pacemaker *chattering* neurons (CHING). We find that all three mechanisms generate features consistent with human recordings, but that the ING mechanism is most consistent with the firing rate change inside Gamma bursts seen in the human data. We next evaluated the responsiveness and resonant properties of these networks, contrasting Gamma oscillations with the asynchronous mode. We find that for both slowly-varying stimuli and precisely-timed stimuli, the responsiveness is generally lower during Gamma compared to asynchronous states, while resonant properties are similar around the Gamma band. We could not find conditions where Gamma oscillations were more responsive. We therefore predict that asynchronous states provide the highest responsiveness to external stimuli, while Gamma oscillations tend to overall diminish responsiveness.

Author summary

In the awake and attentive brain, the activity of neurons is typically asynchronous and irregular. It also occasionally displays oscillations in the Gamma frequency range (30–90 Hz), which are believed to be involved in information processing. Here, we use computational models to investigate how brain circuits generate oscillations in a manner

Funding: A.D was supported by the Centre National de la Recherche Scientifique (CNRS) and the European Community (Human Brain Project, H2020-785907). E.S. acknowledges a PhD fellowship from the École des Neurosciences de Paris (ENP) and from the Fondation pour la Recherche Médicale (FRM) - grant FDT202012010566 - and the financial support from La Fondation des Treilles. The funders had no role in study design, data collection and analysis, decision to publish, or preparation of the manuscript. CNRS: www.cnrs.fr Human Brain Project: www.humanbrainproject.eu ENP: www.paris-neuroscience.fr FRM: www.frm.org La Fondation des Treilles: https://www.les-treilles.com/la-recherche/le-prix-jeune-chercheur/.

Competing interests: The authors have declared that no competing interests exist.

consistent with microelectrode recordings in humans. We then study how these networks respond to external input, comparing asynchronous and oscillatory states. This is tested according to several paradigms, an *integrative mode*, where slowly varying inputs are progressively integrated, a *coincidence detection mode*, where brief inputs are processed according to the phase of the oscillations, and a *resonance mode* where the network is probed with oscillatory inputs. Surprisingly, we find that in all cases, the presence of Gamma oscillations tends to diminish the responsiveness to external inputs. We discuss possible implications of this responsiveness decrease on information processing and propose new directions for further exploration.

Introduction

Gamma oscillations appear in many brain states and brain regions [1] and are detectable mostly from the local field potential (LFP) as oscillations in the 30–90 Hz frequency range. During sensory responses, oscillations in this frequency range were initially proposed to serve as a mechanism for coordination of neural activity among cells coding for different aspects of the same stimulus [2–5]. Strengthening of synaptic input due to temporal summation led to the hypothesis that Gamma synchrony was necessary to effectively transmit specific sets of information across cortical networks in the very noisy conditions in which the brain operates. This concept was later expanded by proposing that synchronous Gamma also engages inhibition in target networks. Phase-locked inhibition creates strong suppression around the excitatory drive and creates windows of low and high neuronal excitability. Such observations led to hypotheses that Gamma oscillations are important for information processing and coding. The most popular theories are the Binding-by-synchronization Hypothesis [4, 5], the Phase Coding Theory [6, 7], the Communication Through Coherence Theory [8, 9] and Communication through Resonance Theory [10].

An alternative hypothesis, instead of relying on oscillations for efficient cortical communication, posits that *desynchronized states* are optimal for the transfer of signals between cortical networks [11, 12]. Desynchronized states, called *Asynchronous-Irregular* (AI) [13] because of its features, are characterized in cortical cells in vivo by irregular firing with very weak correlations and stationary global activity [14–18]. This type of activity can be modeled by networks with balanced excitatory and inhibitory inputs [19].

In the present work, we aim at testing these two discrepant points of view using computational models. We take advantage of previously published electrophysiological data, measured extracellularly in human temporal cortex [20, 21], to characterize the behavior of individual neurons during Gamma oscillations in resting awake states, and to compare such experimental features to spiking neural networks generating Gamma. We exploit different network structures to investigate three well-known mechanisms of Gamma generation [22–27]: either by the exclusive interaction between inhibitory neurons [*Interneuron Gamma* (ING)] or by the interaction of inhibitory and excitatory neurons via *Pyramidal-Interneuron Gamma* (PING) or via *Chattering Induced Gamma* (CHING). First we compare to what degree each mechanism can reproduce the observed experimental features of human Gamma oscillations and what are the specificities of each mechanism, in the way neurons behave during Gamma. Subsequently, we examine network responsiveness due to three types of stimulus: Gaussian slowly-varying inputs (*integration mode*), precisely-timed Gaussian inputs (*coincidence detection mode*) and a sinusoidal varying Poissonian input (*resonance*).

Materials and methods

Neuron and network models

Each of the three networks developed in this work uses the *Adaptive Exponential Integrate-And-Fire Model* (Adex) [28] for its neural units. In this model, each neuron i is described by its membrane potential V_i, which evolves according to the following equations:

$$\begin{aligned} C\frac{dV_i(t)}{dt} &= -g_L(V_i - E_L) + g_L\Delta exp\left[\frac{(V_i(t) - V_{th})}{\Delta}\right] - w_i(t) - I_{Syn_i}(t) \\ I_{Syn_i}(t) &= g_{E_i}(t)(V_i(t) - E_E) + g_{I_i}(t)(V_i(t) - E_I) \\ \tau_{E,I}\frac{dg_{E,I_i}(t)}{dt} &= -g_{E,I_i}(t) + Q_{E,I_i}\sum_k \delta(t - t_k) \\ \tau_{w_i}\frac{dw_i(t)}{dt} &= a(V_i(t) - E_L) - w_i(t) + b\sum_j \delta(t - t_j) \end{aligned} \quad (1)$$

where C is the membrane capacitance, g_L is the leakage conductance, E_L is the leaky membrane potential, V_{th} is the effective threshold and Δ is the threshold slope factor. The synaptic current (I_{Syn_i} (t)) received from other neurons to neuron i is taken into account as conductance based: every time a presynaptic neuron spikes at time t_k, the excitatory (g_{E_i}) or the inhibitory (g_{I_i}) synaptic conductance increase by a discrete amount Q_E or Q_I (excitatory or inhibitory synaptic strength), depending on the nature of the presynaptic neuron. Synaptic conductances subsequently decay exponentially with a time constant τ_E or τ_I. E_E and E_I are the reversal potential of excitatory (E_E) and inhibitory (E_I) synapses. The Σ_k runs over all the presynaptic excitatory or inhibitory neurons spike times. During the simulations, the equation characterizing the membrane potential V_i is numerically integrated until a spike is generated. Formally this happens when V_i grows rapidly toward infinity. In practice, the spiking time is defined as the moment in which V_i reaches a certain threshold (V_{th}). When $V_i = V_{th}$ the membrane potential is reset to V_{rest}, which is kept constant until the end of the refractory period T_{ref}. After the refractory period the equations start being integrated again. The adaptation current is described by the variable w_i. It increases by an amount b every time neuron i emits a spike at times t_j and decays exponentially with time scale τ_w. The parameter a indicates the subthreshold adaptation.

Three types of cells were used in our models: Regular Spiking Cells (RS), Chattering Cells (Ch) and Fast Spiking Cells (FS). The cell specific activities are displayed in Fig 1 and their parameters are indicated in Table 1.

Each of the three developed networks are composed of N = 25000 neurons, 80% excitatory and 20% of inhibitory. All neurons are connected randomly. Additionally to recurrent connections, each neuron receive an external drive (noise). This noise was implemented as N_{Ext} = 20000 independent and identically distributed excitatory Poissonian spike trains with a spiking frequency μ_{Ext}, being sent to the network with a 2% probability of connection. These spike trains were computed inside of the synaptic current term $I_{syn}(t)$, by means of a discontinuous increase of the excitatory synaptic conductance g_E by an amount Q_{Ext} (at every spike time). This type of implementation adds to the network a low degree of correlation, since some neurons share the same drive. Nevertheless, this extra correlation does not affect our results, which kept being qualitatively the same when a drive with no correlations was applied. The

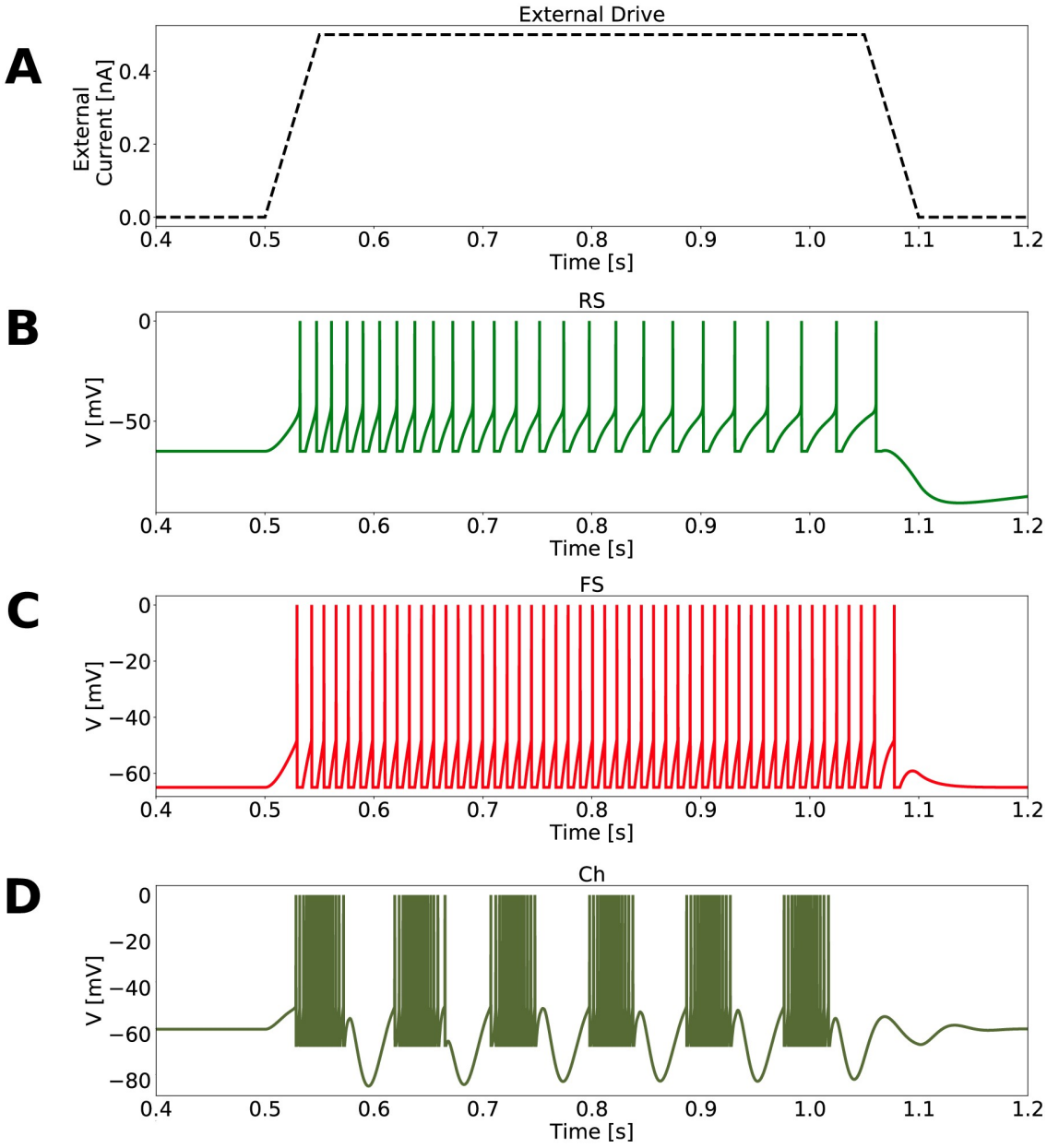

Fig 1. Neuronal response to an external current. A: External drive fluctuation. External current, in each neuron, varied from 0 to 0.5 nA in a linear way, was kept constant for 500 ms, subsequently decreasing to 0 nA in a linear way. B: Isolated RS cell in response to the external drive presented in A. C: Isolated FS cell in response to the external drive presented in A. D: Activity of one Ch cell, in a network exclusively composed of 1000 Ch cells connected randomly with a probability of 2%.

https://doi.org/10.1371/journal.pcbi.1009416.g001

patterns of connection and neuron type composition of each network model, as well as the specific values of Poissonian stimulation (μ_{Ext} and Q_{Ext}), are described bellow.

- ***PING Network***: It is composed of 25000 Adex neurons (20000 excitatory Regular Spiking and 5000 inhibitory Fast Spiking cells). All neurons are connected randomly with a probability of connection of 2%. All synapses are delayed by a time delay of 1.5 ms. The synaptic excitatory (inhibitory) time scales are $\tau_E = 1.5$ ms ($\tau_I = 7.5$ ms), with synaptic strengths of

Table 1. Specific neuron model parameters.

Parameter	RS	FS	Ch
V_{th}	-40 mV	-47.5 mV	-47.5 mV
Δ	2 mV	0.5 mV	0.5 mV
T_{ref}	5 ms	5 ms	1 ms
τ_w	500 ms	500 ms	50 ms
a	4 nS	0 nS	80 nS
b	20 pA	0 pA	150 pS
C	150 pF	150 pF	150 pF
g_L	10 nS	10 nS	10 nS
E_L	-65 mV	-65 mV	-58 mV
E_E	0 mV	0 mV	0 mV
E_I	−80 mV	−80 mV	−80 mV
V_{rest}	-65 mV	-65 mV	-65 mV

https://doi.org/10.1371/journal.pcbi.1009416.t001

Q_E = 5 nS (Q_I = 3.34 nS). Synaptic time scales were chosen accordingly to the parameter search indicated in S1 Fig. For Gamma activity, the network was stimulated with an external noise of μ_{Ext} = 3 Hz and Q_{Ext} = 4 nS. For an activity similar to an Asynchronous and Irregular activity (AI-like), the network was stimulated with an external noise of μ_{Ext} = 2 Hz and Q_{Ext} = 4 nS.

- ***Asynchronous and Irregular (AI) Network***: The *AI Network* was used in this work as one of the building blocks for the ING and the CHING Network. It is composed of 25000 neurons (20000 excitatory Regular Spiking and 5000 inhibitory Fast Spiking). All neurons are connected randomly with a probability of connection of 2%. All synapses have synaptic strengths of Q_E = 1 nS or Q_I = 5 nS, and are delayed by a time delay of 1.5 ms. This network, independently of the strength of the the external noise, can not generate Gamma rhythms. This is the case because the chosen synaptic excitatory and inhibitory time scales ($\tau_E = \tau_I$ = 5 ms) are in a region of the parameter space in which the regime is asynchronous and irregular. See S1 Fig. Because of this feature, the *AI Network* was used as a control to study network responsiveness (see Results section).
- ***Gamma Network***: The *Gamma Network* was used in this work as one of the building blocks for the ING Network. It is composed of 1000 inhibitory Fast Spiking neurons, highly connected between each other. All neurons are connected randomly with a probability of connection of 60%. All synapses have synaptic strengths of Q_I = 5 nS and synaptic time constant of τ_I = 5 ms, and are delayed by a time delay of 1.5 ms. This network is capable of generating oscillations by its own due to the exclusive presence of inhibitory neurons excited by an external drive [29, 30]. Low oscillation frequencies in the Gamma range (≈70 Hz) are possible thanks to the high connectivity patterns used (60%). S2 Fig displays the parameter space of network connectivity vs. inhibitory synaptic strengths for this network. The parameters chosen in our simulations (p = 60% and Q_I = 5 nS) are indicated.
- ***ING Network***: The *ING Network* is constructed as a mixture of *AI network* with the *Gamma Network*. It is composed of 25000 neurons: 20000 RS and 4000 FS from the *AI network* plus 1000 FS neurons from the *Gamma Network*. The Fast Spiking neurons in the original *AI network* and the ones in the *Gamma Network* share all the same parameters of FS cells in Table 1. The only difference among them is their pattern of connectivity. To make it clear, we call as FS2, the FS neurons that were part of the *Gamma Network*, and we keep calling as FS the ones that were part of the *AI Network*. In the *ING Network*, FS2 cells send and receive

random connections to RS neurons with a probability of 15%, FS2 cells send random connections to FS neurons with a probability of 15% while FS cells send random connections to FS2 neurons with a probability of 3%. This combination of the *Gamma network* with the *AI Network* allows the oscillation frequency to slow down further, reaching ≈ 55 Hz. All synapses have synaptic strengths of Q_E = 1 nS or Q_I = 5 nS and synaptic time scales of $\tau_E = \tau_I$ = 5 ms. Synapses are delayed by a time of 1.5 ms. For Gamma activity the network was stimulated with an external noise of μ_{Ext} = 3 Hz, while for Asynchronous and Irregular activity, the network was stimulated with an external noise of μ_{Ext} = 2 Hz. The external noise used had a synaptic strength of Q_{Ext} = 0.9 nS.

- ***CHING Network***: The *CHING Network* is constructed the same way as the *AI network*, with the difference that 5% of the RS cells were replaced by Chattering Cells (Ch). This way, the *CHING Network* is composed of 25000 neurons: 19000 RS, 1000 Ch and 5000 FS. All cells in the network are randomly connected to each other with a probability of 2%. All synapses have synaptic time scales of $\tau_E = \tau_I$ = 5 ms and are delayed by a time delay of 1.5 ms. Excitatory synapses have synaptic strengths of Q_E = 1 nS, while inhibitory synapses from FS cells to Ch or to RS have synaptic strengths of Q_I = 7 nS. Synapses from FS to FS have synaptic strengths of Q_I = 5 nS. The network receives external noise with synaptic strength of Q_{Ext} = 1 nS in excitatory cells (RS and Ch) and Q_{Ext} = 0.75 nS in FS cells. For Gamma, external noise of μ_{Ext} = 2 was used, while for Asynchronous and Irregular activity, μ_{Ext} = 1 Hz.

Simulations

All neural networks were constructed using Brian2 simulator [31]. All equations were numerically integrated using Euler Methods and dt = 0.1 ms as integration time step. The codes for each one of the three developed networks are available at ModelDB platform: http://modeldb.yale.edu/267039.

LFP model

To model the LFP generated by each of the three developed networks, we used a recent method developed by [32]. This approach calculates the contribution of individual neurons to the LFP by means of the convolution of individual neuron spike trains (generated by the networks) with a phenomenological Kernel $\mathcal{K}$, which had its parameters fitted from unitary LFPs (the LFP generated by a single axon, *uLFP*) measured experimentally [32]. Each neuron spike train is convoluted with a particular Kernel $\mathcal{K}^p$ that depends on the particular neuron position $\vec{x_p}$ in a 2-D space.

$$\begin{aligned} \mathcal{K}^p(\vec{x},t) &= A(\vec{x})exp[-(t-t_{pick})^2/(2\sigma^2)] \\ t_{pick} &= t_0 + d + |\vec{x}-\vec{x_p}|/v_a \\ A(\vec{x}) &= A_0 exp[-|\vec{x}-\vec{x_p}|/\lambda] \end{aligned} \quad (2)$$

in which σ is the standard deviation in time, t_{pick} is the peak time of the *uLFP*, t_0 is the time of the spike of a particular cell p, d is a constant delay, v_a is the axonal speed, and $|\vec{x} - \vec{x_p}|$ is the distance between the position of particular cell ($\vec{x_p}$) and the position of the electrode ($\vec{x}$). $A(\vec{x})$ gives the space-dependent amplitude, in which A_0 is the maximal amplitude, and λ is the space constant of the decay. These parameters were estimated separately for excitatory and

inhibitory contributions ($\mathcal{K}_E^p$ and $\mathcal{K}_I^p$) [32, 33]. The LFP, at a particular electrode position $\vec{x}$, is given by the sum of all individual neuron contributions:

$$LFP(\vec{x}, t) = \tag{3}$$

$$\sum_p \int \mathcal{K}_E^p(\vec{x}, t-\tau)\left(\sum_j \delta(t - t_p^j)\right)d\tau + \sum_p \int \mathcal{K}_I^p(\vec{x}, t-\tau)\left(\sum_j \delta(t - t_p^j)\right)d\tau \tag{4}$$

In which Σ_p runs over neurons p, and Σ_j runs over all spike times of neuron p. To be able to apply this method to our simulations (which don't presume any neuronal localization in space), we randomly displaced the network neurons in 2-D grid, assuming that the electrode was displaced on its center and was measuring the LFP in the same layer as neuronal soma. The program code of the kernel method is available in ModelDB (http://modeldb.yale.edu/266508), using python 3 or the *hoc* language of NEURON.

Detection of Gamma rhythms and Gamma phase

In both, experimental and simulated signals, Gamma rhythms were detected by means of the Hilbert transform of the band-filtered LFP. The identification of Gamma bursts was done separately for each electrode. We considered as Gamma bursts periods in which the amplitude of Hilbert Transform envelope (absolute value) differed from the mean, by at least 2 standard deviations for the experimental data, and by at least 1 standard deviation for the numerical ones, for a minimum duration of 3 Gamma cycles. This criteria were not enough to identify all Gamma bursts (some Gamma bursts were ignored). On the other hand, no false positives were included in the analysis. All the Gamma bursts automatically identified by the algorithm were individually confirmed visually. The oscillation phase was acquired using the angle of the imaginary part of the transform. The LFP was band-pass filtered in the band of 30–50 Hz (unless indicated otherwise). To band-pass the LFP signals, we used a FIR (Finite Impulse Response) filter using the Kaiser window method with a 60 dB stop-band attenuation and a 5Hz width from pass to stop transition [34]. To implement the filter we used the following functions from the Python-based ecosystem *Scipy*: *signal.kaiserord*, *signal.lfilter* and *signal.firwin* [35].

Spike-LFP phase-locking

Every time a Gamma period was identified, in both experimental and simulated signals, the spiking times of each neuron was stored and compared to the Gamma rhythm phase. This information allowed the construction of the phase distribution of each neuron. For the experimental data, considering that the identification of Gamma bursts was done separately for each electrode, neurons measured in particular electrode, had their phases and firing rates analyzed exclusively with respect to the rhythm measured in this electrode. Neuron phases were calculated from $-\pi$ to π. In this way neurons with negative phases should be interpreted as spiking preferentially before than neurons with positive phases. The phase distribution of each neuron was tested for circular uniformity using a Bonferroni-corrected Rayleigh test [36, 37]. A neuron was considered phase-locked if we could reject circular uniformity at $P < 0.01$. See S3 Fig. Neurons that spiked less then 5 times inside Gamma bursts, or neurons whose electrode measured less then 1 second of Gamma, in the respective data segment, were classified as *inconclusive*.

Firing rate change

The average firing rate of each neuron outside Gamma bursts (f_{out}) was computed based in the total time, excluding the activity inside Gamma bursts and their duration. In accordance, the

average firing rate inside Gamma bursts (f_γ) was calculated based on the total Gamma duration and the activity occurring exclusively inside Gamma bursts. A neuron was considered to increase its firing significantly if the observed number of spikes in the measured time was higher than the *percent point function* of a 95% Interval of Confidence of a Poissonian distribution with average firing rate f_{out}. Cells that had firing rates smaller then 0.1 Hz or cells whose electrode measured less then 1 second of Gamma bursts, in the respective data segment, were classified as *inconclusive*. See S4 Fig.

Responsiveness

The level of *responsiveness* (R) of a network, due to a stimulus (S) in a time window of duration T, is defined as the difference between the total number of spikes generated by the whole network due to a stimulus (N^S_{spikes}) and the total number of spikes generated in the absence of the stimulus (N_{spikes}), normalized by the network size (total number of neurons N_n) and the duration of the time window T.

$$R = \frac{N^S_{spikes} - N_{spikes}}{TN_n} \tag{5}$$

Phase-dependent responsiveness

The *Phase-dependent responsiveness* of a network $R(\theta)$, in a time window of duration T, due to a stimulus S presented to the network in a particular phase θ of the Gamma cycle, is defined as the difference between the total number of spikes generated by the whole network due to a stimulus at the θ phase, $N^S_{spikes}(\theta)$, and the total number of spikes generated in the absence of the stimulus at the θ phase, $N_{spikes}(\theta)$, normalized by the network size (total number of neurons N_n) and the time window T.

$$R(\theta) = \frac{N^S_{spikes}(\theta) - N_{spikes}(\theta)}{TN_n} \tag{6}$$

Human recordings

In one epileptic patient with intractable seizures, 10x10 Neuroprobe silicon multielectrode arrays (400-μm inter-electrode separation, 1 mm electrode length, Blackrock Microsystems) were implanted in the middle temporal gyrus (layers II/III). Electrodes were implanted in regions expected to be removed, and after the monitoring session, the implant area was excised. The patient consented to the procedure, which was approved by the Massachusetts General Hospital Institutional Review Board in accordance with the ethical standards of the Declaration of Helsinki. This data set have already been published previously [20, 21]. Neurons could be classified through clustering based on the spike shape and functional interactions (determined using cross-correlograms) [20, 38] as Regular Spiking Cell (RS), putative excitatory, and Fast Spiking Cells (FS), putative inhibitory. From 81 electrodes, 91 neurons could be detected: 23 FS and 68 RS.

Results

We first analyze Gamma oscillations from human recordings, then examine network models of Gamma oscillations and compare them to the experimental data. Finally, we examine the

responsiveness and resonant properties of these networks, comparing Gamma and asynchronous states.

Human recordings analysis

In this paper, aiming to constrain our computational models to observed experimental features, we extend the human data analysis performed in [20, 21], focusing on awake states. The data was acquired extracellularly in patients suffering of intractable epilepsy, who had multielectrode arrays implanted during therapeutic procedures. The arrays registered simultaneously local field potential (LFP) and unit activity. We considered here one patient for which the recording was very stable, and in which several periods of wakefulness could be analyzed.

In each electrode, Gamma rhythms were identified and neural activity was characterized with respect to the Gamma cycles. Fig 2A illustrates a specific instant in which Gamma bursts were observed in most of the electrodes (spiking activity and the respective electrode band-filtered LFP are shown). Gamma rhythms were determined through the Hilbert transform of the filtered LFP (30–50 Hz). Fig 2B and 2C give an example of how Gamma is detected and how neural phase with respect to the oscillation is extracted (see *Detection of Gamma rhythms and Gamma phase* in Materials and methods Section). The data were acquired during the night. Five awake periods could be recorded, having a mean duration of 27 minutes, containing on average 13 seconds of Gamma (Fig 2D). During these periods the patient was in a resting awake condition.

In accordance with other studies, the spiking activity during Gamma bursts was observed to be very irregular and close to a Poissonian process, with a spiking frequency much smaller than the population frequency [21, 39–41]. Moreover, conformable to [21], on average, only 4% of RS cells and 17% of FS cells were Phase-Locked (Fig 2E), with RS cells having a phase preference later in the cycle than the FS cells (see S5 Fig). Furthermore, by measuring the firing rate change of each cell inside and outside Gamma bursts (Fig 2F), we encountered on average 47% of FS cells that increased their firing inside Gamma bursts, while only 17% of RS cells did. These observations suggest that Gamma oscillations modulate spiking activity in two manners: by means of firing rate increase and by defining time windows were some neurons are more likely to spike (phase-locking).

Contrary to the intuition that all neurons in a network generating Gamma would be *participating* to the rhythm, this analysis indicates that, only a small percentage of neurons has its activity modulated by the oscillation (either by phase-locking or by firing rate increase). We call this group of neurons as *Gamma participating* cells.

To better characterize the *non-participation* to Gamma rhythms, we followed each cell in each of the 5 waking periods present in the recordings, searching for behavioral changes. We observed that in different data segments, different groups of neurons were identified to participate to Gamma, indicating that the group of *Gamma participating* cells varies with time (see S6 Fig). Furthermore, cells that were classified as phase-locked in different data segments, had their preferred phase changed from one recording to the other (see cells 65 and 22 in S5 Fig). We called this feature as *dynamical phase preference*. Fig 3 indicates the individual cell *behavior consistency*, that is, how frequently a cell keeps being identified to a certain behavior: either being phase-locked or to have its firing rate changed inside Gamma bursts in a particular data segment. Stacked bars of Fig 3A and 3B indicate a color-coded behavior distribution of individual neurons, inside of the 5 data segments, with respect to firing rate change and phase-locking respectively. Neurons are ordered in a way in which inhibitory cells are displayed in the beginning. Red neuron indexes stand for FS cells and green neuron indexes stand for RS cells. Fig 3C and 3D depict the distribution among all recorded neurons of each behavior (C:

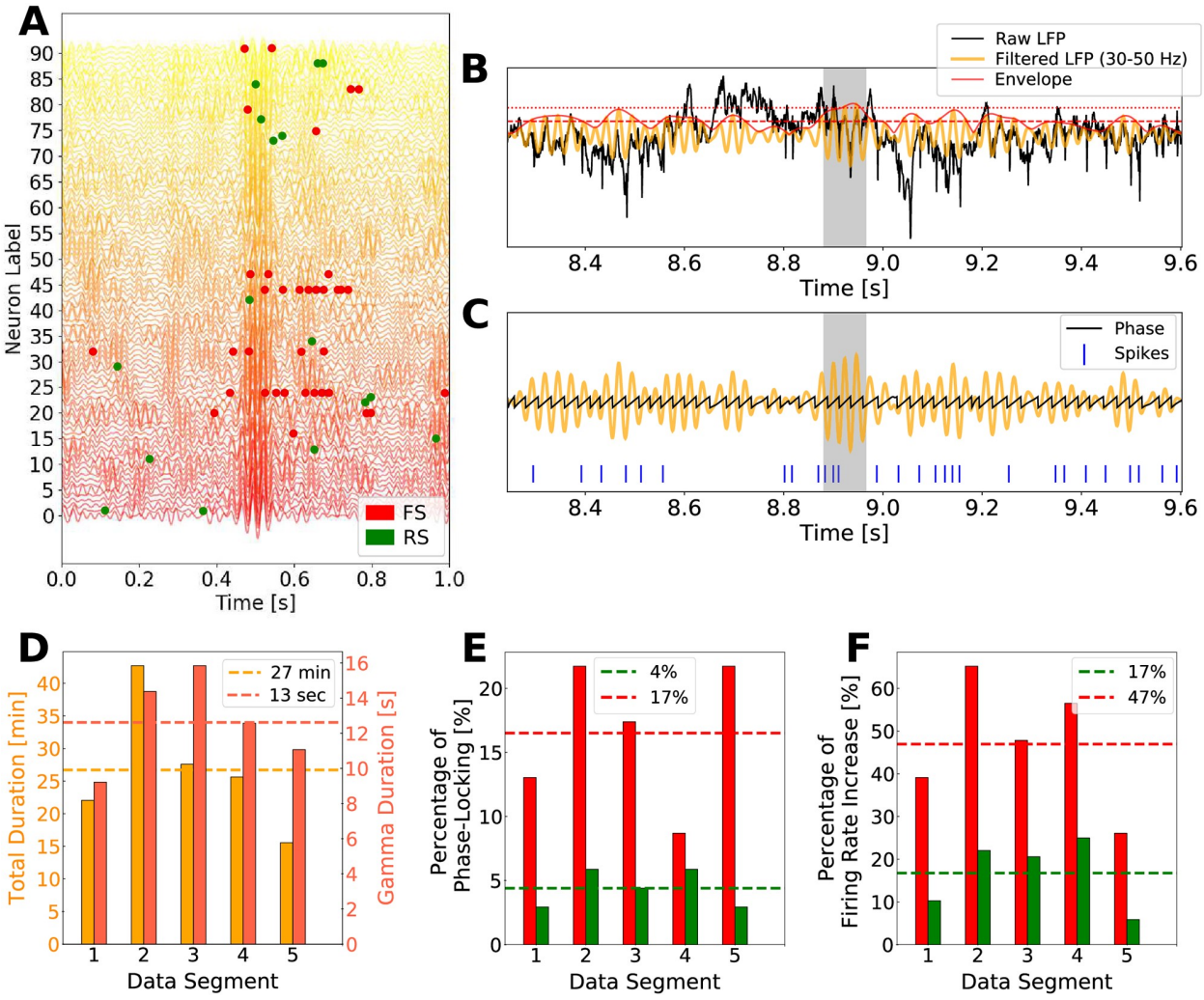

Fig 2. Human electrophysiological data. A: Simultaneously recorded LFP and multi-units activity. The Filtered LFP (30–50 Hz) of the 81 electrodes are shown together with the spiking times of 91 neurons. Some neurons were recorded by the same electrode, which had its LFP duplicated in the figure. The identification of Gamma bursts was done separately for each electrode. This way, neurons measured in a particular electrode, had their phases and firing rates analyzed exclusively with respect to the rhythm measured in its respective electrode. Spikes of Fast Spiking (FS) neurons, presumably inhibitory, are shown in red, and spikes from Regular Spiking (RS) neurons, presumably excitatory, are shown in green. B: Gamma periods detection. Raw LFP (black), band-pass filtered LFP (yellow) and Hilbert Transform Envelope (red) are shown. Gamma bursts were detected by means of the deviation from the average of the Hilbert Transform envelope (dashed red line) of at least 2 SDs (dotted red line), with a minimum duration of 3 Gamma cycles. The gray shaded region indicates one example of identified Gamma burst. C: Oscillation Phase extraction. The oscillation phases were obtained by the angle of the imaginary part of the Hilbert Transform. The phase distributions of each neuron were computed based on the oscillation phases where each neuron spiked. D: Data organization. Five awake periods could be recorded during one night. Each period had a different total time duration (yellow bars in minutes) and a different average duration of total Gamma occurrences (orange bars in seconds). Since each electrode was analyzed individually, the average indicated in the bars is the average among all the electrodes in the respective segment. E: Percentage of neurons identified as phase-locked in each data segment. The average amount of Phase-locked neurons in the five data segments was of 4% in RS and 17% in FS. RS neurons are shown in green and FS neuron in red. F: Percentage of neurons that increased their firing during Gamma, in each data segment. The average amount neurons in the five data segments which increased their firing during Gamma was of 17% in RS and 47% in FS. Same color scheme as in E.

https://doi.org/10.1371/journal.pcbi.1009416.g002

Firing Rate Increase, D: Phase-Locking). A behavior consistency of zero denotes that the indicated percentage of neurons never presented that behavior, while a behavior consistency of 5 denotes that the indicated percentage of neurons presented that behavior in all 5 data segments. FS cells tended to participate of Gamma bursts with higher consistency than RS cells.

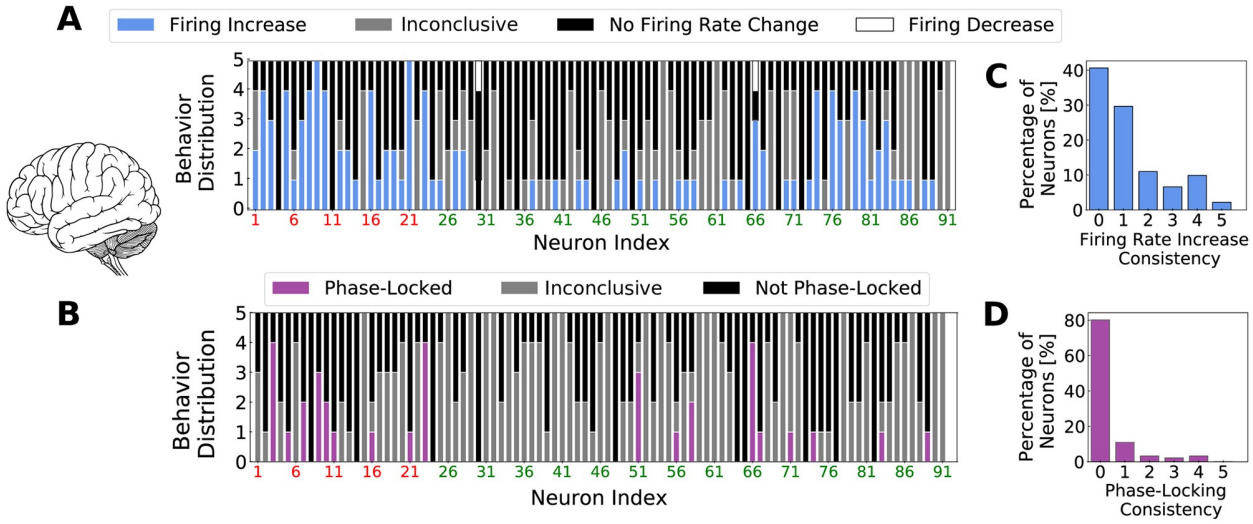

Fig 3. Individual neural behavior consistency on human recordings. Stacked bars indicating the color-coded distribution, inside of the 5 data segments, of individual neural behavior relative to firing rate change (*A*) and phase-locking (*B*). Neurons are ordered in a way in which inhibitory neurons are displayed in the beginning of the graph. Red neuron indexes stand for FS cells and green neuron indexes stand for RS cells. Items *C* and *D* indicate respectively the statistics of the consistency indexes among the recorded neurons for Firing Rate Increase and Phase-Locking.

https://doi.org/10.1371/journal.pcbi.1009416.g003

While 34.8% of FS increased their firing inside Gamma bursts in at least 4 of the 5 data segments, only 4.4% of RS cells did the same. Moreover 8.7% of FS cells kept being phase-locked in at least 4 data segments, in comparison to only 1.5% in RS population (see S7 Fig). Likewise, we call the reader's attention to the significant number of cells that never increase their firing rate inside Gamma bursts (Fig 3C, ≈ 40% of the recorded neurons) and to the significant number of cells that never presented phase-locking (Fig 3D, ≈ 80% of the recorded neurons). The behavior of individual cells during Gamma is quantified in S8 Fig.

Furthermore, another important aspect to be acknowledge is a possible correlation between high firing rate cells (inside Gamma bursts) and those cells that show higher phase locking. Nonetheless, the human data set used in this study is too small to be able to arrive to any conclusion. In our analysis cells with high firing rates were observed to be not phase-locked (or phase-locked), the same way as cells with lower firing rates were observed to phase-locked (or not phase-locked). See S9 Fig. The same is true if we try do drive conclusions about the co-occurrences of firing rate increase and phase-locking (see S6 Fig).

In summary our analysis shows that, during Gamma bursts, only a small percentage of the recorded neurons participate of the rhythm. This participation takes place in two ways: phase-locking and/or firing rate increase. FS cells presented significant higher level of phase-locking and firing rate increase in comparison to RS cells. Likewise the level of consistency behavior were also more marked in FS cells than RS cells. Our analysis further indicates that, the group of *Gamma participating* cells changes with time as well as their phase-preference.

Network models of Gamma oscillations

Gamma oscillations have been extensively modeled in the literature with different neuronal models and networks structures [23, 42]. The low and irregular firing rates observed during Gamma oscillations have been reproduced in recurrent networks of spiking neurons [13, 30, 43–45] by means of strong recurrent inhibition and strong noise (due to external inputs and/or due to synaptic disorder). Networks displaying this type of activity are known to be in the

firing rate regime [30]; in contrast to models fully synchronized, in which neurons behave as periodic oscillators. In this last regime, known as an *spike-to-spike regime*, neurons spike at every cycle (or once every two cycles), with an average firing rate close to the frequency of oscillatory network activity [46–54]

It is well established, experimentally and theoretically, that inhibition plays a crucial role in generating Gamma rhythms [21, 23, 29, 42, 55–59]. Nonetheless, it is still controversial [22–25] whether Gamma oscillations are generated by the exclusively interaction among inhibitory neurons [*Interneuron Gamma* (ING)] or via the interaction of inhibitory and excitatory neurons [*Pyramidal-Interneuron Gamma* (PING)]. Furthermore, a third mechanism, less explored in the literature, relies on the presence of pacemaker excitatory cells known as *Chattering neurons* [26, 27]. We named this third mechanism as *Chattering Induced Gamma* (CHING).

To compare to what degree each of three previously mentioned mechanisms can reproduce the observed experimental features, and what are the consequences of each mechanism, we constructed three neural networks working in the *firing rate regime*, adapted to generate Gamma by means of ING, PING or CHING. Network and neuronal parameters were chosen in a way to allow each model to reproduce experimental features as well as possible, with physiologically plausible firing rates and membrane conductance distributions (see S10 and S11 Figs). We call the reader's attention to the fact that, while networks with a structure similar to our *PING Network* have been largely used in the literature, the structures of *ING* and *CHING Networks* were developed exclusively for this study.

Like in previous works [60], all three networks are capable of generating spontaneous Gamma bursts. These Gamma bursts are controlled by fluctuations of recurrent drive generated by the network dynamics, which for this reason occur irregularly and in an unpredictable fashion. However, more predictable Gamma bursts can be obtained by increasing the external drive (in all three networks). Fig 4 shows the behavior of the three networks when a fluctuation on the Poissonian input generates Gamma, mimicking the Gamma bursts observed experimentally. Note however that, outside of Gamma bursts (low input amplitude), the networks do not necessarily display a pure AI state: all three networks display reminiscent low-amplitude oscillations. In all cases, the firing dynamics remained irregular and with low synchrony, so we called them *AI-like states*.

We next performed on the network models an equivalent analysis as in the human data recordings. Each cell was followed in 5 different simulations containing on average 13 seconds of Gamma bursts (same duration as in the experimental recordings, mimicking the five experimental data segments) and statistical tests to identify phase-locking and firing rate changes were performed. Fig 5A, 5B and 5C display respectively the quantification of behavior consistency for *PING*, *ING* and *CHING* Networks. Accordingly to the unit recordings [21], the cells were generally more depolarized and increased their firing during Gamma. On the other hand, within the three models, only the *ING Network* (Fig 5Bc) is capable of describing the appropriate amount of neurons that increase their firing in different data segments, during Gamma. The *PING* and *CHING* networks predict an over-estimation of this number. The presence of a sub-population of highly connected inhibitory neurons, capable of generating Gamma rhythms by their own (see *Neuron and Network Models: Gamma Network* in Materials and methods Section), allows the *ING Network* to provide a compensation for external excitatory fluctuations: whenever there is an augmentation of input in the network (generating Gamma), there is in addition a concomitant augmentation of inhibition thanks to the FS2 population.

In comparison to the experimental data analysis performed previously, all three models are capable of correctly describing the frequency of re-occurrence of phase-locking inside of a group of neurons in different data segments. That is, all three models predict the same the

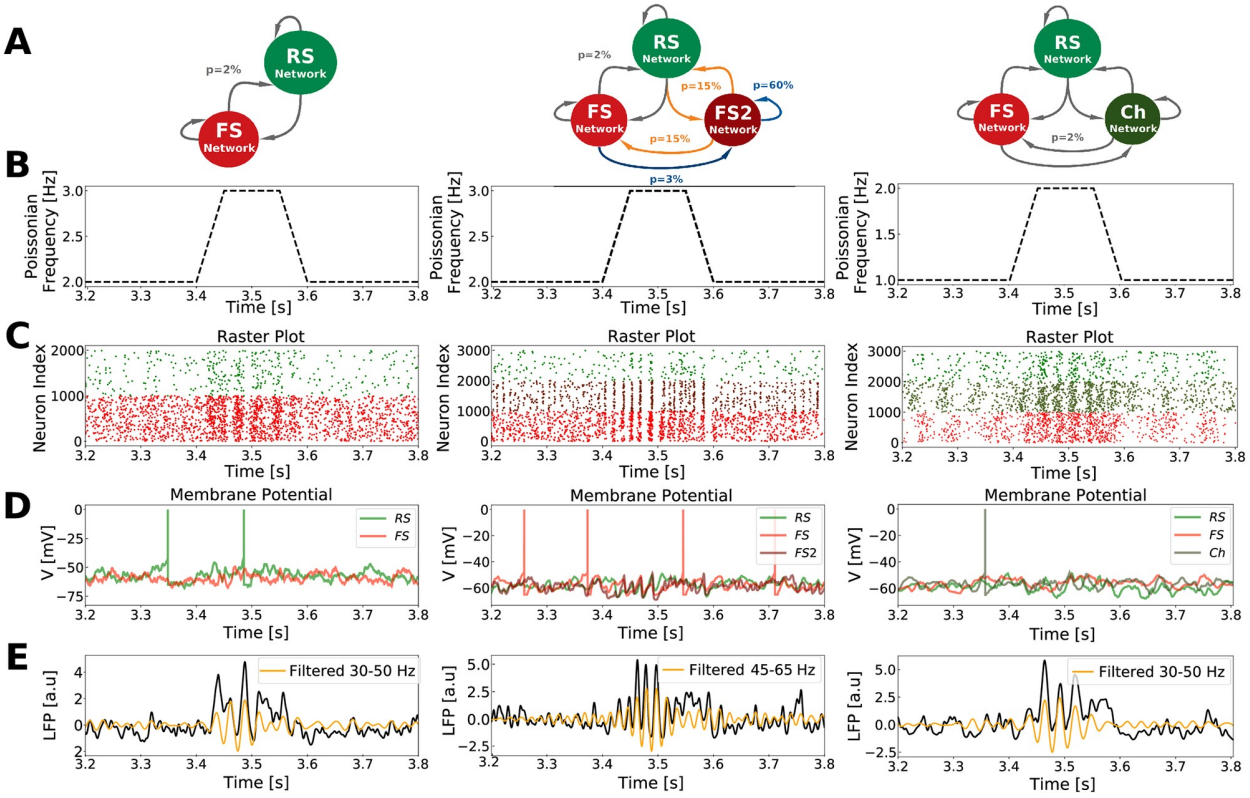

Fig 4. Neural activity of different Gamma generation mechanisms networks. *PING Network* (left), *ING Network* (middle) and *CHING Network* (right). A: Scheme of each network structure and pattern of connectivity. B: External Poissonian noise fluctuation generating Gamma bursts. C: Raster plot of network activity inside and outside Gamma bursts. Only 1000 neurons of each cell type are shown. D: Membrane potential activity of randomly picked neurons of each type. Pay attention to the well defined subthreshold oscillation exclusively present in the *ING Network*. E: Simulated LFP (raw—in black) and its filtered version (yellow).

https://doi.org/10.1371/journal.pcbi.1009416.g004

same intensity of *phase-locking consistency* as the one observed on the human recordings (Fig 3D). On the other hand, regardless of the mechanisms of Gamma generation, all networks predict an over estimated phase-locking level (total number of phase-locked neurons per data segment) (see S12 Fig). With respect to the human data set, the *PING* and *ING* networks predict a comparable level of phase-locking in the excitatory population but an exaggerated level in the inhibitory population. In contrast, the *CHING Network* predicts a comparable level of phase-locking in the inhibitory population but an exaggerated level in the excitatory one. Side by side, the *CHING Network* is the one that still captures the best the level of phase-locking in both populations (excitatory and inhibitory).

The right prediction of phase-locking consistency can be explained by the type of activity regime in which each network works: the *fluctuation-driven regime*. Since this regime allows neurons to spike with low firing rates in an irregular fashion, participating of the global Gamma oscillation only in certain cycles due to the subthreshold randomness. Nonetheless, the over-estimation of phase-locking level, indicates that the simple fact of being in the *fluctuation-driven regime* is not enough to capture all levels of description. We hypothesize that the network structure play a key role in the way neurons behave during oscillations. Fig 5 illustrates how different network structures (different connectivities in the ING Network or different neuron types in the CHING Network) influence network activity.

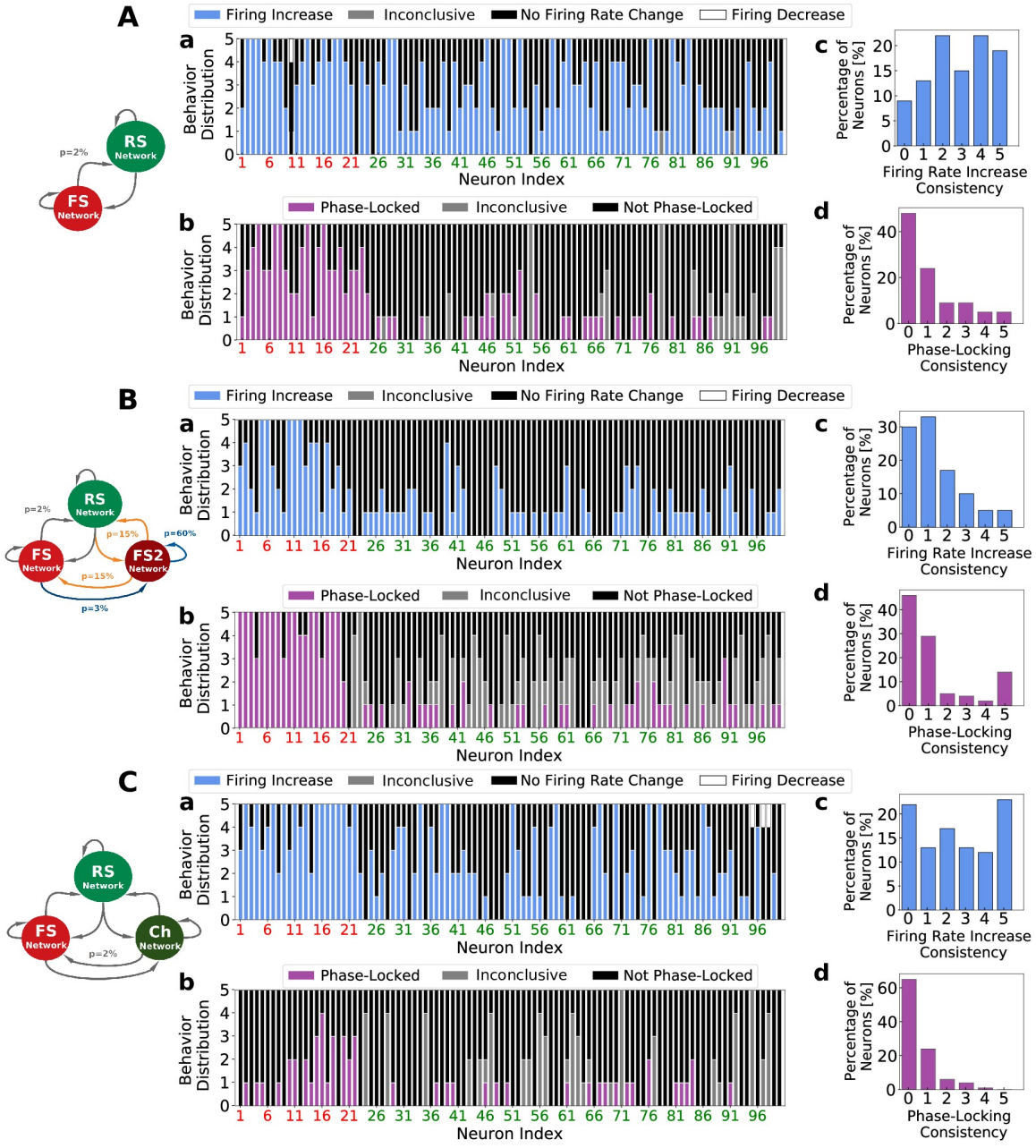

Fig 5. Individual neural behavior consistency in computational models. A: *PING Network*. B: *ING Network*. C: *CHING Network*. Same analysis and color codes used in Fig 3. To mimic the five experimental independent data segments in the Human data recordings (Fig 3) on the network models, five simulations (per model) were performed, containing on average the same amount of total Gamma bursts duration as in the experimental data (13 seconds). In addition, to match the number of recorded neurons in the experimental data, in the models a subset of 100 randomly picked neurons were selected in each case.

https://doi.org/10.1371/journal.pcbi.1009416.g005

In the presented human recordings, inhibitory neurons tended to spike earlier in the cycle than excitatory neurons. Fig 6 shows the phase preference with respect to the Gamma cycle of all the neurons considered phase-locked in the human data recordings (Fig 6A) and in each of the three developed networks (Fig 6B, 6C and 6D). The *ING* and *CHING* networks predict the

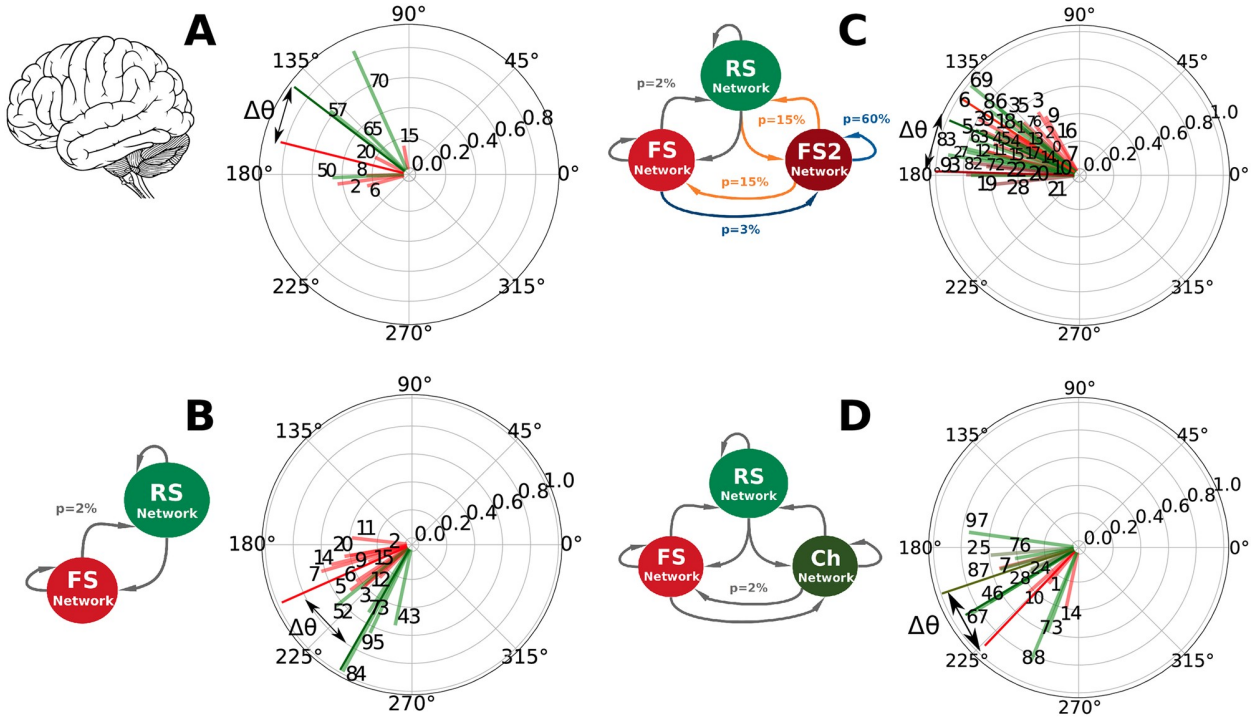

Fig 6. Phase preference of phase-locked cells. A: Human Data (Data segment 2). B: *PING Network* Data. C: *ING Network* Data. D: *CHING Network* Data. The preferred phases of each phase-locked cell are displayed in polar graph representation. Note that, since phases were calculated from $-\pi$ to π (see *Spike-LFP phase-locking* in Materials and methods Section), these polar graphs should be interpreted clockwise with time. The vector size gives a measure of the phase distribution of each cell. Big amplitude vectors indicate very concentrated distributions while small amplitude vectors indicate less concentrated ones (see S3 Fig). The color of each vector encodes the type of the cell of whom it represents the phase: red (FS), dark red (FS2), green (RS) and dark green (Ch). Cell number IDs are indicated. Dark colored vectors indicate the average phase among each neuron type and $\Delta\theta$ the phase difference among them. Data segment 2 presented 43 minutes of recordings, containing 14 seconds of Gamma activity.

https://doi.org/10.1371/journal.pcbi.1009416.g006

same relationship as observed in the human recordings (inhibition preceding excitation) while the *PING Network* predicts the opposite. Moreover, in the same way as the human data set (S5 Fig), cells that were classified as phase-locked, have their preferred phase changed from one simulation to other (dynamical phase preference). We argue that this feature is also a consequence of the *fluctuation-driven regime*.

The phase relationship between excitation and inhibition is an important aspect to be discussed, since it has been suggested to be a marker of the type of Gamma generation mechanism [25]. It has been shown theoretically by [45] that, in models composed of conductance based neurons (neurons that include non-linear spike generation mechanisms on their equations) the spiking order of excitatory and inhibitory populations depends exclusively on single-cell characteristics. Based on their analysis, when the I_{AMPA}/I_{GABA} ratio is the same in excitatory and inhibitory neurons, excitatory cells tend to follow the inhibitory ones in most of the physiologically plausible parameter space. On the other hand, when the ratio of excitation to inhibition is weaker in excitatory cells than in inhibitory ones, excitatory cells tend to precede inhibitory neurons [30, 45]. In our simulations, the only network in which this theory can be directly applied (because of the network structure) is the *PING Network*, in which the I_{AMPA}/I_{GABA} ratio in excitatory cells is weaker than in inhibitory cells. Interesting discussions about neural properties and population phase-differences can also be found on [61, 62].

Concluding this section, we showed that network models working in the *firing rate regime*, regardless of the mechanism of Gamma generation, can reproduce qualitatively some of the

most important features of experimental neural activity during Gamma: phase-locking consistency and dynamical phase preference. On the other hand, all models predict an overestimation of the phase-locking levels. Additionally, only the *ING Network* model was capable of describing a reasonable level of firing rate increase inside Gamma bursts, as found in the human recordings. We advocate that just the simple fact of being in the fluctuation-driven regime is not enough to capture all levels of description of Gamma oscillations, and hypothesize that the network structure play a key role in the way neurons behave during oscillations.

Considering that the different types of spontaneous activity exhibited by the three presented models could greatly influence how the network processes external input, we have investigated this issue of responsiveness to external input in the next section.

Responsiveness and resonance during Gamma oscillations

Responsiveness. The way information is encoded and processed in the brain is still a largely investigated enigma. Several ways of encoding information have been considered, such as firing rates [63, 64], pairwise correlations [65, 66], spike pattern irregularity [67–70] and spike packets [71], among others. In particular, two main theories have been dominating the debate: *Temporal Coding* in which individual neurons encode information by means of precise spike timings (working as coincidence detectors), and the *Rate Coding* in which neurons encode information by means of changes in their spike rates (working as temporal integrators). Regardless of the encoded strategy used to encode information, the way the network is capable of responding to a certain stimulus is of prime importance. To identify how Gamma rhythms change the response properties of a network to an external stimulus with respect to AI, in this section we applied two protocols, investigating the effect of Gamma in both, the *coincidence detection mode* and in the *integration mode* [72, 73].

In the *integration mode* protocol, we compared how each of the three developed models responded to slowly-varying inputs (occurring in a time window much bigger than the Gamma period). In this protocol, each network received Poissonian drive (spikes from an external network) with firing rates varying in time, in a Gaussian manner, both during Gamma and AI-like states. The applied Gaussian inputs had a standard deviation of 50 ms, allowing the stimulus to interact with different Gamma cycles. Several amplitudes of slowly-varying Gaussian were tested, and the *responsiveness* of excitatory and inhibitory populations were measured separately. *Responsiveness* (see Eq 5) was defined as the difference between the total number of spikes (in a time window of duration T) generated by the whole network in the presence and in the absence of the stimulus (normalized by the network size and the time window duration T).

Fig 7 shows the *responsiveness* of the *PING Network*, the *ING Network* and the *CHING Network*, when the *integration mode* protocol was applied. To be able to measure the real impact of Gamma oscillations on network responsiveness, we used as a control the responsiveness curves from the AI-Network, in which no oscillation is generated, independently of the level of external drive. See *Neuron and Network Models: AI Network* in Materials and methods Section and S13 Fig. All models, regardless of the mechanism of Gamma generation, were less responsive during Gamma bursts in comparison with their baseline responsiveness during AI-like states. Furthermore, the responsiveness of a network in a real AI-state (gray curve generated by the AI Network) is equal or higher to the AI-like responsiveness, in each of the networks, and is always higher then the Gamma state responsiveness in all cases. In addition, to further investigate this result, we examined the responsiveness of individual cells (S14 Fig). Due to the previous finding that only a restricted group of cells *participate* to Gamma, one could imagine that there could still be few cells (*Gamma participating* cells) that would be more responsive,

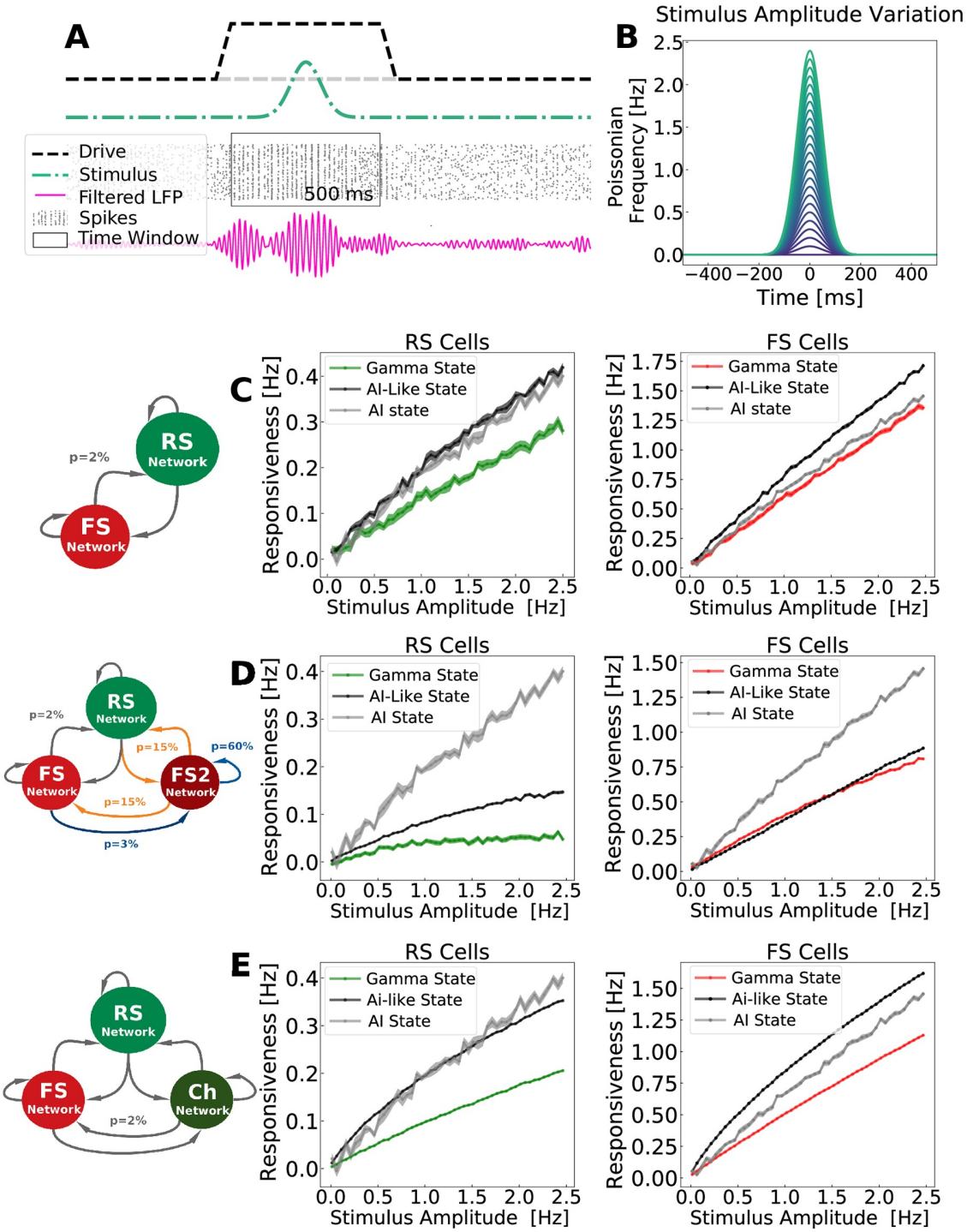

Fig 7. Network responsiveness to a Gaussian input with varying amplitude. The *responsiveness*, in different states (Gamma and AI-like), was measured in the three developed networks and compared to the responsiveness of the *AI Network* as a control. A: Responsiveness protocol scheme for Gamma state. A Gamma burst is generated due to fluctuations of the external drive (black dashed line). During the Gamma activity, a Gaussian input (green line) is applied. The total number of spikes due to the stimulus, in time window of 500 ms, is measured. To measure the total number of spikes in the absence of the stimulus, another drive fluctuation is created generating Gamma. The total number of spikes inside of a time window of 500 ms is measured again (this time, without the Gaussian input). Only the situation in response to a stimulus is depicted in the scheme. This procedure was repeated 100 times per each Gaussian amplitude input. To measure responsiveness in AI and AI-like states no drive fluctuation was applied (the black dashed line in the figure

was kept constant). B: Input Amplitude Variation. The stimulus consisted of a Gaussian fluctuation in the firing rate of the external drive. The Gaussian amplitude varied from 0.05 Hz to 2.5 Hz (step of 0.05 Hz) and had a standard deviation of 50 ms. Items C, D and E display respectively the responsiveness of the *PING Network*, the *ING Network* and the *CHING Network*, inside Gamma bursts (green for excitatory cells, red for inhibitory cells), and outside Gamma bursts—AI-like activity—(black for both types of cells). Every point corresponds to the average responsiveness measured in 100 simulations. Standard error of the mean are indicated by the shaded region around each curve. The responsiveness of the *AI-Network* was added as a control in each case (gray curve in C, D and E). To implement the responsiveness protocol the *AI-Network* received a constant drive with $\mu_{Ext} = 3$ Hz, in addition to the Gaussian inputs. See S13 Fig.

https://doi.org/10.1371/journal.pcbi.1009416.g007

while all others (*Gamma non-participating* cells) would be less responsive, leading to a yet overall less prominent responsiveness. Nonetheless, S14 Fig shows the contrary. All cells seem to follow the same decrease of responsiveness during Gamma oscillations, and we found no evidence that some subset of cells would be more responsive, for all amplitudes tested.

In the *coincidence detection mode* protocol, the responsiveness at different Gamma phases was measured. To do this, precisely-timed inputs (occurring in a time window much smaller than the Gamma period) were applied and related to Gamma cycles in each of the three developed networks. In this protocol the amplitude of the stimulation was kept constant, while the time of the application of the Gaussian stimulus changed with respect to the phase of the Gamma oscillation. This procedure allowed each network to be stimulated at different Gamma phases (see S15 Fig). Fig 8 indicates the network response of excitatory cells per Gamma phase, in different states: Gamma state (blue), AI-like (black) and AI-like modulated by a control external current oscillating at Gamma frequency (gray). All responses were normalized by the average response of AI-like states without external current modulation (black).

AI-like states, when modulated by an external oscillatory current, displayed, in all network models, preferred phases in which the network response was higher in comparison to the non-modulated AI-like state. This constitutes an important control, because the external current creates periods of higher and lower excitability in the network, which is translated in a phase-dependent response (as shown by the gray curves in Fig 8). Likewise, when generating Gamma, our models (PING and ING) demonstrate an equivalent type of phase-dependence response (even-tough with a narrow amplitude range). On the other hand, in agreement with the *integration mode* protocol, our simulations show that the responsiveness during Gamma states at all phases are less or equal to that during AI-like states.

Resonance. In Physics, when dealing with an oscillatory system, one of the first features to be explored is its resonant properties. In general, *resonance* describes the phenomenon of increased amplitude in a system, that occurs due to the application of an oscillatory stimulus whose frequency is equal or close to the natural frequency of the system. It has been shown experimentally that this phenomenon can also be observed in inhibitory [56] and excitatory [74] neuronal populations. Furthermore, theoretical studies [75] have shown that resonance is a fundamental property of spiking networks composed of excitatory and inhibitory neurons. Resonance has also been proposed as a mechanism to gate neuronal signals [76] and to communicate information [10].

We tested the resonant properties of each of our networks in AI-like and Gamma states. In this protocol, each network received Poissonian drive with firing rates varying in time in a sinusoidal manner, with different frequencies (Fig 9A). Fig 9B, 9C and 9D depict, for each frequency and oscillation phase, the average number of spikes per RS neuron and time bin, during Gamma and AI-like states, for the *PING*, *ING* and *CHING* Networks. All values were normalized by the average firing inside of each state to exclude the state dependent firing rate level (which is higher on Gamma). To enhance the comprehension of the responsive properties of each network, a linear version of the color maps depicted in Fig 9 (amplitude vs. phase)

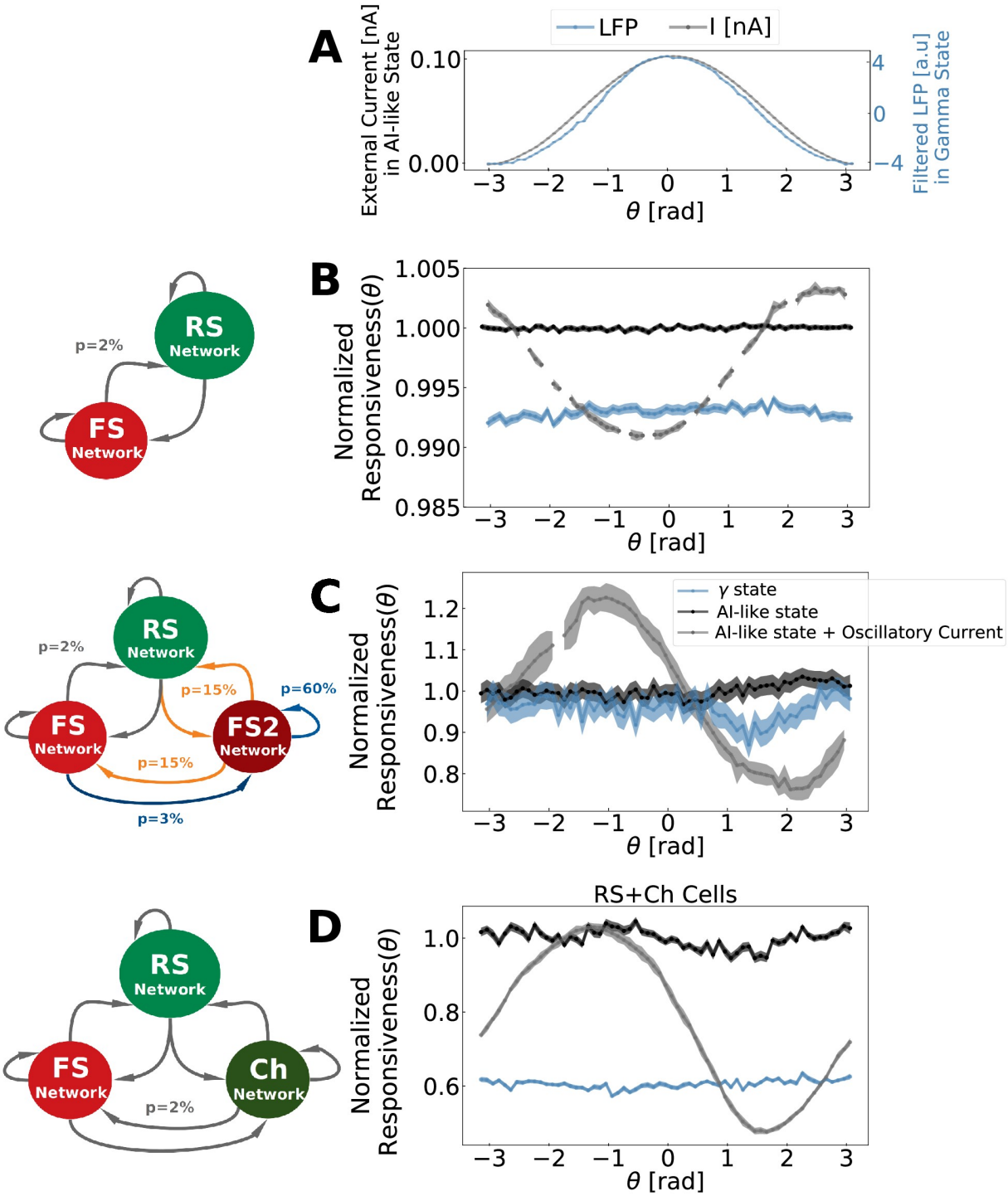

Fig 8. Phase-dependent network response. A: External oscillatory current applied at AI-like state as function of its oscillation phases (gray curve) and the filtered LFP measured during Gamma states as function of its oscillation phases (blue curve). All networks received a current oscillating from 0 to 0.1 nA in a sinusoidal manner with a Gamma frequency F_γ. To match the Gamma oscillation frequency generated by each network, the frequency of the external current applied to PING and CHING networks was $F_\gamma = 40$ Hz, while the one applied to ING network was $F_\gamma = 55$ Hz. The LFP depicted is the one from PING network. ING and CHING also displayed a similar LFP pattern. B: *PING Network* phase-dependent response C: *ING Network* phase-dependent response. D:*CHING Network* phase-dependent response. The phase-dependent network response was calculated according to Eq 6, in a time window of duration T equal to one Gamma cycle (T = 25ms for the PING and CHING Networks and T = 18ms for

ING). Responses measured inside AI-like activity (outside Gamma bursts) are shown in black, and in gray when the networks received a supplementary oscillatory external current. Responses measured inside Gamma bursts are displayed in blue. All curves were normalized by the average response inside AI-like activity without external current modulation. Solid lines indicate the average, and the shaded region indicates the standard error of the mean. The curves were calculated based on the output of 12000 simulations (120 positions of the Gaussian stimulus in 100 numerical seeds for external Poissonian drive). The Gaussian stimulus used had an amplitude of 50 Hz and standard deviation of 1 ms.

https://doi.org/10.1371/journal.pcbi.1009416.g008

is provided in S16 Fig. In addition, S17 Fig depicts the resonant properties in other cell types (FS, FS2 or Ch) during Gamma state for each one of the networks.

We observe that, in both AI-like and Gamma states, all models display resonant properties around the Gamma band, with the main difference in between these two states being a shift of the resonance frequency center. In this protocol we detect a similar level of responsiveness per phase (reflected in the measured number of spikes per time bin) in AI and Gamma, indicating that networks receiving oscillatory inputs have the same latent potential to resonate at Gamma ranges regardless if they are displaying AI or Gamma oscillations. One should note that each model presents its own particularities. While the PING network presents just a shift of the center frequency of resonance, the ING network presents an enlarged potential of resonance in AI (in addition to the frequency shift). During AI, the ING network presents an equal resonance in several bands other than Gamma. Moreover, when a Gamma oscillation is triggered in this network, this resonance is shrunk and becomes more concentrated in the Gamma band. The CHING network, on the other hand, presents a strong resonance in the 15–25 Hz frequency range during AI, while during Gamma this resonance is lost.

Concluding this section, we investigated three dynamical properties (Responsiveness, Phase-dependent-responsiveness and Resonance) in different states (AI-like and Gamma) of each of the three developed networks. We encounter that, regardless of Gamma generating mechanism (PING, ING or CHING), the network responsiveness, in both *coincidence detection* and *integrative* mode, is decreased at Gamma states with respect to AI. On the other hand, the resonant properties around the Gamma band in all networks did not change significantly from one state to the other. The main resonant properties changes between AI and Gamma states in each model were most prominent around other bands. The implications of these observations on the role Gamma rhythms in neural computations and information transfer will be discussed in the next section.

Discussion

In this paper, we have examined the genesis and responsiveness of Gamma oscillations constrained by human recordings. We analyzed Gamma oscillations from previous studies [20, 21], where the recordings were stable, and in which RS and FS cells were discriminated. We compared the results of this analysis to conductance-based network models implementing three different mechanisms that were proposed for Gamma oscillations, PING, ING and CHING. We next examined these three networks with respect to their responsiveness and resonance to external inputs. We discuss these aspects below.

Human data analysis

Compared to a previous analysis of the cellular correlates of Gamma oscillations [21], we confirm here the low level of cellular engagement and a greater participation of FS cells during Gamma, either through phase-locking or through firing rate increase. FS cells not only presented a higher percentage of phase-locking or firing rate increase during Gamma, but they also presented a more consistent behavior compared to RS cells which were much more variable. Our analysis further indicates that, the group of Gamma participating cells changes with

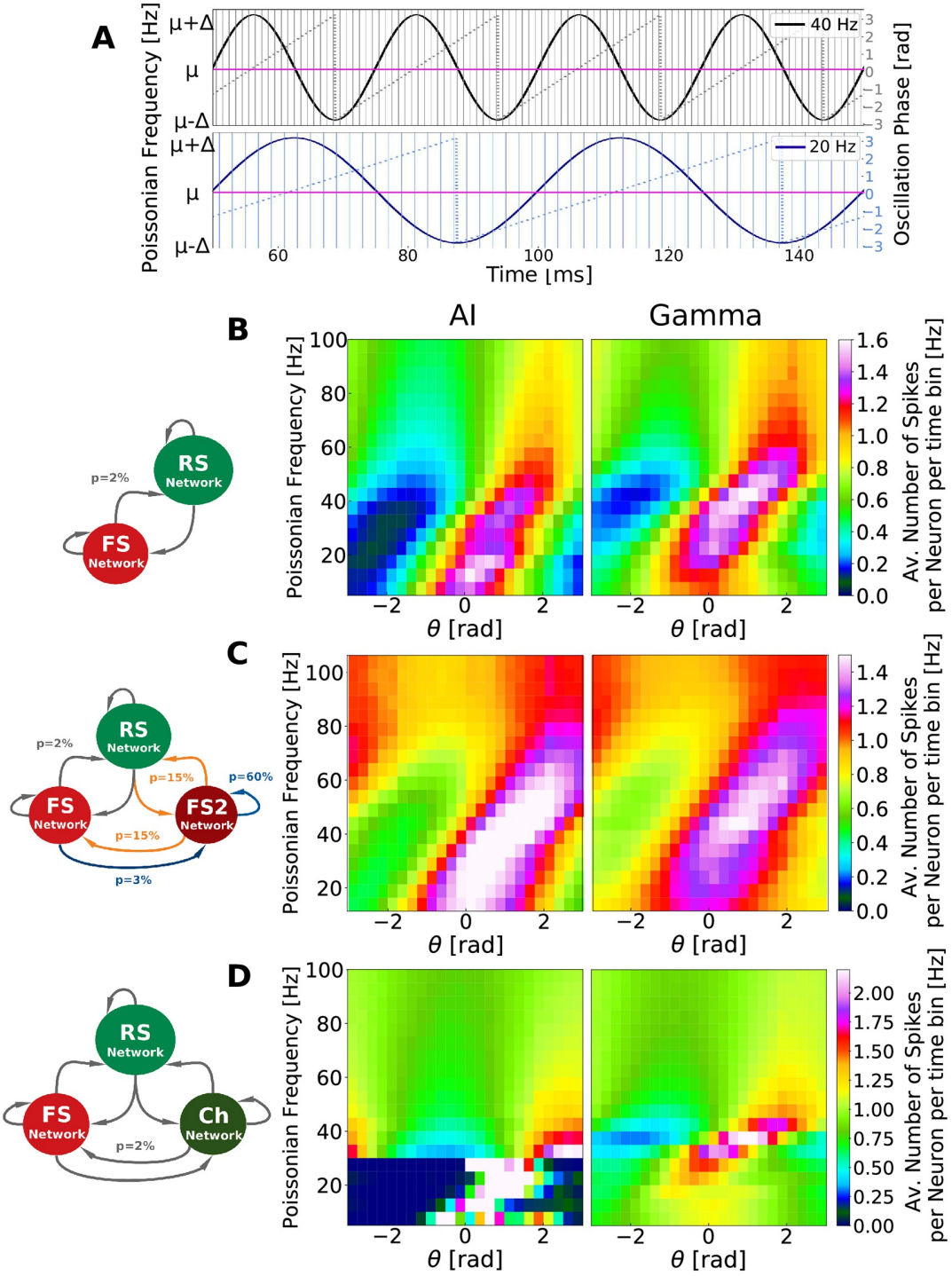

Fig 9. Resonant properties of computational models. A: Representation of external Poissonian noise varying in time in a sinusoidal manner around μ_{noise}. In this protocol sinusoidal frequencies varied from 5 Hz to 100 Hz (step of 5 Hz). Two oscillatory frequencies are depicted: 20Hz (blue) and 40 Hz (black), together with their phases (second axis) and time bins (vertical line). For all frequencies the average Poissonian noise (μ_{noise}) was kept the same, varying from $\mu_{noise} - \Delta_{noise}$ and $\mu_{noise} + \Delta_{noise}$. The bins were chosen in a way in which the oscillatory phases (from $-\pi$ to π) were divided into 25 intervals (for all frequencies), resulting in time bins of different duration for each oscillatory frequency. B: Resonant properties of *PING* Network. C: Resonant properties of *ING* Network. D: Resonant properties of *CHING* Network. The color maps displayed in B, C and D depict, for each oscillatory frequency and oscillation phase, the average number of spikes per RS neuron per time bin, during Gamma and AI-like states. All

values were normalized by the average firing inside of each state to exclude the state dependent firing rate level (which is higher on Gamma). Δ_{noise} = 0.5 Hz in all network models but μ_{noise} varied in each case. For AI, in PING and ING Networks μ_{noise} = 2 Hz and in CHING Network μ_{noise} = 1 Hz, while for Gamma, μ_{noise} = 3 Hz in in PING and ING Networks and μ_{noise} = 2 Hz in CHING Network.

https://doi.org/10.1371/journal.pcbi.1009416.g009

time as well as their phase-preference. The analysis performed on this work is very qualitative, since it was based on a single patient. Nonetheless, this very sparse participation of RS and FS cells during Gamma was seen in different patients, and the same was observed in monkey for beta oscillations [21].

Responsiveness

The occurrence of Gamma rhythms have been correlated with conscious perception [77–81] and several authors support these rhythms as being a suitable marker of consciousness. On the other hand, it has been proposed that the Asynchronous and Irregular activity, observed during awake and aroused states, due to its specific responsiveness properties, is an ideal setting for integrating multiple external inputs [12]. In support of this, it was concluded in a review that asynchronous states constitute the most reliable correlate of conscious states [82].

Previous work [12] has compared the responsiveness of a fully synchronized network (spike-to-spike regime) with a network in AI state, showing that the AI state is the best state to integrate multiple external inputs. It was also shown that, in rate-based networks, the most chaotic states could display the highest responsiveness, as measured using Shannon information [83]. In the present work, we compared the responsive properties of AI state with Gamma states generated by means of three different mechanism: PING, ING and CHING. Each of these networks were submitted to two types of inputs. First, a slowly-varying input integrated by the population of neurons over a substantial period of time (*integrative mode*). Second, we examined precisely-timed inputs, occurring in a time window smaller than the Gamma period (*coincidence detection mode*). For the *integrative mode*, we systematically found that the Gamma oscillations yielded less responsiveness than the AI-like states and even lesser responsiveness than real AI states (generated by the *AI Network*, used as a control). In the *coincidence detection mode*, we found that the response was only weakly modulated by the phase of the Gamma. This was assessed by comparing the Gamma oscillation to a sinusoidal control input, in which case the response was clearly phase-dependent. In agreement with the *integrative mode*, the responsiveness measured in the *coincidence detection mode* protocol was generally higher for the AI-like states. In addition, in the *coincidence detection mode*, among the three models, the *ING Network* is the only one that presents a similar responsiveness between Gamma and AI states, which stresses again the importance of network topology on networks behaviors.

A smaller responsiveness during Gamma states is somehow surprising since neurons are in general more depolarized in this state and additionally increase their firing, as we showed in our data analysis. On the other hand this observation is intuitively easy to understand, if we take into account the fact that Gamma oscillation are composed of successions of periods of high inhibition, which define time windows in which neurons are less likely to spike. While during Gamma states, these time windows of high inhibition constrain the times a certain neuron can spike, during AI states neurons can spike at all moments with the same probability. Indeed, we observed that the response during Gamma oscillations is phase-dependent, while there is no phase preference during AI states. However, although there was a phase dependence, Gamma oscillations did not provide a preferred phase where the network is more responsive than during AI states. The fact that higher levels of inhibition during Gamma could

explain their diminished responsiveness should be testable experimentally using intracellular recordings *in vivo*.

Given our model results, what this decrease of responsiveness could be useful for, and what are the advantages of a higher responsive state in AI? This questions can be approached in the light of the *Phase Coding Theory* (PC). This theory was initially formulated with respect to Theta rhythm [6], but lately extended to Gamma [7]. This theory states that, within the Gamma cycle, the excitatory input to pyramidal cells is converted into a temporal code whereby the amplitude of excitation is re-coded in the time of occurrence of output spikes relative to the cycle [7]. In this view, the cells that are most excited fire earlier in the cycle, while cells that are not excited enough are prohibited to spike due the new wave of inhibition composing the cycle. This process can be seen as a winner-take-all phenomena (or more precisely a few-winners-take-all phenomena, since it involves several neurons neurons) [7]. Such a coding strategy enables transmission and read out of amplitude information within a single Gamma cycle without requiring rate integration, proving a fast processing and readout by means of coincidence detection, rather than on rate integration [84], in agreement with more recent work [60, 76, 85]. Furthermore, this type of encoding strategy would, in principle, allow an improvement of signal-to-noise ratios, since neurons not conveying information would be hindered to spike. In this perspective, according to our models, Gamma oscillations would allow a network to respond quicker at the expense of decreasing the strength of its response. On the other hand, more responsive states such as AI, would be better suited to respond to low amplitude stimulus (due to their high sensitivity) at the cost of loosing temporal precision. Thus, AI states, because of their high responsiveness, seem well suited to detect inputs, while gamma oscillations, due to their tighter time precision, seem better suited to transmit timing information. Such possibilities constitute interesting directions to explore by future models.

Resonance

In this work we reproduced previous results [75] showing that resonance is a fundamental property of spiking networks composed of excitatory and inhibitory neurons. We compared the resonant properties during AI and Gamma states generated by three different mechanism (ING, PING and CHING) and verified that, apart from a shift on the resonant frequency center, the resonant properties around the Gamma band in all networks did not change significantly from one state to the other. We call the reader attention to the particularities of each network model, especially the enlarged potential of resonance of ING network during AI.

Even though previous work proposed the importance of resonance in information transfer and processing in the brain [10], this aspect has been left aside until recently [86]. The most popular view, known as the Communication Through Coherence (CTC) Theory [8, 9], proposes a mechanistic explanation for how different neural regions could communicate by means of *coherence* [60]. This theory advocates that, since oscillations generate a rhythmic modulations in neuronal excitability (defining time windows in which neurons are capable to respond), only coherently oscillating groups can effectively communicate. In contrast, a recent work [86] present results indicating that, to the contrary, *coherence* is a consequence of communication, not a cause of it. This study shows that if an oscillating network is connected to another network that owns resonant properties around this same frequency, these two networks present *coherent* activity, and that the presence of these resonant interactions could explain more than 50% of the observed *coherence*. Furthermore, they show that the oscillating network sends information to the resonant one (the *Granger-causality* between field potentials is dominated by oscillatory synchronization in the sending area).

In this perspective, the enlarged potential of resonance of ING network in different bands during AI, indicates that this type of network structure (with heterogeneous connectivity patterns in between inhibitory neurons) could potentially convey information equally well in several bands. This stress the importance of network topology for neuronal information processing and also constitutes interesting directions to further explore.

Supporting information

S1 Fig. Synaptic time scale parameter search of a network composed of RS and FS neurons randomly connected. The network used to produce this figure was composed of 20000 excitatory Regular Spiking and 5000 inhibitory Fast Spiking neurons connected randomly with a probability of connection of 2%. All synapses were delayed by a time delay of 1.5 ms, and had reference synaptic strengths of $Q_e^R = 1$ nS or $Q_i^R = 5$ nS and reference synaptic time scales of $\tau_e^R = \tau_i^R = 5$ ms. Synaptic strengths ($Q_{e,i}$) were normalized at each tested time scale ($\tau_{e,i}$) to keep the same synaptic gain, such that: $Q_{e,i} = (Q_{e,i}^R.\tau_{e,i}^R)/\tau_{e,i}$. A: Network oscillation frequency depicted in a color scheme as a function of excitatory and inhibitory synaptic time scales. White color corresponds to regions in which no oscillation was identified in RS population. B: Synchrony Index of RS population (top) and network balance (bottom) as a function of synaptic time scales. The Synchrony Index (SI) is based on the auto-correlation of the population frequency of RS cells. To be calculated, the autocorrelation of the population frequency was fitted by a damped cosine function and the value of this fitted function at zero time lag was defined as the SI. If the exponential decay rate was higher then 100, it was considered that there was no global oscillation at the population scale. The network balance was defined as the rate between the average excitatory and inhibitory synaptic currents, $\langle \frac{\langle I_{exc} \rangle_N}{\langle I_{inh} \rangle_N} \rangle_t$, in which $\langle \rangle_N$ stand for average among neurons and $\langle \rangle_t$ average on time. White squares indicate the two different parameter sets used in our simulations ($\tau_e = \tau_i = 5$ ms for *AI Network*, and $\tau_e = 1$ ms, $\tau_i = 7.5$ ms for *PING Network*). C: Same as B but calculated for the FS population. D: Population frequency autocorrelation of RS (green dots) and FS population (blue dots) neurons of the two used parameter sets. Solid lines indicate the damped cosine fitted function.
(TIF)

S2 Fig. *Gamma Network* parameter search. The network connectivity (p) vs. inhibitory synaptic strengths (Q_i) parameter space of the Gamma Network are displayed as color-plots. A: Average spiking frequency. B: Network oscillation frequency. C: Network balance: rate between the average excitatory and inhibitory synaptic currents, $\langle \frac{\langle I_{exc} \rangle_N}{\langle I_{Inh} \rangle_N} \rangle_t$, in which $\langle \rangle_N$ stand for average among neurons and $\langle \rangle_t$ average on time. D: Membrane Potential Synchrony (χ), calculated by means of the equation: $\chi^2 = \frac{\sigma_V^2}{\frac{1}{N}\Sigma_i^N \sigma_{V_i}^2}$, in which $V(t) = \frac{1}{N}\Sigma_i^N V_i(t)$, ${\sigma_V}^2 = \langle [V(t)]^2 \rangle_t - [\langle V(t) \rangle_t]^2$ and ${\sigma_{V_i}}^2 = \langle [V_i(t)]^2 \rangle_t - [\langle V_i(t) \rangle_t]^2$. The set of parameter which allowed Gamma Network to oscillate in the Gamma range are indicated by a star symbol. The white and yellow curves depict parameter choices in which the product between p and Q_i are the same. The yellow curve indicates all parameters equivalent to a choice of $p = 60\%$ and $Q_i = 5$ nS ($Q_i' = 3/p'$), while the white curve indicates all parameters equivalent to a choice of $p = 10\%$ and $Q_i = 5$ nS ($Q_i' = 0.5/p'$), like it is usually used in other works [30]. Every point in each graph is given by the average output of 10 simulations of 5 seconds each. In this simulations each neuron of the *Gamma Network* received 400 independent and identically distributed excitatory Poissonian spike trains with a spiking frequency $\mu_{Ext} = 5$ Hz and a synaptic strength of $Q_{Ext} = 1$ nS that decayed with synaptic time constant of $\tau_E = 5$ ms. E: Network activity for the parameters indicated with a start in A, B, C and ($p = 60\%$ and $Q_i = 5$ nS). The raster

plot of the whole network (e1), the population frequency (e2), the membrane potential of 3 randomly chosen neurons (e3) and the power spectrum of the population frequency (e4) are indicated. The population frequency is calculated as the total number of spikes (spikes of the whole network) in a time bin of 1 ms, divided by the duration of this time bin. Because of the exclusive presence of inhibitory neurons and its high level of recurrent inhibition, this network is capable of generating Gamma rhythms with frequencies around 70Hz by means of an ING mechanism.
(TIF)

S3 Fig. Phase-locking statistical test. A and B: Phase distribution of two randomly picked cells from the human recordings (Data segment 1): one excitatory (A, green) and one inhibitory (B, red). The phase distribution of each cell was fitted to a Von Mises curve, which allowed the estimation of its preferred phase $\overline{\theta_{VM}}$. The phase distribution of each neuron was tested for circular uniformity using a Bonferroni-corrected Rayleigh test [36, 37]. C and D: Rayleigh Z calculated for all recorded neurons: excitatory (C, green) and inhibitory (D, red). A neuron was considered phase-locked if the circular uniformity at $P < 0.01$, ($Z > Z_c$) could be rejected. In these plots, neurons were ordered according to their Z value and not according to their original indexes. E: Preferred phases, $\overline{\theta_{VM}}$, of each phase-locked cell, displayed in polar graph representation. Dark colored vectors indicate the average phase among each neuron type and $\Delta\theta$ the phase difference among RS and FS. Data segment 1 presented 22 minutes of recordings, containing 9 seconds of Gamma activity.
(TIF)

S4 Fig. Firing rate change statistical test. A: Activity of two randomly picked cells during several Gamma bursts: neuron 13 (inhibitory, left) and neuron 75 (excitatory, right). The graphs display the firing patter around Gamma bursts (indicated by the black doted lines). Each point corresponds to one spike in the correspondent tuple of time and burst ID (y-axis). B: Histogram computing the distributions of all spikes inside all Gamma bursts of neuron 13 (left) and neuron 75 (right). C: Exemplification of firing rate change statistical test. The Poissonian distribution of these two neurons is constructed based on their average firing rate calculated outside of Gamma bursts. The critical number of spikes n_c, indicated by the dotted lines, is calculated based on the *Percent Point Function* of the respective Poissonian Distribution for a period T, with an 95% Interval of Confidence. The observed number of spikes n_{obsv} is depict as a dot over the curve. According to this procedure, only neuron 75 is considered to increase its firing, since $n_{obsv} > n_c$.
(TIF)

S5 Fig. Phase preference of phase-locked cells per data segment in the human recordings. A: Data segment 1—containing 22 minutes of recordings and 9 seconds of total Gamma activity. B: Data segment 2—containing 43 minutes of recordings and 14 seconds of total Gamma activity. C: Data segment 3—containing 28 minutes of recordings and 16 seconds of total Gamma activity. D: Data segment 4—containing 26 minutes of recordings and 13 seconds of total Gamma activity. E: Data segment 5—containing 16 minutes of recordings and 11 seconds of total Gamma activity. The preferred phases of each phase-locked cell are displayed in polar graph representation. Phases were calculated from $-\pi$ to π. The vector size gives a measure of the phase distribution of each cell. Big amplitude vectors indicate very concentrated distributions while small amplitude vectors indicate less concentrated ones. The color of each vector encodes the type of the cell of whom it represents the phase: red (FS), and green (RS). Cell number IDs are indicated. Dark colored vectors indicate the

average phase among each neuron type and $\Delta\theta$ the phase difference among them.
(TIF)

S6 Fig. Change of *Gamma participating cells* with time in experimental data. The middle panel represents each cell by a circle in each of the 5 data segments. FS and RS phase-locked cells are depicted respectively as red and green circles, while not phase-locked or inconclusive (with respect to phase locked) cells of both types are depicted as blue and gray circles respectively. Superposed to each cell circle, pointing up and down triangles were added to indicate if the cell increased ($\triangle$) or decreased ($\triangledown$) its firing. If the cell didn't change its firing significantly a minus sign (-) was added. Side box plots indicate, on the left, the percentage of phase-locked FS (red) and RS (green) cells in each of the 5 data segments, and, on the right, the percentage of firing rate increase. Dotted lines indicate the average value (phase-locking level: left and firing rate increase: right) between the 5 data segments. The bottom box plot depicts the superposed counts of phase-locking or firing rate increase behavior of each individual cell, computed in the 5 data segments.
(TIF)

S7 Fig. Behavior consistency of RS and FS cells in human recordings. Distributions of consistency indexes among the recorded neurons with respect to to firing rate increase are displayed respectively in A and B for RS cells and FS cells, while C and D display the consistency indexes distribution of phase-locking for RS and FS.
(TIF)

S8 Fig. Neural behavior time distribution in the human data. The activity of each neuron inside and outside Gamma bursts in all 5 data segments were quantified. Taking into account that each data segment had a different duration, containing a different total Gamma duration, and that some neurons were silent in some data segments, each neuron was analyzed individually, taking into account the percentage of the total amount of time in which the neuron was active. A: Phase-locking time distribution. The grid plot in the middle displays the amount of time (with respect to the total recording time) in which each neuron was considered phase-locked (A, y axis), and the the amount of time in which each neuron was considered not phase-locked (A, x axis). RS neurons are depicted in green and FS neurons in red, together with their ID number. Neurons lying outside of the diagonal are neurons of whom statistical analysis was inconclusive at some data segments, due to the reduced number of spikes. At the top left corner, lie neurons that were always considered phase-locked, while neurons that were never considered phase-locked are placed at the bottom right corner. Pie plots indicate the percentage of neurons that passed at least 50% of the total time being either phase-locked or not phase-locked (neurons that fall inside of the colored quadrants) and the neurons lying on the left white quadrant. B: Same analysis as A but displaying the firing rate change time distribution. This analysis indicates that only a small percentage of neurons passed at least 50% of the total time being either phase-locked (RS: 4.4%, FS: 13%) or increasing its firing (RS: 20.6%, FS: 52.2%). Moreover, even though no cell was 100% of the time phase-locked to Gamma, some cells were 100% of the time not phase-locked to Gamma (RS: 22.1%, FS: 13%) and others never increased their firing (RS: 41.2%, FS: 17.4%).
(TIF)

S9 Fig. Firing rate distribution of individual neurons inside Gamma bursts and their phase-locking classification in human data recordings. The average firing rate of each neuron in each of the 5 data segments (inside Gamma bursts) is depicted as a point in this graph (each neuron presents 5 points). The color of each point corresponds to the neuron classification with respect to phase-locking in the correspondent data segment (purple: phase-locked,

red: not phase-locked and gray: inconclusive). The average firing rate inside Gamma bursts was calculated based on the total Gamma duration (recorded by the electrode, that also recorded the particular neuron, in the respective data segment) and the total number of spikes emitted by this particular neuron exclusively inside the Gamma bursts of the respective data segment. Cells classified as inconclusive are cells that spiked less then 5 times inside Gamma bursts, or cells whose electrode measured less then 1 second of Gamma bursts in the respective data segment. FS neurons are depicted on the left and RS neurons on the right. Box plots referent to each neuron distribution are added to help in the visualization (regardless of the reduced number of points). The box extends from the lower to upper quartile values of the data, with a line at the median. The whiskers extend from the box to show the range of the data. Flier points are those past the end of the whiskers and are depicted with black circle together with the color point. This graph illustrates the fact that phase-locking and not phase-locking behaviors are observed both in cells with high and low firing rates.
(TIF)

S10 Fig. Firing rate distributions. Firing rate distributions of different neuron types (inside and outside Gamma bursts) are depicted in A, B, C and D for each studied system. A: Human recordings. B: *PING Network*. C: *ING Network* and D: *CHING Network*. Average firing rates of each cell type is indicated by the dotted line.
(TIF)

S11 Fig. Average excitatory and inhibitory synaptic conductances. A: Illustration of the analyzed system: *PING Network*, *ING Network* and *CHING Network*. B: Ratio between excitatory conductance (G_e) and leakage conductance (G_L). C: Ratio between inhibitory conductance (G_i) and leakage conductance (G_L). Averages are indicated by the dotted line. The distributions fall inside of the physiological range observed experimentally [87].
(TIF)

S12 Fig. Average level of phase-locking. The average level of phase-locking is defined as the averaged percentage of cells in the network considered to be phase-locked, across the 5 segments of data recorded. The analysis was done separately for excitation and inhibition. A: Human Data recordings, B:*PING Network*, C: *ING Network* and D: *CHING Network*. The percentage of cells signaled as *inconclusive* relates to cells in which the number of spikes inside Gamma burst were too small to allow statistical significant phase-locking.
(TIF)

S13 Fig. Network responsiveness of a network composed of RS and FS neurons randomly connected with different synaptic time scales. A: *AI network* receiving a Poissonian drive of 3Hz. B: *PING network* receiving a Poissonian drive of 3Hz (inducing Gamma). C: *PING network* receiving a Poissonian drive of 2Hz (not inducing Gamma). In addition to the drive each network received a Gaussian stimulus of 2Hz pick and a standard deviation of 50 ms. The drive and stimulus are depicted in each case in a1, b1 and c1. The raster plot of each network during the stimulation is depicted in each case in a2, b2 and c2. The membrane potential of 3 randomly picked neurons are depicted in each case in a3, b3 and c3. The raw and the filtered simulated LFP are depicted in each case in a4, b4 and c4.
(TIF)

S14 Fig. Responsiveness of individual cells in computational models. A: *PING Network*. B: *ING Network*. C: *CHING Network*. To estimate the individual cell responsiveness, we calculated the average spiking frequency of each cell inside (y-axis) and outside stimulus (x-axis) during AI-like states (left) and Gamma states (right). RS cells are displayed in green and FS

cells in red. In each plot the linear regression from the points is depicted with the identity. We observe that all cells follow the same rule of responsiveness (proportional to their firing outside the stimulus). No difference can be seen between the responsiveness of neurons classified as *Gamma participating* and the *Gamma non-participating* cells.
(TIF)

S15 Fig. Phase-dependent network response protocol. A: Protocol scheme in ING Network when it displays Gamma oscillations (45-65 Hz). Top: stimulus used to measure network phase-dependent response. The stimulus consisted of fast Gaussian fluctuation (standard deviation of 1 ms) which modulated the firing rate of the external Poissonian spike trains injected into network from 0 to 50 Hz. Middle: Raster plot indicating the network response to the Gaussian stimulus. The network responsiveness was calculated according to Eq 6, in a time window T = 18ms (shaded gray area). Bottom: Gamma oscillation phase around the the stimulus pick. The phase at the time the stimulus was applied is indicated. The Phase-dependent network responsiveness was measured in three different network states: B: AI state (Poissonian noise = 2Hz, no external current). C: AI-modulated states (Poissonian noise = 1Hz, with sinusoidal external current). D: Gamma state (Poissonian noise = 3Hz, no external current). Items A, B and C display the Raster activity of ING Network without the Gaussian stimulation. Only 20% of network is shown.
(TIF)

S16 Fig. Linear representation of color maps depicted in Fig 9. A: Resonant properties of *PING* Network. B: Resonant properties of *ING* Network. C: Resonant properties of *CHING* Network. The curves displayed in B, C and D depict, for each oscillatory frequency (color scheme) the amplitude (average number of spikes per neuron per time bin) as a function of the oscillation phase, during Gamma and AI-like states. All values were normalized by the average firing inside of each state to exclude the state dependent firing rate level (which is higher on Gamma). Δ_{noise} = 0.5 Hz in all network models but μ_{noise} varied in each case. For AI, in PING and ING Networks μ_{noise} = 2 Hz and in CHING Network μ_{noise} = 1 Hz, while for Gamma, μ_{noise} = 3 Hz in in PING and ING Networks and μ_{noise} = 2 Hz in CHING Network.
(TIF)

S17 Fig. Resonant properties of computational models during Gamma in each cell type. A: Resonant properties of *PING* Network. B: Resonant properties of *ING* Network. C: Resonant properties of *CHING* Network. The color maps displayed in A, B and C depict, for each oscillatory frequency and oscillation phase, the average number of spikes per cell type (RS, FS, FS2 or Ch) and time bin, during Gamma state. Differently than Fig 9 no normalization was applied. Δ_{noise} = 0.5 Hz in all network models but μ_{noise} varied in each case. In PING and ING Networks μ_{noise} = 3 Hz and in CHING Network μ_{noise} = 2 Hz.
(TIF)

Acknowledgments

We thank Damien Depannemaecker and Mallory Carlu for enlightening discussions and insights.

Author Contributions

Conceptualization: Eduarda Susin, Alain Destexhe.

Data curation: Eduarda Susin.

Formal analysis: Eduarda Susin.

Funding acquisition: Eduarda Susin, Alain Destexhe.

Investigation: Eduarda Susin.

Methodology: Eduarda Susin, Alain Destexhe.

Project administration: Eduarda Susin, Alain Destexhe.

Resources: Alain Destexhe.

Software: Eduarda Susin.

Supervision: Alain Destexhe.

Visualization: Eduarda Susin.

Writing – original draft: Eduarda Susin.

Writing – review & editing: Alain Destexhe.

References

1. Buzsaki G. Rhythms of the Brain. Oxford University Press; 2006.
2. Gray CM, Singer W. Stimulus-specific neuronal oscillations in orientation columns of cat visual cortex. Proceedings of the National Academy of Sciences. 1989; 86(5):1698–1702. https://doi.org/10.1073/pnas.86.5.1698 PMID: 2922407
3. Gray CM, König P, Engel AK, Singer W. Oscillatory responses in cat visual cortex exhibit inter-columnar synchronization which reflects global stimulus properties. Nature. 1989; 338(6213):334–337. https://doi.org/10.1038/338334a0 PMID: 2922061
4. Singer W, Gray CM. Visual feature integration and the temporal correlation hypothesis. Annual review of neuroscience. 1995; 18(1):555–586. https://doi.org/10.1146/annurev.ne.18.030195.003011 PMID: 7605074
5. Singer W. Neuronal synchrony: a versatile code for the definition of relations? Neuron. 1999; 24(1):49–65. https://doi.org/10.1016/S0896-6273(00)80821-1 PMID: 10677026
6. O'Keefe J, Recce ML. Phase relationship between hippocampal place units and the EEG theta rhythm. Hippocampus. 1993; 3(3):317–330. https://doi.org/10.1002/hipo.450030307 PMID: 8353611
7. Fries P, Nikolić D, Singer W. The gamma cycle. Trends in neurosciences. 2007; 30(7):309–316. https://doi.org/10.1016/j.tins.2007.05.005 PMID: 17555828
8. Fries P. A mechanism for cognitive dynamics: neuronal communication through neuronal coherence. Trends in cognitive sciences. 2005; 9(10):474–480. https://doi.org/10.1016/j.tics.2005.08.011 PMID: 16150631
9. Fries P. Rhythms for cognition: communication through coherence. Neuron. 2015; 88(1):220–235. https://doi.org/10.1016/j.neuron.2015.09.034 PMID: 26447583
10. Hahn G, Bujan AF, Frégnac Y, Aertsen A, Kumar A. Communication through resonance in spiking neuronal networks. PLoS Comput Biol. 2014; 10(8):e1003811. https://doi.org/10.1371/journal.pcbi.1003811 PMID: 25165853
11. Destexhe A, Contreras D. Neuronal computations with stochastic network states. Science. 2006; 314 (5796):85–90. https://doi.org/10.1126/science.1127241 PMID: 17023650
12. Zerlaut Y, Destexhe A. Enhanced responsiveness and low-level awareness in stochastic network states. Neuron. 2017; 94(5):1002–1009. https://doi.org/10.1016/j.neuron.2017.04.001 PMID: 28595044
13. Brunel N. Dynamics of sparsely connected networks of excitatory and inhibitory spiking neurons. Journal of computational neuroscience. 2000; 8(3):183–208. https://doi.org/10.1023/A:1008925309027 PMID: 10809012
14. Softky WR, Koch C. The highly irregular firing of cortical cells is inconsistent with temporal integration of random EPSPs. Journal of neuroscience. 1993; 13(1):334–350. https://doi.org/10.1523/JNEUROSCI.13-01-00334.1993 PMID: 8423479
15. Holt GR, Softky WR, Koch C, Douglas RJ. Comparison of discharge variability in vitro and in vivo in cat visual cortex neurons. Journal of neurophysiology. 1996; 75(5):1806–1814. https://doi.org/10.1152/jn.1996.75.5.1806 PMID: 8734581

16. Shadlen MN, Newsome WT. The variable discharge of cortical neurons: implications for connectivity, computation, and information coding. Journal of neuroscience. 1998; 18(10):3870–3896. https://doi.org/10.1523/JNEUROSCI.18-10-03870.1998 PMID: 9570816

17. Destexhe A, Rudolph M, Paré D. The high-conductance state of neocortical neurons in vivo. Nature reviews neuroscience. 2003; 4(9):739–751. https://doi.org/10.1038/nrn1198 PMID: 12951566

18. Henrie JA, Shapley R. LFP power spectra in V1 cortex: the graded effect of stimulus contrast. Journal of neurophysiology. 2005; 94(1):479–490. https://doi.org/10.1152/jn.00919.2004 PMID: 15703230

19. Van Vreeswijk C, Sompolinsky H. Chaos in neuronal networks with balanced excitatory and inhibitory activity. Science. 1996; 274(5293):1724–1726. https://doi.org/10.1126/science.274.5293.1724 PMID: 8939866

20. Peyrache A, Dehghani N, Eskandar EN, Madsen JR, Anderson WS, Donoghue JA, et al. Spatiotemporal dynamics of neocortical excitation and inhibition during human sleep. Proceedings of the National Academy of Sciences. 2012; 109(5):1731–1736. https://doi.org/10.1073/pnas.1109895109 PMID: 22307639

21. Le Van Quyen M, Muller LE, Telenczuk B, Halgren E, Cash S, Hatsopoulos NG, et al. High-frequency oscillations in human and monkey neocortex during the wake–sleep cycle. Proceedings of the National Academy of Sciences. 2016; 113(33):9363–9368. https://doi.org/10.1073/pnas.1523583113 PMID: 27482084

22. Traub RD, Jefferys JG, Jefferys JG, Whittington MA. Fast oscillations in cortical circuits. MIT press; 1999.

23. Buzsáki G, Wang XJ. Mechanisms of gamma oscillations. Annual review of neuroscience. 2012; 35:203–225. https://doi.org/10.1146/annurev-neuro-062111-150444 PMID: 22443509

24. Traub RD. Fast oscillations. Scholarpedia. 2006; 1(12):1764. https://doi.org/10.4249/scholarpedia.1764

25. Tiesinga P, Sejnowski TJ. Cortical enlightenment: are attentional gamma oscillations driven by ING or PING? Neuron. 2009; 63(6):727–732. https://doi.org/10.1016/j.neuron.2009.09.009 PMID: 19778503

26. Gray CM, McCormick DA. Chattering cells: superficial pyramidal neurons contributing to the generation of synchronous oscillations in the visual cortex. Science. 1996; 274(5284):109–113. https://doi.org/10.1126/science.274.5284.109 PMID: 8810245

27. Cunningham MO, Whittington MA, Bibbig A, Roopun A, LeBeau FE, Vogt A, et al. A role for fast rhythmic bursting neurons in cortical gamma oscillations in vitro. Proceedings of the National Academy of Sciences. 2004; 101(18):7152–7157. https://doi.org/10.1073/pnas.0402060101 PMID: 15103017

28. Brette R, Gerstner W. Adaptive exponential integrate-and-fire model as an effective description of neuronal activity. Journal of neurophysiology. 2005; 94(5):3637–3642. https://doi.org/10.1152/jn.00686.2005 PMID: 16014787

29. Van Vreeswijk C, Abbott L, Ermentrout GB. When inhibition not excitation synchronizes neural firing. Journal of computational neuroscience. 1994; 1(4):313–321. https://doi.org/10.1007/BF00961879 PMID: 8792237

30. Brunel N, Wang XJ. What determines the frequency of fast network oscillations with irregular neural discharges? I. Synaptic dynamics and excitation-inhibition balance. Journal of neurophysiology. 2003; 90(1):415–430. https://doi.org/10.1152/jn.01095.2002 PMID: 12611969

31. Stimberg M, Brette R, Goodman DF. Brian 2, an intuitive and efficient neural simulator. eLife. 2019; 8:e47314. https://doi.org/10.7554/eLife.47314 PMID: 31429824

32. Telenczuk B, Telenczuk M, Destexhe A. A kernel-based method to calculate local field potentials from networks of spiking neurons. Journal of Neuroscience Methods. 2020; 344:108871. https://doi.org/10.1016/j.jneumeth.2020.108871 PMID: 32687850

33. Teleńczuk B, Dehghani N, Le Van Quyen M, Cash SS, Halgren E, Hatsopoulos NG, et al. Local field potentials primarily reflect inhibitory neuron activity in human and monkey cortex. Scientific reports. 2017; 7:40211. https://doi.org/10.1038/srep40211 PMID: 28074856

34. Widmann A, Schröger E, Maess B. Digital filter design for electrophysiological data–a practical approach. Journal of neuroscience methods. 2015; 250:34–46. https://doi.org/10.1016/j.jneumeth.2014.08.002 PMID: 25128257

35. Virtanen P, Gommers R, Oliphant TE, Haberland M, Reddy T, Cournapeau D, et al. SciPy 1.0: Fundamental Algorithms for Scientific Computing in Python. Nature Methods. 2020; 17:261–272. https://doi.org/10.1038/s41592-019-0686-2 PMID: 32015543

36. Jacobs J, Kahana MJ, Ekstrom AD, Fried I. Brain oscillations control timing of single-neuron activity in humans. Journal of Neuroscience. 2007; 27(14):3839–3844. https://doi.org/10.1523/JNEUROSCI.4636-06.2007 PMID: 17409248

37. Le Van Quyen M, Staba R, Bragin A, Dickson C, Valderrama M, Fried I, et al. Large-scale microelectrode recordings of high-frequency gamma oscillations in human cortex during sleep. Journal of Neuroscience. 2010; 30(23):7770–7782. https://doi.org/10.1523/JNEUROSCI.5049-09.2010 PMID: 20534826

38. Barthó P, Hirase H, Monconduit L, Zugaro M, Harris KD, Buzsaki G. Characterization of neocortical principal cells and interneurons by network interactions and extracellular features. Journal of neurophysiology. 2004; 92(1):600–608. https://doi.org/10.1152/jn.01170.2003 PMID: 15056678

39. Destexhe A, Contreras D, Steriade M. Spatiotemporal analysis of local field potentials and unit discharges in cat cerebral cortex during natural wake and sleep states. Journal of Neuroscience. 1999; 19 (11):4595–4608. https://doi.org/10.1523/JNEUROSCI.19-11-04595.1999 PMID: 10341257

40. Fries P, Reynolds JH, Rorie AE, Desimone R. Modulation of oscillatory neuronal synchronization by selective visual attention. Science. 2001; 291(5508):1560–1563. https://doi.org/10.1126/science.1055465 PMID: 11222864

41. Pesaran B, Pezaris JS, Sahani M, Mitra PP, Andersen RA. Temporal structure in neuronal activity during working memory in macaque parietal cortex. Nature neuroscience. 2002; 5(8):805–811. https://doi.org/10.1038/nn890 PMID: 12134152

42. Bartos M, Vida I, Jonas P. Synaptic mechanisms of synchronized gamma oscillations in inhibitory interneuron networks. Nature reviews neuroscience. 2007; 8(1):45–56. https://doi.org/10.1038/nrn2044 PMID: 17180162

43. Brunel N, Hakim V. Fast global oscillations in networks of integrate-and-fire neurons with low firing rates. Neural computation. 1999; 11(7):1621–1671. https://doi.org/10.1162/089976699300016179 PMID: 10490941

44. Tiesinga P, José JV. Robust gamma oscillations in networks of inhibitory hippocampal interneurons. Network: Computation in Neural Systems. 2000; 11(1):1–23. https://doi.org/10.1088/0954-898X_11_1_301 PMID: 10735526

45. Geisler C, Brunel N, Wang XJ. Contributions of intrinsic membrane dynamics to fast network oscillations with irregular neuronal discharges. Journal of neurophysiology. 2005; 94(6):4344–4361. https://doi.org/10.1152/jn.00510.2004 PMID: 16093332

46. Abbott L, van Vreeswijk C. Asynchronous states in networks of pulse-coupled oscillators. Physical Review E. 1993; 48(2):1483. https://doi.org/10.1103/PhysRevE.48.1483 PMID: 9960738

47. Gerstner W. Time structure of the activity in neural network models. Physical review E. 1995; 51(1):738. https://doi.org/10.1103/PhysRevE.51.738 PMID: 9962697

48. Gerstner W, Van Hemmen JL, Cowan JD. What matters in neuronal locking? Neural computation. 1996; 8(8):1653–1676. https://doi.org/10.1162/neco.1996.8.8.1653 PMID: 8888612

49. Hansel D, Mato G, Meunier C. Synchrony in excitatory neural networks. Neural computation. 1995; 7 (2):307–337. https://doi.org/10.1162/neco.1995.7.2.307 PMID: 8974733

50. Kopell N, Ermentrout G. Symmetry and phaselocking in chains of weakly coupled oscillators. Communications on Pure and Applied Mathematics. 1986; 39(5):623–660. https://doi.org/10.1002/cpa.3160390504

51. Kuramoto Y. Chemical oscillations, waves, and turbulence. Courier Corporation; 2003.

52. Marder E. From biophysics to models of network function. Annual review of neuroscience. 1998; 21 (1):25–45. https://doi.org/10.1146/annurev.neuro.21.1.25 PMID: 9530490

53. Traub R, Whittington M, Colling S, Buzsaki G, Jefferys J. Analysis of gamma rhythms in the rat hippocampus in vitro and in vivo. The Journal of physiology. 1996; 493(2):471–484. https://doi.org/10.1113/jphysiol.1996.sp021397 PMID: 8782110

54. Wang XJ, Buzsáki G. Gamma oscillation by synaptic inhibition in a hippocampal interneuronal network model. Journal of neuroscience. 1996; 16(20):6402–6413. https://doi.org/10.1523/JNEUROSCI.16-20-06402.1996 PMID: 8815919

55. Whittington MA, Traub RD, Jefferys JG. Synchronized oscillations in interneuron networks driven by metabotropic glutamate receptor activation. Nature. 1995; 373(6515):612–615. https://doi.org/10.1038/373612a0 PMID: 7854418

56. Cardin JA, Carlén M, Meletis K, Knoblich U, Zhang F, Deisseroth K, et al. Driving fast-spiking cells induces gamma rhythm and controls sensory responses. Nature. 2009; 459(7247):663–667. https://doi.org/10.1038/nature08002 PMID: 19396156

57. Sohal VS, Zhang F, Yizhar O, Deisseroth K. Parvalbumin neurons and gamma rhythms enhance cortical circuit performance. Nature. 2009; 459(7247):698–702. https://doi.org/10.1038/nature07991 PMID: 19396159

58. Zemankovics R, Veres JM, Oren I, Hájos N. Feedforward inhibition underlies the propagation of cholinergically induced gamma oscillations from hippocampal CA3 to CA1. Journal of Neuroscience. 2013; 33 (30):12337–12351. https://doi.org/10.1523/JNEUROSCI.3680-12.2013 PMID: 23884940

59. Susin E, Destexhe A. Cellular correlates of wakefulness and slow-wave sleep: evidence for a key role of inhibition. Current Opinion in Physiology. 2020; 15:68–73. https://doi.org/10.1016/j.cophys.2019.12.006

60. Palmigiano A, Geisel T, Wolf F, Battaglia D. Flexible information routing by transient synchrony. Nature neuroscience. 2017; 20(7):1014. https://doi.org/10.1038/nn.4569 PMID: 28530664

61. Viriyopase A, Memmesheimer RM, Gielen S. Cooperation and competition of gamma oscillation mechanisms. Journal of neurophysiology. 2016; 116(2):232–251. https://doi.org/10.1152/jn.00493.2015 PMID: 26912589

62. Viriyopase A, Memmesheimer RM, Gielen S. Analyzing the competition of gamma rhythms with delayed pulse-coupled oscillators in phase representation. Physical Review E. 2018; 98(2):022217. https://doi.org/10.1103/PhysRevE.98.022217 PMID: 30253475

63. Barlow HB. Single units and sensation: a neuron doctrine for perceptual psychology? Perception. 1972; 1(4):371–394. https://doi.org/10.1068/p010371 PMID: 4377168

64. Churchland MM, Byron MY, Cunningham JP, Sugrue LP, Cohen MR, Corrado GS, et al. Stimulus onset quenches neural variability: a widespread cortical phenomenon. Nature neuroscience. 2010; 13(3):369–378. https://doi.org/10.1038/nn.2501 PMID: 20173745

65. Riehle A, Grün S, Diesmann M, Aertsen A. Spike synchronization and rate modulation differentially involved in motor cortical function. Science. 1997; 278(5345):1950–1953. https://doi.org/10.1126/science.278.5345.1950 PMID: 9395398

66. Vaadia E, Haalman I, Abeles M, Bergman H, Prut Y, Slovin H, et al. Dynamics of neuronal interactions in monkey cortex in relation to behavioural events. Nature. 1995; 373(6514):515–518. https://doi.org/10.1038/373515a0 PMID: 7845462

67. Thorpe S, Delorme A, Van Rullen R. Spike-based strategies for rapid processing. Neural networks. 2001; 14(6-7):715–725. https://doi.org/10.1016/S0893-6080(01)00083-1 PMID: 11665765

68. Deneve S. Bayesian spiking neurons I: inference. Neural computation. 2008; 20(1):91–117. https://doi.org/10.1162/neco.2008.20.1.91 PMID: 18045002

69. Shinomoto S, Kim H, Shimokawa T, Matsuno N, Funahashi S, Shima K, et al. Relating neuronal firing patterns to functional differentiation of cerebral cortex. PLoS Comput Biol. 2009; 5(7):e1000433. https://doi.org/10.1371/journal.pcbi.1000433 PMID: 19593378

70. Maimon G, Assad JA. Beyond Poisson: increased spike-time regularity across primate parietal cortex. Neuron. 2009; 62(3):426–440. https://doi.org/10.1016/j.neuron.2009.03.021 PMID: 19447097

71. Luczak A, McNaughton BL, Harris KD. Packet-based communication in the cortex. Nature Reviews Neuroscience. 2015; 16(12):745–755. https://doi.org/10.1038/nrn4026 PMID: 26507295

72. Maršálek P, Koch C, Maunsell J. On the relationship between synaptic input and spike output jitter in individual neurons. Proceedings of the National Academy of Sciences. 1997; 94(2):735–740. https://doi.org/10.1073/pnas.94.2.735 PMID: 9012854

73. Rudolph M, Destexhe A. Tuning neocortical pyramidal neurons between integrators and coincidence detectors. Journal of computational neuroscience. 2003; 14(3):239–251. https://doi.org/10.1023/A:1023245625896 PMID: 12766426

74. Lepousez G, Lledo PM. Odor discrimination requires proper olfactory fast oscillations in awake mice. Neuron. 2013; 80(4):1010–1024. https://doi.org/10.1016/j.neuron.2013.07.025 PMID: 24139818

75. Ledoux E, Brunel N. Dynamics of networks of excitatory and inhibitory neurons in response to time-dependent inputs. Frontiers in computational neuroscience. 2011; 5:25. https://doi.org/10.3389/fncom.2011.00025 PMID: 21647353

76. Akam T, Kullmann DM. Oscillations and filtering networks support flexible routing of information. Neuron. 2010; 67(2):308–320. https://doi.org/10.1016/j.neuron.2010.06.019 PMID: 20670837

77. Melloni L, Molina C, Pena M, Torres D, Singer W, Rodriguez E. Synchronization of neural activity across cortical areas correlates with conscious perception. Journal of neuroscience. 2007; 27(11):2858–2865. https://doi.org/10.1523/JNEUROSCI.4623-06.2007 PMID: 17360907

78. McCarley RW. Brainstem control of Wakefulness and Sleep. New York: Plenum Press; 1990.

79. Fries P, Roelfsema PR, Engel AK, König P, Singer W. Synchronization of oscillatory responses in visual cortex correlates with perception in interocular rivalry. Proceedings of the National Academy of Sciences. 1997; 94(23):12699–12704. https://doi.org/10.1073/pnas.94.23.12699 PMID: 9356513

80. Uhlhaas PJ, Singer W. Abnormal neural oscillations and synchrony in schizophrenia. Nature reviews neuroscience. 2010; 11(2):100–113. https://doi.org/10.1038/nrn2774 PMID: 20087360

81. Kulli J, Koch C. Does anesthesia cause loss of consciousness? Trends in neurosciences. 1991; 14(1):6–10. https://doi.org/10.1016/0166-2236(91)90172-Q PMID: 1709532

82. Koch C, Massimini M, Boly M, Tononi G. Neural correlates of consciousness: progress and problems. Nature Reviews Neuroscience. 2016; 17(5):307–321. https://doi.org/10.1038/nrn.2016.22 PMID: 27094080

83. Destexhe A. Oscillations, complex spatiotemporal behavior, and information transport in networks of excitatory and inhibitory neurons. Phys Rev E Stat Phys Plasmas Fluids Relat Interdiscip Topics. 1994; 50(2):1594–1606. PMID: 9962131

84. VanRullen R, Thorpe SJ. Surfing a spike wave down the ventral stream. Vision research. 2002; 42 (23):2593–2615. https://doi.org/10.1016/S0042-6989(02)00298-5 PMID: 12446033

85. Sherfey J, Ardid S, Miller EK, Hasselmo ME, Kopell NJ. Prefrontal oscillations modulate the propagation of neuronal activity required for working memory. Neurobiology of learning and memory. 2020; 173:107228. https://doi.org/10.1016/j.nlm.2020.107228 PMID: 32561459

86. Schneider M, Dann B, Sheshadri S, Scherberger H, Vinck M. A general theory of coherence between brain areas. bioRxiv. 2020.

87. Rudolph M, Pospischil M, Timofeev I, Destexhe A. Inhibition determines membrane potential dynamics and controls action potential generation in awake and sleeping cat cortex. Journal of neuroscience. 2007; 27(20):5280–5290. https://doi.org/10.1523/JNEUROSCI.4652-06.2007 PMID: 17507551

A network model of the modulation of Gamma oscillations by NMDA receptors in cerebral cortex

---

French Abstract:

Des médicaments psychotiques, tels que la kétamine, induisent des symptômes proches de la schizophrénie et stimulent l'augmentation d'oscillations Gamma, similaires à ce que s'observe chez les patients touches par cette maladie. Toutefois, les mécanismes sous-jacents à ces effets ne sont toujours pas bien décrits. Dans cette étude, nous avons utilisé des modèles informatiques de réseaux de neurones corticaux générant des oscillations Gamma, où nous avons intégré l'action de médicaments tels que la kétamine pour bloquer partiellement les récepteurs de n-méthyl-d-aspartate (NMDA). Le modèle développé décrit la modulation des oscillations Gamma par des antagonistes des récepteurs de NMDA, en supposant que les antagonistes affectent davantage les récepteurs de NMDA sur les interneurones inhibiteurs. Le modèle a ensuite été utilisé pour comparer la réactivité du réseau aux stimuli externes. Nous avons constaté que lorsque les canaux de NMDA sont bloqués, une augmentation de la puissance des oscillations Gamma est observée, conjointement avec une augmentation de la réactivité du réseau. Cependant, cette augmentation de la réactivité s'applique non seulement aux états oscillatoires dans la fréquence Gamma, mais également aux états asynchrones sans oscillations apparentes. Nous concluons que les antagonistes des canaux de NMDA induisent un état d'excitabilité accru, qui produit une réponse aux stimuli externes exacerbée, et qui peut ou non produire des oscillations Gamma. Nous cogitons que cet effet stimulant peut expliquer des phénomènes tels qu'une perception altérée ou des hallucinations.

A network model of the modulation of gamma oscillations by NMDA receptors in cerebral cortex

Eduarda Susin[1,*], Alain Destexhe[1]
1 Paris-Saclay University, Centre National de la Recherche Scientifique (CNRS), Institute of Neuroscience (NeuroPSI), Gif-sur-Yvette, France * eduardadsusin@gmail.com

***Abstract*—Psychotic drugs such as ketamine induce symptoms close to schizophrenia, and stimulates the production of gamma oscillations, as also seen in patients, but the underlying mechanisms are still unclear. Here, we have used computational models of cortical networks generating gamma oscillations, and have integrated the action of drugs such as ketamine to partially block n-methyl-d-Aspartate (NMDA) receptors. The model can reproduce the modulation of gamma oscillations by NMDA-receptor antagonists, assuming that antagonists affect NMDA receptors predominantly on inhibitory interneurons. We next used the model to compare the responsiveness of the network to external stimuli, and found that when NMDA channnels are blocked an increase of Gamma power is observed altogether with an increase of network responsiveness. However, this responsiveness increase applies not only to gamma states, but also to asynchronous states with no apparent gamma. We conclude that NMDA antagonists induce increased excitability state, which may or may not produce gamma oscillations, but the response to external inputs is exacerbated, which may explain phenomena such as altered perception or hallucinations.**

***Index Terms*—Schizophrenia, NMDAR hypofunction, Gamma oscillations, Network Model, Psychosis**

I. Introduction

SCHIZOPHRENIA is a mental disorder characterized by three classes of symptoms: positive symptoms (such as delusions, hallucinations and disordered thoughts or speech), negative symptoms (comprehending poverty of speech and deficits of normal emotional response), and cognitive deficits [1–3]. Several abnormalities have been identified in schizophrenic patients, including important differences in neurotransmitters systems, anatomical deficits and abnormal neural rhythms [4, 5].

Gamma oscillations (30-90 Hz) in early-course schizophrenia patients are commonly reported to present increased power and/or phase synchronization [6–8]. In parallel, positive correlation between psychotic symptoms and the Gamma power have been identified in schizophrenic patients, in which higher Gamma-band activity corresponded to increased symptom load [9–12]. These findings indicate that hallucinations and delusions could be related to an excess of oscillatory synchronization in the Gamma band.

NMDA receptor (NMDAR) antagonists, commonly used in sub-anesthetic doses as animal and human models to study Schizophrenia [13], induce a psychotic state that resembles all three classes of symptoms of the disease [14–16]. Furthermore, NMDAR antagonists also increase Gamma power amplitude, both in human and in animal models [17–24].

In this study we investigate by means of computational models how NMDAR antagonists, such as ketamine, affect the dynamics of neural networks and how the generated boosting of Gamma activity affects the network response, providing an interpretation for the observed correlation between Gamma Power and psychotic episodes.

II. Results

Computational model reproduces experimental features

Several preparations with sub-anesthetics doses of NMDAR antagonists have reported to produce neural excitation [25–30]. Since NMDAR mediate excitatory synaptic transmission, this behavior is intriguing. Several hypothesis have been proposed to explain this apparent paradox [3]. One of the possible explanations is that NMDAR antagonists in sub-anesthetics doses act preferentially on inhibitory neurons, increasing network activity indirectly by means of desinhibition. Even though some contrasting results have been observed [31], this interpretation has been supported experimentally by several works [32–35]. Network excitability have also been reported to increase in schizophrenic patients [36, 37], and its increase in sensory and association cortex have been correlated with hallucinations [38, 39].

Another important effect of NMDAR antagonists in sub-anesthetics doses is the increase of Gamma-band activity. These observations were reported in human [17–19], monkey [24] and rats [20–23], both during cognitive tasks or free movement.

The network model developed in the present work (see Methods) is able to reproduce both of these features (increase of network excitability and increase of Gamma power). Figure 1 depicts the network behavior with respect to the to different NMDA synaptic strengths, Q^{NMDA}, in excitatory Regular Spiking (RS) and in inhibitory Fast Spiking (FS) cells. We mimic the block of NMDA channels due to the action of NMDAR antagonists by decreasing Q^{NMDA} in RS and FS cells according to Figure 1A (see Methods). Points of higher synaptic strengths are associated with healthy conditions, while points with lower synaptic strengths are associated to pathological conditions supposedly similar to the schizophrenic brain. The network dynamics for two sets of NMDA synaptic strengths are shown in Figure 1B and Figure 1C by means of a Raster Plot. As the synaptic strengths of NMDA channels decreased (higher concentration of NMDAR antagonists), the firing rate of excitatory RS cells increased

while the firing rate of inhibitory FS cells decreased (Figure 1D). In addition, the Gamma power of the population activity (see Methods) presented an increase (Figure 1E and F).

Network Responsiveness during Gamma rhythms in different levels of NMDAR block

We investigated how the decrease of NMDA synaptic strength changed the network dynamics and its capacity to respond to external stimulus.

While network *excitability* is related to an overall increase of spiking activity, network *responsiveness* relates to the network capacity to react to a certain stimulus, producing additional spikes then the ones generated by spontaneous activity. These two dynamical measurements (excitability and responsiveness) are not always congruent, meaning that it is possible to observe an increase in excitability but a concomitant decrease in responsiveness [40].

Network responsiveness was defined as the difference between the total number of spikes generated by the whole network in the presence and in the absence of the stimulus (see Eq 6). We measured network responsiveness at different levels of NMDAR block for different stimulus amplitudes (Figure 2). The stimulus consisted of a variation in time of the external Poissonian drive, in a Gaussian manner (see Methods).

Network responsiveness in RS cells increased with the increased level of NMDAR block, while the responsiveness of FS neurons decreased. In this case, both, network excitability and network responsiveness, behave in the same direction.

The increase of network responsiveness can be understood from Figure 3. The NMDA receptors block depolarizes RS cells, while FS neurons are overall hyperpolarized. For weak levels of NMDA receptors block, no or weak depolarization is observed in FS cells, while for strong levels of NMDA block a significant hyperpolarization is observed.

Gamma states vs. AI states

Gamma oscillations (30-90 Hz) are believed to be involved in information processing [41–46], and have been associated to different high-level cognitive functions, such as memory [47–49], perception [50–53], attention [54–57], focused arousal [58] and prediction [59]. In parallel, studies with schizophrenic patients have reported a positive correlation between psychotic symptoms and the power of Gamma oscillations [9–12].

In contrast, Asynchronous-and-Irregular (AI) states [60] are usually associated to conscious states [61], being observed during awake and aroused states [62]. This regime are characterized by irregular and sustained firing with very weak correlations [63–67].

In a previous study [40] we reported that AI states, in comparison to oscillatory states in Gamma band, provide the highest responsiveness to external stimuli, indicating that Gamma oscillations tend to overall diminish responsiveness. This observation could indicate that Gamma rhythms present a *masking effect*, conveying information in its cycles on spike timing at the expense of decreasing the strength of the network response.

In the present study, we compare AI and Gamma states at different levels of NMDAR block. Figure 4 depicts the responsiveness of RS neurons, with respect to different stimulus amplitudes (same protocol as Figure 2), for different ensembles of NMDA synaptic strengths. In agreement with Figure 2, parameter sets in which NMDA synaptic strengths are decreased (mimicking the action NMDAR antagonists) correspond to regions of the parameter space with higher responsiveness. For example, Q_{FS}^{NMDA}= 0.4 nS and Q_{FS}^{NMDA}=0.36 nS displayed higher responsiveness then the networks in which the NMDA synaptic strengths wrere Q_{FS}^{NMDA}= 1 nS and Q_{FS}^{NMDA}=0.8 nS. Interestingly, in both conditions, responsiveness in AI states were always superior to the one in Gamma. This result was also observed in a similar model in the obscene of NMDA channels [40]. This example illustrates a general tendency, which was also observed with other parameter sets.

III. Discussion

In this work, we used computational models to investigate the effect of psychotic drugs such as ketamine in cerebral cortex, and how gamma oscillations relate to these effects. Our findings are (1) NMDA receptors antagonists modulate the rhythms produced by a simple network model consisting of two distinct cell types, RS and FS cells, which generate Gamma oscillations by means of the PING mechanism [68]. This modulation is obtained assuming that the NMDAR block predominantly affects interneurons. (2) The boosted gamma oscillations following partial block of NMDA receptors, was accompanied by an increased responsiveness to external inputs. (3) This increase of responsiveness could also be seen for asynchronous states, with no apparent gamma. We discuss below the implications of these findings.

A first prediction of the model is that it was necessary that the antagonism affects predominantly NMDAR receptors on interneurons. This feature is supported by a number of observations. Intuitively, if the NMDAR block would occur predominantly on excitatory cells, then it is difficult to see how diminishing excitation could augment the activity and excitability of the network. This long-standing question was resolved recently by finding that indeed, NMDAR antagonists primarily affects NMDA receptors on interneurons. It was observed that the application of Ketamine or MK-801 in subanesthetic doses leads to an increased activity of glutamatergic neurons both in cortex [25, 35] and in hippocampus [33], and that this increase of glutamatergic activity is a consequence of the disinhibition of GABAergic neurons [32, 34]. In addition, it has also been reported in hippocampus that inhibitory neurons are more sensitive to NMDAR antagonists than glutamatergic neurons [69, 70]. Thus, our model completely supports these findings, and could reproduce the increase of Gamma power induced by NMDA receptor antagonists. On the other hand, contrasting results also exist. For example, [31] argue that NMDAR have less impact on the activity of inhibitory neurons than on the one of excitatory neurons, since they and other authors observed that NMDAR block depressed large EPSP–spike coupling more strongly in excitatory than in inhibitory neurons [31, 71, 72].

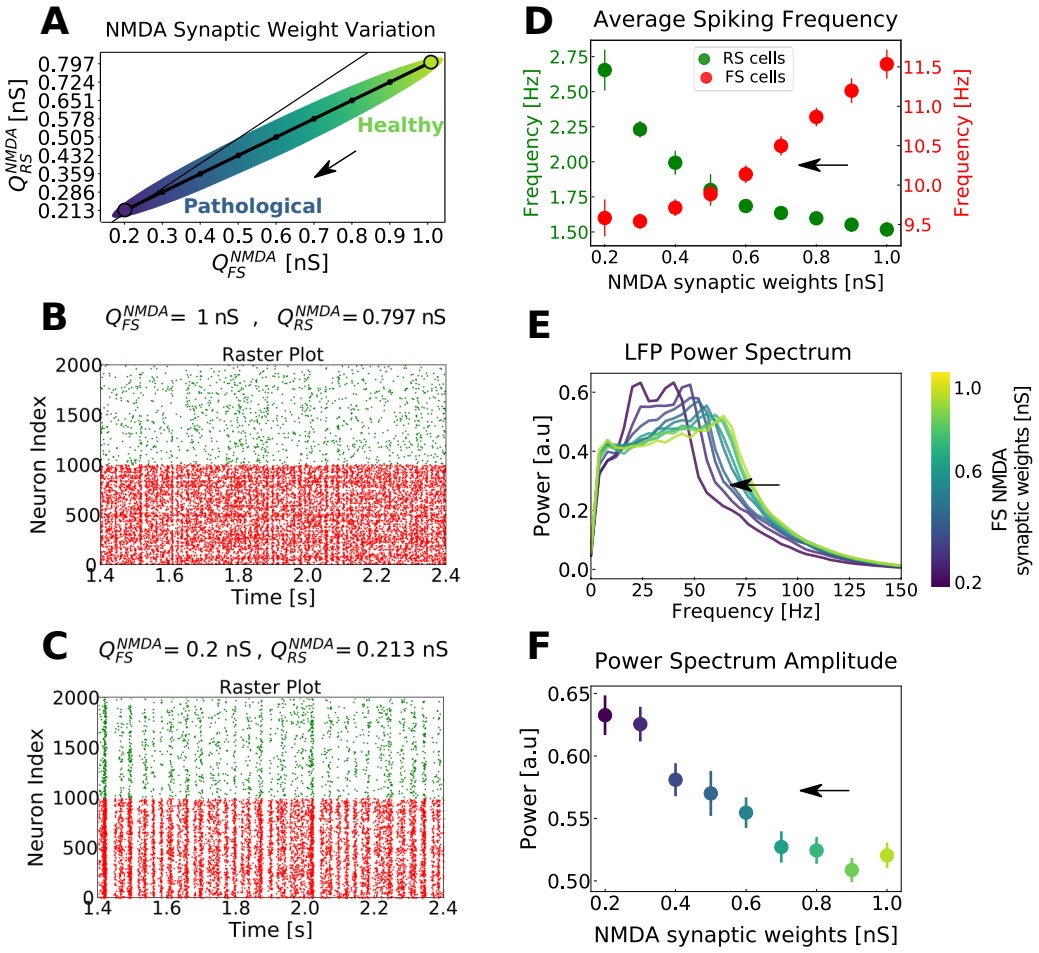

Fig. 1. **Network dynamics with respect to different levels of NMDA channels block in the network**. A) Possible trajectory in the parameter space of Q_{RS}^{NMDA} vs. Q_{FS}^{NMDA}, mimicking the action of NMDA receptor (NMDAR) antagonists (the higher the intensity of the NMDAR antagonists, the smaller the NMDA synaptic strengths). The thin line indicates the identity for reference. The arrow indicates the sens of action of NMDAR antagonists. Points of higher synaptic strengths are associated with healthy conditions, while points with lower synaptic strengths are associated to pathological conditions supposedly similar to the schizophrenic brain. B) and C) Raster plots indicating the activity of only 1000 cells of each type (FS in red and RS in green), for two parameter sets. B: Q_{RS}^{NMDA}= 0.8 nS and Q_{FS}^{NMDA}= 1 nS, and C: Q_{RS}^{NMDA}= 0.213 nS and Q_{FS}^{NMDA}= 0.2 nS. D) Average firing rate of RS (green) and FS cells (red) with respect to the trajectory in parameter space depicted in A. Only the values of Q_{FS}^{NMDA} are indicated in the x axis. Standard errors of the mean (SEM) are indicated as error bars. E) Average normalized Power Spectrum of the network LFP for different NMDA synaptic strength. Like in D, the synaptic strengths follow the curve indicated in A, but only the values of Q_{FS}^{NMDA} are indicated in the color scheme. Notice the shift of the Power Spectrum pick toward smaller frequencies with the increase of NMDA channel block. F) Power Spectrum peak amplitude with respect to the levels of NMDA channels block (following the synaptic strengths indicated in A). The color scheme (presented for better visualization) are the same as in E. Standard errors of the mean (SEM) are indicated as error bars. Results expressed in D, E and F are the outcome of 50 simulations average. The arrows indicate the sense of the behavior according to amount of block of NMDA channels.

The second finding, which is probably the main finding of our study, is that the network has a marked increased responsiveness under the boosted Gamma condition. This increased responsiveness could be tested experimentally either *in vitro*, by testing the response of cortical slices with and without application of NMDAR antagonists, or *in vivo*, by monitoring their response following administration of NMDA antagonists.

The third finding is that the increase of responsiveness is not specific to gamma oscillations, because it was also present for asynchronous states with no apparent gamma. The underlying mechanism is that the antagonism of NMDA receptors produce an overall depolarization of RS cells, and hyperpolarization of FS cells. Consequently, there is an increase of responsiveness of RS cells, with a corresponding decrease for FS cells, as we observed. In this model, the increase of responsiveness is due to the depolarizing effect on RS cells, and are not due to gamma oscillations. Indeed, the highest responsiveness was seen for asynchronous states, also in agreement with a previous modeling study [40].

Possible implications to understand brain pathologies

Our model exhibits several interesting properties that can be related to pathologies. First, the model provides a possible explanation for the symptoms associated to ketamine and others NMDA receptor antagonists, such as hallucinations. The

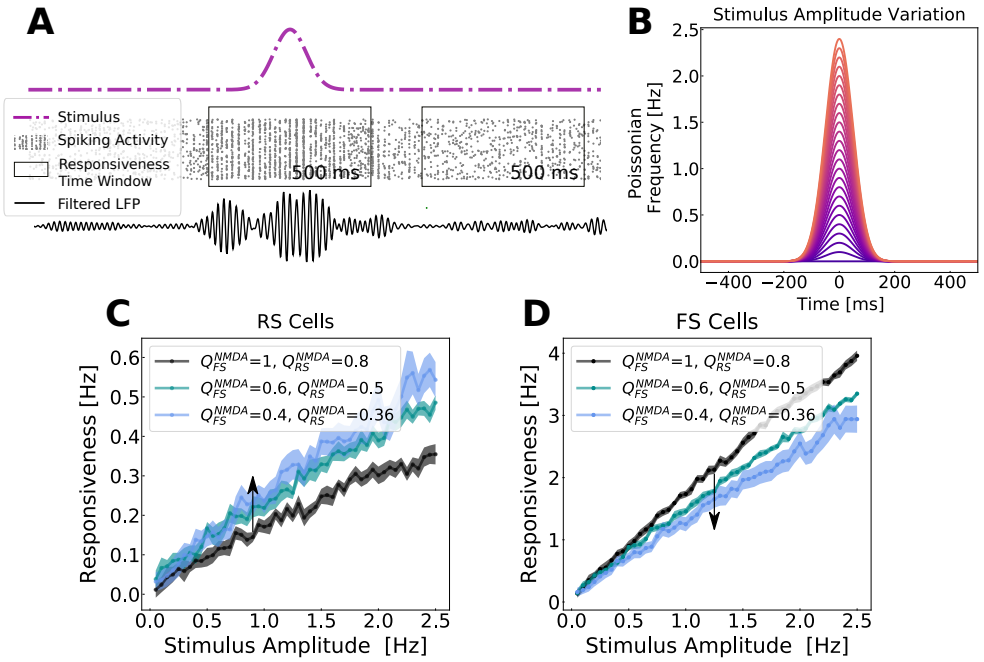

Fig. 2. **Network responsiveness to broad Gaussian inputs in different levels of NMDA channel blocked during Gamma rhythms**. A) Responsiveness protocol scheme. The total number of spikes generated by the network were measured during an external stimulus and in its absence in a time window of 500 ms. The stimulus consisted of a Gaussian fluctuation in the firing rate of the external noise input. Responsiveness was calculated according to Equation 6. B) Gaussian input amplitude variation. The Gaussian amplitude varied from 0.05 Hz to 2.5 Hz (step of 0.05 Hz), always keeping the same standard deviation of 50 ms. C and D depict respectively the responsiveness of RS (C) and FS (D) neurons for different Gaussian amplitudes in different levels of NMDAR block, when the network was displaying Gamma activity. The color-scheme indicates the synaptic weights of NMDA synapses (Q^{NMDA}) in RS and FS cells. The arrow indicates the sense of the simulated action of NMDA antagonist (decreasing synaptic strength). Every point corresponds to the average responsiveness measured in 15 simulations. Standard error of the mean are indicated by the shaded region around each curve.

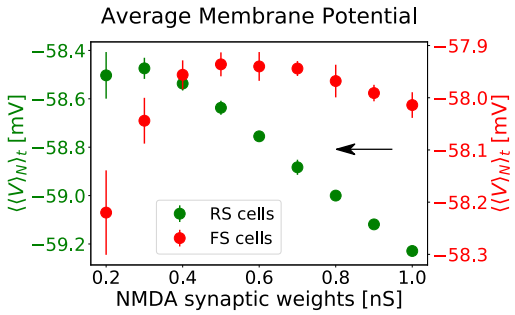

Fig. 3. **Membrane potential polarization as a function of NMDA receptor block**. The average membrane potential of RS (green, left y-axis) and FS (red, right y-axis) is expressed as function of NMDA synaptic weights of RS and FS cells. The values of Q_{RS}^{NMDA} and Q_{FS}^{NMDA} follow the trajectory in the parameter space indicated in Figure 1A. Only the values of Q_{FS}^{NMDA} are indicated in the x axis. The average was performed first in between neurons ($\langle\rangle_N$), obtaining an average curve as a function of time, and subsequently with respect time ($\langle\rangle_t$). The values plotted correspond to the average of $\langle\langle V\rangle_N\rangle_t$ in between 10 simulations. The error bars indicate the standard error of the mean between these simulations.

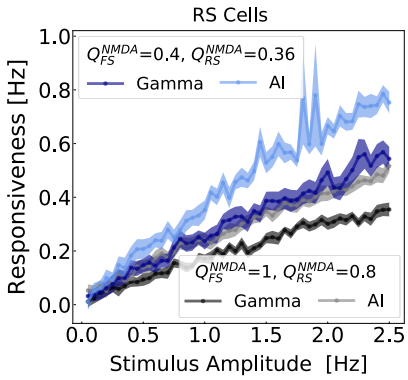

Fig. 4. **Network responsiveness to broad Gaussian inputs of different amplitudes during Gamma and AI states**. The responsiveness of RS neurons, due to different Gaussian amplitudes stimuli (same as in the protocol of Figure 2), was measured in different states AI and Gamma for NMDA synaptic parameter sets: Q_{RS}^{NMDA}= 0.8 nS and Q_{FS}^{NMDA}= 1 nS (Gamma: black, AI: gray), and Q_{RS}^{NMDA}= 0.36 nS and Q_{FS}^{NMDA}= 0.4 nS (Gamma: blue, AI: light blue). The Gaussian amplitude varied from 0.05 Hz to 2.5 Hz (step of 0.05 Hz), always keeping the same standard deviation of 50 ms.

enhanced responsiveness produced by antagonizing NMDA receptors may explain exacerbated responses to sensory stimuli, which may be related to phenomena such as altered perception or hallucinations. Indeed, it is well documented that ketamine produces hallucinations together with a marked increase of gamma oscillations [73–75].

Besides hallucinations, the model seems also a priori consistent with the previously reported role for FS neurons in schizophrenia. Post-mortem analysis of schizophrenic patient brains have shown a reduced expression of parvalbumin (PV) and GAD67 [1, 76–80]. In parallel, genetic ablation of NMDA receptors in PV-positive interneurons in rodents mimics important behavioral [81] and phenotypical features of of the disease

(reduction of GAD67 [82], increase of neuronal excitability [82] and increase of spontaneous Gamma power [83–85]). These observations support the idea that the hypofunction of NMDA receptors in PV-positive interneurons are specially important in this illness.

However, NMDA receptors are expressed in both GABAergic and glutamatergic neurons [32], and it still remains unclear in which types of cells the NMDA receptor hypofunction causes schizophrenia [3, 86]. Some works reported conflicting results and have questioned the hypothesis that PV-positive Fast Spiking neurons play a role in Schizophrenia [31, 86].

In our model, the effect of NMDAR antagonists is to increase excitability due to desinhibition, consistent with a number of experimental observations [25–30]. This increased excitability is accompanied by a Gamma power increase, as also found in experiments with ketamine [17–19] or in schizophrenic patients [6–12]. The model could reproduce all these experimental observations only assuming a larger decrease of the NMDA synaptic strengths in FS cells than in RS cells (see Figure 1A). These results support the idea sustained by some authors [87], that PV-positive Fast Spiking inhibitory neurons play a key role in schizophrenia. Another modeling study also stressed the importance of NMDA channels into FS neurons [88]. Thus, models support the view that the hypofunction of NMDA receptors on FS cells could explain a number of features typical of schizophrenia, such as anomalous responses and boosted gamma oscillations.

IV. Methods

Neuronal Model

Neural units are described by the *Adaptive Exponential Integrate-And-Fire Model* (Adex) [89]. In this model, each neuron i is described by its membrane potential V_i, which evolves according to the following equations:

$$\begin{aligned} C\frac{dV_i(t)}{dt} = & -g_L(V_i - E_L) + g_L\Delta exp\left[\frac{(V_i(t) - V_{th})}{\Delta}\right] \\ & - w_i(t) - I_i^{Syn}(t) \end{aligned}$$

$$\tau_{w_i}\frac{dw_i(t)}{dt} = a(V_i(t) - E_L) - w_i(t) + b\sum_j \delta(t - t_j) \quad (1)$$

where C is the membrane capacitance, g_L is the leakage conductance, E_L is the leaky membrane potential, V_{th} is the effective threshold, Δ is the threshold slope factor and I_i^{Syn}(t) is postsynaptic current received by the neuron i (see next section). The adaptation current, described by the variable w_i, increases by an amount b every time the neuron i emits a spike at times t_j and decays exponentially with time scale τ_w. The subthreshold adaptation is governed by the parameter a.

During the simulations, the equation characterizing the membrane potential V_i is numerically integrated until a spike is generated. Formally this happens when V_i grows rapidly toward infinity. In practice, the spiking time is defined as the moment in which V_i reaches a certain threshold (V_{th}). When V_i = V_{th} the membrane potential is reset to V_{rest}, which is kept constant until the end of the refractory period T_{ref}. After the refractory period the equations start being integrated again.

In the developed network two types of cells were used: Regular Spiking (RS) excitatory cells and Fast Spiking (FS) inhibitory cells. The cell specific parameters are indicated in Table I.

TABLE I
Specific Neuron Model Parameters

Parameter	RS	FS
V_{th}	-40 mV	-47.5 mV
Δ	2 mV	0.5 mV
T_{ref}	5 ms	5 ms
τ_w	500 ms	500 ms
a	4 nS	0 nS
b	20 pA	0 pA
C	150 pF	150 pF
g_L	10 nS	10 nS
E_L	-65 mV	-65 mV
E_E	0 mV	0 mV
E_I	80 mV	80 mV
V_{rest}	-65 mV	-65 mV

Synaptic Models

The post-synaptic current received by each neuron i is composed by three components: two excitatory, referent to $AMPA$ and $NMDA$ synaptic channels, and one inhibitory, referent to $GABA_A$ channels.

$$I_i^{Syn}(t) = I_i^{AMPA}(t) + I_i^{GABA_A}(t) + I_i^{NMDA}(t)$$

in which

$$\begin{aligned} I_i^{AMPA}(t) &= G_i^{AMPA}(t)(V_i(t) - E^{AMPA}) \\ I_i^{GABA_A}(t) &= G_i^{GABA_A}(t)(V_i(t) - E^{GABA_A}) \\ I_i^{NMDA}(t) &= G_i^{NMDA}(t)(V_i(t) - E^{NMDA})B(V_i(t)) \end{aligned} \quad (2)$$

E^{AMPA}= 0 mV, E^{GABA_A}= -80 mV and E^{NMDA}= 0 mV are the reversal potentials of $AMPA$, $GABA_A$ and $NMDA$ channels. While the $AMPA$ and $GABA_A$-mediated currents are fast, the NMDA-mediated are considerably slower and present a complex relation with respect to the membrane potential [90–93]. This complex relation , due to magnesium block, is accurately modeled by the phenomenological expression B(V) [94] :

$$B(V) = \frac{1}{1 + exp(-0.062V).([Mg^{2+}]_o/3.57)} \quad (3)$$

where $[Mg^{2+}]_o$= 1 mM is the external magnesium concentration (1 to 2 mM in physiological conditions).

Because of the fast dynamicas of $AMPA$ and $GABA_A$ channels, their synaptic conductances (G^X with X=$AMPA$, $GABA_A$) are usually modeled to increase discontinuously by a discrete amount Q^X, every time a presynaptic neuron spikes at time t_k, and to subsequently decay exponentially with a decay time constant τ^X_{decay} according to the following equation:

$$\tau^X_{decay}\frac{dG^X{}_i(t)}{dt} = -G^X{}_i(t) + Q^X\sum_k \delta(t-t_k) \qquad (4)$$

In which, $\sum_k$ runs over all the presynaptic spike times. The synaptic time constantes used for $AMPA$ and $GABA_A$ synapses are τ^{AMPA}_{decay}= 1.5 ms and $\tau^{GABA_A}_{decay}$= 7.5 ms.

NMDA channels synaptic conductances, G^{NMDA}, because of their slow dynamics, are usually modeled as a bi-exponential function characterized by a rise time constant, τ^{NMDA}_{rise}= 2 ms, and a decay time constant τ^{NMDA}_{decay}= 200 ms, according to the following equation:

$$\begin{aligned} G^{NMDA}_i &= Q^{NMDA}_i s_i(t)^{NMDA} \\ \frac{ds_i(t)^{NMDA}}{dt} &= -\frac{s_i(t)^{NMDA}}{\tau^{NMDA}_{decay}} + \alpha x_i(t)(1-s_i(t)^{NMDA}) \\ \frac{dx_i(t)}{dt} &= -\frac{x_i(t)}{\tau^{NMDA}_{rise}} + \sum_k \delta(t-t_k) \end{aligned} \qquad (5)$$

In which, Q^{NMDA}_i is the synaptic strength of the NMDA synapse towards the neuron i, α= 0.5/ms and $x(t)$ is an auxiliary variable. The $\sum_k$ runs over all the presynaptic spike times. Both, $s(t)^{NMDA}$ and $x(t)$, are adimensional.

Synaptic strenghs of $NMDA$ synapses (towards RS and FS neurons) were chosen according to the parameter search expressed in Figure 5, while the synaptic parameters of $AMPA$ and $GABA_A$ synapses were chosen according to previous works [40, 95] (Q^{AMPA}= 5 nS and Q^{GABA_A}= 3.34 nS). All synapses ($AMPA$, $GABA_A$ and $NMDA$) were delayed by time of 1.5 ms. With these choice of parameters the NMDA/AMPA charge ratio in the network is on average higher in RS cells then in FS cells (see Figure IV), in agreement with experimental measurements in prefrontal cortex of adult mice [31] and rat [96].

Network Structure

The network developed in this work is composed of 5000 neurons (4000 RS and 1000 FS). Each neuron (RS or FS) was connected randomly to every other neurons in the network with a probability of 10%, receiving on average 500 excitatory synapses (mediated by both $AMPA$ and $NMDA$ channels) and 100 inhibitory synapses (mediated by $GABA_A$ channels).

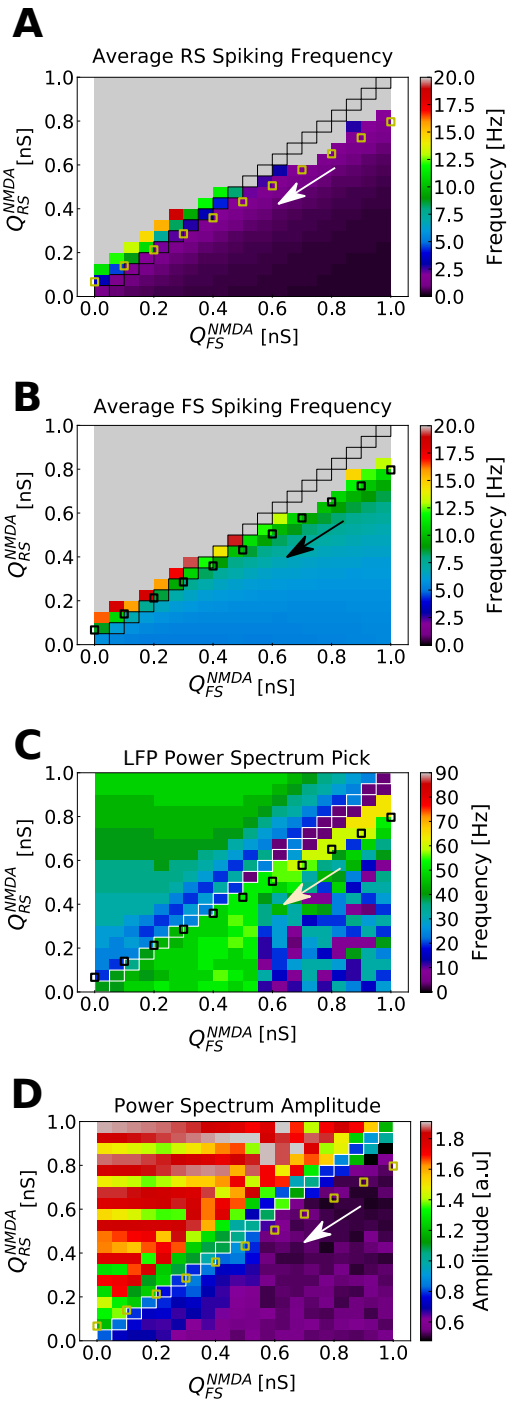

Fig. 5. **Parameter space of NMDA synaptic weights in RS and FS cells**. A) Average spiking rate in RS cells. B) Average spiking rate in FS cells. C) LFP Power Spectrum pick. D) LFP Power Spectrum amplitude. The parameter space of NMDA synaptic weights (Q^{NMDA}) was explored for RS and FS cells in the developed network model. Q^{NMDA}_{RS} and Q^{NMDA}_{FS} varied from 0 nS to 1 nS in steps of 0.05 nS. Each point in the color maps corresponds to the average of 10 simulations of 5 seconds. Points in which Q^{NMDA}_{RS}=Q^{NMDA}_{FS} are highlighted. Small squares indicate a possible trajectory in the parameter space (in the direction of the arrow) generated by the action of NMDAR antagonists. This is the same trajectory indicated in Figure 1A.

External Input

In addition to recurrent connections, each neuron received an external drive to keep the network active. This external drive consisted of $N_{ext} = 5000$ independent and identically distributed excitatory Poissonian spike trains with a spiking frequency μ_{ext}. These spike trains were sent to the network with a 10% probability of connection and were computed inside of the synaptic current term I^{AMPA}, with a synaptic strength of Q_{Ext}^{AMPA}= 0.8 nS. For Gamma activity, the network was stimulated with a drive with μ_{ext}= 3 Hz. For Asynchronous and Irregular activity, the network was stimulated with a drive with μ_{ext}= 2 Hz. The external drive mimicked cortical input, like if the network was embedded in a much bigger one.

To test network responsiveness, an additional external input was included in the simulations. This external input, similar to the external drive, also consisted of $N_{ext} = 5000$ independent and identically distributed excitatory Poissonian spike trains, connected to the network with a 10% probability. The difference of this input was its firing rate time dependence ($\mu_{ext}(t)$). The spiking frequency of the spike trains varied in a Gaussian manner, with a standard deviation of 50 ms and variable amplitude. These spike trains were computed inside of both synaptic current terms I^{AMPA} and I^{NMDA}, with a synaptic strengths of Q_{Ext}^{AMPA}= 0.8 nS, and $Q_{Ext^{RS}}^{NMDA}$ and $Q_{Ext^{FS}}^{NMDA}$ as indicated in each case.

Block of NMDA channels: effect of NMDAR antagonists

In this work, we mimic the effect of NMDAR antagonists by changing the value of the NMDA synaptic weights Q^{NMDA}. In Figure 5 a possible trajectory in the parameter space generated by the action of NMDAR antagonists is depicted. This is the same trajectory indicated in Figure 1A.

Simulations

All neural networks were constructed using Brian2 simulator [97]. All equations were numerically integrated using Euler Methods and dt=0.1 ms as integration time step. The codes for each one of the three developed networks are available at ModelDB platform.

Population activity: LFP model

To measure the global behavior of the neuronal population, we used a simulated Local Field Potential (LFP). This LFP was generated by the network, by means of a recent method developed by [98]. This approach calculates the LFP by convolving the spike trains of the network with a Kernel that have been previously estimated from unitary LFPs (the LFP generated by a single axon, *uLFP*) measured experimentally. Since this method assumes a spatial neuronal displacement, to be able to apply it to our simulations, we randomly displaced part of the network (50 neurons) in 2-D grid, assuming that the electrode was displaced on its center and was measuring the LFP in the same layer as neuronal soma. The program code of the kernel method is available in ModelDB (http://modeldb.yale.edu/266508), using python 3 or the *hoc* language of NEURON.

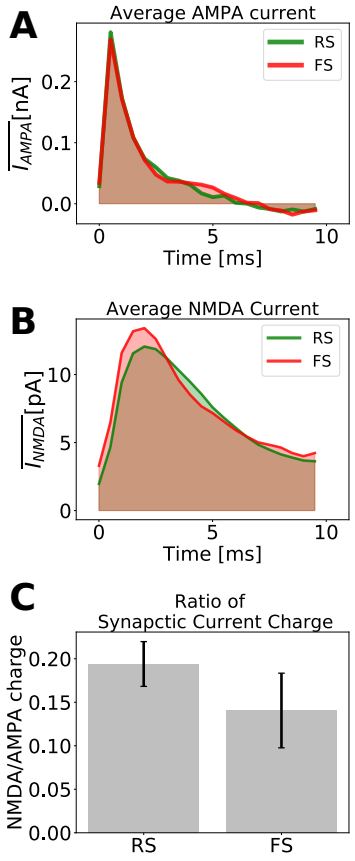

Fig. 6. **Excitatory synaptic currents**. A) Average AMPA current of one randomly picked RS (green) and one randomly picked FS (red) neuron. B) Average NMDA current of one randomly picked RS (green) and one randomly picked FS (red) neuron. C) Ratio of NMDA and AMPA charges for RS and FS cells. The synaptic charge ratio of each neuron was calculated separately. The Bars indicate the mean and the standard deviation among the RS and FS population. The NMDA synaptic strengths in RS and FS cells are Q_{RS}^{NMDA}=0.8 nS and Q_{FS}^{NMDA}= 1 nS (which, in our model, describes a healthy condition).

Power Spectrum

The Power spectrum of the simulated LFP was calculated by means of the Welch's method, using a Hamming window of length 0.25 seconds and 125 overlapping points. We used the Python-based ecosystem Scipy function *signal.welch* to do our calculations.

Synaptic Charge

The synaptic charge (AMPA or NMDA) of each neuron is defined as the area under the curve of the average synaptic current (shaded areas of Figure A or B), which was calculated from the presynaptic input time until 10 ms after it.

Responsiveness

The level of *responsiveness* (R) of a network, due to an stimulus (S) in a time window of duration T, is defined as the difference between the total number of spikes generated by the whole network due to an stimulus (N_{spikes}^{S}) and the total number of spikes generated in the absence of the stimulus

(N_{spikes}), normalized by the network size (total number of neurons N_n) and the duration of the time window T.

$$R = \frac{N^S_{spikes} - N_{spikes}}{TN_n} \tag{6}$$

ACKNOWLEDGMENTS

This research was supported by the Centre National de la Recherche Scientifique (CNRS) and the European Community (Human Brain Project, H2020-785907). E.S. acknowledges a PhD fellowship from the École des Neurosciences de Paris (ENP) and from the Fondation pour la Recherche Médicale (FRM) - grant FDT202012010566 and the financial support from La Fondation des Treilles.

REFERENCES

[1] D. A. Lewis, T. Hashimoto, and D. W. Volk, "Cortical inhibitory neurons and schizophrenia," Nature Reviews Neuroscience, vol. 6, no. 4, pp. 312–324, 2005.

[2] V. P. Bozikas and C. Andreou, "Longitudinal studies of cognition in first episode psychosis: a systematic review of the literature," Australian & New Zealand Journal of Psychiatry, vol. 45, no. 2, pp. 93–108, 2011.

[3] T. Su, Y. Lu, Y. Geng, W. Lu, and Y. Chen, "How could n-methyl-d-aspartate receptor antagonists lead to excitation instead of inhibition?" Brain Science Advances, vol. 4, no. 2, pp. 73–98, 2018.

[4] P. J. Uhlhaas and W. Singer, "Abnormal neural oscillations and synchrony in schizophrenia," Nature reviews neuroscience, vol. 11, no. 2, pp. 100–113, 2010.

[5] M. E. Shenton, C. C. Dickey, M. Frumin, and R. W. McCarley, "A review of mri findings in schizophrenia," Schizophrenia research, vol. 49, no. 1-2, pp. 1–52, 2001.

[6] G. Flynn, D. Alexander, A. Harris, T. Whitford, W. Wong, C. Galletly, S. Silverstein, E. Gordon, and L. M. Williams, "Increased absolute magnitude of gamma synchrony in first-episode psychosis," Schizophrenia research, vol. 105, no. 1-3, pp. 262–271, 2008.

[7] T. Grent, J. Gross, J. Goense, M. Wibral, R. Gajwani, A. I. Gumley, S. M. Lawrie, M. Schwannauer, F. Schultze-Lutter, T. N. Schröder, et al., "Resting-state gamma-band power alterations in schizophrenia reveal e/i-balance abnormalities across illness-stages," Elife, vol. 7, p. e37799, 2018.

[8] A. Perrottelli, G. M. Giordano, F. Brando, L. Giuliani, and A. Mucci, "Eeg-based measures in at-risk mental state and early stages of schizophrenia: A systematic review," Frontiers in psychiatry, vol. 12, p. 582, 2021.

[9] C. Mulert, V. Kirsch, R. Pascual-Marqui, R. W. McCarley, and K. M. Spencer, "Long-range synchrony of gamma oscillations and auditory hallucination symptoms in schizophrenia," International Journal of Psychophysiology, vol. 79, no. 1, pp. 55–63, 2011.

[10] K. M. Spencer, D. F. Salisbury, M. E. Shenton, and R. W. McCarley, "γ-band auditory steady-state responses are impaired in first episode psychosis," Biological psychiatry, vol. 64, no. 5, pp. 369–375, 2008.

[11] K. M. Spencer, P. G. Nestor, R. Perlmutter, M. A. Niznikiewicz, M. C. Klump, M. Frumin, M. E. Shenton, and R. W. McCarley, "Neural synchrony indexes disordered perception and cognition in schizophrenia," Proceedings of the National Academy of Sciences, vol. 101, no. 49, pp. 17 288–17 293, 2004.

[12] K. M. Spencer, M. A. Niznikiewicz, P. G. Nestor, M. E. Shenton, and R. W. McCarley, "Left auditory cortex gamma synchronization and auditory hallucination symptoms in schizophrenia," BMC neuroscience, vol. 10, no. 1, pp. 1–13, 2009.

[13] H. Gunduz-Bruce, "The acute effects of nmda antagonism: from the rodent to the human brain," Brain research reviews, vol. 60, no. 2, pp. 279–286, 2009.

[14] D. C. Javitt and S. R. Zukin, "Recent advances in the phencyclidine model of schizophrenia." The American journal of psychiatry, 1991.

[15] J. H. Krystal, L. P. Karper, J. P. Seibyl, G. K. Freeman, R. Delaney, J. D. Bremner, G. R. Heninger, M. B. Bowers, and D. S. Charney, "Subanesthetic effects of the noncompetitive nmda antagonist, ketamine, in humans: psychotomimetic, perceptual, cognitive, and neuroendocrine responses," Archives of general psychiatry, vol. 51, no. 3, pp. 199–214, 1994.

[16] S. S. Kalsi, D. M. Wood, and P. I. Dargan, "The epidemiology and patterns of acute and chronic toxicity associated with recreational ketamine use," Emerging Health Threats Journal, vol. 4, no. 1, p. 7107, 2011.

[17] A. D. Shaw, N. Saxena, L. E. Jackson, J. E. Hall, K. D. Singh, and S. D. Muthukumaraswamy, "Ketamine amplifies induced gamma frequency oscillations in the human cerebral cortex," European Neuropsychopharmacology, vol. 25, no. 8, pp. 1136–1146, 2015.

[18] G. Plourde, J. Baribeau, and V. Bonhomme, "Ketamine increases the amplitude of the 40-hz auditory steady-state response in humans." British journal of anaesthesia, vol. 78, no. 5, pp. 524–529, 1997.

[19] L. E. Hong, A. Summerfelt, R. W. Buchanan, P. O'donnell, G. K. Thaker, M. A. Weiler, and A. C. Lahti, "Gamma and delta neural oscillations and association with clinical symptoms under subanesthetic ketamine," Neuropsychopharmacology, vol. 35, no. 3, pp. 632–640, 2010.

[20] D. Pinault, "N-methyl d-aspartate receptor antagonists ketamine and mk-801 induce wake-related aberrant γ oscillations in the rat neocortex," Biological psychiatry, vol. 63, no. 8, pp. 730–735, 2008.

[21] B. Kocsis, "Differential role of nr2a and nr2b subunits in n-methyl-d-aspartate receptor antagonist-induced aberrant cortical gamma oscillations," Biological psychiatry, vol. 71, no. 11, pp. 987–995, 2012.

[22] J. Wood, Y. Kim, and B. Moghaddam, "Disruption of prefrontal cortex large scale neuronal activity by different classes of psychotomimetic drugs," Journal of

Neuroscience, vol. 32, no. 9, pp. 3022–3031, 2012.
[23] M. J. Nicolás, J. López-Azcárate, M. Valencia, M. Alegre, M. Pérez-Alcázar, J. Iriarte, and J. Artieda, "Ketamine-induced oscillations in the motor circuit of the rat basal ganglia," PloS one, vol. 6, no. 7, p. e21814, 2011.
[24] M. Slovik, B. Rosin, S. Moshel, R. Mitelman, E. Schechtman, R. Eitan, A. Raz, and H. Bergman, "Ketamine induced converged synchronous gamma oscillations in the cortico-basal ganglia network of nonhuman primates," Journal of neurophysiology, vol. 118, no. 2, pp. 917–931, 2017.
[25] B. Moghaddam, B. Adams, A. Verma, and D. Daly, "Activation of glutamatergic neurotransmission by ketamine: a novel step in the pathway from nmda receptor blockade to dopaminergic and cognitive disruptions associated with the prefrontal cortex," Journal of Neuroscience, vol. 17, no. 8, pp. 2921–2927, 1997.
[26] A. C. Lahti, H. H. Holcomb, D. R. Medoff, and C. A. Tamminga, "Ketamine activates psychosis and alters limbic blood flow in schizophrenia." Neuroreport, vol. 6, no. 6, pp. 869–872, 1995.
[27] A. Breier, A. K. Malhotra, D. A. Pinals, N. I. Weisenfeld, and D. Pickar, "Association of ketamine-induced psychosis with focal activation of the prefrontal cortex in healthy volunteers." The American journal of psychiatry, 1997.
[28] F. Vollenweider, K. Leenders, I. Øye, D. Hell, and J. Angst, "Differential psychopathology and patterns of cerebral glucose utilisation produced by (s)-and (r)-ketamine in healthy volunteers using positron emission tomography (pet)," European Neuropsychopharmacology, vol. 7, no. 1, pp. 25–38, 1997.
[29] Y. Suzuki, E. Jodo, S. Takeuchi, S. Niwa, and Y. Kayama, "Acute administration of phencyclidine induces tonic activation of medial prefrontal cortex neurons in freely moving rats," Neuroscience, vol. 114, no. 3, pp. 769–779, 2002.
[30] M. E. Jackson, H. Homayoun, and B. Moghaddam, "Nmda receptor hypofunction produces concomitant firing rate potentiation and burst activity reduction in the prefrontal cortex," Proceedings of the National Academy of Sciences, vol. 101, no. 22, pp. 8467–8472, 2004.
[31] D. C. Rotaru, H. Yoshino, D. A. Lewis, G. B. Ermentrout, and G. Gonzalez-Burgos, "Glutamate receptor subtypes mediating synaptic activation of prefrontal cortex neurons: relevance for schizophrenia," Journal of Neuroscience, vol. 31, no. 1, pp. 142–156, 2011.
[32] H. Homayoun and B. Moghaddam, "Nmda receptor hypofunction produces opposite effects on prefrontal cortex interneurons and pyramidal neurons," Journal of Neuroscience, vol. 27, no. 43, pp. 11 496–11 500, 2007.
[33] A. J. Widman and L. L. McMahon, "Disinhibition of ca1 pyramidal cells by low-dose ketamine and other antagonists with rapid antidepressant efficacy," Proceedings of the National Academy of Sciences, vol. 115, no. 13, pp. E3007–E3016, 2018.
[34] Y. Zhang, M. M. Behrens, and J. E. Lisman, "Prolonged exposure to nmdar antagonist suppresses inhibitory synaptic transmission in prefrontal cortex," Journal of neurophysiology, vol. 100, no. 2, pp. 959–965, 2008.
[35] V. D. Lazzaro, A. Oliviero, P. Profice, M. Pennisi, F. Pilato, G. Zito, M. Dileone, R. Nicoletti, P. Pasqualetti, and P. Tonali, "Ketamine increases human motor cortex excitability to transcranial magnetic stimulation," The Journal of physiology, vol. 547, no. 2, pp. 485–496, 2003.
[36] R. E. Hoffman and I. Cavus, "Slow transcranial magnetic stimulation, long-term depotentiation, and brain hyperexcitability disorders," American Journal of Psychiatry, vol. 159, no. 7, pp. 1093–1102, 2002.
[37] Z. J. Daskalakis, P. B. Fitzgerald, and B. K. Christensen, "The role of cortical inhibition in the pathophysiology and treatment of schizophrenia," Brain research reviews, vol. 56, no. 2, pp. 427–442, 2007.
[38] R. E. Hoffman, K. A. Hawkins, R. Gueorguieva, N. N. Boutros, F. Rachid, K. Carroll, and J. H. Krystal, "Transcranial magnetic stimulation of left temporoparietal cortex and medication-resistant auditory hallucinations," Archives of general psychiatry, vol. 60, no. 1, pp. 49–56, 2003.
[39] L. B. Merabet, M. Kobayashi, J. Barton, and A. Pascual-Leone, "Suppression of complex visual hallucinatory experiences by occipital transcranial magnetic stimulation: a case report," Neurocase, vol. 9, no. 5, pp. 436–440, 2003.
[40] E. Susin and A. Destexhe, "Integration, coincidence detection and resonance in networks of spiking neurons expressing gamma oscillations and asynchronous states," bioRxiv, 2021.
[41] W. Singer and C. M. Gray, "Visual feature integration and the temporal correlation hypothesis," Annual review of neuroscience, vol. 18, no. 1, pp. 555–586, 1995.
[42] W. Singer, "Neuronal synchrony: a versatile code for the definition of relations?" Neuron, vol. 24, no. 1, pp. 49–65, 1999.
[43] J. O'Keefe and M. L. Recce, "Phase relationship between hippocampal place units and the eeg theta rhythm," Hippocampus, vol. 3, no. 3, pp. 317–330, 1993.
[44] P. Fries, D. Nikolić, and W. Singer, "The gamma cycle," Trends in neurosciences, vol. 30, no. 7, pp. 309–316, 2007.
[45] P. Fries, "A mechanism for cognitive dynamics: neuronal communication through neuronal coherence," Trends in cognitive sciences, vol. 9, no. 10, pp. 474–480, 2005.
[46] ——, "Rhythms for cognition: communication through coherence," Neuron, vol. 88, no. 1, pp. 220–235, 2015.
[47] B. Pesaran, J. S. Pezaris, M. Sahani, P. P. Mitra, and R. A. Andersen, "Temporal structure in neuronal activity during working memory in macaque parietal cortex," Nature neuroscience, vol. 5, no. 8, pp. 805–811, 2002.
[48] L. L. Colgin, T. Denninger, M. Fyhn, T. Hafting, T. Bonnevie, O. Jensen, M.-B. Moser, and E. I. Moser, "Frequency of gamma oscillations routes flow of information in the hippocampus," Nature, vol. 462, no. 7271, pp. 353–

357, 2009.

[49] M. F. Carr, M. P. Karlsson, and L. M. Frank, "Transient slow gamma synchrony underlies hippocampal memory replay," Neuron, vol. 75, no. 4, pp. 700–713, 2012.

[50] A. Rougeul-Buser, J. Bouyer, and P. Buser, "From attentiveness to sleep. a topographical analysis of localized" synchronized" activities on the cortex of normal cat and monkey," Acta Neurobiol Exp (Warsz), vol. 35, no. 5-6, pp. 805–19, 1975.

[51] J. Bouyer, M. Montaron, and A. Rougeul, "Fast fronto-parietal rhythms during combined focused attentive behaviour and immobility in cat: cortical and thalamic localizations," Electroencephalography and clinical neurophysiology, vol. 51, no. 3, pp. 244–252, 1981.

[52] E. Rodriguez, N. George, J.-P. Lachaux, J. Martinerie, B. Renault, and F. J. Varela, "Perception's shadow: long-distance synchronization of human brain activity," Nature, vol. 397, no. 6718, pp. 430–433, 1999.

[53] L. Melloni, C. Molina, M. Pena, D. Torres, W. Singer, and E. Rodriguez, "Synchronization of neural activity across cortical areas correlates with conscious perception," Journal of neuroscience, vol. 27, no. 11, pp. 2858–2865, 2007.

[54] P. Fries, J. H. Reynolds, A. E. Rorie, and R. Desimone, "Modulation of oscillatory neuronal synchronization by selective visual attention," Science, vol. 291, no. 5508, pp. 1560–1563, 2001.

[55] G. G. Gregoriou, S. J. Gotts, H. Zhou, and R. Desimone, "High-frequency, long-range coupling between prefrontal and visual cortex during attention," science, vol. 324, no. 5931, pp. 1207–1210, 2009.

[56] M. Vinck, T. Womelsdorf, E. A. Buffalo, R. Desimone, and P. Fries, "Attentional modulation of cell-class-specific gamma-band synchronization in awake monkey area v4," Neuron, vol. 80, no. 4, pp. 1077–1089, 2013.

[57] S. Rouhinen, J. Panula, J. M. Palva, and S. Palva, "Load dependence of β and γ oscillations predicts individual capacity of visual attention," Journal of Neuroscience, vol. 33, no. 48, pp. 19 023–19 033, 2013.

[58] D. E. Sheer, "Focused arousal and the cognitive 40-hz event-related potentials: differential diagnosis of alzheimer's disease." Progress in clinical and biological research, vol. 317, pp. 79–94, 1989.

[59] T. Womelsdorf, P. Fries, P. P. Mitra, and R. Desimone, "Gamma-band synchronization in visual cortex predicts speed of change detection," Nature, vol. 439, no. 7077, pp. 733–736, 2006.

[60] N. Brunel, "Dynamics of sparsely connected networks of excitatory and inhibitory spiking neurons," Journal of computational neuroscience, vol. 8, no. 3, pp. 183–208, 2000.

[61] C. Koch, M. Massimini, M. Boly, and G. Tononi, "Neural correlates of consciousness: progress and problems," Nature Reviews Neuroscience, vol. 17, no. 5, pp. 307–321, 2016.

[62] J. S. Goldman, N. Tort-Colet, M. Di Volo, E. Susin, J. Bouté, M. Dali, M. Carlu, T.-A. Nghiem, T. Górski, and A. Destexhe, "Bridging single neuron dynamics to global brain states," Frontiers in systems neuroscience, vol. 13, p. 75, 2019.

[63] W. R. Softky and C. Koch, "The highly irregular firing of cortical cells is inconsistent with temporal integration of random epsps," Journal of neuroscience, vol. 13, no. 1, pp. 334–350, 1993.

[64] G. R. Holt, W. R. Softky, C. Koch, and R. J. Douglas, "Comparison of discharge variability in vitro and in vivo in cat visual cortex neurons," Journal of neurophysiology, vol. 75, no. 5, pp. 1806–1814, 1996.

[65] M. N. Shadlen and W. T. Newsome, "The variable discharge of cortical neurons: implications for connectivity, computation, and information coding," Journal of neuroscience, vol. 18, no. 10, pp. 3870–3896, 1998.

[66] A. Destexhe, M. Rudolph, and D. Paré, "The high-conductance state of neocortical neurons in vivo," Nature reviews neuroscience, vol. 4, no. 9, pp. 739–751, 2003.

[67] J. A. Henrie and R. Shapley, "Lfp power spectra in v1 cortex: the graded effect of stimulus contrast," Journal of neurophysiology, vol. 94, no. 1, pp. 479–490, 2005.

[68] P. Tiesinga and T. J. Sejnowski, "Cortical enlightenment: are attentional gamma oscillations driven by ing or ping?" Neuron, vol. 63, no. 6, pp. 727–732, 2009.

[69] D. S. Ling and L. S. Benardo, "Activity-dependent depression of monosynaptic fast ipscs in hippocampus: contributions from reductions in chloride driving force and conductance," Brain research, vol. 670, no. 1, pp. 142–146, 1995.

[70] H. C. Grunze, D. G. Rainnie, M. E. Hasselmo, E. Barkai, E. F. Hearn, R. W. McCarley, and R. W. Greene, "Nmda-dependent modulation of ca1 local circuit inhibition," Journal of Neuroscience, vol. 16, no. 6, pp. 2034–2043, 1996.

[71] D. Ling and L. S. Benardo, "Recruitment of gabaa inhibition in rat neocortex is limited and not nmda dependent," Journal of Neurophysiology, vol. 74, no. 6, pp. 2329–2335, 1995.

[72] T. Karayannis, I. Huerta-Ocampo, and M. Capogna, "Gabaergic and pyramidal neurons of deep cortical layers directly receive and differently integrate callosal input," Cerebral Cortex, vol. 17, no. 5, pp. 1213–1226, 2007.

[73] N. C. Jones, M. Reddy, P. Anderson, M. R. Salzberg, T. J. O'Brien, and D. Pinault, "Acute administration of typical and atypical antipsychotics reduces eeg gamma power, but only the preclinical compound ly379268 reduces the ketamine-induced rise in gamma power," International Journal of Neuropsychopharmacology, vol. 15, no. 5, pp. 657–668, 2012.

[74] T. Hakami, N. C. Jones, E. A. Tolmacheva, J. Gaudias, J. Chaumont, M. Salzberg, T. J. O'Brien, and D. Pinault, "Nmda receptor hypofunction leads to generalized and persistent aberrant γ oscillations independent of hyperlocomotion and the state of consciousness," PloS one, vol. 4, no. 8, p. e6755, 2009.

[75] K.-H. Lee, L. M. Williams, M. Breakspear, and E. Gordon, "Synchronous gamma activity: a review and contribution to an integrative neuroscience model of schizophrenia," Brain Research Reviews, vol. 41, no. 1,

pp. 57–78, 2003.

[76] S. Akbarian, J. J. Kim, S. G. Potkin, J. O. Hagman, A. Tafazzoli, W. E. Bunney, and E. G. Jones, "Gene expression for glutamic acid decarboxylase is reduced without loss of neurons in prefrontal cortex of schizophrenics," Archives of general psychiatry, vol. 52, no. 4, pp. 258–266, 1995.

[77] D. W. Volk, M. C. Austin, J. N. Pierri, A. R. Sampson, and D. A. Lewis, "Decreased glutamic acid decarboxylase67 messenger rna expression in a subset of prefrontal cortical γ-aminobutyric acid neurons in subjects with schizophrenia," Archives of general psychiatry, vol. 57, no. 3, pp. 237–245, 2000.

[78] S. Akbarian and H.-S. Huang, "Molecular and cellular mechanisms of altered gad1/gad67 expression in schizophrenia and related disorders," Brain research reviews, vol. 52, no. 2, pp. 293–304, 2006.

[79] M. Inan, T. J. Petros, and S. A. Anderson, "Losing your inhibition: linking cortical gabaergic interneurons to schizophrenia," Neurobiology of disease, vol. 53, pp. 36–48, 2013.

[80] D. Eyles, J. McGrath, and G. Reynolds, "Neuronal calcium-binding proteins and schizophrenia," Schizophrenia research, vol. 57, no. 1, pp. 27–34, 2002.

[81] T. Korotkova, E. C. Fuchs, A. Ponomarenko, J. von Engelhardt, and H. Monyer, "Nmda receptor ablation on parvalbumin-positive interneurons impairs hippocampal synchrony, spatial representations, and working memory," Neuron, vol. 68, no. 3, pp. 557–569, 2010.

[82] J. E. Belforte, V. Zsiros, E. R. Sklar, Z. Jiang, G. Yu, Y. Li, E. M. Quinlan, and K. Nakazawa, "Postnatal nmda receptor ablation in corticolimbic interneurons confers schizophrenia-like phenotypes," Nature neuroscience, vol. 13, no. 1, pp. 76–83, 2010.

[83] M. Carlen, K. Meletis, J. Siegle, J. Cardin, K. Futai, D. Vierling-Claassen, C. Ruehlmann, S. R. Jones, K. Deisseroth, M. Sheng, et al., "A critical role for nmda receptors in parvalbumin interneurons for gamma rhythm induction and behavior," Molecular psychiatry, vol. 17, no. 5, pp. 537–548, 2012.

[84] E. N. Billingslea, V. M. Tatard-Leitman, J. Anguiano, C. R. Jutzeler, J. Suh, J. A. Saunders, S. Morita, R. E. Featherstone, P. I. Ortinski, M. J. Gandal, et al., "Parvalbumin cell ablation of nmda-r1 causes increased resting network excitability with associated social and self-care deficits," Neuropsychopharmacology, vol. 39, no. 7, pp. 1603–1613, 2014.

[85] K. Nakao and K. Nakazawa, "Brain state-dependent abnormal lfp activity in the auditory cortex of a schizophrenia mouse model," Frontiers in neuroscience, vol. 8, p. 168, 2014.

[86] G. Gonzalez-Burgos and D. A. Lewis, "Nmda receptor hypofunction, parvalbumin-positive neurons, and cortical gamma oscillations in schizophrenia," Schizophrenia bulletin, vol. 38, no. 5, pp. 950–957, 2012.

[87] ——, "Gaba neurons and the mechanisms of network oscillations: implications for understanding cortical dysfunction in schizophrenia," Schizophrenia bulletin, vol. 34, no. 5, pp. 944–961, 2008.

[88] K. M. Spencer, "The functional consequences of cortical circuit abnormalities on gamma oscillations in schizophrenia: insights from computational modeling," Frontiers in human neuroscience, vol. 3, p. 33, 2009.

[89] R. Brette and W. Gerstner, "Adaptive exponential integrate-and-fire model as an effective description of neuronal activity," Journal of neurophysiology, vol. 94, no. 5, pp. 3637–3642, 2005.

[90] D. S. Faber and H. Korn, "Single-shot channel activation accounts for duration of inhibitory postsynaptic potentials in a central neuron," Science, vol. 208, no. 4444, pp. 612–615, 1980.

[91] M. Perouansky and Y. Yaari, "Kinetic properties of nmda receptor-mediated synaptic currents in rat hippocampal pyramidal cells versus interneurones." The Journal of Physiology, vol. 465, no. 1, pp. 223–244, 1993.

[92] T. Götz, U. Kraushaar, J. Geiger, J. Lübke, T. Berger, and P. Jonas, "Functional properties of ampa and nmda receptors expressed in identified types of basal ganglia neurons," Journal of Neuroscience, vol. 17, no. 1, pp. 204–215, 1997.

[93] M. C. Bellingham, R. Lim, and B. Walmsley, "Developmental changes in epsc quantal size and quantal content at a central glutamatergic synapse in rat," The Journal of Physiology, vol. 511, no. 3, pp. 861–869, 1998.

[94] C. E. Jahr and C. F. Stevens, "Voltage dependence of nmda-activated macroscopic conductances predicted by single-channel kinetics," Journal of Neuroscience, vol. 10, no. 9, pp. 3178–3182, 1990.

[95] Y. Zerlaut and A. Destexhe, "Enhanced responsiveness and low-level awareness in stochastic network states," Neuron, vol. 94, no. 5, pp. 1002–1009, 2017.

[96] H.-X. Wang and W.-J. Gao, "Cell type-specific development of nmda receptors in the interneurons of rat prefrontal cortex," Neuropsychopharmacology, vol. 34, no. 8, pp. 2028–2040, 2009.

[97] M. Stimberg, R. Brette, and D. F. Goodman, "Brian 2, an intuitive and efficient neural simulator," eLife, vol. 8, p. e47314, Aug. 2019.

[98] B. Telenczuk, M. Telenczuk, and A. Destexhe, "A kernel-based method to calculate local field potentials from networks of spiking neurons," bioRxiv, 2020.

Part III

Discussion

Discussion

One of the main goals of neuroscience is to understand the underlying processes of cognition, that is, how information is encoded, decoded and processed in the brain [293]. Several ways of encoding information have been hypothesized, such as firing rates [294, 295], pairwise correlations [296, 297], spike pattern irregularity [298, 299, 300, 301] and spike packets [302], among others.

An important aspect to be taken into consideration, when exploring cognitive mechanisms and their related information processes of coding, decoding and transmission, is the environment in which the information is treated. It has been shown, in different studies and protocols, that the brain state promotes major changes in the way the external and internal stimuli are processed. For example, it is well known that attention modulates how neurons respond to external stimuli throughout visual cortex [303]. The same way, the level of responses vary with sleep stage [304] and level of anesthesia [305].

In this thesis we explored in different ways how the activity of individual neurons and their collective behavior interfere in information transmission in the network. We devoted our attention to three particular brain states: Slow-wave sleep, Asynchronous-and-Irregular activity (AI) and Gamma activity. In particular, Gamma and AI activity were studied both in normal and in pathological conditions associated to schizoid brain conditions. To do this, we analyzed LFP and single units in the human cortex, provided by one of our collaborators Sydney S. Cash (Department of Neurology, Massachusetts General Hospital and Harvard Medical School, Boston). In this analysis, we evaluated spiking patterns (firing rate, spike regularity and spiking correlations) and the neuronal participation on Gamma rhythms in Awake and Slow-wave sleep states. In **Work 1**, we compared previously published results with our own analysis, stressing differences and similarities between these two states, with respect to neuronal activity and its contributions on Gamma rhythms.

To investigate the principles of information transmission in the brain, we developed network models constrained by this analysis. These models were capable of generating Gamma rhythms and Asynchronous-and-Irregular activity with spiking activity similar to experimental observations, like it is described in **Work 2**. We developed three different models, each one capable of generating Gamma rhythms by a different mechanism: PING, ING or CHING. The transfer of information was studied in these models, both during Gamma and AI states. Information transmission was measured by means of network *responsiveness*, that is, the the capacity level of the network to produce additional spikes in response to a certain stimulus. This type of measurement, associated to the change in

spiking probability after a stimulus, is easily comparable to experimental measurements, obtained, for example, by EEG, LFP, Calcium imaging, etc. In addition, networks with different level of responsiveness can exhibit drastic changes in their behavior. For example, a decrease in responsiveness imposes important restrictions on the conditions for a cell to fire with respect to the number of necessary coincidental inputs, forbidding network responses due to weak stimuli. Conversely, networks with high levels of responsiveness can easily detect single afferent stimuli, that would be subthreshold otherwise.

In **Work 2**, we compared network responsiveness during Gamma and AI states in different paradigms, and found that in all cases, the presence of Gamma oscillations tends to diminish the responsiveness to external inputs. Our models allowed the interpretation that Asynchronous-and-Irregular states would be better suited to stimulus detection, allowing the perception of even low amplitude stimuli (due to their high sensitivity), while Gamma oscillating states, at the expense of loosing stimulus sensitivity, would be able to encode temporal information. This interpretation comes from the *Phase Coding Theory* [128], which states that input strengths could be converted into spike-timing relative to the cycle (most excited fire earlier in the cycle, while cells that are not excited enough are prohibited to spike). This was observed in our models by the phase-dependence responsiveness present in Gamma states, and absent in AI states.

In a third study, **Work 3**, we compared network responsiveness in healthy and pathological conditions related to the schizoid brain, during Gamma oscillations and AI states. The schizoid condition was simulated in our networks by means of different levels of NMDA receptors block in the respective channels of the models. In this work, as in **Work 2**, a similar result with respect to Gamma and AI states responsiveness was observed. In healthy and pathological conditions (with all levels of NMDA receptors block), AI states displayed a bigger responsiveness than Gamma states. The interesting observation, on the other hand, was that responsiveness increased with the severity of NMDA receptors block, meaning that pathological states were in general, both during Gamma and AI states, more responsive than healthy states. This observation led us to the interpretation that the hallucinations observed during psychotic episodes in schizophrenic patients could be potentially related to an incapacity of the neuronal network to process all the stimuli in the environment, since the network would be excessively responsive, responsive even to stimuli that in normal conditions would be ignored.

Furthermore, our experimental analysis, compared to previous studies on cellular correlates of Gamma oscillations [47], confirmed a sparse participation of neuronal activity during Gamma rhythms. We observed two forms of neuronal participation to the rhythms: phase-locking and/or firing rate increase. FS cells presented significant higher level of phase-locking, firing rate increase, and behavior consistency than RS cells. In addition, we identified that the group of Gamma participating cells changes with time as well as their phase-preference. The combination of this analysis with the developed theoretical

work brought important theoretical insights. In **Work 2**, while most of these features could be obtained by choosing parameters which set the network dynamics into a *firing rate regime*, the right level of firing rate increase could only be reproduced with a particular network configuration, in the ING Network. This network was also the one in which the difference in responsiveness between AI and Gamma was smaller. Furthermore, we showed (**Work 2**) that the resonant properties of each of the developed models (PING, ING and CHING) strongly depended on the patterns of connections and on the neuronal composition. These examples illustrate how network structure drastically change network dynamics and consequently how the information is transmitted by a network.

Another important aspect explored in the thesis is the question if Gamma oscillations have an active role in information processing or alternatively, if they are just an epiphenomenon of this process. Several hypotheses concerning the Gamma role have been proposed. The most popular theories are the Binding-by-synchronization Hypothesis [125, 126], the Phase Coding Theory [127, 128], the Communication Through Coherence Theory [129, 130] and Communication through Resonance Theory [131]. Even though exploring these hypothesis was one of the initial ambitions of this thesis, our models could not provide any evidences in favor or against them. On the contrary, these theories guided us to allow the interpretation of our results. In this perspective, for example, if the Communication through Resonance Theory [131] is indeed one of the mechanism of information transmission, network structure and network resonant properties should be explored in future models.

Albeit no conclusion could be made with respect to the role of Gamma oscillations *per se*, in **Work 3** our models could give a possible interpretation for the role of Gamma oscillations increase in pathological conditions. In our study, we observed an increase of responsiveness in conditions associated to the hyper-production of Gamma, such as in early schizophrenic patients. This increase of responsiveness was accompanied by Gamma power increase. However, since the same effects were also observed during AI states, this increase of responsiveness was not a direct effect of this Gamma increase, but rather, an effect of the increase of excitability generated by alteration of NMDA receptors. In this situation, the Gamma power increase appeared to be a simple side effect of altered or anomalous NMDA function, suggesting that Gamma oscillations have no direct role *per se* in the pathological condition.

In summary, in this thesis we performed an analysis of experimental data from the human cortex, analyzing how neurons participate to Gamma rhythms. We observed that: (1) there are two types of neuronal participation, phase-locking and firing rate increase, that (2) neuronal participation of Gamma rhythms is sparse and that (3) inhibitory neurons participate to the rhythm more expressively than excitatory neurons. Based on

these features, we built and constrained three network models generating Gamma by three different mechanisms: PING, ING and CHING. These models were used as a tool to explore the principles of information transmission in the brain, which was accessed by the measurement of network responsiveness. Our models indicated that network structure should be the center of future studies, since it affects different dynamical properties, such as responsiveness. We explored network responsiveness in healthy and in pathological states similar to that seen in schizophrenia disease, and found that Gamma oscillations diminish network responsiveness in comparison to AI, in both, healthy and pathological conditions. Furthermore, our models indicated that schizoid pathological states were more responsive than healthy states, providing a possible comprehension of positive symptoms associated to schizophrenia. In our interpretation, these symptoms are possibly caused by the hypofunction of NMDA channels, rather than by the the excess of Gamma. In this perspective, we suggest that the increase of Gamma oscillations, observed during early phases of the disease, represents a side effect of the increase of neuronal synchrony, generated by the NMDA anomalies present in the disease.

Part IV

Complement Research Article

Bridging Single Neuron Dynamics to Global Brain States

Reference:

Goldman, J. S., Tort-Colet, N., Di Volo, M., Susin, E., Bouté, J., Dali, M., Carlu, M. Nghiem, T., Górski, T. & Destexhe, A. (2019). Bridging single neuron dynamics to global brain states. Frontiers in systems neuroscience, 13, 75.

French Abstract:

Les réseaux de neurones biologiques produisent de l'information de fonds spontanés à plusieurs échelles. L'activité, qui encapsule ces informations, devient plus complexe dans les états cérébraux qui affichent des capacités plus élevées pour la cognition. Dans cette perspective, les états d'éveil attentif sont plus complexes que les états endormis ou anesthésiés, par exemple. Dans cet article, nous couvrant dès les courants des canaux ioniques (micro-échelle) à l'échelle du cerveau entier (macro-échelle), en exposant différentes études à propos des mécanismes qui contrôlent les différents états dynamiques du cerveau. D'une façon similaire dont les interactions microscopiques entre les molécules sont liées à des structures macroscopiques de la matière, en utilisant la physique statistique, la dynamique des phénomènes neuronaux peuvent être liés à la dynamique macroscopique du cerveau à travers des échelles mésoscopiques. Pendant des états de conscience, on observe que des stimuli externes provoquent des effondrements de complexité au-delà des dynamiques spontanées, accompagnées d'une dynamique multi-dimensionnel, asynchrone et irrégulier. En revanche, la complexité des états d'inconscience ne peut pas être davantage réduite au-delà de la synchronie et de la régularité caractéristiques des activité spontanée observées pendant ces états. Dans cet article, nous proposons que l'augmentation de dimensionnalité des états dynamique spontanée observées pendant les états de conscience promeut la réactivité du cerveau, améliorant la capacité émergente des réseaux de neurones à encoder des informations sur plusieurs échelles.

frontiers in Systems Neuroscience

PERSPECTIVE
published: 06 December 2019
doi: 10.3389/fnsys.2019.00075

Bridging Single Neuron Dynamics to Global Brain States

Jennifer S. Goldman[1], Núria Tort-Colet[1], Matteo di Volo[1†], Eduarda Susin[1], Jules Bouté[1], Melissa Dali[1], Mallory Carlu[1], Trang-Anh Nghiem[2], Tomasz Górski[1] and Alain Destexhe[1]*

[1] Department of Integrative and Computational Neuroscience (ICN), Centre National de la Recherche Scientifique (CNRS), Paris-Saclay Institute of Neuroscience (NeuroPSI), Gif-sur-Yvette, France, [2] Department of Physics, Ecole Normale Supérieure, Paris, France

Biological neural networks produce information backgrounds of multi-scale spontaneous activity that become more complex in brain states displaying higher capacities for cognition, for instance, attentive awake versus asleep or anesthetized states. Here, we review brain state-dependent mechanisms spanning ion channel currents (microscale) to the dynamics of brain-wide, distributed, transient functional assemblies (macroscale). Not unlike how microscopic interactions between molecules underlie structures formed in macroscopic states of matter, using statistical physics, the dynamics of microscopic neural phenomena can be linked to macroscopic brain dynamics through mesoscopic scales. Beyond spontaneous dynamics, it is observed that stimuli evoke collapses of complexity, most remarkable over high dimensional, asynchronous, irregular background dynamics during consciousness. In contrast, complexity may not be further collapsed beyond synchrony and regularity characteristic of unconscious spontaneous activity. We propose that increased dimensionality of spontaneous dynamics during conscious states supports responsiveness, enhancing neural networks' emergent capacity to robustly encode information over multiple scales.

Keywords: computational neuroscience, neural network models, mean-field models, membrane biophysics, low-dimensional manifold, cerebral cortex, coupling, desynchronized

OPEN ACCESS

Edited by:
Per E. Roland,
University of Copenhagen, Denmark

Reviewed by:
Mario Rosanova,
University of Milan, Italy
Sacha Jennifer van Albada,
Julich Research Centre, Germany

****Correspondence:***
Jennifer S. Goldman
jennifer.goldman@mail.mcgill.ca

†Present address:
Matteo di Volo,
Laboratoire de Physique Théorique et Modelisation, Université de Cergy-Pontoise, Cergy-Pontoise, France

Received: *28 June 2019*
Accepted: *19 November 2019*
Published: *06 December 2019*

Citation:
Goldman JS, Tort-Colet N, di Volo M, Susin E, Bouté J, Dali M, Carlu M, Nghiem T-A, GórskiT and Destexhe A (2019) Bridging Single Neuron Dynamics to Global Brain States. Front. Syst. Neurosci. 13:75. doi: 10.3389/fnsys.2019.00075

INTRODUCTION

Brain activity transitions between healthy states, including stages of sleep, restful and aroused waking, as well as pathological states such as epilepsy, coma, and unresponsive wakefulness syndrome. From such a diversity of brain states, phenomenological categories encompassing similar spatio-temporal activity patterns can roughly, but usefully, be defined: unconscious (e.g., sleep and anesthesia) and conscious (e.g., waking and dreaming) brain states. At the macroscopic, global scale, unconscious brain states are dominated by high voltage, low frequency oscillatory brain activity related to the microscopic alternation of synchronous neuronal spiking and near silence (Steriade et al., 1993; Brown et al., 2010). Conversely, conscious states are macroscopically characterized by low voltage, high frequency, complex "disorganized" dynamics resulting from more asynchronous irregular (AI) microscopic network activity (Tsodyks and Sejnowski, 1995; Van Vreeswijk and Sompolinsky, 1996; Brunel, 2000), thought to be important for neural coding (Skarda and Freeman, 1987; Van Vreeswijk and Sompolinsky, 1996; Tononi and Edelman, 1998; Zerlaut and Destexhe, 2017).

Much as different states of matter like solids, liquids, and gases emerge from interactions between populations of molecules, different brain states may emerge from the interactions between populations of neurons. Statistical physics provides a mathematical framework to

uncover structures of microscopic interactions underlying macroscopic properties. In this sense, macroscopically observed high synchrony, low complexity brain signals recorded from unconscious states may be accounted for by an increased coupling in the system's components, behaving more like a solid (Peyrache et al., 2012; Le Van Quyen et al., 2016; Olcese et al., 2016; Nghiem et al., 2018a). In contrast, conscious brain states may be described as higher complexity (Sitt et al., 2014; Engemann et al., 2018; Nghiem et al., 2018a), perhaps liquid-like.

Though quantitative expressions directly linking order and complexity are not straightforward, various definitions and metrics of complexity have been described to vary between brain states. Reports of enhanced complexity in conscious compared to unconscious states may be understood as increased dimensionality (El Boustani and Destexhe, 2010), namely the number of degrees of freedom needed to capture a system's dynamics. Intuitively, dimensionality relates, though is not reducible to, algorithmic complexity which quantifies the length of a deterministic algorithm required to reproduce an exact signal. For a random signal resulting from purely stochastic dynamics (similar to neural activity observed during conscious states), the length of the algorithm would be as long as the signal itself. In contrast, a purely oscillatory signal (reminiscent of unconscious brain dynamics) can be recapitulated by a shorter algorithm, easily described by a periodic trajectory in few dimensions.

Here, we aim to connect spatial scales from microscopic (nanometers to micrometers—molecules to whole neurons) to macroscopic brain activity (centimeters to meters—brain areas to individual subjects' brains), describing both spontaneous and evoked dynamics. Toward linking interpretations of studies between scales, mesoscopic data (micrometers to millimeters—populations of thousands to tens of thousands of neurons) have been useful to inform models of neuronal assemblies. The perspective concludes by discussing a hypothesis best tested with a multi-scale understanding of brain function: the global complexity of neural activity increases in conscious brain states so as to enhance responsiveness to stimuli. We suggest responsiveness may depend on the capacity of neural networks to transiently collapse the dimensionality of collective dynamics—in particular neural assemblies sensitive to stimulus features—into evoked low-dimensional trajectories supporting neural codes (**Figure 1A**).

MACROSCOPIC SIGNALS VARY ROBUSTLY BETWEEN BRAIN STATES

Both spontaneous and evoked (**Figures 1A,B**) neural signals vary macroscopically across brain states, as demonstrated in electroencephalography (EEG), magnetoencephalography (MEG), and functional magnetic resonance imaging (fMRI). In unconscious states, neural activity is dominated by low-frequency, high-amplitude signals (Niedermeyer and Lopes da Silva, 2005). Accordingly, analyses of entropy (Sitt et al., 2014; Engemann et al., 2018), complexity (Tononi and Edelman, 1998), and dimensionality (El Boustani and Destexhe, 2010) during unconscious states indicate a relative simplicity of signals compared to conscious states. In unconscious states, synchronous activity slowly sweeps across the cortex (Massimini et al., 2004) along paths formed by cortical tracts (Capone et al., 2017). In both conscious resting and unconscious states, the default mode network (Raichle et al., 2001; Boly et al., 2008) establishes a pattern of synchronization between brain areas, producing correlations in ultra-slow (< 1 Hz) dynamics (Brookes et al., 2011). Sustained, slow oscillations were initially reported in the thalamocortical system (Steriade, 2003), but are also observed experimentally in isolated cortex, without thalamus (Sanchez-Vives and McCormick, 2000; Timofeev et al., 2000). Thalamocortical connections shape slow wave dynamics (Destexhe et al., 2007; Poulet et al., 2012; David et al., 2013; Crunelli et al., 2015; Zucca et al., 2019) although slow oscillations appear to be the default state of cortical networks (Sanchez-Vives and McCormick, 2000; Sanchez-Vives et al., 2017).

Patterns of neocortical regions activated in resting state networks have been successfully retrieved using eigenmodes of the structural connectivity matrix, i.e., the possible oscillatory patterns at frequencies allowed by white matter tract lengths (Atasoy et al., 2016). In active states, the executive control network replaces the default mode (Fox et al., 2005), and the co-activation of different cortical regions is more strongly controlled by correlations in external stimuli than by white matter structural connectivity (Gilson et al., 2018), with patterns of activity propagating recurrently between low-level, sensory areas and high-level, associative areas.

During conscious states, on the background of globally disorganized neural activity, transient patterns emerge (Duncan-Johnson and Donchin, 1982; Goodin and Aminoff, 1984; Sur and Sinha, 2009; Uhlhaas et al., 2009; Luck and Kappenman, 2011; Churchland et al., 2012; Sato et al., 2012; Singer, 2013; Chemla et al., 2019). Under an interpretation of brain states in analogy to states of matter, microscopic changes in the interactions between neurons could permit the emergence of larger-scale structures in brain activity.

MICROSCOPIC MECHANISMS; BIOPHYSICS OF BRAIN STATES

Experiments have demonstrated that during unconscious brain states, the membrane potential (V_m) of single cells slowly oscillates between hyperpolarized and depolarized potentials associated with alternating periods of silence (Down states, also termed "OFF periods") and AI-like firing (Up states, also termed "ON periods") (Steriade et al., 1993) (**Figure 2A**). During conscious brain states, neurons show sustained but sparse and irregular AI firing patterns (Vreeswijk and Sompolinsky, 1998; Destexhe et al., 1999; Brunel, 2000; Steriade, 2000; Renart et al., 2010; Dehghani et al., 2016; di Volo and Torcini, 2018). It was found that, during AI states, excitatory (E) and inhibitory (I) synaptic inputs are near-balanced (Dehghani et al., 2016), as predicted theoretically (Van Vreeswijk and Sompolinsky, 1996). In AI states, voltage fluctuations drive neurons over the threshold for firing action potentials, resulting in irregular

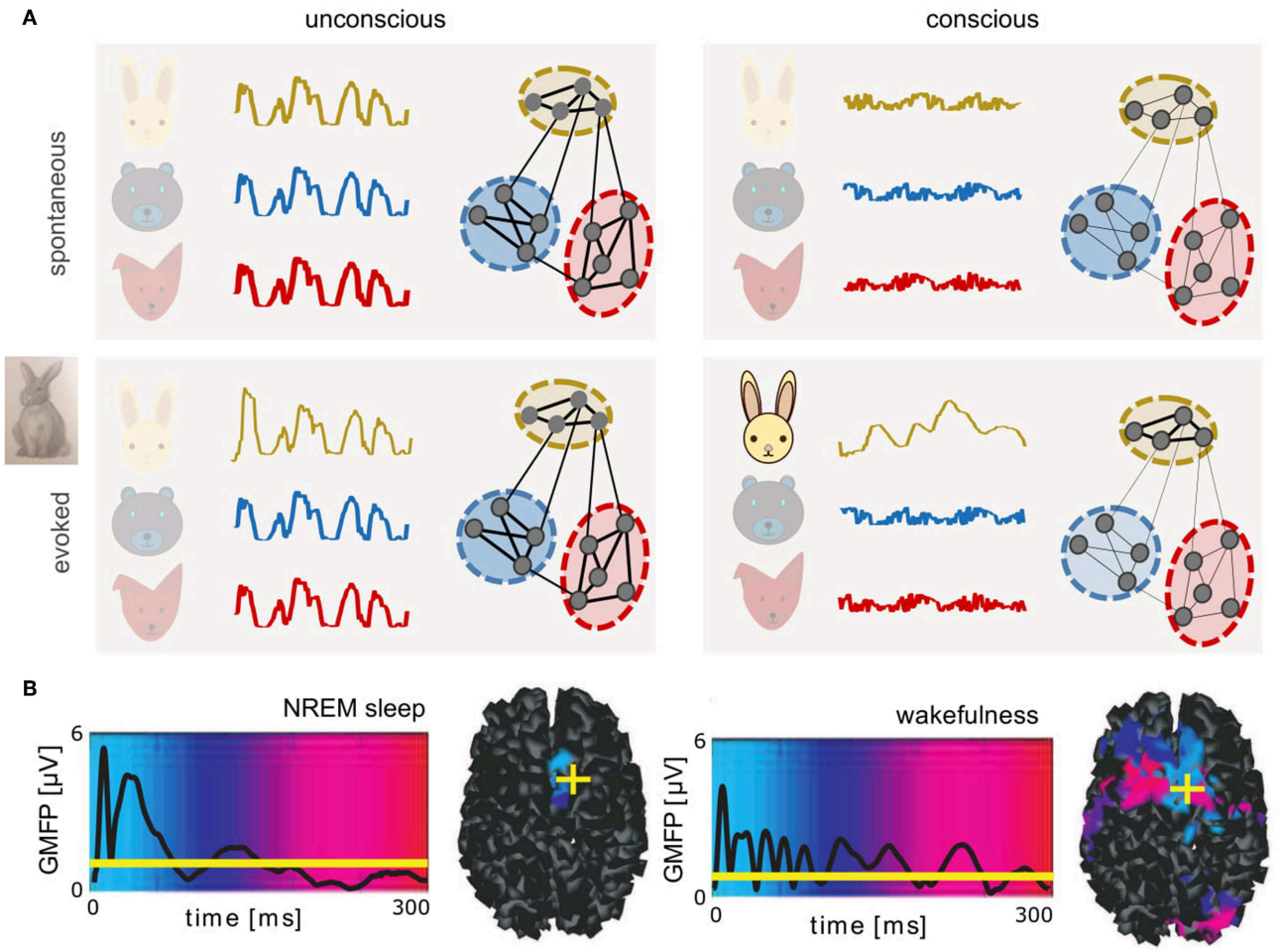

FIGURE 1 | Complex dynamics associated with conscious brain states provide a potential substrate for neural coding. **(A)** Schematics of spontaneous (top) and evoked (bottom) dynamics in connected neuronal assemblies encoding different related concepts (different colors) in unconscious (left) and conscious (right) brain states. In unconscious brain states, slow, synchronous, large amplitude oscillations are observed. Stimuli delivered during unconscious states evoke large amplitude, transient responses similar to spontaneous activity. In contrast, during conscious states, asynchronous, irregular firing of neurons results in macroscopically desynchronized, low amplitude signals. Only networks recruited by the perturbation (here, a rabbit) produce lower-dimensional patterns that propagate relatively further in time and space. **(B)** Global mean-field power (GMFP) recorded with EEG in response to transcranial magnetic stimulation, during deep, non-rapid eye movement (NREM) sleep versus wakefulness. Mean EEG signal is represented by black traces. Background colors represent temporal latency (light blue, 0 ms; red, 300 ms) of maximum current sources, also shown in cortical space on the right, where yellow crosses represent the location of stimulation (right dorsolateral premotor cortex). Reprinted with permission from AAAS (Massimini et al., 2005). If brain dynamics between states may be described in analogy to states of matter, perturbing unconscious brains results in large, brief signals perhaps akin to a small perturbation of a solid, which can displace the solid briefly, but will not modify its internal structure. In contrast, the same perturbation delivered during conscious, liquid-like brain states results in smaller but more complex patterns that propagate further in time and space. Under this interpretation, in coding networks, responses evoked during conscious states could represent a form of transient "crystallization," consistent with neural trajectories lying on low-dimensional manifolds.

spiking dynamics, also known as fluctuation-driven regimes (Kuhn et al., 2004; Destexhe, 2007; Destexhe and Rudolph-Lilith, 2012). To understand mechanisms at work during fluctuation-driven dynamics, computational models have further shown that three parameters are important to capture neuronal responses in this regime, the average membrane voltage V_m, the amplitude of V_m fluctuations, and the conductance state of the membrane (Reig et al., 2015; Zerlaut et al., 2016).

Neuromodulators, including acetylcholine, play important biological roles in modulating the membrane properties of neurons (McCormick, 1992) and thus transitions between AI and slow oscillatory dynamics through the regulation of membrane currents (Hill and Tononi, 2005). Neuromodulators are present at higher concentrations during conscious states (McCormick, 1992; Jones, 2003) and, most generally, inhibit potassium (activity-dependent and leak K^+) channels, which leads to depolarization of cells and suppression of *spike-frequency adaptation*. At low neuromodulatory concentrations, during unconscious states, K^+ leak channels are constitutively open and activity-dependent K^+ channels open when neurons

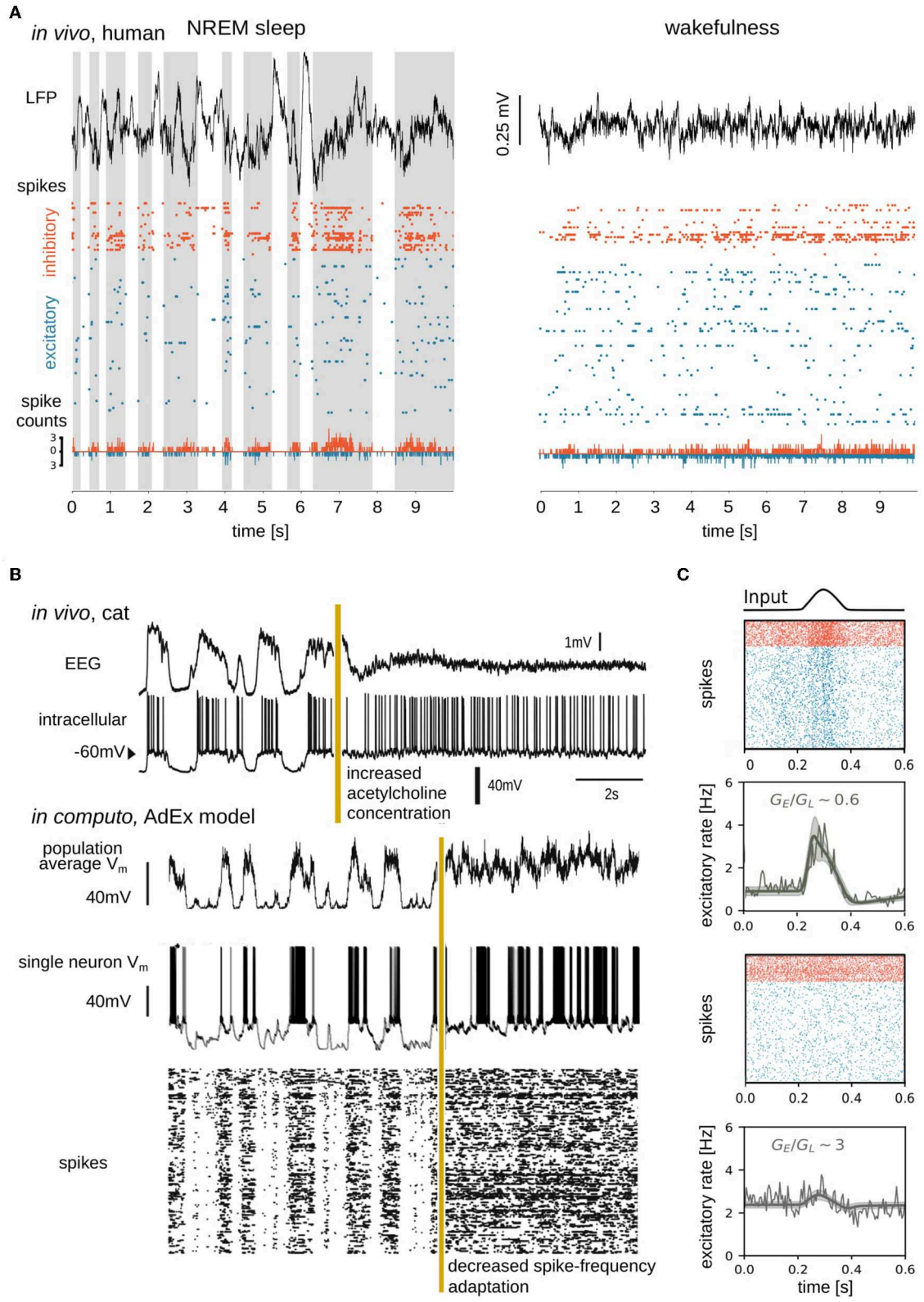

FIGURE 2 | Simple, high-amplitude signals in unconscious brain states are associated with synchronous regular neuronal firing, whereas complex, low-amplitude signals in conscious brain states emerge from asynchronous irregular firing. **(A)** Data sample from Peyrache et al. (2012), Dehghani et al. (2016),

(Continued)

FIGURE 2 | Le Van Quyen et al. (2016), Teleńczuk et al. (2017), and Nghiem et al. (2018b), containing local field potential (LFP; top), spike times (action potentials; middle), and spike counts (bottom) recorded from a human subject during NREM sleep (left) and wakefulness (right). Spikes from inhibitory (orange) and excitatory (blue) neurons were separated and spike counts were calculated in bins of 5ms. Up states shaded in the left panel. **(B)** Transition between slow-wave (unconscious) and activated (conscious) state dynamics *in vivo* (top) and *in silico* (bottom). Experimentally the transition is generated by electrical stimulation of acetylcholine neurons in the pedunculopontine tegmentum (PPT) of anesthetized cat (Volgushev et al., 2011), triggering awake-like, desynchronized dynamics in cortex (Rudolph et al., 2005). A prominent consequence of enhancing cholinergic signaling in cortex is a reduction of spike-frequency adaptation (McCormick, 1992). *In silico*, a similarly desynchronizing effect can be generated by reducing the parameter responsible for spike-frequency adaptation. Simulated traces shown in the bottom were modified from Destexhe (2009), which used a network of adaptive exponential integrate-and-fire neurons. The average V_m of the network, the V_m of a randomly chosen neuron, and the raster plot of the network are shown. Reproduced with permission from Destexhe (2009). **(C)** State dependence of network responsiveness. The responsiveness of two spiking networks to a Gaussian pulse is shown. Raster plots display spike times of excitatory (blue) and inhibitory (orange) neurons connected by conductance-based synapses. Population activity (spike counts, thin line), as well as mean-field model (thick lines), and standard deviation (shaded area) of population firing rate generated by a mean-field model developed in di Volo et al. (2019). Responsiveness is found to vary between different network states, obtained by changing the ratio of the time-averaged global excitatory conductance (G_E) (Destexhe et al., 2003) to membrane leakage conductance (G_L).

spike, allowing K^+ ions to exit cells thus hyperpolarizing the membrane. Accumulating self-inhibition in the form of spike-frequency adaptation during Up periods results in the transition to Down states. Conversely, spike-frequency adaptation wears off during Down states, allowing noise fluctuations (present ubiquitously; Destexhe and Rudolph-Lilith, 2012) to trigger transitions to Up states (Destexhe, 2009; Jercog et al., 2017; Nghiem T.-A. E. et al., 2018; di Volo et al., 2019) (**Figure 2B**). Computationally speaking, for high values of spike-frequency adaptation, bistability can be observed, with solutions at firing rate zero (Down state) and non-zero (Up state) values (Holcman and Tsodyks, 2006; di Volo et al., 2019). The more chaotic dynamics of AI states associated with consciousness allows for more reliable stimulus encoding (D'Andola et al., 2017), more reliable propagation (Zerlaut and Destexhe, 2017), and more sustained responses (Nghiem T.-A. E. et al., 2018) to stimuli over time. In contrast, during unconscious states, neuronal responses are more unreliable and vary greatly depending on the stimulus amplitude and whether cells receive inputs in Up or Down periods (Rosanova and Timofeev, 2005; Reig et al., 2015).

The Ising model for spin glasses (Jaynes, 1982) fitted to neural data (Schneidman et al., 2006) has revealed divergent types of emergent neuronal dynamics in conscious and unconscious states. While neuronal interactions are pairwise in wakefulness (Nghiem et al., 2017), coupling becomes population-wide in deep sleep (Tavoni et al., 2017; Nghiem et al., 2018b). In particular, inhibitory neurons organize synchronous activity across populations (Nghiem et al., 2018b; Zanoci et al., 2019), especially during deep sleep (Peyrache et al., 2012; Le Van Quyen et al., 2016; Olcese et al., 2016) where inhibitory neurons regulate rhythms of slow wave dynamics (Compte et al., 2008; Funk et al., 2017; Zucca et al., 2017, 2019).

To summarize, between unconscious and conscious brain states, microscopic data appear intuitively related to macroscopic data: synchronous microscopic Up and Down states resulting from constitutive and activity-dependent, hyperpolarizing currents due to reduced neuromodulation correspond to relatively simple, high-amplitude macroscopic dynamics observed in unconscious states. Active, disorganized, desynchronized, AI, low adaptation, high neuromodulation conditions correspond to low amplitude, complex, conscious brain signals. On backgrounds of differing spontaneous dynamics, generalizable patterns of activity (a.k.a. neural graphoelements) are observed. Cash et al. have elegantly shown that K-complexes (graphoelements characteristic of sleep stage 2) are complementarily observed both at microscopic and macroscopic scales (Cash et al., 2009). Other identifiable patterns also begin to emerge in empirical and theoretical data, including phase cones (Freeman and Barrie, 2000) and interacting traveling waves (Sato et al., 2012; Chemla et al., 2019). Since statistical physics has successfully described neuronal interactions for different brain states, we ask next whether mesoscale methods from statistical physics can help represent spontaneous and evoked dynamics of neuronal populations, thus formally linking knowledge between micro- and macroscopic scales.

MESOSCALE BRIDGES; POPULATIONS OF NEURONS

Brain dynamics at mesoscopic scales, describing thousands of neurons, are investigated empirically by electrophysiology and more recently, voltage-sensitive dyes (Arieli et al., 1996; Chemla and Chavane, 2010). At mesoscales, brain activity follows the trend of increasing complexity of spontaneous activity with consciousness (**Figure 2A**). Studying the effects of inputs at the mesoscale, studies have shown that perturbations during deep sleep states induce slow waves, but, during waking states, perturbations can result in chains of phase-locked activity (Pigorini et al., 2015) leading to causal global interactions (Rosanova et al., 2018).

Mean-field models offer a formalism for scaling up microscopic detail to collective macroscopic dynamics using few equations, offering a computational advantage for simulations. In describing states of matter, mean-field models simplify the probabilistic behavior of molecules to the relatively more predictable behavior of macroscopic states (Kadanoff, 2009). A rich literature has begun to develop mean-field models of neuronal populations, showing that global variables describing population activity can be usefully derived from the biophysics of neurons and their interactions (Ohira and Cowan, 1993; Ginzburg and Sompolinsky, 1994; El Boustani and Destexhe, 2009; Buice et al., 2010; Dahmen et al., 2016). Mean-field models have qualitatively reproduced temporal features of spontaneous dynamics including AI (El Boustani and Destexhe, 2009), Up and Down dynamics (Compte et al., 2003; Jercog et al., 2017;

Tartaglia and Brunel, 2017; di Volo et al., 2019), and transitions between these states (di Volo et al., 2019; Tort-Colet et al., 2019). In addition, connecting mean-fields provides a tool for simulating the propagation of patterns through time and space, across mesoscale structures. For example, recent work deriving mean-field models of networks with conductance-based synapses has reproduced the suppressive interaction between traveling waves observed in visual cortex during conscious states, a biological phenomenon that could not be captured by current-based networks (Chemla et al., 2019).

Mean-field models have highlighted that, while complicated to apply mathematically in the framework of conductance-based models (di Volo et al., 2019), voltage-dependent interactions constitute a significant non-linearity in the membrane evolution equations. Voltage-dependent interactions appear to be important for explaining non-trivial responses of biological neurons, through the mean and fluctuations of the cells' membrane voltage (Reig et al., 2015). In fact, while these results do not imply that differences in responsiveness are due only to conductances, they show that voltage dependent synapses play a role in the nonlinear state-dependent response of a neural network. As shown in **Figure 2C**, various levels of membrane conductance, regulated by voltage-dependent synapses, are shown to differently shape population responses.

Finally, renormalization group theory, a method of coarse-graining microscopic detail to obtain macroscopic laws helping to understand how order can emerge from apparent disorder (Wilson, 1979; Cardy, 1996; Goldenfeld, 2018) has recently begun to be applied to neural assemblies (Meshulam et al., 2019), laying further foundation for the formal connection of our understanding of brain function across scales.

DISCUSSION

In this paper, we briefly reviewed work on the measurement and modeling of brain states at different scales, from single neurons to cell assemblies and global brain activity, considering both spontaneous and evoked dynamics. In particular, we highlighted that increased complexity in the dynamics of conscious brain states relates to changes in single-neuron biophysics, tuned by neuromodulation. In unconscious states, reduced neuromodulation promotes activity-dependent self-inhibition of excitatory neurons as they spike, leading to alternating, synchronous transients of silence and firing, that produce high-amplitude, low-complexity, synchronous signals, on resonant frequencies of the structural connectome. During conscious states, neuronal discharges are asynchronous, irregular and fluctuation-driven, resulting from sustained membrane depolarization in cortical neurons, promoting effective neural communication.

Beyond conscious and unconscious categories proposed here for the sake of brevity, important differences exist within categories of unconscious and conscious states (Brown et al., 2010; El Boustani and Destexhe, 2010; Nghiem et al., 2018a). Unlike healthy wakefulness and sleep, epileptic networks display both excessively high conductance and strongly synchronized, regular dynamics (El Boustani and Destexhe, 2010). Further, brain signals in coma are both low-amplitude and low-complexity, in contrast to high-amplitude signals observed in other unconscious states, but also to complex signals observed in conscious states (El Boustani and Destexhe, 2010). Such anomalous deviations from the overall trend of coordinated changes in complexity and amplitude may illuminate mechanisms underlying disease-causing deviations from healthy brain states (Mackey and Glass, 1977).

To characterize brain states, it has been useful to consider not only spontaneous dynamics but also patterns evoked by perturbations. It was found that macroscopic responsiveness highly depends on brain state and different patterns of responses are evoked in conscious versus unconscious states (Massimini et al., 2005). Such state-dependent responsiveness can also be seen at the level of local networks *in vivo* and *in silico*, for example in the different reliability of responses to perturbations given during Up and Down periods of slow waves (Reig et al., 2015; Zerlaut and Destexhe, 2017). In simulations, different responsiveness could be accounted for by three parameters: membrane voltage, voltage fluctuation amplitude, and membrane conductance (Reig et al., 2015). These parameters could be well described by mean-field models (di Volo et al., 2019), able to capture fundamental properties of spontaneous dynamics and also state-dependent responses at mesoscales. As such, the data-driven coupling of such mean-field models may serve as natural candidates for modeling the emergence of mesoscopic and macroscopic-scale patterns.

Transient collapses of dimensionality found in encoding networks were also discussed as substrates potentially supporting neural codes. Such collapses in complexity have been observed in active ensembles at scales spanning microscopic (Churchland et al., 2010; Fairhall, 2019) to macroscopic (Quiroga et al., 2001; Zang et al., 2004) activity. This echoes recent work studying recordings of neural populations which highlighted that neural representations of stimuli may lie on low-dimensional manifolds (Churchland et al., 2012; Sadtler et al., 2014; Gallego et al., 2017; Zhao and Park, 2017; Golub et al., 2018; Chaudhuri et al., 2019; Recanatesi et al., 2019; Stringer et al., 2019). Indeed neurons do not fire independently, which would yield dynamics of dimensionality as high as the number of neurons, but instead follow constrained trajectories of activity that can be captured by descriptions of much lower dimensionality that depend on spontaneous and evoked dynamics. For example, a neural population firing in synchrony could be fully described by a periodic orbit trajectory constrained to a low-dimensional space (Churchland et al., 2012). Since spontaneous global network activity increases in dimensionality during conscious states, we ask whether the transient collapse of complexity in specific networks, translating the emergence of simpler dynamical structures from disorder, may be associated to neural codes.

As an analogy, windmills facing all in one direction display low complexity, but can only be synchronously active or inactive. Windmills facing in random directions,

in contrast, are a higher complexity configuration able to represent wind from any direction through the activity of a subset. The activity of an ensemble of windmills tuned to a particular direction of wind could represent a collapse of complexity and the generation of information by that subset (in this case, about the direction of wind). Similarly, enhanced dimensionality associated with conscious states could subserve neural information through the collapse of complexity in neural assemblies tuned to encode particular representations.

AUTHOR CONTRIBUTIONS

All authors listed have made a substantial, direct and intellectual contribution to the work, and approved it for publication.

FUNDING

This research was supported by the Centre National de la Recherche Scientifique (CNRS), the European Community (Human Brain Project, H2020-785907), and by École des Neurosciences de Paris (ENP).

ACKNOWLEDGMENTS

The authors would like to thank Simone Blanco Malerba, Cristiano Capone, Stephen E. Clarke, Damien Depannemaecker, Anton Filipchuk, Enrique Hansen, J. N. K. Jaynes, Vicente Medel, Archibald Parsons, Mattias Peuvrier, Wolf Singer, Kat Uesat, Bahar Hazal Yalçnkaya, and Yann Zerlaut for useful discussion of the manuscript.

REFERENCES

Arieli, A., Sterkin, A., Grinvald, A., and Aertsen, A. (1996). Dynamics of ongoing activity: explanation of the large variability in evoked cortical responses. *Science* 273, 1868–1871. doi: 10.1126/science.273.5283.1868

Atasoy, S., Donnelly, I., and Pearson, J. (2016). Human brain networks function in connectome-specific harmonic waves. *Nat. Commun.* 7:10340. doi: 10.1038/ncomms10340

Boly, M., Phillips, C., Tshibanda, L., Vanhaudenhuyse, A., Schabus, M., Dang-Vu, T. T., et al. (2008). Intrinsic brain activity in altered states of consciousness: how conscious is the default mode of brain function? *Ann. N. Y. Acad. Sci.* 1129:119. doi: 10.1196/annals.1417.015

Brookes, M. J., Woolrich, M., Luckhoo, H., Price, D., Hale, J. R., Stephenson, M. C., et al. (2011). Investigating the electrophysiological basis of resting state networks using magnetoencephalography. *Proc. Natl. Acad. Sci. U.S.A.* 108, 16783–16788. doi: 10.1073/pnas.1112685108

Brown, E. N., Lydic, R., and Schiff, N. D. (2010). General anesthesia, sleep, and coma. *New Engl. J. Med.* 363, 2638–2650. doi: 10.1056/NEJMra0808281

Brunel, N. (2000). Dynamics of sparsely connected networks of excitatory and inhibitory spiking neurons. *J. Comput. Neurosci.* 8, 183–208. doi: 10.1023/A:1008925309027

Buice, M. A., Cowan, J. D., and Chow, C. C. (2010). Systematic fluctuation expansion for neural network activity equations. *Neural Comput.* 22, 377–426. doi: 10.1162/neco.2009.02-09-960

Capone, C., Rebollo, B., Muñoz, A., Illa, X., Del Giudice, P., Sanchez-Vives, M. V., et al. (2017). Slow waves in cortical slices: how spontaneous activity is shaped by laminar structure. *Cereb. Cortex* 29, 319–335. doi: 10.1093/cercor/bhx326

Cardy, J. (1996). *Scaling and Renormalization in Statistical Physics. Vol. 5*. Cambridge: Cambridge University Press.

Cash, S. S., Halgren, E., Dehghani, N., Rossetti, A. O., Thesen, T., Wang, C., et al. (2009). The human k-complex represents an isolated cortical down-state. *Science* 324, 1084–1087. doi: 10.1126/science.1169626

Chaudhuri, R., Gerçek, B., Pandey, B., Peyrache, A., and Fiete, I. (2019). The intrinsic attractor manifold and population dynamics of a canonical cognitive circuit across waking and sleep. *Nat. Neurosci.* 22, 1512–1520. doi: 10.1038/s41593-019-0460-x

Chemla, S., and Chavane, F. (2010). Voltage-sensitive dye imaging: technique review and models. *J. Physiol.* 104, 40–50. doi: 10.1016/j.jphysparis.2009.11.009

Chemla, S., Reynaud, A., di Volo, M., Zerlaut, Y., Perrinet, L., Destexhe, A., et al. (2019). Suppressive traveling waves shape representations of illusory motion in primary visual cortex of awake primate. *J. Neurosci.* 39, 4282–4298. doi: 10.1523/JNEUROSCI.2792-18.2019

Churchland, M. M., Byron, M. Y., Cunningham, J. P., Sugrue, L. P., Cohen, M. R., Corrado, G. S., et al. (2010). Stimulus onset quenches neural variability: a widespread cortical phenomenon. *Nat. Neurosci.* 13, 369–378. doi: 10.1038/nn.2501

Churchland, M. M., Cunningham, J. P., Kaufman, M. T., Foster, J. D., Nuyujukian, P., Ryu, S. I., et al. (2012). Neural population dynamics during reaching. *Nature* 487, 51–56. doi: 10.1038/nature11129

Compte, A., Reig, R., Descalzo, V. F., Harvey, M. A., Puccini, G. D., and Sanchez-Vives, M. V. (2008). Spontaneous high-frequency (10–80 hz) oscillations during up states in the cerebral cortex *in vitro*. *J. Neurosci.* 28, 13828–13844. doi: 10.1523/JNEUROSCI.2684-08.2008

Compte, A., Sanchez-Vives, M. V., McCormick, D. A., and Wang, X.-J. (2003). Cellular and network mechanisms of slow oscillatory activity (< 1 HZ) and wave propagations in a cortical network model. *J. Neurophysiol.* 89, 2707–2725. doi: 10.1152/jn.00845.2002

Crunelli, V., David, F., Lőrincz, M. L., and Hughes, S. W. (2015). The thalamocortical network as a single slow wave-generating unit. *Curr. Opin. Neurobiol.* 31, 72–80. doi: 10.1016/j.conb.2014.09.001

Dahmen, D., Bos, H., and Helias, M. (2016). Correlated fluctuations in strongly coupled binary networks beyond equilibrium. *Phys. Rev. X* 6:031024. doi: 10.1103/PhysRevX.6.031024

D'Andola, M., Rebollo, B., Casali, A. G., Weinert, J. F., Pigorini, A., Villa, R., et al. (2017). Bistability, causality, and complexity in cortical networks: an *in vitro* perturbational study. *Cereb. Cortex* 28, 2233–2242. doi: 10.1093/cercor/bhx122

David, F., Schmiedt, J. T., Taylor, H. L., Orban, G., Di Giovanni, G., Uebele, V. N., et al. (2013). Essential thalamic contribution to slow waves of natural sleep. *J. Neurosci.* 33, 19599–19610. doi: 10.1523/JNEUROSCI.3169-13.2013

Dehghani, N., Peyrache, A., Telenczuk, B., Le Van Quyen, M., Halgren, E., Cash, S. S., et al. (2016). Dynamic balance of excitation and inhibition in human and monkey neocortex. *Sci. Rep.* 6:23176. doi: 10.1038/srep23176

Destexhe, A. (2007). High-conductance state. *Scholarpedia* 2:1341. doi: 10.4249/scholarpedia.1341

Destexhe, A. (2009). Self-sustained asynchronous irregular states and up–down states in thalamic, cortical and thalamocortical networks of nonlinear integrate-and-fire neurons. *J. Comput. Neurosci.* 27, 493–506. doi: 10.1007/s10827-009-0164-4

Destexhe, A., Contreras, D., and Steriade, M. (1999). Spatiotemporal analysis of local field potentials and unit discharges in cat cerebral cortex during natural wake and sleep states. *J. Neurosci.* 19, 4595–4608. doi: 10.1523/JNEUROSCI.19-11-04595.1999

Destexhe, A., Hughes, S. W., Rudolph, M., and Crunelli, V. (2007). Are corticothalamic 'up'states fragments of wakefulness? *Trends Neurosci.* 30, 334–342. doi: 10.1016/j.tins.2007.04.006

Destexhe, A., Rudolph, M., and Paré, D. (2003). The high-conductance state of neocortical neurons *in vivo*. *Nat. Rev. Neurosci.* 4, 739–751. doi: 10.1038/nrn1198

Destexhe, A., and Rudolph-Lilith, M. (2012). *Neuronal Noise*. New York, NY: Springer.

di Volo, M., Romagnoni, A., Capone, C., and Destexhe, A. (2019). Biologically realistic mean-field models of conductance-based networks of spiking neurons with adaptation. *Neural Comput.* 31, 653–680. doi: 10.1162/neco_a_01173

di Volo, M., and Torcini, A. (2018). Transition from asynchronous to oscillatory dynamics in balanced spiking networks with instantaneous synapses. *Phys. Rev. Lett.* 121:128301. doi: 10.1103/PhysRevLett.121.128301

Duncan-Johnson, C. C., and Donchin, E. (1982). The p300 component of the event-related brain potential as an index of information processing. *Biol. Psychol.* 14, 1–52. doi: 10.1016/0301-0511(82)90016-3

El Boustani, S., and Destexhe, A. (2009). A master equation formalism for macroscopic modeling of asynchronous irregular activity states. *Neural Comput.* 21, 46–100. doi: 10.1162/neco.2009.02-08-710

El Boustani, S., and Destexhe, A. (2010). Brain dynamics at multiple scales: can one reconcile the apparent low-dimensional chaos of macroscopic variables with the seemingly stochastic behavior of single neurons? *Int. J. Bifur. Chaos* 20, 1687–1702. doi: 10.1142/S0218127410026769

Engemann, D. A., Raimondo, F., King, J.-R., Rohaut, B., Louppe, G., Faugeras, F., et al. (2018). Robust EEG-based cross-site and cross-protocol classification of states of consciousness. *Brain* 141, 3179–3192. doi: 10.1093/brain/awy251

Fairhall, A. L. (2019). Whither variability? *Nat. Neurosci.* 22, 329–330. doi: 10.1038/s41593-019-0344-0

Fox, M. D., Snyder, A. Z., Vincent, J. L., Corbetta, M., Van Essen, D. C., and Raichle, M. E. (2005). The human brain is intrinsically organized into dynamic, anticorrelated functional networks. *Proc. Natl. Acad. Sci. U.S.A.* 102, 9673–9678. doi: 10.1073/pnas.0504136102

Freeman, W. J., and Barrie, J. M. (2000). Analysis of spatial patterns of phase in neocortical gamma EEGs in rabbit. *J. Neurophysiol.* 84, 1266–1278. doi: 10.1152/jn.2000.84.3.1266

Funk, C. M., Peelman, K., Bellesi, M., Marshall, W., Cirelli, C., and Tononi, G. (2017). Role of somatostatin-positive cortical interneurons in the generation of sleep slow waves. *J. Neurosci.* 37, 9132–9148. doi: 10.1523/JNEUROSCI.1303-17.2017

Gallego, J. A., Perich, M. G., Miller, L. E., and Solla, S. A. (2017). Neural manifolds for the control of movement. *Neuron* 94, 978–984. doi: 10.1016/j.neuron.2017.05.025

Gilson, M., Deco, G., Friston, K. J., Hagmann, P., Mantini, D., Betti, V., et al. (2018). Effective connectivity inferred from fMRI transition dynamics during movie viewing points to a balanced reconfiguration of cortical interactions. *Neuroimage* 180, 534–546. doi: 10.1016/j.neuroimage.2017.09.061

Ginzburg, I., and Sompolinsky, H. (1994). Theory of correlations in stochastic neural networks. *Phys. Rev. E* 50, 3171–3191. doi: 10.1103/PhysRevE.50.3171

Goldenfeld, N. (2018). *Lectures on Phase Transitions and the Renormalization Group*. Boca Raton, FL: CRC Press.

Golub, M. D., Sadtler, P. T., Oby, E. R., Quick, K. M., Ryu, S. I., Tyler-Kabara, E. C., et al. (2018). Learning by neural reassociation. *Nat. Neurosci.* 21, 607–616. doi: 10.1038/s41593-018-0095-3

Goodin, D. S., and Aminoff, M. J. (1984). The relationship between the evoked potential and brain events in sensory discrimination and motor response. *Brain* 107, 241–251. doi: 10.1093/brain/107.1.241

Hill, S., and Tononi, G. (2005). Modeling sleep and wakefulness in the thalamocortical system. *J. Neurophysiol.* 93, 1671–1698. doi: 10.1152/jn.00915.2004

Holcman, D., and Tsodyks, M. (2006). The emergence of up and down states in cortical networks. *PLoS Comput. Biol.* 2:e23. doi: 10.1371/journal.pcbi.0020023

Jaynes, E. T. (1982). On the rationale of maximum-entropy methods. *Proc. IEEE* 70, 939–952. doi: 10.1109/PROC.1982.12425

Jercog, D., Roxin, A., Bartho, P., Luczak, A., Compte, A., and de la Rocha, J. (2017). Up-down cortical dynamics reflect state transitions in a bistable network. *Elife* 6:e22425. doi: 10.7554/eLife.22425

Jones, B. E. (2003). Arousal systems. *Front. Biosci.* 8:438–451. doi: 10.2741/1074

Kadanoff, L. P. (2009). More is the same; phase transitions and mean field theories. *J. Stat. Phys.* 137:777. doi: 10.1007/s10955-009-9814-1

Kuhn, A., Aertsen, A., and Rotter, S. (2004). Neuronal integration of synaptic input in the fluctuation-driven regime. *J. Neurosci.* 24, 2345–2356. doi: 10.1523/JNEUROSCI.3349-03.2004

Le Van Quyen, M., Muller, L. E., Telenczuk, B., Halgren, E., Cash, S., Hatsopoulos, N. G., et al. (2016). High-frequency oscillations in human and monkey neocortex during the wake–sleep cycle. *Proc. Natl. Acad. Sci. U.S.A.* 113, 9363–9368. doi: 10.1073/pnas.1523583113

Luck, S. J., and Kappenman, E. S. (2011). *The Oxford Handbook of Event-Related Potential Components*. Oxford: Oxford University Press.

Mackey, M. C., and Glass, L. (1977). Oscillation and chaos in physiological control systems. *Science* 197, 287–289. doi: 10.1126/science.267326

Massimini, M., Ferrarelli, F., Huber, R., Esser, S. K., Singh, H., and Tononi, G. (2005). Breakdown of cortical effective connectivity during sleep. *Science* 309, 2228–2232. doi: 10.1126/science.1117256

Massimini, M., Huber, R., Ferrarelli, F., Hill, S., and Tononi, G. (2004). The sleep slow oscillation as a traveling wave. *J. Neurosci.* 24, 6862–6870. doi: 10.1523/JNEUROSCI.1318-04.2004

McCormick, D. A. (1992). Neurotransmitter actions in the thalamus and cerebral cortex and their role in neuromodulation of thalamocortical activity. *Prog. Neurobiol.* 39, 337–388. doi: 10.1016/0301-0082(92)90012-4

Meshulam, L., Gauthier, J. L., Brody, C. D., Tank, D. W., and Bialek, W. (2019). Coarse graining, fixed points, and scaling in a large population of neurons. *Phys. Rev. Lett.* 123:178103. doi: 10.1103/PhysRevLett.123.178103

Nghiem, T.-A., Lina, J.-M., di Volo, M., Capone, C., Evans, A. C., Destexhe, A., et al. (2018a). State equation from the spectral structure of human brain activity. *arXiv [preprint]. arXiv:1806.07365*.

Nghiem, T.-A., Marre, O., Destexhe, A., and Ferrari, U. (2017). "Pairwise ising model analysis of human cortical neuron recordings," in *International Conference on Geometric Science of Information* (New York, NY: Springer), 257–264. doi: 10.1007/978-3-319-68445-1_30

Nghiem, T.-A., Telenczuk, B., Marre, O., Destexhe, A., and Ferrari, U. (2018b). Maximum-entropy models reveal the excitatory and inhibitory correlation structures in cortical neuronal activity. *Phys. Rev. E* 98:012402. doi: 10.1103/PhysRevE.98.012402

Nghiem, T.-A. E., Tort-Colet, N., Gorski, T., Ferrari, U., Moghimyfiroozabad, S., Goldman, J. S., et al. (2018). Cholinergic switch between two different types of slow waves in cerebral cortex. *bioRxiv [Preprint]*. doi: 10.1101/430405

Niedermeyer, E., and Lopes da Silva, F. H. (2005). *Electroencephalography: Basic Principles, Clinical Applications, and Related Fields*. Philadelphia, PA: Lippincott Williams & Wilkins.

Ohira, T., and Cowan, J. D. (1993). Master-equation approach to stochastic neurodynamics. *Phys. Rev. E* 48:2259. doi: 10.1103/physreve.48.2259

Olcese, U., Bos, J. J., Vinck, M., Lankelma, J. V., van Mourik-Donga, L. B., Schlumm, F., et al. (2016). Spike-based functional connectivity in cerebral cortex and hippocampus: loss of global connectivity is coupled to preservation of local connectivity during non-REM sleep. *J. Neurosci.* 36, 7676–7692. doi: 10.1523/JNEUROSCI.4201-15.2016

Peyrache, A., Dehghani, N., Eskandar, E. N., Madsen, J. R., Anderson, W. S., Donoghue, J. A., et al. (2012). Spatiotemporal dynamics of neocortical excitation and inhibition during human sleep. *Proc. Natl. Acad. Sci. U.S.A.* 109, 1731–1736. doi: 10.1073/pnas.1109895109

Pigorini, A., Sarasso, S., Proserpio, P., Szymanski, C., Arnulfo, G., Casarotto, S., et al. (2015). Bistability breaks-off deterministic responses to intracortical stimulation during non-rem sleep. *Neuroimage* 112, 105–113. doi: 10.1016/j.neuroimage.2015.02.056

Poulet, J. F., Fernandez, L. M., Crochet, S., and Petersen, C. C. (2012). Thalamic control of cortical states. *Nat. Neurosci.* 15, 370–372. doi: 10.1038/nn.3035

Quiroga, R. Q., Rosso, O. A., Başar, E., and Schürmann, M. (2001). Wavelet entropy in event-related potentials: a new method shows ordering of EEG oscillations. *Biol. Cybern.* 84, 291–299. doi: 10.1007/s004220000212

Raichle, M. E., MacLeod, A. M., Snyder, A. Z., Powers, W. J., Gusnard, D. A., and Shulman, G. L. (2001). A default mode of brain function. *Proc. Natl. Acad. Sci. U.S.A.* 98, 676–682. doi: 10.1073/pnas.98.2.676

Recanatesi, S., Ocker, G. K., Buice, M. A., and Shea-Brown, E. (2019). Dimensionality in recurrent spiking networks: global trends in activity and local origins in connectivity. *PLoS Comput. Biol.* 15:e1006446. doi: 10.1371/journal.pcbi.1006446

Reig, R., Zerlaut, Y., Vergara, R., Destexhe, A., and Sanchez-Vives, M. V. (2015). Gain modulation of synaptic inputs by network state in auditory cortex *in vivo*. *J. Neurosci.* 35, 2689–2702. doi: 10.1523/JNEUROSCI.2004-14.2015

Renart, A., De La Rocha, J., Bartho, P., Hollender, L., Parga, N., Reyes, A., et al. (2010). The asynchronous state in cortical circuits. *Science* 327, 587–590. doi: 10.1126/science.1179850

Rosanova, M., Fecchio, M., Casarotto, S., Sarasso, S., Casali, A., Pigorini, A., et al. (2018). Sleep-like cortical off-periods disrupt causality and complexity in the brain of unresponsive wakefulness syndrome patients. *Nat. Commun.* 9:4427. doi: 10.1038/s41467-018-06871-1

Rosanova, M., and Timofeev, I. (2005). Neuronal mechanisms mediating the variability of somatosensory evoked potentials during sleep oscillations in cats. *J. Physiol.* 562, 569–582. doi: 10.1113/jphysiol.2004.071381

Rudolph, M., Pelletier, J.-G., Paré, D., and Destexhe, A. (2005). Characterization of synaptic conductances and integrative properties during electrically-induced EEG-activated states in neocortical neurons *in vivo*. *J. Neurophysiol.* 94, 2805–2821. doi: 10.1152/jn.01313.2004

Sadtler, P. T., Quick, K. M., Golub, M. D., Chase, S. M., Ryu, S. I., Tyler-Kabara, E. C., et al. (2014). Neural constraints on learning. *Nature* 512, 423–426. doi: 10.1038/nature13665

Sanchez-Vives, M. V., Massimini, M., and Mattia, M. (2017). Shaping the default activity pattern of the cortical network. *Neuron* 94, 993–1001. doi: 10.1016/j.neuron.2017.05.015

Sanchez-Vives, M. V., and McCormick, D. A. (2000). Cellular and network mechanisms of rhythmic recurrent activity in neocortex. *Nat. Neurosci.* 3, 1027–1034. doi: 10.1038/79848

Sato, T. K., Nauhaus, I., and Carandini, M. (2012). Traveling waves in visual cortex. *Neuron* 75, 218–229. doi: 10.1016/j.neuron.2012.06.029

Schneidman, E., Berry II, M. J., Segev, R., and Bialek, W. (2006). Weak pairwise correlations imply strongly correlated network states in a neural population. *Nature* 440, 1007–1012. doi: 10.1038/nature04701

Singer, W. (2013). Cortical dynamics revisited. *Trends Cogn. Sci.* 17, 616–626. doi: 10.1016/j.tics.2013.09.006

Sitt, J. D., King, J.-R., El Karoui, I., Rohaut, B., Faugeras, F., Gramfort, A., et al. (2014). Large scale screening of neural signatures of consciousness in patients in a vegetative or minimally conscious state. *Brain* 137, 2258–2270. doi: 10.1093/brain/awu141

Skarda, C. A., and Freeman, W. J. (1987). How brains make chaos in order to make sense of the world. *Behav. Brain Sci.* 10, 161–173. doi: 10.1017/S0140525X00047336

Steriade, M. (2000). Corticothalamic resonance, states of vigilance and mentation. *Neuroscience* 101, 243–276. doi: 10.1016/S0306-4522(00)00353-5

Steriade, M. (2003). *Neuronal Substrates of Sleep and Epilepsy*. Cambridge: Cambridge University Press.

Steriade, M., Nunez, A., and Amzica, F. (1993). A novel slow (< 1 Hz) oscillation of neocortical neurons *in vivo*: depolarizing and hyperpolarizing components. *J. Neurosci.* 13, 3252–3265. doi: 10.1523/JNEUROSCI.13-08-03252.1993

Stringer, C., Pachitariu, M., Steinmetz, N., Carandini, M., and Harris, K. D. (2019). High-dimensional geometry of population responses in visual cortex. *Nature* 571, 361–365. doi: 10.1038/s41586-019-1346-5

Sur, S., and Sinha, V. (2009). Event-related potential: an overview. *Ind. Psychiatry J.* 18, 70–73. doi: 10.4103/0972-6748.57865

Tartaglia, E. M., and Brunel, N. (2017). Bistability and up/down state alternations in inhibition-dominated randomly connected networks of lif neurons. *Sci. Rep.* 7:11916. doi: 10.1038/s41598-017-12033-y

Tavoni, G., Ferrari, U., Battaglia, F. P., Cocco, S., and Monasson, R. (2017). Functional coupling networks inferred from prefrontal cortex activity show experience-related effective plasticity. *Netw. Neurosci.* 1, 275–301. doi: 10.1162/NETN_a_00014

Teleńczuk, B., Dehghani, N., Le Van Quyen, M., Cash, S. S., Halgren, E., Hatsopoulos, N. G., et al. (2017). Local field potentials primarily reflect inhibitory neuron activity in human and monkey cortex. *Sci. Rep.* 7:40211. doi: 10.1038/srep40211

Timofeev, I., Grenier, F., Bazhenov, M., Sejnowski, T., and Steriade, M. (2000). Origin of slow cortical oscillations in deafferented cortical slabs. *Cereb. Cortex* 10, 1185–1199. doi: 10.1093/cercor/10.12.1185

Tononi, G., and Edelman, G. M. (1998). Consciousness and complexity. *Science* 282, 1846–1851. doi: 10.1126/science.282.5395.1846

Tort-Colet, N., Capone, C., Sanchez-Vives, M. V., and Mattia, M. (2019). Attractor competition enriches cortical dynamics during awakening from anesthesia. *bioRxiv [Preprint]*. doi: 10.1101/517102

Tsodyks, M. V., and Sejnowski, T. (1995). Rapid state switching in balanced cortical network models. *Network* 6, 111–124. doi: 10.1088/0954-898X_6_2_001

Uhlhaas, P., Pipa, G., Lima, B., Melloni, L., Neuenschwander, S., Nikolić, D., et al. (2009). Neural synchrony in cortical networks: history, concept and current status. *Front. Integr. Neurosci.* 3:17. doi: 10.3389/neuro.07.017.2009

Van Vreeswijk, C., and Sompolinsky, H. (1996). Chaos in neuronal networks with balanced excitatory and inhibitory activity. *Science* 274, 1724–1726. doi: 10.1126/science.274.5293.1724

Volgushev, M., Chauvette, S., and Timofeev, I. (2011). "Long-range correlation of the membrane potential in neocortical neurons during slow oscillation," in *Progress in Brain Research, Vol. 193* (Amsterdam: Elsevier), 181–199.

Vreeswijk, C. V., and Sompolinsky, H. (1998). Chaotic balanced state in a model of cortical circuits. *Neural Comput.* 10, 1321–1371. doi: 10.1162/089976698300017214

Wilson, K. G. (1979). Problems in physics with many scales of length. *Sci. Am.* 241, 158–179. doi: 10.1038/scientificamerican0879-158

Zang, Y., Jiang, T., Lu, Y., He, Y., and Tian, L. (2004). Regional homogeneity approach to fMRI data analysis. *Neuroimage* 22, 394–400. doi: 10.1016/j.neuroimage.2003.12.030

Zanoci, C., Dehghani, N., and Tegmark, M. (2019). Ensemble inhibition and excitation in the human cortex: an ising-model analysis with uncertainties. *Phys. Rev. E* 99:032408. doi: 10.1103/PhysRevE.99.032408

Zerlaut, Y., and Destexhe, A. (2017). Enhanced responsiveness and low-level awareness in stochastic network states. *Neuron* 94, 1002–1009. doi: 10.1016/j.neuron.2017.04.001

Zerlaut, Y., Teleńczuk, B., Deleuze, C., Bal, T., Ouanounou, G., and Destexhe, A. (2016). Heterogeneous firing rate response of mouse layer V pyramidal neurons in the fluctuation-driven regime. *J. Physiol.* 594, 3791–3808. doi: 10.1113/JP272317

Zhao, Y., and Park, I. M. (2017). Variational latent gaussian process for recovering single-trial dynamics from population spike trains. *Neural Comput.* 29, 1293–1316. doi: 10.1162/NECO_a_00953

Zucca, S., D'Urso, G., Pasquale, V., Vecchia, D., Pica, G., Bovetti, S., et al. (2017). An inhibitory gate for state transition in cortex. *Elife* 6:e26177. doi: 10.7554/eLife.26177

Zucca, S., Pasquale, V., de Leon Roig, P. L., Panzeri, S., and Fellin, T. (2019). Thalamic drive of cortical parvalbumin-positive interneurons during down states in anesthetized mice. *Curr. Biol.* 29, 1481–1490. doi: 10.1016/j.cub.2019.04.007

Conflict of Interest: The authors declare that the research was conducted in the absence of any commercial or financial relationships that could be construed as a potential conflict of interest.

Bibliography

[1] Andrea Volterra, Pierre Julius Magistretti, and Philip G Haydon. *The tripartite synapse: glia in synaptic transmission*. BOOK. Oxford University Press, 2002.

[2] Eric R Kandel et al. *Principles of neural science*. Vol. 4. McGraw-hill New York, 2013.

[3] Roger D Traub et al. "A model of gamma-frequency network oscillations induced in the rat CA3 region by carbachol in vitro". In: *European Journal of Neuroscience* 12.11 (2000), pp. 4093–4106.

[4] Mario Galarreta and Shaul Hestrin. "Spike transmission and synchrony detection in networks of GABAergic interneurons". In: *Science* 292.5525 (2001), pp. 2295–2299.

[5] Roger D Traub et al. "Gap junctions between interneuron dendrites can enhance synchrony of gamma oscillations in distributed networks". In: *Journal of Neuroscience* 21.23 (2001), pp. 9478–9486.

[6] Sheriar G Hormuzdi et al. "Impaired electrical signaling disrupts gamma frequency oscillations in connexin 36-deficient mice". In: *Neuron* 31.3 (2001), pp. 487–495.

[7] Derek L Buhl et al. "Selective impairment of hippocampal gamma oscillations in connexin-36 knock-out mouse in vivo". In: *Journal of Neuroscience* 23.3 (2003), pp. 1013–1018.

[8] Robert S Zucker. "Calcium-and activity-dependent synaptic plasticity". In: *Current opinion in neurobiology* 9.3 (1999), pp. 305–313.

[9] Donald S Faber and Henri Korn. "Single-shot channel activation accounts for duration of inhibitory postsynaptic potentials in a central neuron". In: *Science* 208.4444 (1980), pp. 612–615.

[10] MICHAEL Perouansky and YOEL Yaari. "Kinetic properties of NMDA receptor-mediated synaptic currents in rat hippocampal pyramidal cells versus interneurones." In: *The Journal of Physiology* 465.1 (1993), pp. 223–244.

[11] Thomas Götz et al. "Functional properties of AMPA and NMDA receptors expressed in identified types of basal ganglia neurons". In: *Journal of Neuroscience* 17.1 (1997), pp. 204–215.

[12] Mark C Bellingham, Rebecca Lim, and Bruce Walmsley. “Developmental changes in EPSC quantal size and quantal content at a central glutamatergic synapse in rat”. In: *The Journal of Physiology* 511.3 (1998), pp. 861–869.

[13] Craig E Jahr and Charles F Stevens. “Voltage dependence of NMDA-activated macroscopic conductances predicted by single-channel kinetics”. In: *Journal of Neuroscience* 10.9 (1990), pp. 3178–3182.

[14] Ziv Gil and Yael Amitai. “Adult thalamocortical transmission involves both NMDA and non-NMDA receptors”. In: *Journal of neurophysiology* 76.4 (1996), pp. 2547–2554.

[15] Houman Homayoun and Bita Moghaddam. “NMDA receptor hypofunction produces opposite effects on prefrontal cortex interneurons and pyramidal neurons”. In: *Journal of Neuroscience* 27.43 (2007), pp. 11496–11500.

[16] Alain Destexhe, Zachary F Mainen, and Terrence J Sejnowski. “Kinetic models of synaptic transmission”. In: *Methods in neuronal modeling* 2 (1998), pp. 1–25.

[17] Yasuo Kawaguchi and Yoshiyuki Kubota. “GABAergic cell subtypes and their synaptic connections in rat frontal cortex.” In: *Cerebral cortex (New York, NY: 1991)* 7.6 (1997), pp. 476–486.

[18] Carsten K Pfeffer et al. “Inhibition of inhibition in visual cortex: the logic of connections between molecularly distinct interneurons”. In: *Nature neuroscience* 16.8 (2013), pp. 1068–1076.

[19] Yoshiyuki Kubota. “Untangling GABAergic wiring in the cortical microcircuit”. In: *Current opinion in neurobiology* 26 (2014), pp. 7–14.

[20] Bruce P Bean. “The action potential in mammalian central neurons”. In: *Nature Reviews Neuroscience* 8.6 (2007), pp. 451–465.

[21] David A McCormick et al. “Comparative electrophysiology of pyramidal and sparsely spiny stellate neurons of the neocortex”. In: *Journal of neurophysiology* 54.4 (1985), pp. 782–806.

[22] Barry W Connors and Michael J Gutnick. “Intrinsic firing patterns of diverse neocortical neurons”. In: *Trends in neurosciences* 13.3 (1990), pp. 99–104.

[23] Petilla Interneuron Nomenclature Group (PING et al. “Petilla terminology: nomenclature of features of GABAergic interneurons of the cerebral cortex”. In: *Nature reviews. Neuroscience* 9.7 (2008), p. 557.

[24] Javier DeFelipe et al. “New insights into the classification and nomenclature of cortical GABAergic interneurons”. In: *Nature Reviews Neuroscience* 14.3 (2013), pp. 202–216.

[25] Camille Allene, Joana Lourenço, and Alberto Bacci. "The neuronal identity bias behind neocortical GABAergic plasticity". In: *Trends in neurosciences* 38.9 (2015), pp. 524–534.

[26] János Szabadics et al. "Excitatory effect of GABAergic axo-axonic cells in cortical microcircuits". In: *Science* 311.5758 (2006), pp. 233–235.

[27] Charles M Gray and David A McCormick. "Chattering cells: superficial pyramidal neurons contributing to the generation of synchronous oscillations in the visual cortex". In: *Science* 274.5284 (1996), pp. 109–113.

[28] Mircea Steriade et al. "Dynamic properties of corticothalamic neurons and local cortical interneurons generating fast rhythmic (30–40 Hz) spike bursts". In: *Journal of Neurophysiology* 79.1 (1998), pp. 483–490.

[29] Mircea Steriade. *The intact and sliced brain*. MIT press, 2001.

[30] Ariel Agmon and Barry W Connors. "Correlation between intrinsic firing patterns and thalamocortical synaptic responses of neurons in mouse barrel cortex". In: *Journal of Neuroscience* 12.1 (1992), pp. 319–329.

[31] Gordon M Shepherd. *The synaptic organization of the brain*. Oxford university press, 2004.

[32] Lennart Heimer. *The human brain and spinal cord: functional neuroanatomy and dissection guide*. Springer Science & Business Media, 2012.

[33] Steven Laureys. "The neural correlate of (un) awareness: lessons from the vegetative state". In: *Trends in cognitive sciences* 9.12 (2005), pp. 556–559.

[34] Florian Mormann and Christof Koch. "Neural correlates of consciousness". In: *Scholarpedia* 2.12 (2007), p. 1740.

[35] Cathy Jones. *Glasgow coma scale*. 1979.

[36] Olivier Le Bon. "Relationships between REM and NREM in the NREM-REM sleep cycle: a review on competing concepts". In: *Sleep medicine* 70 (2020), pp. 6–16.

[37] Conrad Iber. "The AASM manual for the scoring of sleep and associated events: Rules". In: *Terminology and Technical Specification* (2007).

[38] Alain Destexhe, Diego Contreras, and Mircea Steriade. "Spatiotemporal analysis of local field potentials and unit discharges in cat cerebral cortex during natural wake and sleep states". In: *Journal of Neuroscience* 19.11 (1999), pp. 4595–4608.

[39] David H Hubel. "Single unit activity in striate cortex of unrestrained cats". In: *The Journal of physiology* 147.2 (1959), pp. 226–238.

[40] Edward V Evarts. "Temporal patterns of discharge of pyramidal tract neurons during sleep and waking in the monkey". In: *Journal of neurophysiology* 27.2 (1964), pp. 152–171.

[41] M Steriade, M Deschênes, and G Oakson. “Inhibitory processes and interneuronal apparatus in motor cortex during sleep and waking. I. Background firing and responsiveness of pyramidal tract neurons and interneurons.” In: *Journal of neurophysiology* 37.5 (1974), pp. 1065–1092.

[42] Rodolfo Llinas and Urs Ribary. “Coherent 40-Hz oscillation characterizes dream state in humans.” In: *Proceedings of the National Academy of Sciences* 90.5 (1993), pp. 2078–2081.

[43] H Berger. “On the use of the encephalogram in humans”. In: *Arch Psychiatr Nervenkr* 87 (1929), pp. 527–570.

[44] Marie Engelene J Obien et al. “Revealing neuronal function through microelectrode array recordings”. In: *Frontiers in neuroscience* 8 (2015), p. 423.

[45] Sylvain Baillet. “Magnetoencephalography for brain electrophysiology and imaging”. In: *Nature neuroscience* 20.3 (2017), pp. 327–339.

[46] Paul L Nunez and Ramesh Srinivasan. “Electroencephalogram”. In: *Scholarpedia* 2.2 (2007), p. 1348.

[47] Michel Le Van Quyen et al. “High-frequency oscillations in human and monkey neocortex during the wake-sleep cycle”. In: *Proceedings of the National Academy of Sciences* 113.33 (2016), pp. 9363–9368.

[48] Steffen Gais et al. “Early sleep triggers memory for early visual discrimination skills”. In: *Nature neuroscience* 3.12 (2000), pp. 1335–1339.

[49] Robert Stickgold, LaTanya James, and J Allan Hobson. “Visual discrimination learning requires sleep after training”. In: *Nature neuroscience* 3.12 (2000), pp. 1237–1238.

[50] Pierre Maquet. “The role of sleep in learning and memory”. In: *science* 294.5544 (2001), pp. 1048–1052.

[51] Mircea Steriade and Igor Timofeev. “Neuronal plasticity in thalamocortical networks during sleep and waking oscillations”. In: *Neuron* 37.4 (2003), pp. 563–576.

[52] Reto Huber et al. “Local sleep and learning”. In: *Nature* 430.6995 (2004), pp. 78–81.

[53] Mircea Steriade, David A McCormick, and Terrence J Sejnowski. “Thalamocortical oscillations in the sleeping and aroused brain”. In: *Science* 262.5134 (1993), pp. 679–685.

[54] Mircea Steriade, Angel Nunez, and Florin Amzica. “Intracellular analysis of relations between the slow ($<$ 1 Hz) neocortical oscillation and other sleep rhythms of the electroencephalogram”. In: *Journal of Neuroscience* 13.8 (1993), pp. 3266–3283.

[55] I Timofeev and M Steriade. “Low-frequency rhythms in the thalamus of intact-cortex and decorticated cats”. In: *Journal of neurophysiology* 76.6 (1996), pp. 4152–4168.

[56] Maria V Sanchez-Vives and David A McCormick. “Cellular and network mechanisms of rhythmic recurrent activity in neocortex”. In: *Nature neuroscience* 3.10 (2000), pp. 1027–1034.

[57] Maxim Bazhenov and Igor Timofeev. “Thalamocortical oscillations”. In: *Scholarpedia* 1.6 (2006), p. 1319.

[58] Jaekyung Kim, Tanuj Gulati, and Karunesh Ganguly. “Competing roles of slow oscillations and delta waves in memory consolidation versus forgetting”. In: *Cell* 179.2 (2019), pp. 514–526.

[59] Caroline Geisler et al. “Hippocampal place cell assemblies are speed-controlled oscillators”. In: *Proceedings of the National Academy of Sciences* 104.19 (2007), pp. 8149–8154.

[60] Michael E Hasselmo. “What is the function of hippocampal theta rhythm?—Linking behavioral data to phasic properties of field potential and unit recording data”. In: *Hippocampus* 15.7 (2005), pp. 936–949.

[61] Joshua Jacobs et al. “Brain oscillations control timing of single-neuron activity in humans”. In: *Journal of Neuroscience* 27.14 (2007), pp. 3839–3844.

[62] Han Lee et al. “Phase locking of single neuron activity to theta oscillations during working memory in monkey extrastriate visual cortex”. In: *Neuron* 45.1 (2005), pp. 147–156.

[63] Omkar N Markand. “Alpha rhythms”. In: *Journal of Clinical Neurophysiology* 7.2 (1990), pp. 163–190.

[64] Xiao-Jing Wang. “Neurophysiological and computational principles of cortical rhythms in cognition”. In: *Physiological reviews* 90.3 (2010), pp. 1195–1268.

[65] György Buzsáki and Andreas Draguhn. “Neuronal oscillations in cortical networks”. In: *science* 304.5679 (2004), pp. 1926–1929.

[66] Charles M Gray and Wolf Singer. “Stimulus-specific neuronal oscillations in orientation columns of cat visual cortex”. In: *Proceedings of the National Academy of Sciences* 86.5 (1989), pp. 1698–1702.

[67] György Buzsáki, Cornelius H Vanderwolf, et al. “Cellular bases of hippocampal EEG in the behaving rat”. In: *Brain Research Reviews* 6.2 (1983), pp. 139–171.

[68] Anatol Bragin et al. “Gamma (40-100 Hz) oscillation in the hippocampus of the behaving rat”. In: *Journal of Neuroscience* 15.1 (1995), pp. 47–60.

[69] Jozsef Csicsvari et al. “Mechanisms of gamma oscillations in the hippocampus of the behaving rat”. In: *Neuron* 37.2 (2003), pp. 311–322.

[70] Marlene Bartos, Imre Vida, and Peter Jonas. “Synaptic mechanisms of synchronized gamma oscillations in inhibitory interneuron networks”. In: *Nature reviews neuroscience* 8.1 (2007), pp. 45–56.

[71] Christof Brücke et al. “Thalamic gamma oscillations correlate with reaction time in a Go/noGo task in patients with essential tremor”. In: *Neuroimage* 75 (2013), pp. 36–45.

[72] Christine Pedroarena and Rodolfo Llinás. “Dendritic calcium conductances generate high-frequency oscillation in thalamocortical neurons”. In: *Proceedings of the National Academy of Sciences* 94.2 (1997), pp. 724–728.

[73] D Pinault and M Deschenes. “Control of 40-Hz firing of reticular thalamic cells by neurotransmitters”. In: *Neuroscience* 51.2 (1992), pp. 259–268.

[74] Bijan Pesaran et al. “Temporal structure in neuronal activity during working memory in macaque parietal cortex”. In: *Nature neuroscience* 5.8 (2002), pp. 805–811.

[75] Laura Lee Colgin et al. “Frequency of gamma oscillations routes flow of information in the hippocampus”. In: *Nature* 462.7271 (2009), p. 353.

[76] Margaret F Carr, Mattias P Karlsson, and Loren M Frank. “Transient slow gamma synchrony underlies hippocampal memory replay”. In: *Neuron* 75.4 (2012), pp. 700–713.

[77] A Rougeul-Buser, JJ Bouyer, and P Buser. “From attentiveness to sleep. A topographical analysis of localized" synchronized" activities on the cortex of normal cat and monkey”. In: *Acta Neurobiol Exp (Warsz)* 35.5-6 (1975), pp. 805–19.

[78] JJ Bouyer, MF Montaron, and A Rougeul. “Fast fronto-parietal rhythms during combined focused attentive behaviour and immobility in cat: cortical and thalamic localizations”. In: *Electroencephalography and clinical neurophysiology* 51.3 (1981), pp. 244–252.

[79] Eugenio Rodriguez et al. “Perception’s shadow: long-distance synchronization of human brain activity”. In: *Nature* 397.6718 (1999), pp. 430–433.

[80] Lucia Melloni et al. “Synchronization of neural activity across cortical areas correlates with conscious perception”. In: *Journal of neuroscience* 27.11 (2007), pp. 2858–2865.

[81] Pascal Fries et al. “Modulation of oscillatory neuronal synchronization by selective visual attention”. In: *Science* 291.5508 (2001), pp. 1560–1563.

[82] Georgia G Gregoriou et al. “High-frequency, long-range coupling between prefrontal and visual cortex during attention”. In: *science* 324.5931 (2009), pp. 1207–1210.

[83] Martin Vinck et al. “Attentional modulation of cell-class-specific gamma-band synchronization in awake monkey area v4”. In: *Neuron* 80.4 (2013), pp. 1077–1089.

[84] Sateri Rouhinen et al. “Load dependence of β and γ oscillations predicts individual capacity of visual attention”. In: *Journal of Neuroscience* 33.48 (2013), pp. 19023–19033.

[85] Daniel E Sheer. “Focused arousal and the cognitive 40-Hz event-related potentials: differential diagnosis of Alzheimer’s disease.” In: *Progress in clinical and biological research* 317 (1989), pp. 79–94.

[86] Thilo Womelsdorf et al. “Gamma-band synchronization in visual cortex predicts speed of change detection”. In: *Nature* 439.7077 (2006), pp. 733–736.

[87] Jozsef Csicsvari et al. “Oscillatory coupling of hippocampal pyramidal cells and interneurons in the behaving rat”. In: *Journal of Neuroscience* 19.1 (1999), pp. 274–287.

[88] Ryan T Canolty et al. “High gamma power is phase-locked to theta oscillations in human neocortex”. In: *science* 313.5793 (2006), pp. 1626–1628.

[89] Supratim Ray et al. “Neural correlates of high-gamma oscillations (60–200 Hz) in macaque local field potentials and their potential implications in electrocorticography”. In: *Journal of Neuroscience* 28.45 (2008), pp. 11526–11536.

[90] Kevin Whittingstall and Nikos K Logothetis. “Frequency-band coupling in surface EEG reflects spiking activity in monkey visual cortex”. In: *Neuron* 64.2 (2009), pp. 281–289.

[91] Mariano A Belluscio et al. “Cross-frequency phase–phase coupling between theta and gamma oscillations in the hippocampus”. In: *Journal of Neuroscience* 32.2 (2012), pp. 423–435.

[92] Supratim Ray and John HR Maunsell. “Different origins of gamma rhythm and high-gamma activity in macaque visual cortex”. In: *PLoS biology* 9.4 (2011), e1000610.

[93] Xi Jiang, Jorge Gonzalez-Martinez, and Eric Halgren. “Coordination of human hippocampal sharpwave ripples during NREM sleep with cortical theta bursts, spindles, downstates, and upstates”. In: *Journal of Neuroscience* 39.44 (2019), pp. 8744–8761.

[94] György Buzsáki. “Hippocampal sharp wave-ripple: A cognitive biomarker for episodic memory and planning”. In: *Hippocampus* 25.10 (2015), pp. 1073–1188.

[95] Dion Khodagholy, Jennifer N Gelinas, and György Buzsáki. “Learning-enhanced coupling between ripple oscillations in association cortices and hippocampus”. In: *Science* 358.6361 (2017), pp. 369–372.

[96] Alex P Vaz et al. “Coupled ripple oscillations between the medial temporal lobe and neocortex retrieve human memory”. In: *Science* 363.6430 (2019), pp. 975–978.

[97] Nikos K Logothetis et al. “Hippocampal–cortical interaction during periods of subcortical silence”. In: *Nature* 491.7425 (2012), pp. 547–553.

[98] Richard B Berry et al. “The AASM manual for the scoring of sleep and associated events”. In: *Rules, Terminology and Technical Specifications, Darien, Illinois, American Academy of Sleep Medicine* 176 (2012), p. 2012.

[99] Oren M Weiner and Thien Thanh Dang-Vu. “Spindle oscillations in sleep disorders: a systematic review”. In: *Neural plasticity* 2016 (2016).

[100] Thien Thanh Dang-Vu et al. “Interplay between spontaneous and induced brain activity during human non-rapid eye movement sleep”. In: *Proceedings of the National Academy of Sciences* 108.37 (2011), pp. 15438–15443.

[101] Hiroharu Noda and W Ross Adey. “Firing variability in cat association cortex during sleep and wakefulness”. In: *Brain research* 18.3 (1970), pp. 513–526.

[102] Mircea Steriade, Igor Timofeev, and F Grenier. “Natural waking and sleep states: a view from inside neocortical neurons”. In: *Journal of neurophysiology* 85.5 (2001), pp. 1969–1985.

[103] Alexander S Ecker et al. “Decorrelated neuronal firing in cortical microcircuits”. In: *science* 327.5965 (2010), pp. 584–587.

[104] Alfonso Renart et al. “The asynchronous state in cortical circuits”. In: *science* 327.5965 (2010), pp. 587–590.

[105] Carl Van Vreeswijk and Haim Sompolinsky. “Chaos in neuronal networks with balanced excitatory and inhibitory activity”. In: *Science* 274.5293 (1996), pp. 1724–1726.

[106] Yousheng Shu, Andrea Hasenstaub, and David A McCormick. “Turning on and off recurrent balanced cortical activity”. In: *Nature* 423.6937 (2003), pp. 288–293.

[107] Bilal Haider et al. “Neocortical network activity in vivo is generated through a dynamic balance of excitation and inhibition”. In: *Journal of Neuroscience* 26.17 (2006), pp. 4535–4545.

[108] Nima Dehghani et al. “Dynamic balance of excitation and inhibition in human and monkey neocortex”. In: *Scientific reports* 6.1 (2016), pp. 1–12.

[109] Daniel J Amit and Nicolas Brunel. "Model of global spontaneous activity and local structured activity during delay periods in the cerebral cortex." In: *Cerebral cortex (New York, NY: 1991)* 7.3 (1997), pp. 237–252.

[110] Nicolas Brunel. "Dynamics of sparsely connected networks of excitatory and inhibitory spiking neurons". In: *Journal of computational neuroscience* 8.3 (2000), pp. 183–208.

[111] Nicolas Brunel and Xiao-Jing Wang. "What determines the frequency of fast network oscillations with irregular neural discharges? I. Synaptic dynamics and excitation-inhibition balance". In: *Journal of neurophysiology* 90.1 (2003), pp. 415–430.

[112] Caroline Geisler, Nicolas Brunel, and Xiao-Jing Wang. "Contributions of intrinsic membrane dynamics to fast network oscillations with irregular neuronal discharges". In: *Journal of neurophysiology* 94.6 (2005), pp. 4344–4361.

[113] Charles F Stevens and Anthony M Zador. "Input synchrony and the irregular firing of cortical neurons". In: *Nature neuroscience* 1.3 (1998), pp. 210–217.

[114] David M Groppe et al. "Dominant frequencies of resting human brain activity as measured by the electrocorticogram". In: *Neuroimage* 79 (2013), pp. 223–233.

[115] Priyanka A Abhang, Bharti W Gawali, and Suresh C Mehrotra. *Introduction to EEG-and speech-based emotion recognition*. Academic Press, 2016.

[116] Edgar D Adrian. "Olfactory reactions in the brain of the hedgehog". In: *The Journal of physiology* 100.4 (1942), pp. 459–473.

[117] Canan Başar-Eroglu et al. "Gamma-band responses in the brain: a short review of psychophysiological correlates and functional significance". In: *International journal of psychophysiology* 24.1-2 (1996), pp. 101–112.

[118] Mircea Steriade, Florin Amzica, and Diego Contreras. "Synchronization of fast (30-40 Hz) spontaneous cortical rhythms during brain activation". In: *Journal of Neuroscience* 16.1 (1996), pp. 392–417.

[119] Andreas Gabriel and Reinhard Eckhorn. "A multi-channel correlation method detects traveling γ-waves in monkey visual cortex". In: *Journal of neuroscience methods* 131.1-2 (2003), pp. 171–184.

[120] Robert Galambos. "A comparison of certain gamma band (40-Hz) brain rhythms in cat and man". In: *Induced rhythms in the brain*. Springer, 1992, pp. 201–216.

[121] Albert Compte et al. "Spontaneous high-frequency (10–80 Hz) oscillations during up states in the cerebral cortex in vitro". In: *Journal of Neuroscience* 28.51 (2008), pp. 13828–13844.

[122] Nikos K Logothetis et al. “Neurophysiological investigation of the basis of the fMRI signal”. In: *Nature* 412.6843 (2001), p. 150.

[123] Reinhard Eckhorn et al. “Coherent oscillations: A mechanism of feature linking in the visual cortex?” In: *Biological cybernetics* 60.2 (1988), pp. 121–130.

[124] Le Bon-Jego, Rafael Yuste, et al. “Persistently active, pacemaker-like neurons in neocortex”. In: *Frontiers in neuroscience* 1 (2007), p. 9.

[125] Wolf Singer and Charles M Gray. “Visual feature integration and the temporal correlation hypothesis”. In: *Annual review of neuroscience* 18.1 (1995), pp. 555–586.

[126] Wolf Singer. “Neuronal synchrony: a versatile code for the definition of relations?” In: *Neuron* 24.1 (1999), pp. 49–65.

[127] John O’Keefe and Michael L Recce. “Phase relationship between hippocampal place units and the EEG theta rhythm”. In: *Hippocampus* 3.3 (1993), pp. 317–330.

[128] Pascal Fries, Danko Nikolić, and Wolf Singer. “The gamma cycle”. In: *Trends in neurosciences* 30.7 (2007), pp. 309–316.

[129] Pascal Fries. “A mechanism for cognitive dynamics: neuronal communication through neuronal coherence”. In: *Trends in cognitive sciences* 9.10 (2005), pp. 474–480.

[130] Pascal Fries. “Rhythms for cognition: communication through coherence”. In: *Neuron* 88.1 (2015), pp. 220–235.

[131] Gerald Hahn et al. “Communication through resonance in spiking neuronal networks”. In: *PLoS Comput Biol* 10.8 (2014), e1003811.

[132] György Buzsáki and Xiao-Jing Wang. “Mechanisms of gamma oscillations”. In: *Annual review of neuroscience* 35 (2012), pp. 203–225.

[133] Mark O Cunningham et al. “A role for fast rhythmic bursting neurons in cortical gamma oscillations in vitro”. In: *Proceedings of the National Academy of Sciences* 101.18 (2004), pp. 7152–7157.

[134] Charles M Gray. “Synchronous oscillations in neuronal systems: mechanisms and functions”. In: *Journal of computational neuroscience* 1.1-2 (1994), pp. 11–38.

[135] Miles A Whittington et al. “Inhibition-based rhythms: experimental and mathematical observations on network dynamics”. In: *International journal of psychophysiology* 38.3 (2000), pp. 315–336.

[136] Andre Fisahn et al. “Cholinergic induction of network oscillations at 40 Hz in the hippocampus in vitro”. In: *Nature* 394.6689 (1998), pp. 186–189.

[137] André Fisahn et al. “Distinct roles for the kainate receptor subunits GluR5 and GluR6 in kainate-induced hippocampal gamma oscillations”. In: *Journal of Neuroscience* 24.43 (2004), pp. 9658–9668.

[138] Roger D Traub et al. *Fast oscillations in cortical circuits*. MIT press, 1999.

[139] Roger D Traub. "Fast oscillations". In: *Scholarpedia* 1.12 (2006), p. 1764.

[140] Paul Tiesinga and Terrence J Sejnowski. "Cortical enlightenment: are attentional gamma oscillations driven by ING or PING?" In: *Neuron* 63.6 (2009), pp. 727–732.

[141] David A Lewis. "GABAergic local circuit neurons and prefrontal cortical dysfunction in schizophrenia". In: *Brain Research Reviews* 31.2-3 (2000), pp. 270–276.

[142] David A Lewis, Takanori Hashimoto, and David W Volk. "Cortical inhibitory neurons and schizophrenia". In: *Nature Reviews Neuroscience* 6.4 (2005), pp. 312–324.

[143] Vasilis P Bozikas and Christina Andreou. "Longitudinal studies of cognition in first episode psychosis: a systematic review of the literature". In: *Australian & New Zealand Journal of Psychiatry* 45.2 (2011), pp. 93–108.

[144] Tonghui Su et al. "How could N-methyl-D-aspartate receptor antagonists lead to excitation instead of inhibition?" In: *Brain Science Advances* 4.2 (2018), pp. 73–98.

[145] Martha E Shenton et al. "A review of MRI findings in schizophrenia". In: *Schizophrenia research* 49.1-2 (2001), pp. 1–52.

[146] Lynn D Selemon and Patricia S Goldman-Rakic. "The reduced neuropil hypothesis: a circuit based model of schizophrenia". In: *Biological psychiatry* 45.1 (1999), pp. 17–25.

[147] Daniel C Javitt and Stephen R Zukin. "Recent advances in the phencyclidine model of schizophrenia." In: *The American journal of psychiatry* (1991).

[148] John H Krystal et al. "Subanesthetic effects of the noncompetitive NMDA antagonist, ketamine, in humans: psychotomimetic, perceptual, cognitive, and neuroendocrine responses". In: *Archives of general psychiatry* 51.3 (1994), pp. 199–214.

[149] Sarbjeet S Kalsi, David M Wood, and Paul I Dargan. "The epidemiology and patterns of acute and chronic toxicity associated with recreational ketamine use". In: *Emerging Health Threats Journal* 4.1 (2011), p. 7107.

[150] John W Newcomer et al. "Ketamine-induced NMDA receptor hypofunction as a model of memory impairment and psychosis". In: *Neuropsychopharmacology* 20.2 (1999), pp. 106–118.

[151] Joseph T Coyle. "Glutamate and schizophrenia: beyond the dopamine hypothesis". In: *Cellular and molecular neurobiology* 26.4 (2006), pp. 363–382.

[152] Craig W Lindsley et al. "Progress towards validating the NMDA receptor hypofunction hypothesis of schizophrenia". In: *Current topics in medicinal chemistry* 6.8 (2006), pp. 771–785.

[153] Herbert Y Meltzer. “Dopamine receptors and average clinical doses”. In: *Science* 194.4264 (1976), pp. 545–546.

[154] Solomon H Snyder. “Dopamine receptors, neuroleptics, and schizophrenia.” In: *The American journal of psychiatry* (1981).

[155] Stephanie M Perez and Daniel J Lodge. “New approaches to the management of schizophrenia: focus on aberrant hippocampal drive of dopamine pathways”. In: *Drug design, development and therapy* 8 (2014), p. 887.

[156] B Pakkenberg, J Scheel-Krüger, and LV Kristiansen. “Schizophrenia; from structure to function with special focus on the mediodorsal thalamic prefrontal loop”. In: *Acta Psychiatrica Scandinavica* 120.5 (2009), pp. 345–354.

[157] Jefferson W Kinney et al. “A specific role for NR2A-containing NMDA receptors in the maintenance of parvalbumin and GAD67 immunoreactivity in cultured interneurons”. In: *Journal of Neuroscience* 26.5 (2006), pp. 1604–1615.

[158] Lavinia Albéri et al. “The calcium-binding protein parvalbumin modulates the firing 1 properties of the reticular thalamic nucleus bursting neurons”. In: *Journal of neurophysiology* 109.11 (2013), pp. 2827–2841.

[159] Olivier Caillard et al. “Role of the calcium-binding protein parvalbumin in short-term synaptic plasticity”. In: *Proceedings of the National Academy of Sciences* 97.24 (2000), pp. 13372–13377.

[160] M Margarita Behrens et al. “Ketamine-induced loss of phenotype of fast-spiking interneurons is mediated by NADPH-oxidase”. In: *Science* 318.5856 (2007), pp. 1645–1647.

[161] Susan M Cochran et al. “Induction of metabolic hypofunction and neurochemical deficits after chronic intermittent exposure to phencyclidine: differential modulation by antipsychotic drugs”. In: *Neuropsychopharmacology* 28.2 (2003), pp. 265–275.

[162] Yuchun Zhang, M Margarita Behrens, and John E Lisman. “Prolonged exposure to NMDAR antagonist suppresses inhibitory synaptic transmission in prefrontal cortex”. In: *Journal of neurophysiology* 100.2 (2008), pp. 959–965.

[163] Schahram Akbarian et al. “Gene expression for glutamic acid decarboxylase is reduced without loss of neurons in prefrontal cortex of schizophrenics”. In: *Archives of general psychiatry* 52.4 (1995), pp. 258–266.

[164] David W Volk et al. “Decreased glutamic acid decarboxylase67 messenger RNA expression in a subset of prefrontal cortical γ-aminobutyric acid neurons in subjects with schizophrenia”. In: *Archives of general psychiatry* 57.3 (2000), pp. 237–245.

[165] Schahram Akbarian and Hsien-Sung Huang. “Molecular and cellular mechanisms of altered GAD1/GAD67 expression in schizophrenia and related disorders”. In: *Brain research reviews* 52.2 (2006), pp. 293–304.

[166] Melis Inan, Timothy J Petros, and Stewart A Anderson. “Losing your inhibition: linking cortical GABAergic interneurons to schizophrenia”. In: *Neurobiology of disease* 53 (2013), pp. 36–48.

[167] DW Eyles, JJ McGrath, and GP Reynolds. “Neuronal calcium-binding proteins and schizophrenia”. In: *Schizophrenia research* 57.1 (2002), pp. 27–34.

[168] Takanori Hashimoto et al. “Gene expression deficits in a subclass of GABA neurons in the prefrontal cortex of subjects with schizophrenia”. In: *Journal of Neuroscience* 23.15 (2003), pp. 6315–6326.

[169] Juan E Belforte et al. “Postnatal NMDA receptor ablation in corticolimbic interneurons confers schizophrenia-like phenotypes”. In: *Nature neuroscience* 13.1 (2010), pp. 76–83.

[170] Marie Carlen et al. “A critical role for NMDA receptors in parvalbumin interneurons for gamma rhythm induction and behavior”. In: *Molecular psychiatry* 17.5 (2012), pp. 537–548.

[171] Eddie N Billingslea et al. “Parvalbumin cell ablation of NMDA-R1 causes increased resting network excitability with associated social and self-care deficits”. In: *Neuropsychopharmacology* 39.7 (2014), pp. 1603–1613.

[172] Kazuhito Nakao and Kazu Nakazawa. “Brain state-dependent abnormal LFP activity in the auditory cortex of a schizophrenia mouse model”. In: *Frontiers in neuroscience* 8 (2014), p. 168.

[173] Tatiana Korotkova et al. “NMDA receptor ablation on parvalbumin-positive interneurons impairs hippocampal synchrony, spatial representations, and working memory”. In: *Neuron* 68.3 (2010), pp. 557–569.

[174] Diana C Rotaru et al. “Glutamate receptor subtypes mediating synaptic activation of prefrontal cortex neurons: relevance for schizophrenia”. In: *Journal of Neuroscience* 31.1 (2011), pp. 142–156.

[175] Guillermo Gonzalez-Burgos and David A Lewis. “NMDA receptor hypofunction, parvalbumin-positive neurons, and cortical gamma oscillations in schizophrenia”. In: *Schizophrenia bulletin* 38.5 (2012), pp. 950–957.

[176] Madhuri S Kurdi, Kaushic A Theerth, and Radhika S Deva. “Ketamine: current applications in anesthesia, pain, and critical care”. In: *Anesthesia, essays and researches* 8.3 (2014), p. 283.

[177] Bita Moghaddam et al. “Activation of glutamatergic neurotransmission by ketamine: a novel step in the pathway from NMDA receptor blockade to dopaminergic and cognitive disruptions associated with the prefrontal cortex”. In: *Journal of Neuroscience* 17.8 (1997), pp. 2921–2927.

[178] Adrienne C Lahti et al. “Ketamine activates psychosis and alters limbic blood flow in schizophrenia.” In: *Neuroreport* 6.6 (1995), pp. 869–872.

[179] Alan Breier et al. “Association of ketamine-induced psychosis with focal activation of the prefrontal cortex in healthy volunteers.” In: *The American journal of psychiatry* (1997).

[180] FX Vollenweider et al. “Differential psychopathology and patterns of cerebral glucose utilisation produced by (S)-and (R)-ketamine in healthy volunteers using positron emission tomography (PET)”. In: *European Neuropsychopharmacology* 7.1 (1997), pp. 25–38.

[181] Y Suzuki et al. “Acute administration of phencyclidine induces tonic activation of medial prefrontal cortex neurons in freely moving rats”. In: *Neuroscience* 114.3 (2002), pp. 769–779.

[182] Mark E Jackson, Houman Homayoun, and Bita Moghaddam. “NMDA receptor hypofunction produces concomitant firing rate potentiation and burst activity reduction in the prefrontal cortex”. In: *Proceedings of the National Academy of Sciences* 101.22 (2004), pp. 8467–8472.

[183] Allie J Widman and Lori L McMahon. “Disinhibition of CA1 pyramidal cells by low-dose ketamine and other antagonists with rapid antidepressant efficacy”. In: *Proceedings of the National Academy of Sciences* 115.13 (2018), E3007–E3016.

[184] V Di Lazzaro et al. “Ketamine increases human motor cortex excitability to transcranial magnetic stimulation”. In: *The Journal of physiology* 547.2 (2003), pp. 485–496.

[185] Alexander D Shaw et al. “Ketamine amplifies induced gamma frequency oscillations in the human cerebral cortex”. In: *European Neuropsychopharmacology* 25.8 (2015), pp. 1136–1146.

[186] Gilles Plourde, Jacinthe Baribeau, and Vincent Bonhomme. “Ketamine increases the amplitude of the 40-Hz auditory steady-state response in humans.” In: *British journal of anaesthesia* 78.5 (1997), pp. 524–529.

[187] L Elliot Hong et al. “Gamma and delta neural oscillations and association with clinical symptoms under subanesthetic ketamine”. In: *Neuropsychopharmacology* 35.3 (2010), pp. 632–640.

[188] Didier Pinault. “N-methyl d-aspartate receptor antagonists ketamine and MK-801 induce wake-related aberrant γ oscillations in the rat neocortex”. In: *Biological psychiatry* 63.8 (2008), pp. 730–735.

[189] Bernat Kocsis. “Differential role of NR2A and NR2B subunits in N-methyl-D-aspartate receptor antagonist-induced aberrant cortical gamma oscillations”. In: *Biological psychiatry* 71.11 (2012), pp. 987–995.

[190] Jesse Wood, Yunbok Kim, and Bita Moghaddam. “Disruption of prefrontal cortex large scale neuronal activity by different classes of psychotomimetic drugs”. In: *Journal of Neuroscience* 32.9 (2012), pp. 3022–3031.

[191] María Jesús Nicolás et al. “Ketamine-induced oscillations in the motor circuit of the rat basal ganglia”. In: *PloS one* 6.7 (2011), e21814.

[192] Maya Slovik et al. “Ketamine induced converged synchronous gamma oscillations in the cortico-basal ganglia network of nonhuman primates”. In: *Journal of neurophysiology* 118.2 (2017), pp. 917–931.

[193] Klaus Linkenkaer-Hansen et al. “Genetic contributions to long-range temporal correlations in ongoing oscillations”. In: *Journal of Neuroscience* 27.50 (2007), pp. 13882–13889.

[194] L Elliot Hong et al. “Sensory gating endophenotype based on its neural oscillatory pattern and heritability estimate”. In: *Archives of general psychiatry* 65.9 (2008), pp. 1008–1016.

[195] L Elliot Hong et al. “Evoked gamma band synchronization and the liability for schizophrenia”. In: *Schizophrenia research* 70.2-3 (2004), pp. 293–302.

[196] Mei-Hua Hall et al. “The early auditory gamma-band response is heritable and a putative endophenotype of schizophrenia”. In: *Schizophrenia bulletin* 37.4 (2011), pp. 778–787.

[197] Gregor Leicht et al. “Alterations of the early auditory evoked gamma-band response in first-degree relatives of patients with schizophrenia: hints to a new intermediate phenotype”. In: *Journal of psychiatric research* 45.5 (2011), pp. 699–705.

[198] Peter J Uhlhaas and Wolf Singer. “Abnormal neural oscillations and synchrony in schizophrenia”. In: *Nature reviews neuroscience* 11.2 (2010), pp. 100–113.

[199] Peter J Uhlhaas and Wolf Singer. “High-frequency oscillations and the neurobiology of schizophrenia”. In: *Dialogues in clinical neuroscience* 15.3 (2013), p. 301.

[200] Johanna Kissler et al. “MEG gamma band activity in schizophrenia patients and healthy subjects in a mental arithmetic task and at rest”. In: *Clinical Neurophysiology* 111.11 (2000), pp. 2079–2087.

[201] Jun Soo Kwon et al. “Gamma frequency–range abnormalities to auditory stimulation in schizophrenia”. In: *Archives of general psychiatry* 56.11 (1999), pp. 1001–1005.

[202] Colleen A Brenner et al. “EEG synchronization to modulated auditory tones in schizophrenia, schizoaffective disorder, and schizotypal personality disorder”. In: *American Journal of Psychiatry* 160.12 (2003), pp. 2238–2240.

[203] Gregory A Light et al. “Gamma band oscillations reveal neural network cortical coherence dysfunction in schizophrenia patients”. In: *Biological psychiatry* 60.11 (2006), pp. 1231–1240.

[204] Dorea Vierling-Claassen et al. “Modeling GABA alterations in schizophrenia: a link between impaired inhibition and altered gamma and beta range auditory entrainment”. In: *Journal of neurophysiology* 99.5 (2008), pp. 2656–2671.

[205] Kevin M Spencer et al. “γ-Band auditory steady-state responses are impaired in first episode psychosis”. In: *Biological psychiatry* 64.5 (2008), pp. 369–375.

[206] Tony W Wilson et al. “Cortical gamma generators suggest abnormal auditory circuitry in early-onset psychosis”. In: *Cerebral cortex* 18.2 (2008), pp. 371–378.

[207] Giri P Krishnan et al. “Steady state and induced auditory gamma deficits in schizophrenia”. In: *Neuroimage* 47.4 (2009), pp. 1711–1719.

[208] Kwang-Hyuk Lee et al. “An integration of 40 Hz Gamma and phasic arousal: novelty and routinization processing in schizophrenia”. In: *Clinical neurophysiology* 112.8 (2001), pp. 1499–1507.

[209] Kevin M Spencer et al. “Neural synchrony indexes disordered perception and cognition in schizophrenia”. In: *Proceedings of the National Academy of Sciences* 101.49 (2004), pp. 17288–17293.

[210] Kevin M Spencer et al. “Sensory-evoked gamma oscillations in chronic schizophrenia”. In: *Biological psychiatry* 63.8 (2008), pp. 744–747.

[211] Jürgen Gallinat et al. “Reduced oscillatory gamma-band responses in unmedicated schizophrenic patients indicate impaired frontal network processing”. In: *Clinical Neurophysiology* 115.8 (2004), pp. 1863–1874.

[212] Kevin M Spencer. “Baseline gamma power during auditory steady-state stimulation in schizophrenia”. In: *Frontiers in human neuroscience* 5 (2012), p. 190.

[213] Noah C Venables, Edward M Bernat, and Scott R Sponheim. “Genetic and disorder-specific aspects of resting state EEG abnormalities in schizophrenia”. In: *Schizophrenia bulletin* 35.4 (2009), pp. 826–839.

[214] Yoji Hirano et al. “Spontaneous gamma activity in schizophrenia”. In: *JAMA psychiatry* 72.8 (2015), pp. 813–821.

[215] Georg Winterer et al. “Prefrontal broadband noise, working memory, and genetic risk for schizophrenia”. In: *American Journal of Psychiatry* 161.3 (2004), pp. 490–500.

[216] Canan Basar-Eroglu et al. “Working memory related gamma oscillations in schizophrenia patients”. In: *International journal of psychophysiology* 64.1 (2007), pp. 39–45.

[217] Gary Flynn et al. “Increased absolute magnitude of gamma synchrony in first-episode psychosis”. In: *Schizophrenia research* 105.1-3 (2008), pp. 262–271.

[218] Corinna Haenschel et al. “Cortical oscillatory activity is critical for working memory as revealed by deficits in early-onset schizophrenia”. In: *Journal of Neuroscience* 29.30 (2009), pp. 9481–9489.

[219] RY Cho, RO Konecky, and Cameron S Carter. “Impairments in frontal cortical γ synchrony and cognitive control in schizophrenia”. In: *Proceedings of the National Academy of Sciences* 103.52 (2006), pp. 19878–19883.

[220] Lindsay Rutter et al. “Magnetoencephalographic gamma power reduction in patients with schizophrenia during resting condition”. In: *Human brain mapping* 30.10 (2009), pp. 3254–3264.

[221] Balaji Narayanan et al. “Resting state electroencephalogram oscillatory abnormalities in schizophrenia and psychotic bipolar patients and their relatives from the bipolar and schizophrenia network on intermediate phenotypes study”. In: *Biological psychiatry* 76.6 (2014), pp. 456–465.

[222] Erol Başar. “A review of gamma oscillations in healthy subjects and in cognitive impairment”. In: *International Journal of Psychophysiology* 90.2 (2013), pp. 99–117.

[223] Andrea Perrottelli et al. “EEG-Based Measures in At-Risk Mental State and Early Stages of Schizophrenia: A Systematic Review”. In: *Frontiers in psychiatry* 12 (2021), p. 582.

[224] Matthew B Symond et al. ““Gamma synchrony” in first-episode schizophrenia: a disorder of temporal connectivity?” In: *American Journal of Psychiatry* 162.3 (2005), pp. 459–465.

[225] C Mulert et al. “Long-range synchrony of gamma oscillations and auditory hallucination symptoms in schizophrenia”. In: *International Journal of Psychophysiology* 79.1 (2011), pp. 55–63.

[226] Kevin M Spencer et al. “Left auditory cortex gamma synchronization and auditory hallucination symptoms in schizophrenia”. In: *BMC neuroscience* 10.1 (2009), pp. 1–13.

[227] Tineke Grent et al. “Resting-state gamma-band power alterations in schizophrenia reveal E/I-balance abnormalities across illness-stages”. In: *Elife* 7 (2018), e37799.

[228] Maciej T Lazarewicz et al. “Ketamine modulates theta and gamma oscillations”. In: *Journal of cognitive neuroscience* 22.7 (2010), pp. 1452–1464.

[229] Alan Anticevic et al. “N-methyl-D-aspartate receptor antagonist effects on prefrontal cortical connectivity better model early than chronic schizophrenia”. In: *Biological psychiatry* 77.6 (2015), pp. 569–580.

[230] Zheng Wang et al. “Comparison of first-episode and chronic patients diagnosed with schizophrenia: Symptoms and childhood trauma”. In: *Early intervention in psychiatry* 7.1 (2013), pp. 23–30.

[231] Nicolas Brunel and Mark CW Van Rossum. “Lapicque’s 1907 paper: from frogs to integrate-and-fire”. In: *Biological cybernetics* 97.5-6 (2007), pp. 337–339.

[232] Larry F Abbott. “Lapicque’s introduction of the integrate-and-fire model neuron (1907)”. In: *Brain research bulletin* 50.5-6 (1999), pp. 303–304.

[233] Frederic B Fitch. “McCulloch Warren S. and Pitts Walter. A logical calculus of the ideas immanent in nervous activity. Bulletin of mathematical biophysics, vol. 5, pp. 115–133”. In: (1944).

[234] Andreas Knoblauch. “Neural associative memory for brain modeling and information retrieval”. In: *Information Processing Letters* 95.6 (2005), pp. 537–544.

[235] Alan L Hodgkin and Andrew F Huxley. “A quantitative description of membrane current and its application to conduction and excitation in nerve”. In: *The Journal of physiology* 117.4 (1952), pp. 500–544.

[236] Catherine Morris and Harold Lecar. “Voltage oscillations in the barnacle giant muscle fiber”. In: *Biophysical journal* 35.1 (1981), pp. 193–213.

[237] W Rall et al. “Matching dendritic neuron models to experimental data”. In: *Physiological Reviews* 72.suppl_4 (1992), S159–S186.

[238] Romain Brette and Wulfram Gerstner. “Adaptive exponential integrate-and-fire model as an effective description of neuronal activity”. In: *Journal of neurophysiology* 94.5 (2005), pp. 3637–3642.

[239] Richard FitzHugh. “Impulses and physiological states in theoretical models of nerve membrane”. In: *Biophysical journal* 1.6 (1961), pp. 445–466.

[240] RM Rose and JL Hindmarsh. “The assembly of ionic currents in a thalamic neuron III. The seven-dimensional model”. In: *Proc. R. Soc. Lond. B* 237.1288 (1989), pp. 313–334.

[241] Eugene M Izhikevich. “Simple model of spiking neurons”. In: *IEEE Transactions on neural networks* 14.6 (2003), pp. 1569–1572.

[242] Bard Ermentrout. “Type I membranes, phase resetting curves, and synchrony”. In: *Neural computation* 8.5 (1996), pp. 979–1001.

[243] Eugene M Izhikevich. “Which model to use for cortical spiking neurons?” In: *IEEE transactions on neural networks* 15.5 (2004), pp. 1063–1070.

[244] Romain Brette. “What is the most realistic single-compartment model of spike initiation?” In: *PLoS computational biology* 11.4 (2015), e1004114.

[245] Jan Benda and Andreas VM Herz. “A universal model for spike-frequency adaptation”. In: *Neural computation* 15.11 (2003), pp. 2523–2564.

[246] Boris Gutkin and Fleur Zeldenrust. “Spike frequency adaptation”. In: *Scholarpedia* 9.2 (2014), p. 30643.

[247] Yoshiki Kuramoto. *Chemical oscillations, waves, and turbulence*. Courier Corporation, 2003.

[248] Michael Breakspear, Stewart Heitmann, and Andreas Daffertshofer. “Generative models of cortical oscillations: neurobiological implications of the Kuramoto model”. In: *Frontiers in human neuroscience* 4 (2010), p. 190.

[249] Jianxia Cui, Carmen C Canavier, and Robert J Butera. “Functional phase response curves: a method for understanding synchronization of adapting neurons”. In: *Journal of Neurophysiology* 102.1 (2009), pp. 387–398.

[250] Arthur T Winfree. *The geometry of biological time*. Vol. 12. Springer Science & Business Media, 2001.

[251] Leon Glass and Michael C Mackey. *From clocks to chaos: the rhythms of life*. Princeton University Press, 1988.

[252] Xiao-Jing Wang and György Buzsáki. “Gamma oscillation by synaptic inhibition in a hippocampal interneuronal network model”. In: *Journal of neuroscience* 16.20 (1996), pp. 6402–6413.

[253] Anastasiia Panchuk et al. “Synchronization of coupled neural oscillators with heterogeneous delays”. In: *International Journal of Bifurcation and Chaos* 23.12 (2013), p. 1330039.

[254] LF Abbott and Carl van Vreeswijk. “Asynchronous states in networks of pulse-coupled oscillators”. In: *Physical Review E* 48.2 (1993), p. 1483.

[255] Wulfram Gerstner. “Time structure of the activity in neural network models”. In: *Physical review E* 51.1 (1995), p. 738.

[256] Wulfram Gerstner, J Leo Van Hemmen, and Jack D Cowan. “What matters in neuronal locking?” In: *Neural computation* 8.8 (1996), pp. 1653–1676.

[257] David Hansel, Germán Mato, and Claude Meunier. “Synchrony in excitatory neural networks”. In: *Neural computation* 7.2 (1995), pp. 307–337.

[258] Nancy Kopell and GB Ermentrout. “Symmetry and phaselocking in chains of weakly coupled oscillators”. In: *Communications on Pure and Applied Mathematics* 39.5 (1986), pp. 623–660.

[259] RD Traub et al. “Analysis of gamma rhythms in the rat hippocampus in vitro and in vivo.” In: *The Journal of physiology* 493.2 (1996), pp. 471–484.

[260] Alessandro Treves. “Mean-field analysis of neuronal spike dynamics”. In: *Network: Computation in Neural Systems* 4.3 (1993), pp. 259–284.

[261] Theoden I Netoff et al. “Synchronization in hybrid neuronal networks of the hippocampal formation”. In: *Journal of neurophysiology* 93.3 (2005), pp. 1197–1208.

[262] Michael A Schwemmer and Timothy J Lewis. “The theory of weakly coupled oscillators”. In: *Phase response curves in neuroscience*. Springer, 2012, pp. 3–31.

[263] Klaus M Stiefel and G Bard Ermentrout. “Neurons as oscillators”. In: *Journal of neurophysiology* 116.6 (2016), pp. 2950–2960.

[264] Roy M Smeal, G Bard Ermentrout, and John A White. “Phase-response curves and synchronized neural networks”. In: *Philosophical Transactions of the Royal Society B: Biological Sciences* 365.1551 (2010), pp. 2407–2422.

[265] MR Jarvis and PP Mitra. “Sampling properties of the spectrum and coherency of sequences of action potentials”. In: *Neural Computation* 13.4 (2001), pp. 717–749.

[266] Nicolas Brunel and Vincent Hakim. “Fast global oscillations in networks of integrate-and-fire neurons with low firing rates”. In: *Neural computation* 11.7 (1999), pp. 1621–1671.

[267] Nicolas Brunel and Vincent Hakim. “Sparsely synchronized neuronal oscillations”. In: *Chaos: An Interdisciplinary Journal of Nonlinear Science* 18.1 (2008), p. 015113.

[268] Stephen Coombes, Peter beim Graben, and Roland Potthast. “Tutorial on neural field theory”. In: *Neural fields*. Springer, 2014, pp. 1–43.

[269] G Bard Ermentrout and David H Terman. *Mathematical foundations of neuroscience*. Vol. 35. Springer Science & Business Media, 2010.

[270] Wulfram Gerstner et al. *Neuronal dynamics: From single neurons to networks and models of cognition*. Cambridge University Press, 2014.

[271] Hugh R Wilson and Jack D Cowan. “Excitatory and inhibitory interactions in localized populations of model neurons”. In: *Biophysical journal* 12.1 (1972), pp. 1–24.

[272] Hugh R Wilson and Jack D Cowan. “A mathematical theory of the functional dynamics of cortical and thalamic nervous tissue”. In: *Kybernetik* 13.2 (1973), pp. 55–80.

[273] Federico Devalle, Alex Roxin, and Ernest Montbrió. “Firing rate equations require a spike synchrony mechanism to correctly describe fast oscillations in inhibitory networks”. In: *PLoS computational biology* 13.12 (2017), e1005881.

[274] Stephen Keeley et al. “Firing rate models for gamma oscillations”. In: *Journal of neurophysiology* 121.6 (2019), pp. 2181–2190.

[275] Xiao-Jing Wang and John Rinzel. “Alternating and synchronous rhythms in reciprocally inhibitory model neurons”. In: *Neural computation* 4.1 (1992), pp. 84–97.

[276] Miles A Whittington, Roger D Traub, and John GR Jefferys. “Synchronized oscillations in interneuron networks driven by metabotropic glutamate receptor activation”. In: *Nature* 373.6515 (1995), pp. 612–615.

[277] Xiao-Jing Wang and György Buzsáki. “Gamma oscillation by synaptic inhibition in a hippocampal interneuronal network model”. In: *Journal of neuroscience* 16.20 (1996), pp. 6402–6413.

[278] Carl Van Vreeswijk, LF Abbott, and G Bard Ermentrout. “When inhibition not excitation synchronizes neural firing”. In: *Journal of computational neuroscience* 1.4 (1994), pp. 313–321.

[279] LS Leung. “Nonlinear feedback model of neuronal populations in hippocampal CAl region”. In: *Journal of neurophysiology* 47.5 (1982), pp. 845–868.

[280] G Bard Ermentrout and Nancy Kopell. “Fine structure of neural spiking and synchronization in the presence of conduction delays”. In: *Proceedings of the National Academy of Sciences* 95.3 (1998), pp. 1259–1264.

[281] Christoph Börgers and Nancy Kopell. “Synchronization in networks of excitatory and inhibitory neurons with sparse, random connectivity”. In: *Neural computation* 15.3 (2003), pp. 509–538.

[282] David Hansel and Germán Mato. “Asynchronous states and the emergence of synchrony in large networks of interacting excitatory and inhibitory neurons”. In: *Neural computation* 15.1 (2003), pp. 1–56.

[283] Atthaphon Viriyopase, Raoul-Martin Memmesheimer, and Stan Gielen. “Cooperation and competition of gamma oscillation mechanisms”. In: *Journal of neurophysiology* 116.2 (2016), pp. 232–251.

[284] Atthaphon Viriyopase, Raoul-Martin Memmesheimer, and Stan Gielen. "Analyzing the competition of gamma rhythms with delayed pulse-coupled oscillators in phase representation". In: *Physical Review E* 98.2 (2018), p. 022217.

[285] X-J Wang. "Fast burst firing and short-term synaptic plasticity: a model of neocortical chattering neurons". In: *Neuroscience* 89.2 (1999), pp. 347–362.

[286] Roger D Traub et al. "Single-column thalamocortical network model exhibiting gamma oscillations, sleep spindles, and epileptogenic bursts". In: *Journal of neurophysiology* 93.4 (2005), pp. 2194–2232.

[287] Roger D Traub et al. "Persistent gamma oscillations in superficial layers of rat auditory neocortex: experiment and model". In: *The Journal of physiology* 562.1 (2005), pp. 3–8.

[288] Adrien Peyrache et al. "Spatiotemporal dynamics of neocortical excitation and inhibition during human sleep". In: *Proceedings of the National Academy of Sciences* 109.5 (2012), pp. 1731–1736.

[289] Peter Barthó et al. "Characterization of neocortical principal cells and interneurons by network interactions and extracellular features". In: *Journal of neurophysiology* 92.1 (2004), pp. 600–608.

[290] Michel Le Van Quyen et al. "Large-scale microelectrode recordings of high-frequency gamma oscillations in human cortex during sleep". In: *Journal of Neuroscience* 30.23 (2010), pp. 7770–7782.

[291] Yann Zerlaut and Alain Destexhe. "Enhanced responsiveness and low-level awareness in stochastic network states". In: *Neuron* 94.5 (2017), pp. 1002–1009.

[292] Yann Zerlaut et al. "Modeling mesoscopic cortical dynamics using a mean-field model of conductance-based networks of adaptive exponential integrate-and-fire neurons". In: *Journal of computational neuroscience* 44.1 (2018), pp. 45–61.

[293] Robert Friedman. "Themes of advanced information processing in the primate brain". In: *AIMS neuroscience* 7.4 (2020), p. 373.

[294] Horace B Barlow. "Single units and sensation: a neuron doctrine for perceptual psychology?" In: *Perception* 1.4 (1972), pp. 371–394.

[295] Mark M Churchland et al. "Stimulus onset quenches neural variability: a widespread cortical phenomenon". In: *Nature neuroscience* 13.3 (2010), pp. 369–378.

[296] Alexa Riehle et al. "Spike synchronization and rate modulation differentially involved in motor cortical function". In: *Science* 278.5345 (1997), pp. 1950–1953.

[297] E Vaadia et al. "Dynamics of neuronal interactions in monkey cortex in relation to behavioural events". In: *Nature* 373.6514 (1995), pp. 515–518.

[298] Simon Thorpe, Arnaud Delorme, and Rufin Van Rullen. “Spike-based strategies for rapid processing”. In: *Neural networks* 14.6-7 (2001), pp. 715–725.

[299] Sophie Deneve. “Bayesian spiking neurons I: inference”. In: *Neural computation* 20.1 (2008), pp. 91–117.

[300] Shigeru Shinomoto et al. “Relating neuronal firing patterns to functional differentiation of cerebral cortex”. In: *PLoS Comput Biol* 5.7 (2009), e1000433.

[301] Gaby Maimon and John A Assad. “Beyond Poisson: increased spike-time regularity across primate parietal cortex”. In: *Neuron* 62.3 (2009), pp. 426–440.

[302] Artur Luczak, Bruce L McNaughton, and Kenneth D Harris. “Packet-based communication in the cortex”. In: *Nature Reviews Neuroscience* 16.12 (2015), pp. 745–755.

[303] Sabine Kastner. “Attentional Response Modulation in the Human Visual System.” In: (2004).

[304] Thomas Andrillon et al. “Neural markers of responsiveness to the environment in human sleep”. In: *Journal of Neuroscience* 36.24 (2016), pp. 6583–6596.

[305] SL Shafer and DR Stanski. “Defining depth of anesthesia”. In: *Modern Anesthetics* (2008), pp. 409–423.